SOLIDS SUSPENSION IN VISCOUS NEWTONIAN AND NON-NEWTONIAN LIQUIDS

Submitted for the degree of Doctor of Philosophy
in the University of London by:

Louis Al-Dhahir, B.Eng. (Hons)

November, 1990

ABSTRACT

Mechanically agitated solid mixing has been investigated for many years. A multitude of empirical correlations and theoretical models have been proposed in order to predict the minimum impeller speed, N_{JS}, required for complete solids suspension. Hitherto, nearly all this research has focussed on low viscosity Newtonian liquids, typically water.

This study has been concerned with extending the acquisition of solids suspension data into the transition and laminar regimes using both high viscosity Newtonian liquids as well as non-Newtonian as well as non-Newtonian liquids.

The Newtonian liquids were mixtures of glycerol and water or corn syrup and water. Their viscosities varied from 0.022 to 11.35 Pas. The non-Newtonian liquids were made of aqueous solutions of Carbonyl Methyl Cellulose. These were found to conform to a simple power-law rheology. The flow index, n, varied from 0.95 to 0.73, and the consistency index from 0.012 to 0.700.

Suspension speed experiments were carried out in unbaffled, flat-bottomed tanks. Agitation was provided by a range of 45^{o} pitch, six-bladed turbine impellers. Baffles, when used were found to hinder suspension.

Solids distribution experiments were carried out in fully profiled vessels. A non-intrusive optical technique was used to sample local solids concentrations.

By using such viscous liquids, it was found possible to suspend solids well within the laminar regime. Under such circumstances, those empirical and theoretical relationships derrived from turbulent conditions proved unsatisfactory for either a prediction of N_{JS} or an explaination of the solids suspension mechanism. Instead, an attempt has been made to explain the suspension mechanism, and hence to predict N_{JS}, using the mean liquid velocities found at close proximity to particles at the base of an agitated vessel.

The Newtonian and non-Newtonian liquids were found to have markedly different axial solids concentration profiles both form each other and as compared with water.

Acknowledgements

I would like to thank Professor J.Mullin and Dr A.Burgess for their advice and encouragement especially during the later stages of the research.

My gratitude is also extended to Tunnel Refineries for providing corn syrup for the research free of charge.

ERRATA

Abstract

2nd paragraph "...as well as non-Newtonian .." is repeated
6th paragraph "derived" not "derrived"
7th paragraph "from" not "form"

Chapter 2

p5 Zweitering not Zwietering
p17 2nd paragraph "possible" not "possilble"
4th paragraph "..inside of a pipe.."
p30 1st paragraph "Schwartzberg & Treybal"

Chapter 3

p53 top paragraph "equalled" not "equaled"
p59 mid-page "...of n in equation 3.1.10.." not 3.1.9

Chapter 5

p101 2nd paragraph "these" not "thee"
p119 1st paragraph " ...note that..." not "....note that that.."

CONTENTS

1.1 Suspension of Solids in Agitated Vessels

Suspension of solid particles in liquids is an important unit operation in the chemical process industry. Mechanically agitated vessels are often used in those processes that require the greatest possible contact between the solid phase and the surrounding liquid phase.

Impeller agitated systems have been, and are continuing to be, used in a wide range of industrial applications, with perhaps the widest application in relatively low concentration suspensions in which intense agitation is required to lift the solids into suspension and maintain them there. Typical examples are crystallization, ion-exchange, solid catalyzed liquid reactions, and preparation of slurries for hydraulic conveying.

The liquids encountered in such applications can either be Newtonian or non-Newtonian. The present work is concerned with those suspension systems that involve either relatively high viscosity Newtonian or non-Newtonian liquids. This is an area that has been neglected in terms of systematic research in spite of its industrial significance.

With such applications, the point at which complete particle suspension is initiated and the degree of solids distribution are of considerable practical importance, particularly in the case of low concentrations of dense solids where the particles will tend to settle out to the bottom of the vessel if sufficient agitation is not provided. An essential parameter for the design of mechanically agitated vessels is the minimum impeller speed at which all the particles become suspended. This is termed the "just suspension speed", N_{JS}. Mass transfer studies have shown that in many cases an increase in impeller speed beyond N_{JS} can result in much higher power consumption whilst hardly improving the rate of mass transfer. The importance of N_{JS} in agitated vessels is shown by the

relatively large number of published papers and books (tables 2.1.1 and 2.3.1).

Several criteria and experimental techniques have been proposed in the literature for the determination of N_{JS}. However, even upto the present day, there is no universally agreed definition and no accepted method for determining the just suspension speed condition. This has had the consequence of widely differing results and conclusions from apparently similar empirical work reported by different authors (table 2.3.1).

In many cases it is acceptable to operate a suspension process at the just suspension condition. However, there are some applications, e.g. continuously stirred tank reactors, where it is desirable to operate as close as possible to homogeneous suspension conditions, i.e. the solid particles are uniformly distributed throughout the agitated vessel.

Although it is easy to define a homogeneous suspension, it is more difficult to achieve it. A variety of experimental techniques and definitions have been employed in an attempt to to measure and evaluate the quality of the solids suspension. These have included visual observation, photography, sample removal, electrical conductivity probes, and optical techniques, both intrusive and non-intrusive. These investigations tend to show the practical difficulties of attaining homogeneity. Consequently, some investigators have resorted to defining an optimum degree of suspension homogeneity which a given agitated system can ultimately achieve. This is commonly referred to as the "pseudo-homogeneous" state of suspension.

Although solid-liquid suspensions have been utilized for centuries and systematically studied for the last half century, the basic mechanism, responsible for lifting solids from the base of the tank into suspension, is still a matter of contention. Furthermore, perhaps due to the complexity of the hydrodynamics of agitated systems, little progress has been achieved in developing theoretical models to describe the distribution of suspended solids. Much of

the published work and the proposed predictive equations rely on a statistical analysis of large quantities of experimental data. This approach has proved useful for design purposes, but it is not comprehensive enough to provide a complete answer to the full range of suspension problems.

Many of the industrial applications of mechanically agitated vessels involve vessels of considerable size. It is rarely feasible to conduct suspension studies in full, plant size vessels. The usual practice is to conduct suspension studies in smaller, geometrically similar tanks and then use the results as a basis for scale-up. A number of researchers have attempted to tackle the problem of scale-up but their results rarely agree with each other and can be very misleading. This has been mainly attributed to inconsistent scale-up procedures, different experimental techniques, and the several definitions employed for determining the just suspension speed.

1.2 Objectives of this Study

Most of the empirical work conducted into the field of solids suspension has involved suspending solids in low viscosity liquids, typically water. The principal aim of this work was to extend the range of experimental data from the low viscosity, high Reynolds number régime to lower Reynolds number régimes using high viscosity Newtonian and non-Newtonian liquids. This meant recording just suspension speeds for a variety of solids in different liquids and also measuring the local concentrations of suspended solids to find the quality of mixing in a variety of agitated systems.

An important part of this thesis is taken up by the theoretical aspects of the solids suspension mechanism, i.e. the mechanism by which solids are lifted up into suspension from the base of the vessel. Hitherto, most of the prevailing theories have relied to some extent on fully turbulent conditions, with high impeller Reynolds numbers. Since the agitated systems in this study have much lower

Reynolds numbers, these turbulent models can not provide a satisfactory answer to solids suspension under such conditions. This has meant developing a model based on mean liquid velocities present at the base of the agitated vessel. The suspension speed data gathered by this and other studies were then compared with the predictions made by this proposed model to test its validity and utility for predicting N_{JS}, and as a basis for scale-up.

This thesis does not propose a new model for the distribution of solids in an agitated vessel but the experimental data gathered can be usefully compared with the data and correlations produced by other researchers.

CHAPTER TWO: LITERATURE SURVEY

Solid suspension has been an important part of many industrial processes for many centuries. The first (known) written review of the subject dates back to the Sixteenth Century. Agricola, 1553, devoted a chapter of his book to means by which Central European miners used a series of agitated tanks, and paddle impellers, to suspend solid particles to separate the useful minerals from the debris. However, the first real attempts to systematically study the subject of solids suspension in this first half of this century with the work of White & Summerford, 1932. This work, in common with nearly all subsequent research, only dealt with the suspension of solids in low viscosity Newtonian liquids. Only a narrow range of experimental conditions were examined by White & Summerford and the conclusions drawn from the their studies are of limited applicability for design purposes.

The first successful attempt to produce general rules for predicting the just suspension speed, N_{JS} (see 2.1.1 for definition), came with the work of Zweitering, 1958. In various baffled tanks with different stirrer types and geometries, over 1000 experiments were conducted, suspending solids of varying size and density in low viscosity Newtonian liquids. The impeller Reynolds number, required for suspension, was always found to be greater than 3000.

Although a great deal of work, of both empirical and theoretical nature, has been published in the last 30 years, Zweitering's work has still remained as the benchmark by which subsequent research has been frequently compared.

For the purposes of this study, the survey of literature is limited to work published on low concentration and inert, two-phase suspensions, where the solids are denser than the surrounding liquid.

2.1 Definitions of the State of Suspension and of the Just Suspension Condition

2.1.1 Definitions of the State of Suspension

There are three main states of suspension which have been described in the literature.

a) Complete or Just Suspension

Complete suspension is said to be reached when all the particles are in motion and no particle remains at the base of the agitated vessel for more than a short time (see 2.1.2 for more detail). When there is complete suspension, the particle/liquid interfacial area is maximized. This can be important for optimizing any mass transfer operation. The term "just suspension" is defined as the minimum condition (or level of agitation) when complete suspension occurs. The significance of the just suspension condition can be gauged from the numerous publications devoted to either the recording or attempting to predict the occurrence of this condition. When the agitation is provided by the rotary action of an impeller, the minimum rotational speed required to achieve complete suspension is referred to as the "just suspension speed", N_{JS}.

b) Bottom or Corner Fillets Suspension

During the course of agitation, solids may be trapped at the peripheries of the vessel (in "dead zones"). This often occurs with flat-bottomed cylindrical vessels where particles collect at the corners of the vessel, where the base joins the walls. If the impeller speed is increased sufficiently, the numbers of particles trapped as corner fillets may decrease, but to achieve complete suspension may require a very substantial increase in power consumption.

c) Homogeneous or Uniform Suspension

A homogeneous suspension occurs when the local concentration of solids is the same as the bulk holdup

concentration at all locations within the agitated liquid. This condition is often desirable in continuous flow systems such as crystallizers, where the concentration of suspended crystals in the discharge stream should be as close as possible to that within the agitated vessel. Complete homogeneity is an ideal that is rarely achievable in practice.

2.1.2 Definitions of the Just Suspension Speed

One of the major problems in conducting quantitative research into solids suspension has been to determine accurately the "just suspension speed". This is the minimum impeller speed, normally in terms of revolutions per unit time, required to completely suspend all the particles from the base of an agitated vessel. This has given rise to many definitions of this just suspension condition.

"1 to 2 seconds" criterion

The first practical criterion for determining N_{JS} was introduced by Zweitering, 1958. This requires visual observation of the base of the tank. Above a certain impeller speed, solid particles are constantly lifting into suspension and then settling out. At equilibrium, the rates at which these two processes take place will be the same. At the transition point between incomplete and complete suspension, small piles of solids remain at the bottom for more than 1 or 2 seconds before being broken up. Zweitering judged that when no deposits remained at the bottom for more than 1 second, the suspension was considered complete and the impeller speed recorded. Zweitering reported that this technique was reproducible to 2 to 3 per cent. This is the so called "1 to 2 seconds" criterion. This method relies on good visibility and has been confined to use in small, transparent vessels where the solids concentration is not so high that the suspended solids obscure the base from sight.

"C-break" criterion

Another, less subjective means of finding N_{JS} is the C-break method. Musil, 1976, used an optical probe to

measure local solid concentrations near the base of an agitated vessel, at various impeller speeds, see figure 2.1.1. This graph of local concentration vs. impeller speed has been referred to as the C-curve (Koutsakos, 1989). This break can either manifest itself as a maximum (Koutsakos, 1989) or as a sharp change of slope (Musil, 1976). The reasoning by which this point is taken as the N_{JS} value is conjecture. As the impeller speed is increased from zero, particles begin to move into suspension, and further increases in speed cause more and more particles to go into suspension. At N_{JS}, all the particles have become suspended. Further increases beyond N_{JS} cause some of those particles near the base of the tank to be suspended at a higher plane in the liquid resulting in lower local concentrations near the base of the vessel, causing the break in the C-curve.

In order to accurately determine this break, the experimenter would have to ensure that the increments between successive impeller speeds was sufficiently small near this critical region of the curve. This would mean the experimenter knowing, approximately, the value of N_{JS} before conducting the experiment.

The C-break criterion has been used by many investigators that have sampled the local concentration using electrical conductivity sampling, or optical probes (Musil, 1976; Bourne & Sharma, 1974; Ohiaeri, 1981), and non-intrusive light sensitive methods (Shamlou & Koutsakos, 1986)

"98% suspension" criterion

Chudacek, 1982, pointed out that induced recirculation loops, figure 2.1.2, near the base of the vessel hindered the visual observation of N_{JS}. In response, Chudacek introduced a new criterion for N_{JS} to be the impeller speed required to suspend 98 per cent of the total solids content of the vessel. This was suggested to overcome the disproportionate increase in impeller speed,

required by the 1 to 2 seconds criterion, to suspend the last few particles. However, this criterion has been found to be highly impractical because of the difficulties in determining when 98 per cent of the solids are in suspension.

"Suspension Height" criterion

Einenkel & Mersmann, 1977, defined N_{JS} as being the impeller speed required to reduce the height of clear liquid, at the top of the vessel, to one tenth of the total liquid height. This criterion is completely arbitrary. It also suffers from a practical problem when suspending small particles, when it is difficult to identify the interface between the suspension and the clear liquid because these small particles travel to the top of the liquid before the last particles are suspended (Chapman, 1981).

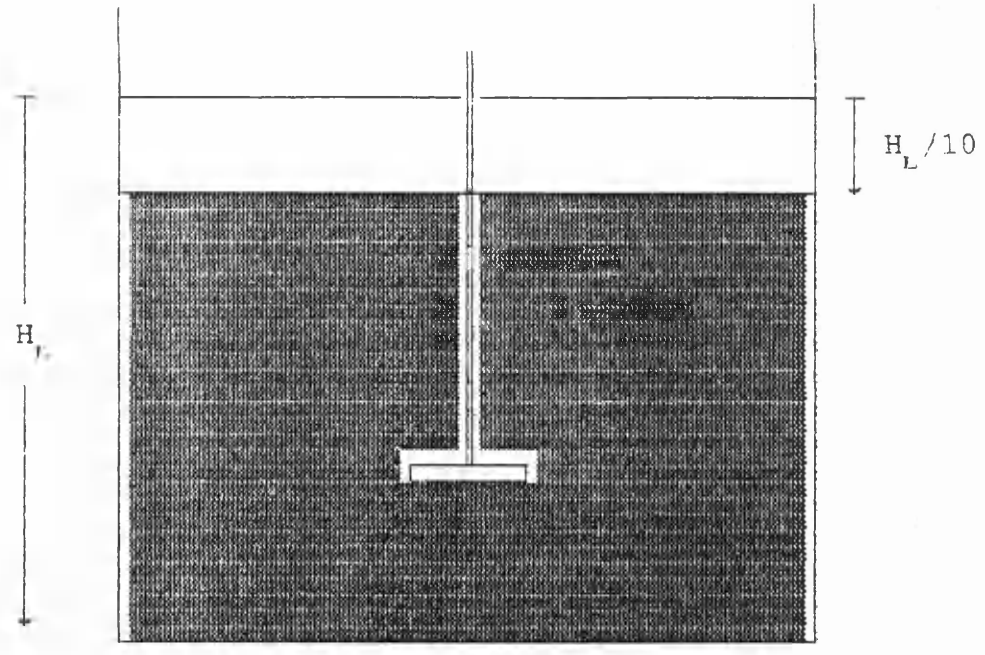

Figure 2.1.3 Suspension height criterion (Einenkel & Mersmann, 1977)

Table 2.1.1 Suspension Speed Studies

Author(s)	ρ_s (kg/m^3)	d_p (μm)	ρ_f (kg/m^3)	μ mPas	C_w %wt
Baldi et al 1978	2650	5 -> 550	1000	1->3	0.2->2.0
Bohnet & Niesmak, 1980	1050 -> 8850	100 -> 1150	1000	1	0.2->25.0
Bourne & Sharma, 1974	2640	200 -> 1000	1000	1	< 5.3
Chapman et al 1983	1050 -> 2900	180 -> 2800	1000	1	< 30.0
Chudacek,1982	2650	290	1000	1	32.2
Conti et al 1978	1200 -> 2650	440 -> 3400	1000	0.7->7	0.05->0.6
Ditl & Reiger 1985	2600 -> 3590	180 -> 2800	1000	1	< 5.0
Einenkel, 1980	2870	200 -> 630	1000	1	10->40
Einenkel & Mersmann, 1977	2480	80 -> 250	1000	1	2 -> 35
Herringe 1979	2650 -> 4470	20 -> 5000	1000	1	16 ->25

Table 2.1.1 Solids Suspension Studies (continued)

Author(s)	ρ_s (kg/m^3)	d_p (μm)	ρ_f (kg/m^3)	μ mPas	C_w %wt
Kneule & Weinspach,1967	2630 -> 11100	100-> 10000	1000	1	0.2 -> 25
Kolar, 1967	1150 -> 2980	130 -> 1640	800 -> 1000	1 -> 2	0.3 -> 3
Koutsakos 1989	1513 -> 2900	175 -> 1100	1000	1	< 10
Molerus & Latzel, 1987	2480 -> 7841	34 -> 1937	1000	1 ->13	1.2->23.5
Musil & Vlk 1978	<2900	700 -> 1100	1000	1	11.6->23.2
Narayanan et al, 1969	1140 -> 2600	68 -> 211	1000	1	2.5 -> 10
Nienow 1968	1530 -> 2660	153 -> 9000	1000	1	0.1 -> 10
Shamlou & Zolfagharian1987	2540 -> 2960	175 -> 3015	1000	1	1 -> 5
Weismann & Efferding, 1960	2600 -> 9700	4 -> 140	1000	1	10.5 ->23
Zweitering 1958	2150 -> 2650	125 -> 800	790 -> 1600	0.3->9	0.5 -> 20
This work 1990	1270 -> 3820	390 -> 10000	1000 -> 1390	20 -> 11400	0.03->1.0

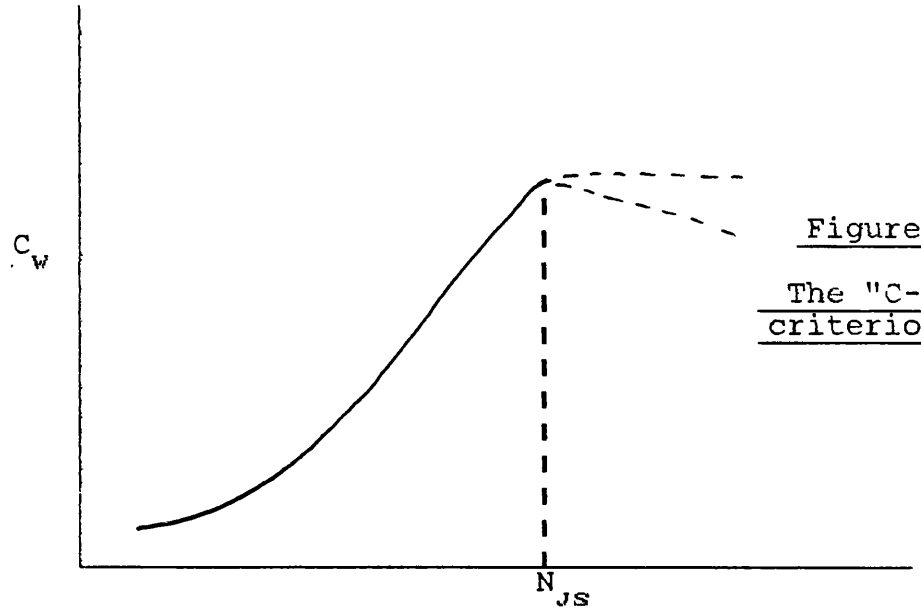

Figure 2.1.1

The "C-break" criterion for N_{JS}

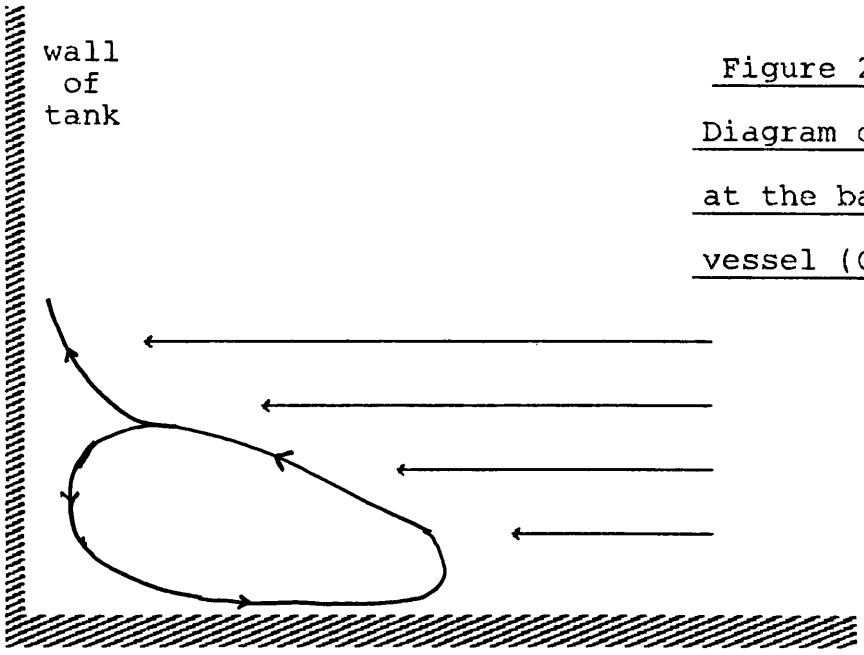

Figure 2.1.2

Diagram of recirculation at the base of a flat vessel (Chudacek, 1982)

2.2 Solids Suspension in High Viscosity Newtonian Liquids and in non-Newtonian Liquids

Very little work of a quantitative nature has been accomplished with suspension in high viscosity liquids, whether they are Newtonian or otherwise. Zweitering, 1958; Baldi et al, 1978; Molerus & Latzel, 1987, and all the others listed in tables 2.1.1, 2.3.1 and 2.4.1 all conducted experiments exclusively with low viscosity liquids. The maximum kinematic viscosity examined by these researchers was that of an ethylene glycol solution, 13 x 10^{-6} m^2/s. Even those researchers who conducted experiments with a view to verifying the mean flow approach for modeling the suspension mechanism never exceeded this value.

The only work that has been found concerning suspension in high viscosity liquids is that of Hirsekorn & Miller, 1953. This paper showed that it was possible to suspend particles, such as glass ballotini, in Newtonian corn syrup solutions of absolute viscosity 20 to 30 Pas. Under such viscous conditions, the impeller Reynolds number, required for suspension, was found to be less than 12. This shows that turbulence is not required to lift particles into suspension.

The Hirsekorn & Miller paper is more interesting from a qualitative perspective than quantitative. Photographs taken by the researchers show that the suspension characteristics are different in high viscosity liquids as compared with visual observations made in the low viscosity régime.

It has been conventional with those experiments conducted in the low viscosity/high Reynolds number régime to design the agitation system such that there are four symmetrically arranged baffles and the stirrer, if axial, to be set pumping downwards. The ratio of impeller diameter to tank diameter (D/T) is normally set at 1/3. The width of the baffles is typically one tenth of the vessel diameter.

Amongst many others, Molerus & Latzel, 1987, for

example, have observed that under such a geometry in low viscosity liquids, the particles are generally thrown radially outwards and that the last particles to suspend are to be found at the periphery of the vessel base next to the baffles.

For the high viscosity Newtonian liquids investigated by Hirsekorn & Miller, the most efficient suspension was found by setting D/T at 0.6. In contrast to Molerus & Latzel's observations, Hirsekorn & Miller's photographic evidence shows that the particles are drawn inwards to the centre of the base and form a mound directly beneath the impeller (see figure 2.2.1). From the top of this mound, particles lift off into suspension. As the impeller speed is increased, this mound decreases in size until only a few particles are left, almost stationary at the centre. At this point, a large increase in impeller speed is required before these last particles are suspended. Such mound formation has been observed for low viscosity liquids but only under extreme geometries when D/T is large or if the impeller clearance is very low.

These high viscosity experiments were conducted in a cylindrical, flat bottomed, transparent tank without baffles. Agitation was provided by a simple two bladed paddle.

In a discussion following on from their 1953 paper, Miller remarked that under such low Reynolds number conditions, the effect of the baffles was minimal on the just suspension speed. This is because the impeller, unless it approaches the same diameter as the tank, does not feel the the effects of the tank walls only the liquid in the immediate vicinity of the impeller blades. Indeed, Miller went on to point out that baffles in low Reynolds number conditions may actually hinder suspension because what little liquid motion there may be at the extremes of the tank will be stopped by the baffles, so that solids can trapped behind the baffles.

As for solids suspension in non-Newtonian liquids, there has been no work, qualitative or quantitative, that has been published to date. There have been papers

concerning the agitation of non-Newtonian liquids (see Appendix 2) and the results of these papers show the difficulties found when experimenting with such liquids. In this study, the non-Newtonian liquids under examination exhibit a pseudoplastic rheology. With non-Newtonian liquids, the viscosity of the liquid will not be constant throughout the tank. Instead, it will be a function of the local shear rate experienced by the liquid. In a pseudoplastic fluid, the viscosity will be at a minimum at the point of highest shear, i.e near the blades of an impeller, and at its maximum at the periphery, where the local shear rate is lowest, i.e. at the walls and base of the tank.

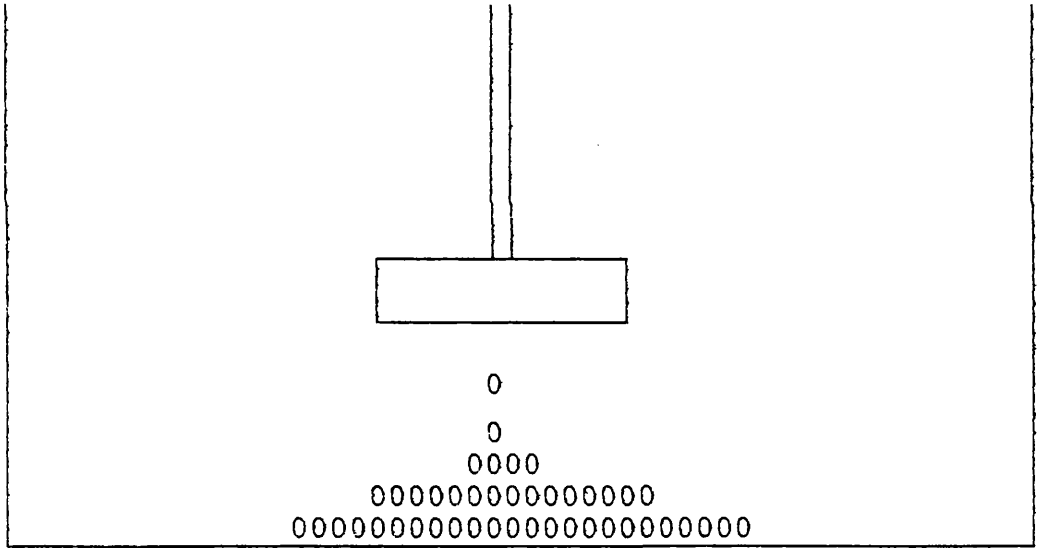

Figure 2.2.1 Mound formation in high viscosity corn syrup solutions (Hirsekorn & Miller, 1953)

2.3 Predictions of Suspension Speeds

The first successful attempt to predict just suspension speeds was made by Zweitering, 1958. Whilst many previous researchers had investigated solids suspension, none had been able to set out definite general rules for predicting N_{JS} for a given system. The experiments were conducted in transparent baffled vessels. N_{JS} was determined visually using the "1 to 2 seconds" criterion. By studying the following design variables: vessel diameter, stirrer type and geometry, solid density, concentration and density, liquid density and viscosity, a great number of combinations could be examined (see table 2.3.1). All the liquids used were low viscosity Newtonian liquids, whose kinematic viscosities ranged from 0.39 to 11.1 x 10^{-6} m^2/s.

Zweitering arranged these variables into dimensionless groups and employed dimensional analysis arguments in conjunction with the results of over 1000 experiments to determine a relationship to predict N_{JS}. The end result is an empirical correlation

$$N_{JS} = \frac{S\,\nu^{0.1} d_p^{0.2} g^{0.45} C_w^{0.13}}{D^{0.85}} \left[\frac{\rho_s - \rho_f}{\rho_f}\right]^{0.45} \qquad 2.3.1$$

where S is a geometrical constant that takes into account the stirrer type, clearance and diameter as well as the vessel diameter. In order to determine S, Zweitering used the data he had gathered at different geometries and presented them in graphical form. Each graph corresponds to a different impeller type. Typical graphs are shown in figures 2.3.1 and 2.3.2.

Zweitering's correlation is just one of many empirical correlations that emerged, with varying degrees of success, in the last 30 years (see table 2.3.1). However, because of the large amount of experimental data gathered by Zweitering, the subsequent analysis of the data, and the generally good predictions made from 2.3.1, his correlation remains as a standard by which to compare

other equations and data.

Such empirical correlations can be a useful aid for design purposes, but this approach gives little theoretical insight into the mechanisms responsible for suspension of solids from the base of an agitated vessel into the bulk of the liquid.

A more general relationship, relying more on theory rather than empiricism, has been the goal of much research in the last 20 years. With a more general relationship, it might then be possible to predict N_{JS} over much wider ranges of solid/liquid properties and for the purposes of scaling up from the laboratory to the industrial scale. By doing so, it might also be possilble to optimize the design of the agitation system. To satisfy this aim, a greater understanding is required of the mechanism by which solids are suspended. These mechanisms fall into two distinct, and apparently contradictory categories: a) those that rely on turbulence in the bulk of the fluid and b) those that rely on the mean (or time averaged) liquid velocities at the base of the vessel.

The first of these, type a), is the one that has received the most attention and can be regarded as the current orthodoxy.

Einstein and El-Samni, 1949, attempted to show that turbulence was the mechanism that suspended solids. Hemispheres were fixed to the inside if a pipe through which a liquid was allowed to flow. Strain gauges attached to the surface of these hemispheres were used to determine the pressure distribution and hence the lift-force on the hemisphere. Separate measurements gave data on the mean and fluctuating liquid velocity in the pipe. The conclusions drawn by the researchers' statistical analysis indicated that the lift-force was better correlated with the fluctuating velocity than the mean velocity, and hence turbulence must be the suspension mechanism. In a paper by Thomas, 1961, it was asserted that the suspension of particles in a pipe was primarily caused by turbulent fluctuations penetrating the laminar sub-layer. Without some critical degree of turbulence, suspension would be

impossible.

Further, more indirect, evidence of the turbulence mechanism might be found from those researchers who investigated the phenomenon of vibratory agitation. Tojo et al, 1981, suspended solids using a reciprocating disc agitator in a flat bottomed cylindrical tank. The range of experimental conditions used are shown in figure 2.3.3. As well as studying the suspension of solids, they also measured the rate of solid-liquid mass transfer. The results of their work showed that for a given mass transfer rate, vibratory agitation was more energy efficient than conventional rotary agitation.

Part of the reason why the suspension mechanism is contentious, is that all rotary agitators generate a mixture of turbulence and mean bulk flow of liquid. Low amplitude, high frequency vibratory agitation is regarded as one way to provide the liquid with a high degree of turbulence whilst minimizing the amount of mean bulk liquid motion. Therefore, one possible implication of Tojo et al's results is that for a given power input to an agitated system, the more energy is converted to turbulence, rather than mean flow, the more efficient the system will be for suspending solids. However, it is interesting to note that the results could only be used to show that mass transfer operations were enhanced by vibratory agitation, and not the actual suspension of solids. It has long been established that the mass transfer rate will be increased by increasing the fluid Reynolds number, and hence the degree of turbulence. It is quite possible for the rotary agitation to have suspended the solids more efficiently than vibratory by promoting the mean flow mechanism, and yet, find that having suspended the solids , the rate of mass transfer is less because the degree of turbulence in the bulk of the liquid is considerably less than in the vibratory agitator system.

More recently, Yung et al, 1989, conducted experiments with a monolayer of particles submerged within the viscous sublayer (see figure 2.3.4). The flow through the channel varied with Reynolds Numbers in the range 17000

to 47000. The turbulent burst-particle interactions were recorded using high speed photography and a dual laser beam technique. Yung et al were able to conclude that turbulent burst activity is insignificant in the re-entrainment (i.e. suspension) of the deposited particles in the viscous sub-layer.

Of those researchers who have attempted to predict N_{JS} by using the turbulent mechanism, one of the most successful for design purposes is that of Baldi, Conti and Alaria, 1978. The reasoning by which they disregarded the mean flow mechanism seems to be based on heuristic or intuitive principles. They give no reference to any other work or experiments to give further credence to their basic assumption that turbulence is the suspension mechanism, only to their visual observation that the continuous interchange of particles from a state of rest to a state of suspension is an indication of turbulent disturbances at the base of the vessel.

Associated with these disturbances is the production of eddies that have a certain critical size. If these eddies are too small, then they will not have the energy required to lift the particles. Those eddies that are too large will have low frequencies and will have a smaller probability of "hitting" and suspending the particle.

These critical eddies are thought to be on a similar scale as, or proportional to, the particle diameter. It is also assumed that these eddies have sufficient energy to lift each particle approximately one particle diameter from the base of the tank.

One can equate the kinetic energy of the liquid to the potential energy gained by each suspended particle.

$$\rho_f v'^2 \propto d_p \Delta\rho g \qquad 2.3.2$$

If the scale of the critical eddies is much higher than that of the eddies which dissipate their energy by viscous action, then for isotropic (Levich, 1962) or anisotropic turbulence (Schwartzburg & Treybal, 1968)

$$v' \propto \left(\frac{\varepsilon_b d_p}{\rho_f}\right)^{0.33} \qquad 2.3.3$$

where ε_b is the local dissipated power per unit volume near the base of the vessel. ε_b changes with distance from the impeller but as a first approximation

$$\varepsilon_b \propto \bar{\varepsilon} \qquad 2.3.4$$

If the height of the liquid in the vessel is equal to the diameter, T, then at the minimum stirrer velocity, N_{JS}:

$$\bar{\varepsilon} = \frac{4\ Po\ \rho_f\ N_{JS}^3\ D^5}{\Pi\ T^3} \qquad 2.3.5$$

incorporating these equations together

$$Z_B = \left(\frac{\Delta\rho\ g}{\rho_f}\right)^{0.5} \frac{T\ d_p^{1/6}}{P_o^{1/3} D^{5/3} N_{JS}} \qquad 2.3.6$$

so that Z_B would be a constant for a given geometry. However, the assumption that

$$\varepsilon_b \propto \bar{\varepsilon}$$

can be modified.

In real situations, there will be a decay of turbulence with distance from the impeller, dependant on the viscosity of the fluid.

For a stirred tank, an empirical relationship can written in a general form

$$\varepsilon_b = k_1\ \bar{\varepsilon}^{\alpha} \mu^{\beta} u^{\gamma} l^{\delta} + \ldots\ldots \qquad 2.3.7$$

where u is the mean velocity of the fluid element leaving the impeller zone and following a pathlength, l, to the base of the tank. From dimensional analysis,

$$\frac{\varepsilon_b}{\varepsilon} = k_1\left(\frac{\mu\, u^2}{l^2\,\bar{\varepsilon}}\right)^{1-\alpha} + \ldots = f_1\left(\frac{\mu\, u^2}{l^2\,\bar{\varepsilon}}\right) \qquad 2.3.8$$

Assuming that l is a function of T and clearance, ΔZ, then

$$\frac{l}{D} = f\ (\ T/D,\ \Delta Z/D\ ) \qquad 2.3.9$$

Schwartzenburg & Treybal, 1968, suggest that the mean velocity, u, is related to the impeller speed by

$$u \ \alpha \ \ N\ D\ (D/T) \qquad 2.3.10$$

Substituting for u from equation 2.3.10 and ε_b from equation 2.3.5 then

$$\frac{\varepsilon_b}{\varepsilon} = f_1\left(\frac{\mu}{l^2}\ \frac{N^2D^4}{T^2}\ \frac{T^3}{\rho_f N^3 D^5}\right)$$

$$= f_1\left(\frac{\mu}{\rho_f}\ \frac{T}{D^3N}\ (D/l)^2\right)$$

$$= f_1\left(\frac{1}{Re^*}\ (D/l)^2\right) \qquad 2.3.11$$

therefore Z_B is no longer a constant but is a function of Re^*, T/D, $\Delta Z/D$ so that

$$\left(\frac{\Delta\rho\, g}{\rho_f}\right)^{0.5} \frac{T\, d_p^{1/6}}{N_{JS}\, P_o^{1/3} D^{5/3}} = f_4\ (Re^*;T/D;\Delta Z/D) \qquad 2.3.12$$

The concentration C_w is taken account of empirically and

not as a result of theoretical considerations.

Figure 2.3.5 shows Z_B as a function of Re^* for different D/T ratios, hence giving an empirically determined relationship

$$Z_B \propto \left(\frac{\mu T}{\rho_f D^3 N_{JS}}\right)^{-0.2} C_W^{0.15} \qquad 2.3.13$$

N_{JS} is then found to related to the other variables by

$$N_{JS} \propto \left(\frac{\Delta\rho\, g}{\rho_f}\right)^{0.42} \frac{T\,\mu^{0.17} C_W^{0.125} d_p^{0.14}}{P_O^{0.28}\, D^{1.89}} \qquad 2.3.14$$

Figure 2.3.6 shows the experimentally recorded (by Baldi et al, 1978) variation of N_{JS} with particle diameter. This shows that d_p has much greater influence at small particle diameters then after some critical size, the influence of particle diameter can be neglected. The final relationship, equation 2.3.14 shows that

$$N_{JS} \propto d_p^{0.14} \qquad 2.3.15$$

for all particle diameters which does not satisfactorily explain the shape of the N_{JS} vs. d_p curve.

A comparison of equation 2.3.14 with that of Zweitering shows many similarities. The only major difference is that Baldi et al remarked upon is the complex influence of the clearance on N_{JS}. Zweitering treats the clearance more simply in as much as it only changes the value of S, the geometric constant of proportionality, in equation 2.3.1. According to Baldi et al, the clearance will also effect the value of some of the exponents in equation 2.3.14.

In a related paper presented by Conti and Baldi, 1978, it was noted that their proposed model gave satisfactory results for particle sizes above 0.2mm. However, below this size, they suggested that some other

mechanism was responsible for suspension.

Molerus & Latzel, part I, 1987, examined the immediate vicinity of the walls of an agitated vessel in order to determine the liquid velocities in the boundary layer. The type of tank is shown in figure 2.3.7. Visual observations indicated that the last particles to suspend are located at the transition from the curved surface to the vertical, point F. From their velocity measurements, a characteristic reference velocity, u_c, was determined, as shown in figure 2.3.8. This velocity was shown to be proportional to the stirrer velocity by the authors, so that:

$$u_c = K_M D\, N \qquad 2.3.16$$

The universal non-dimensional representation of turbulent boundary layer flow is given by

$$\frac{u_y}{u_t} = \begin{cases} y^* & \text{viscous sublayer } y^* \leq 5 \\ 10\arctan(0.1y^*) + 1.2 & \text{buffer layer } 5 \leq y^* \leq 30 \\ 5.5 + 2.5\ln y^* & \text{turbulent layer } y^* \geq 30 \end{cases}$$

where u_t is the friction velocity defined by

$$u_t = \left(\tau_w/\rho_f\right)^{0.5} \qquad 2.3.18$$

and the non-dimensional wall distance given by

$$y^* = \frac{y\, u_t}{\nu} \qquad 2.3.19$$

As an approximation, the wall shear stress at point F can found by treating the shallow curve as a flat plane so that point F is T/2 from the leading edge of the plane, so that:

$$\tau_w = 1/2\ c_f \rho_f u_c^2 \qquad 2.3.20$$

where $$c_f = \frac{0.056}{Re_D^{0.2}} \qquad 2.3.21$$

It is this relationship between c_f and Re_D where the authors use the properties of bulk fluid turbulence. If the fluid were laminar, then:

$$c_f = \frac{0.65}{Re_D^{0.5}} \qquad 2.3.22$$

The Reynolds number is defined as

$$Re_D = \frac{T\ u_c}{2\ \nu} \qquad 2.3.23$$

and so by substitution using 2.3.20 and 2.3.21,

$$u_t = 0.182\ \frac{\nu^{0.1} u_c^{0.1}}{T^{0.1}} \qquad 2.3.24$$

Molerus & Latzel then went on to examine the forces acting on a particle in the boundary layer, figure 2.3.9. At the centre of gravity of the particle, the undisturbed liquid velocity, at $d_p/2$, is u. They then pointed out that two types of flow forces act on particles settled in the boundary layer:

(i) shear stress for a particle layer covering the wall surface.

(ii) the drag exerted on a single particle by a uniform flow field with velocity u.

Molerus & Latzel only considered (i) to be important. Results from classical pipe flow work on surface roughness and wall friction have shown that case (i) will only be appropriate as long as the particles lie in the viscous sublayer. This is the case when the Archemedes number of the solid liquid system is less than 40.

The point at which the particle is just about to lift into suspension is defined by the balance of forces

$$\frac{\Pi\, d_p^2\, \tau_w}{4} = \frac{(\rho_s - \rho_f)\Pi\, d_p^3 g}{6} \qquad 2.3.25$$

so that

$$\tau_w = 2/3\; d_p g(\rho_s - \rho_f) \qquad 2.3.26$$

Frictional forces between the particles and the wall are considered to be insignificant. Substitution of equation 2.3.18 into equation 2.3.26 gives a relationship between two dimensionless groups.

$$Re_t^2 \equiv \left[\frac{d_p u_t}{\nu}\right]^2 = 2/3\; \frac{d_p^3 g}{\nu^2}\left[\frac{\rho_s - \rho_f}{\rho_f}\right] = 2/3\; Ar \qquad 2.3.27$$

Incorporating all these equations together, N_{JS} can be predicted by

$$N_{JS} = \frac{45.3\; d_p^{0.55}\; T^{0.11}}{D\; \nu^{0.11}}\left[\frac{\rho_s - \rho_f}{\rho_f}\right]^{0.55} g^{0.55} \qquad 2.3.2$$

Comparision of the exponents with those of Zweitering shows good agreement for the influence of impeller diameter and particle-liquid densities, but the exponent for d_p is much higher than 0.2 found by Zweitering's data. Even more interesting is the influence of kinematic viscosity; whilst Zweitering and most of the other researchers in the field have found that increasing viscosity also increases the impeller speed required for complete suspension, if only by a slight amount, the implication of equation 2.3.27 is the reverse. It may well be that previous researchers did not conduct sufficient experiments for Ar < 40. In a liquid of such low viscosity as water, experiments with glass ballotini would have to be conducted with particle diameters less than 150μm. Molerus & Latzel's experiments show that their equation holds for Ar < 40 but increasingly deviate as Ar becomes larger and the particle protrudes out of the viscous sublayer. Surprisingly, in view of the importance attached to the viscous sublayer, the experiments were conducted with low viscosity liquids upto a maximum of 13 x 10^{-6} m^2/s.

The solids concentration was not taken into account

in the derivation, and Molerus suggests that the boundary layer flow is no longer applicable at high solids concentration.

As mentioned previously, Hirsekorn & Miller, 1953, were able to suspend solids in corn syrup solutions where the impeller Reynolds number was less than 12, i.e in the laminar regime. Therefore, those models based on turbulence can not be expected to yield satisfactory results when the conditions are less than fully turbulent. Many of the assumptions concerning the nature of the turbulence made in the theoretical derivations can no longer be valid. This has led some researchers, a small minority, to explore the possibility of developing a model based on mean liquid velocities at the base of the tank.

One model that utilizes the mean liquid flow mechanism was presented by Shamlou & Zolfagharian, 1987. It was suggested that for particles to lift off into suspension, from the base, these particles have to be dislodged from their stable resting position, figure 2.3.10. For this dislodgement to take place, the moment of the forces acting on the particle about point O must be zero.

$$\frac{\Pi\ \rho_f u_h^2 d_p^2}{2}(C_L + \xi C_D) = \frac{\Pi\ d_p^3}{6}(\rho_s - \rho_f)g \qquad 2.3.29$$

where u_h is the mean horizontal flow at the vessel base and C_D and C_L are the drag and lift co-efficients respectively. By definition:

$$C_L = \frac{F_L}{1/2\ \rho_f u_h^2\ A_p} \qquad C_D = \frac{F_D}{1/2\ \rho_f u_h^2\ A_p} \qquad 2.3.30$$

The mean liquid velocity was related to the impeller speed (Mersmann & Laufthutte, 1985), N by

$$u_h \propto ND(D/T) \qquad 2.3.31$$

It was further assumed that when the particle Reynolds number is in the turbulent régime, C_D would tend

towards some constant value, and that C_L would behave in a similar way and also tend towards some constant value. Substituting for u_h and after some rearrangement

$$N_{JS} = K_S \left(\frac{\rho_s - \rho_f}{\rho_f} \right)^{0.5} d_p^{0.5} \, (T/D) \; 1/D \qquad 2.3.32$$

This equation does not explicitly take into account the viscosity of the liquid, but the constant of proportionality in equation 2.3.32 may be a function of liquid properties as well as geometry as a consequence of 2.3.31 although the authors did not investigate this possibility. There is no provision at all for solids concentration. However, the main difference with Zweitering, 2.3.1, lies in the influence of particle diameter.

A major disadvantage of the dislodgement approach is that it can only give an indication of when the first particles, resting on top of others, will go into suspension, and there is no established relationship between the beginning of the suspension process and the final N_{JS} condition. Furthermore, for the equation to be generally applicable, then it must hold when conditions are not turbulent i.e. when C_D and C_L can not be considered to constant. The authors have not attempted to explore what might happen to equation 2.3.32 under such low particle Reynolds number conditions. Indeed, the problem of determining C_D and C_L has been one of the major problems faced by the mean flow approach.

Another mean flow mechanism has been to draw an analogy between the base of an agitated vessel and a solid-liquid fluidized bed. Subbarao and Taneja, 1979, have used this analogy to propose a simple model which balances the forces exerted on a particle from the liquid velocity and the particle settling velocity. The theoretical expression that was developed did not even agree with the experimental data of the authors themselves.

In part II of Molerus & Latzel's (1987) paper, it was proposed that the orderly nature of a fluidized bed could

be extended to solids suspension in agitated vessels. Molerus suggested a force balance between the total static pressure drop of the agitated vessel and the weight of the solid-liquid bed. This resulted in a complex set of correlations. However, after some manipulation, the just suspension speed was found to be related to the other system parameters by

$$N_{JS} \alpha \frac{(\rho_s - \rho_f) d_p^{0.4} C_w}{\nu^{0.24} D} \qquad 2.3.33$$

The values of the exponents clearly show that this approach is unsatisfactory. The most flawed aspect of the analogy lies in the assumption that the uniform suspension conditions found in fluidized beds are replicated in agitated vessels.

The model proposed by Nienow & Miles (1978) is based on the convective flow in the immediate vicinity of the vessel base. The particles are assumed to suspend when there is a critical average velocity, u_B. This velocity is independent of direction. Using experimental evidence from studies conducted by Nienow & Bartlett (1974) as well as Nayaranan et al, 1969, it was shown that under isotropic conditions, the mean linear velocity, u, is directly proportional to the RMS fluctuating velocity, u', so that:

$$\bar{u} = \frac{A(ND^2)}{(T^2H)^{1/3}} \qquad 2.3.34$$

where A is a dimensionless co-efficient which in turn is a function of impeller clearance. As the impeller clearance is increased, u falls. For geometrically similar systems, 2.3.34 reduces to 2.3.31.

Without any theoretical or empirical evidence, it was further assumed that u_B is proportional to $\bar{u}$ so that:

$$u_B \alpha ND(D/T) \qquad 2.3.35$$

However, there is no implied dependence of u_B with

distance from the base. The authors, Nienow & Miles, seem to have assumed that the liquid's velocity profile at the base of the tank is completely uniform.

Nayaranan et al (1969) derived an expression for N_{JS} based on force balance on a particle already in suspension. Assuming that there is no slip between the particle and fluid velocities, the downward force of gravity is balanced by the upward drag force due to the upward vertical component of the liquid velocity, u_v

$$\frac{\rho_f u_v^2}{2g} = 2/3\ d_p(\rho_s - \rho_f) + H_{SL}\rho_{SL} \qquad 2.3.36$$

where H_{SL} is the net hydrostatic head of the suspension

$$\rho_{SL} = \frac{\left(\frac{C_w}{\rho_s(\rho_s - \rho_f)}\right)}{\left(\frac{1}{\rho_f} + \frac{C_w}{\rho_s}\right)} \qquad 2.3.37$$

The fluid velocity, u , was related to the impeller speed and diameter by the work of Holmes et al (1964). The final expression for N_{JS} can be represented as:

$$N_{JS} = \frac{\left[0.9\{2g\Delta\rho(\frac{2d_p}{3\rho_f} + \frac{C_w H_{SL}}{\rho_s} + C_w\rho_f)\}^{0.5}(T/D)^2\right]}{\left(2T - D\right)} \qquad 2.3.38$$

The nature of equation 2.3.38 can be more clearly seen at low solids concentrations when N_{JS} can be approximated by:

$$N_{JS} \simeq \frac{0.9\left(\frac{4g\ \Delta\rho\ d_p}{3\rho_f}\right)^{0.5}(T/D)^2}{\left(2T - D\right)} \qquad 2.3.39$$

Although the exponents for $\Delta\rho$ and g are in good agreement with Zweitering, the dependence on d_p is too high as is the influence of C_w on N_{JS} as predicted by the full equation, 2.3.38. Nayararan et al's approach considers a force balance on a particle already in suspension but does

not explain how the particle was initially lifted from the vessel base.

As mentioned previously, the two different approaches to developing models based on either turbulence or mean bulk flow seem to be contradictory. However, some similarities may still exist because of the relationship between the fluctuating velocity and the mean velocity in an agitated vessel. Work by Schwartzenburg & Tribal, 1968, has shown that the root mean squared value of the fluctuating velocity is proportional to the impeller tip speed. If the mean velocity at the base of the tank is also proportional to the impeller tip
speed, then the fluctuating velocity will be proportional to the mean velocity. This result, in combination with other considerations, may have two possible implications:
(i) that the mechanisms merge together so that both turbulence and mean flow contribute to the suspension process, with each contribution determined by the agitation system.
(ii) that the mean flow criterion, alone, is responsible for suspending solids at all Reynolds number conditions, but that because of the direct proportionality between the fluctuating velocity and the mean, a model based on mean flow will come, with increasing Reynolds number, to resemble the more successful theoretical and empirical expressions derived under turbulent conditions.

This second implication has been chosen by the present study, and has led to the formation of a novel mean flow model whose derivation is shown in chapter 3.

Table 2.3.1 Exponents of Parameters Pertinent to the Prediction of N_{JS}

Author(s)	d_p	$\Delta\rho/\rho_f$	D	υ	C_w
Baldi et al 1978 (ΔZ)	0.17	0.42	-1.67 (R)	0.1	0.13
Chapman et al, 1983	0.15	0.40	-1.5;-2.45 (A) (R)	-	0.12
Ditl & Reiger, 1985	0.10*	0.50	-0.5 (A)	0.1	-
Einenkel 1980	0.17*	0.50*	-1.0*(A)	0.1*	0.2*
Herringe 1979	0.30	0.44	-0.71(A)	-	0.18
Koutsakos 1989	0.24	0.45	-1.06(A)	-	0.17
Molerus & Latzel, 1987 Ar>40	0.40	1.0	-1.0 (A)	-0.24	0.30
Molerus & Latzel, 1987 Ar<40	0.55	0.55	-1.0 (A)	-0.11	-
Narayanan et al, 1969	<0.5	0.50	-2.0 (R)	-	0.22
Nienow 1968	0.21	0.43	-2.21 (R)	-	0.12
Shamlou & Zolfagharian 1987	0.50	0.50	-1.0 (A)	-	-
Wichterle** 1988	-0.33 ->0.67	0.33 ->0.67	-1.33	-0.33 ->0.3	-
Zweitering 1958	0.20	0.45	-1.67;-2.3 (A) (R)	0.1	0.13

ΔZ - depending on impeller clearance;* - depending on d_p

**-depending on Archemedes number

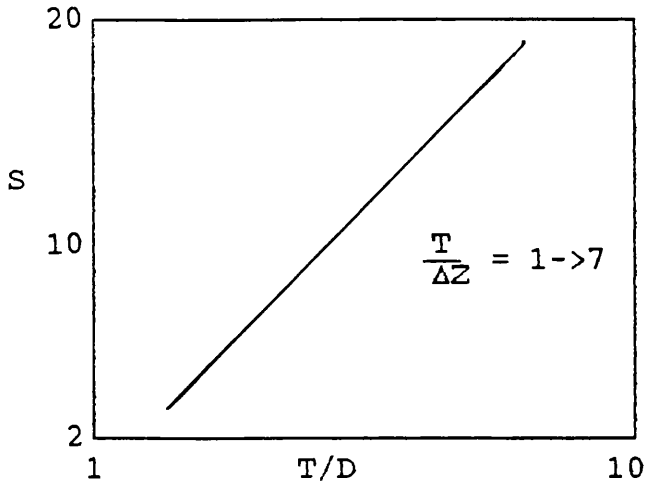

Figure 2.3.1 Correlation for complete suspension with a six (flat) bladed turbine (Zweitering, 1958)

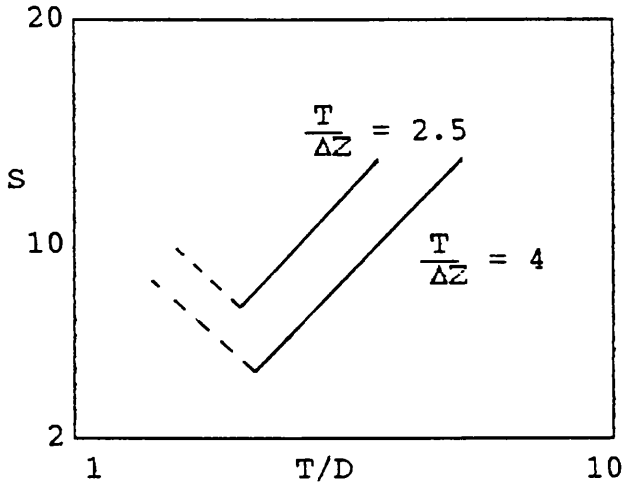

Figure 2.3.2 Correlation for complete suspension with a propeller (Zweitering, 1958)

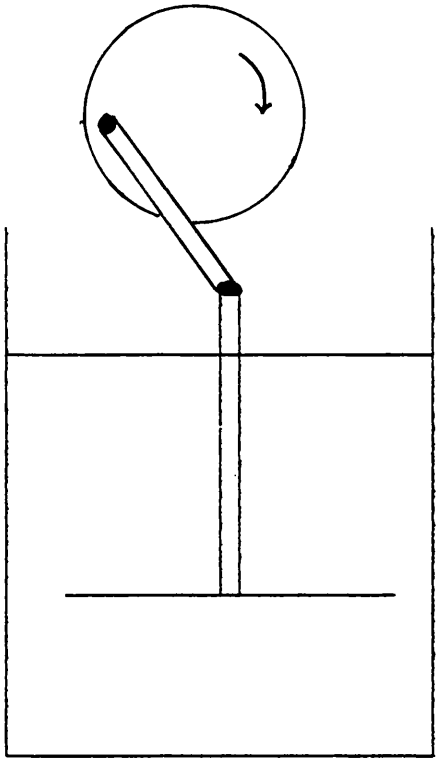

Figure 2.3.3 Reciprocating disc agitator (Tojo et al, 1981)

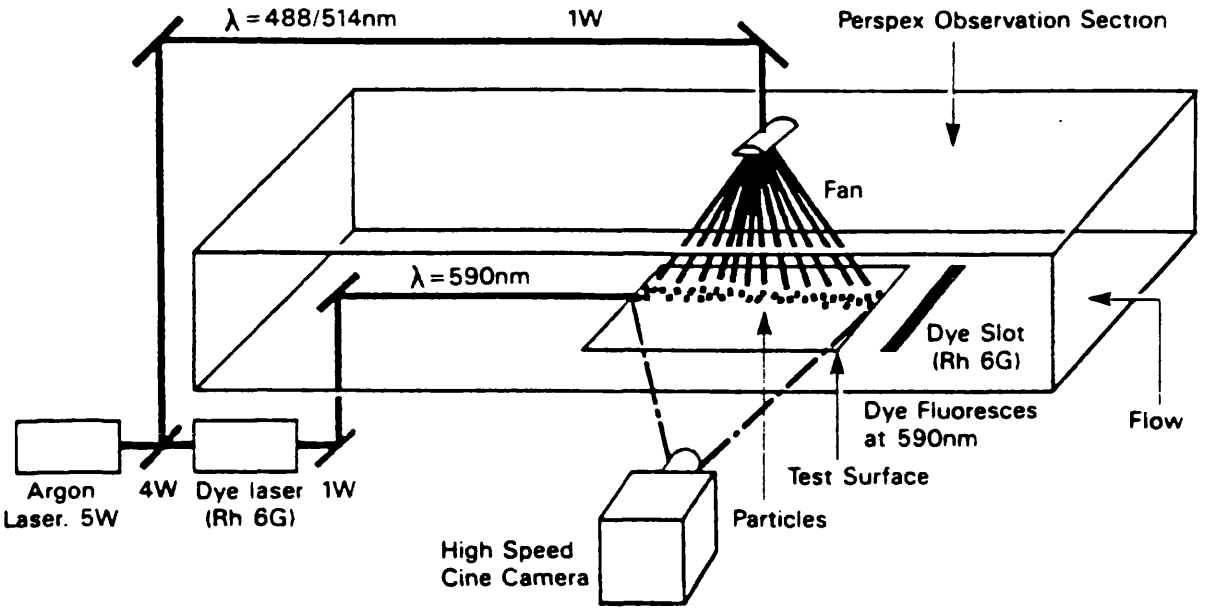

Figure 2.3.4 Apparatus of Yung et al, 1989

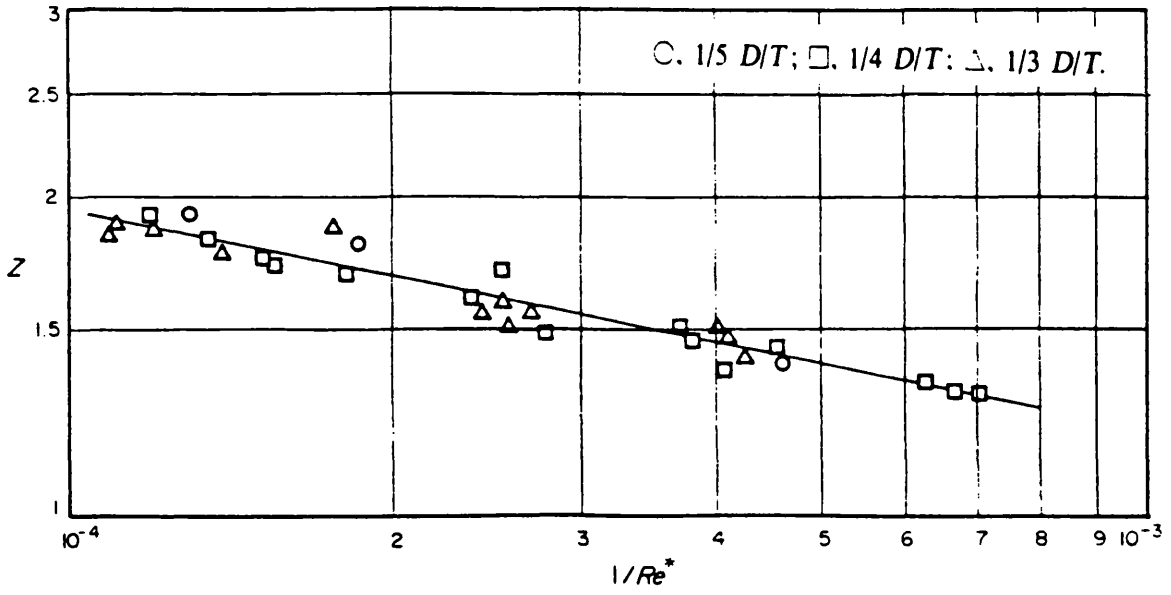

Figure 2.3.5 Z_B as a function of Re^* at $\Delta Z/T=1$, C_w=0.5%wt (Baldi et al, 1978)

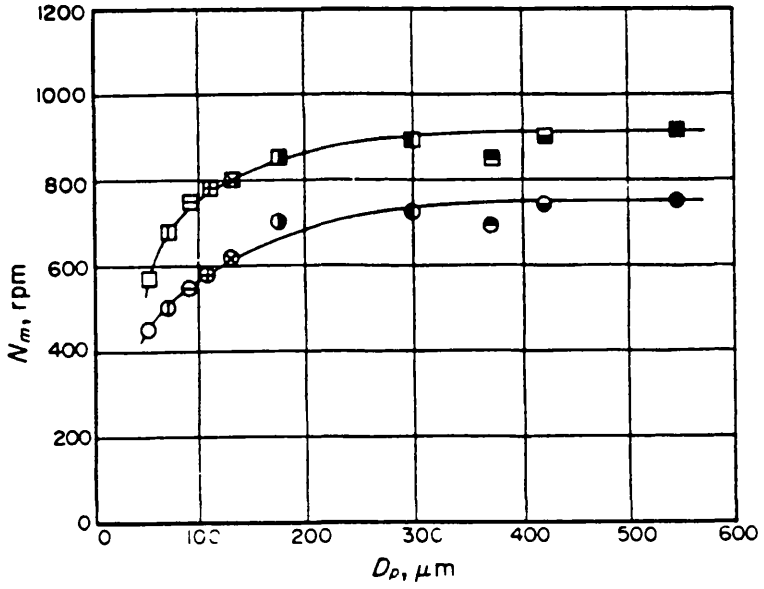

Figure 2.3.6 Effect of d_p on N_{JS} for mono- and bi-modal sizes (Baldi et al, 1978)

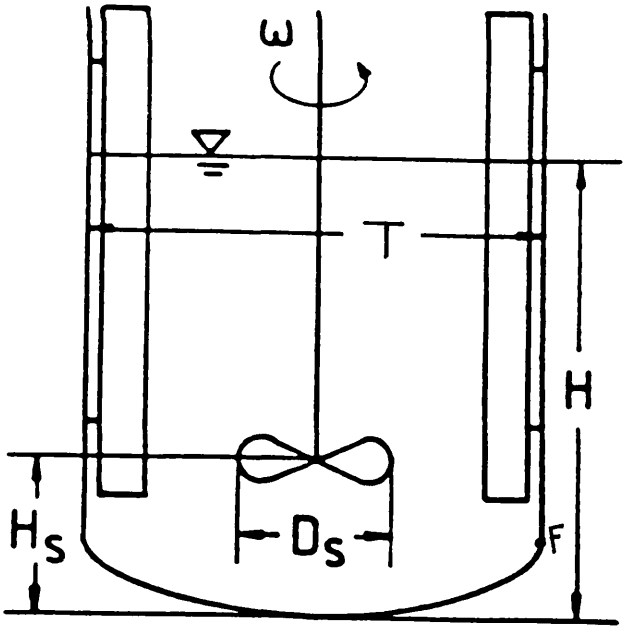

Figure 2.3.7 Geometrical configuration of the agitated vessel (Molerus & Latzel, 1987)

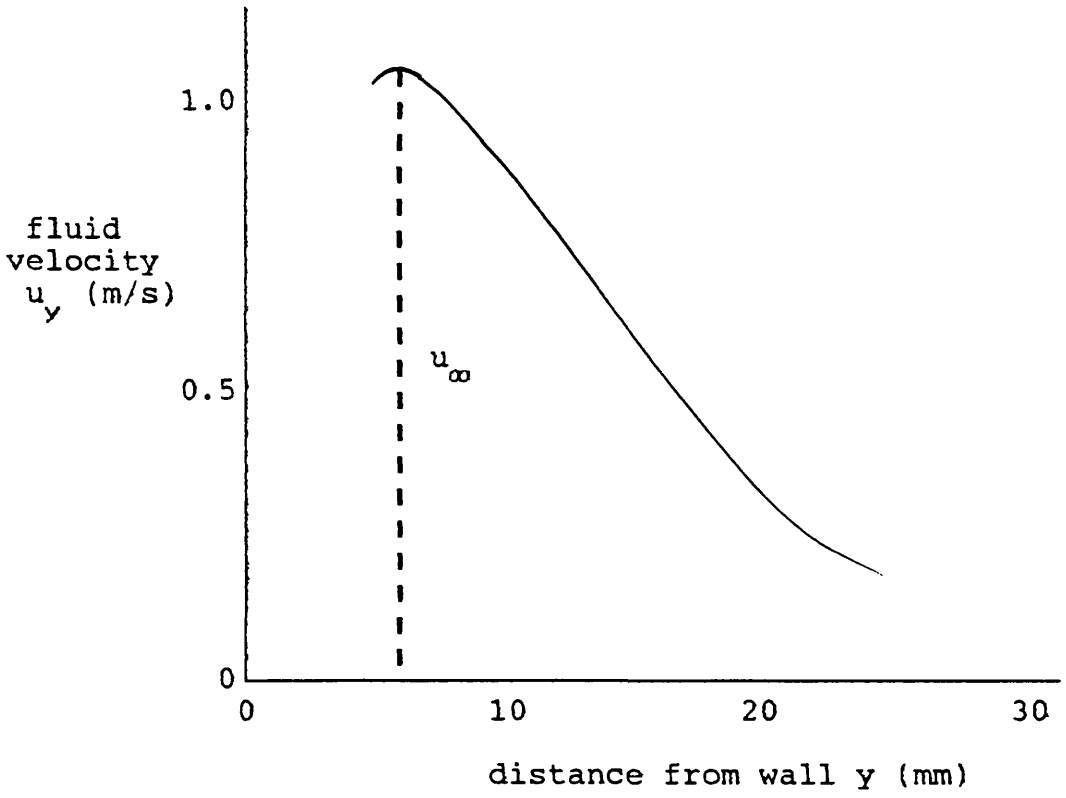

Figure 2.3.8 Time-averaged fluid velocity vs wall distance (Molerus & Latzel, 1987)

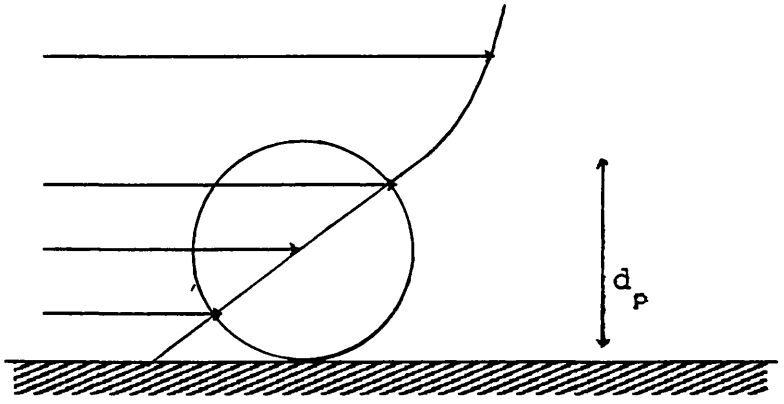

Figure 2.3.9 A single particle settled in the boundary layer (Molerus & Latzel, 1987)

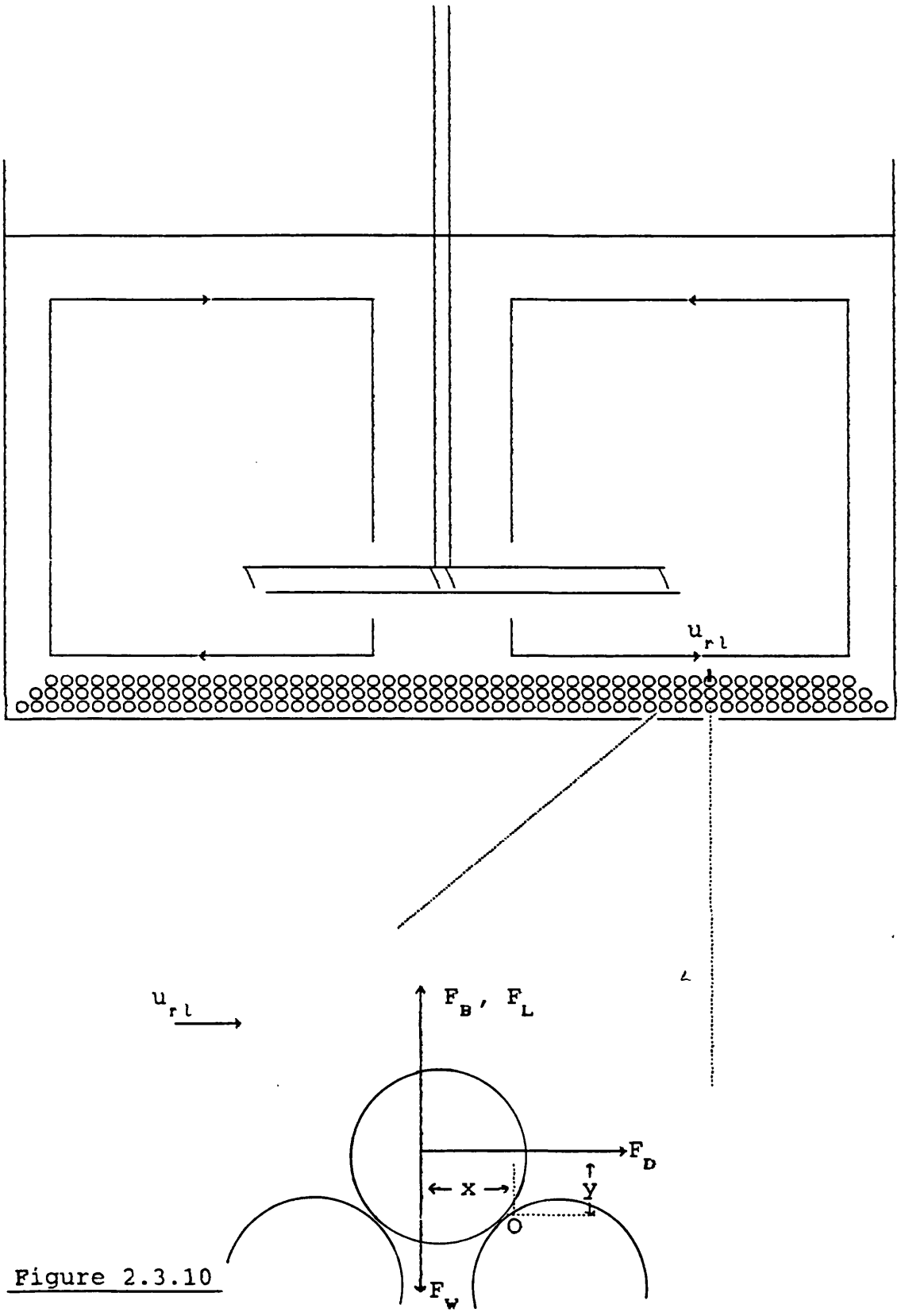

Figure 2.3.10

Forces acting on a particle at rest just before suspension (Shamlou & Zolfagharian, 1987)

2.4 Distribution of Suspended Solids

As well as suspending solids, as efficiently as possible, from the base of an agitated vessel, some researchers have been interested in designing systems that promote a uniform solids distribution throughout the liquid. Homogeneity is an ideal in agitated vessels that is rarely achievable. Instead, for some industrial applications, agitated vessels are required to attain a certain degree of suspension homogeneity.

An initial assessment of the solids distribution can be found from visual or photographic evidence (Kolar, 1961, Nienow & Miles, 1978). However, such methods cannot give a quantitative measure of the local solids concentrations or the overall degree of homogeneity, and give misleading results in systems where the particles have a high concentration or have small diameters.

Electrical conductivity methods have been used successfully to measure the local solids concentration. These methods rely on changes to the local electrical conductivity of the liquid caused by the presence of suspended particles which generally lower the local conductivity because of their insulating properties. However, no attempt was made by those using conductivity methods to quantify the degree of suspension homogeneity (Musil & Vlk, 1978; Musil & Vlk, 1984; Machon, Fort, & Skrivanek, 1982).

Optical methods have also been used to determine the axial solid concentration profile (Calderbank & MooYoung, 1961; Musil, 1976). Shamlou & Koutsakos, 1986, used a laser and photocell arrangement to measure the local solids concentration. The main advantage of these optical methods is their non-intrusive nature. However, they are not so reliable when there is significant radial concentration profile. In the case of the laser/photocell arrangement, it would be ideal if a pair of identical lasers and photocells aligned such that the beams of light intersected at right angles to one another within the suspension. The local solids concentration could then be determined at this

intersection rather than as an averaged quantity along the path length of the light through the suspension. More recently, attempts have been made to measure solids concentration using ultrasonic spectrometry (Riebel & Loffler, 1989). This has had a high degree of success for solids concentrations upto about 10%wt.

The most widely used method to measure local solids concentrations is by sample removal. The problem with such intrusive methods is ensuring that the sampling is isokinetic, so that the withdrawn sample is truly representative. To be isokinetic, the device has to be aligned so that the withdrawal direction is the same as that of the suspended solids in the vicinity of the sampler. In systems where there is a high degree of turbulence, the local flow is not sufficiently well defined to ensure that isokinetic sampling is achieved. The intrusive nature of the sampling device can compound these problems by interfering with the local hydrodynamics of the liquid flow.

Weissmann & Efferding, 1960, proposed that the height of the solid-liquid interface could act as a measure of the suspension quality. But this technique does not try to take into account the distribution of solid particles within the bulk of the vessel.

A more useful way of determining the degree of suspension uniformity is proposed by Bohnet & Niesmak, 1980. The local solids concentration measurements are used to calculate a relative distribution factor.

$$\Phi = \left(\frac{1}{n} \sum_{h=1}^{h=n} \left\{ \frac{C_{vh} - C_v}{C_v} \right\}^2 \right)^{0.5} \left(\frac{C_v}{C_{vb} - C_v} \right)^{0.5} \qquad 2.4.1$$

where n is the number of samples, C_{vh} is the volume ratio at sample height, h, C_v is the solid hold-up concentration, and C_{vb} is the solid concentration deposited at the base of the vessel.

Einenkel, 1980, used the sample variance, σ^2, of the local concentrations to define the degree of homogeneity.

$$\sigma^2 = \frac{1}{n^2}\sum_{h=1}^{h=n} \frac{(C_{wh} - C_w)^2}{C_w^2} \qquad 2.4.2$$

When the suspension is homogeneous, $C_{wh} - C_w$ will be zero for all h, and so σ^2 will also be zero. σ^2 will be 1 when there is no suspension at all.

During Einenkel's experiments, complete homogeneity was never achieved but a "pseudo-homogeneous" condition was defined when $\sigma^2 = 0.5$. This condition was suggested to be the equivalent to the "suspension height" criterion discussed earlier.

In their study of solids suspension in a continuously stirred tank, Aeschbach & Bourne, 1972, proposed that homogeneity had been attained when the particle size distribution and concentration in the vessel and the exit or sample stream were the same. This is an important condition for the design of continuous flow crystallizers. Aeschbach & Bourne measured deviations of the particle size distribution from their expected values using a Segregation Co-efficient, S.C.

$$S.C. = \frac{1}{n}\sum_{i=1}^{i=n}\left(\frac{M_i - M_{io}}{M_{io}}\right)^2 \qquad 2.4.3$$

where M_i is the mass of particles in size fraction i in the tank at time t. M_{io} is the hold-up value of M_i.

Experimental investigations into solids distribution within agitated vessels date back to Rouse, 1938. Using a vibratory agitator, Rouse was able to suspend sand particles in water. The design of the agitator ensured the maximum degree of turbulence whilst minimizing the bulk flow of liquid within the vessel, with low amplitude/high frequency oscillations (figure 2.4.1). During agitation, Rouse was able to use a device that withdrew samples of sand in order to determine the local solids concentrations. The experimental data gathered was fitted, with good agreement, to a one-dimensional turbulent diffusion model suggested by von Karman, 1935.

Einenkel, 1980, was one of the first to measure solids concentrations throughout the agitated vessel at

impeller speeds well beyond the just suspension speed, N_{JS}. The local solids concentration was measured by removing samples at different heights. The results are shown in figure 2.4.2 and indicate that solids concentration does not continuously increase with depth from the liquid surface, but reaches a maximum near the impeller zone.

Einenkel used equation 2.4.2 as a means of quantifying the homogeneity of the suspension. As the impeller speed is increased beyond N_{JS}, there is little increase in homogeneity and the graph of $1-\sigma^2$ vs. N tends towards a plateau beyond which increasing N will not change σ^2.

For a given degree of homogeneity, Einenkel proposed that the impeller speed N could be related to other system variables by the empirical relationship:

$$\frac{Fr^* W_s}{C_w u_s} \propto Re^{0.27} \qquad 2.4.4$$

where Fr^* is a modified Froude number

$$Fr^* = \frac{N^2 d_p \rho_f}{(\rho_s - \rho_f) g} \qquad 2.4.5$$

W_s is the impeller tip speed and u_s is the settling velocity of the particles in suspension. The left hand side of the equation represents the ratio of power input to settling power. Einenkel found that for suspending glass particles in water, a suspension of $\sigma^2 = 0.95$ required a tenfold increase in power input to make $\sigma^2 = 0.25$.

Barresi & Baldi, 1987, measured the local concentrations of suspended particles in water using various stirrer types, particles sizes and concentrations. The vessel used had a torispherical base and was fitted with four symmetrically arranged baffles. The local concentrations were measured using radially aligned withdrawal tubes. The results show broad agreement with those of Einenkel, 1980,except that in the region of the impeller, Barresi & Baldi did not show the steep oscillations shown in figure 2.4.2 and found that there was

little variation in the radial concentration profile.

Using the square root of the variance

$$\sigma = \frac{1}{n} \sum_{h=1}^{h=n} \frac{\sqrt{(C_{wh} - C_w)^2}}{C_w} \qquad 2.4.6$$

Barresi and Baldi were able to quantify the quality of suspension. They then developed a theoretical "iconic" model with which they attempted to correlate the quality of suspension. This iconic model considers a stationary and regular velocity field determined by time-averaged values of the local speed, with a superimposed turbulent velocity field.

Assuming that dispersion of particles is caused by both turbulent diffusion and anisotropic turbulent motion, Barresi & Baldi suggested that σ can be correlated to a modified Peclet number, K

$$K = \frac{P_o^{1/3} ND}{u_t} \qquad 2.4.7$$

where P_o is the Power number, ND is the impeller tip speed, and u_t is the terminal settling velocity of the suspended particles.

For a system that consists of a large number of particles, the time-averaged continuity equation becomes

$$\frac{d}{dx_i}\left(\hat{U}_{pi} \hat{C}_v \right) + \frac{d}{dx_i}\left(\hat{u}_{pi} \hat{c}_v \right) = 0 \qquad 2.4.8$$

where $\hat{U}_{pi}$ is the time averaged Eulerian velocity

C_v is the time-averaged local volumetric concentration

$\hat{u}_{pi}$ is the time averaged turbulent component of the Eulerian velocity

$\hat{c}_{pi}$ is the time averaged turbulent volumetric fluctuation.

Neglecting radial concentration profiles and the inertia forces, the local mean-time solid velocity in the

axial direction is the vector sum of the axial component of the liquid velocity and the terminal particle velocity.

$$\hat{U}_{pz} = \hat{U}_{fz} - u_t \qquad 2.4.9$$

However, u_t for turbulent liquids is less than for still liquids, but it cannot be predicted by how much, the authors, Barresi and Baldi, have taken the still liquid values for u_t.

Through any cross-section, the net flow of liquid is zero, integrating 2.4.9. over a volume element

$$\bar{U}_{pz} = - u_t \qquad 2.4.10$$

where $\bar{U}_{pz}$ is the time and section mean value. Integrating 2.4.8. for the monodimensional case, from z=0 to z

$$\bar{U}_{pz}\bar{C}_v + \bar{u}_{pz}\bar{c}_v = 0 \qquad 2.4.11$$

substituting for $\bar{U}_{pz}$ from 2.4.10

$$-u_t\bar{C}_v + \bar{u}_{pz}\bar{c}_v = 0 \qquad 2.4.12$$

For monodimensional turbulent diffusion involving isotropic small scale perturbations

$$\bar{u}_{pz}\bar{c}_v = - D_p \frac{d\bar{c}}{dz} \qquad 2.4.13$$

where D_p is the turbulent diffusion co-efficient. Taking into account the convective contribution of large scale anisotropic turbulent motions so that 2.4.13. may be modified so that

$$\bar{u}_{pz}\bar{c}_v = - D_p \frac{d\bar{c}}{dz} + \bar{v}\,\bar{c}_v \qquad 2.4.14$$

However, as a first approximation the authors neglected this convective contribution so that substituting for $\bar{u}_{pz}\bar{c}_v$ from equation 2.4.12. into 2.4.13.

$$u_t \bar{c}_v = - D_p \frac{d\bar{c}}{dz} \qquad 2.4.15$$

therefore the local concentration depends on D_p/u_t which can be incorperated into the dimensionless Péclet Number

$$Pe^* = \frac{u_t L^*}{D_p} \qquad 2.4.16$$

where L^* is a characteristic linear dimension of the system.

The dissipated power and turbulence intensity will be a function of position within the tank so that D_p and Pe^* will not be constant for all r and z. The axial concentration profiles found experimentally by the authors (see figure 2.4.3.), confirm that a simple exponential function arising from the solution of 2.4.15., with D_p/u_t constant, cannot accurately describe the real situation. Sysova et al, 1984, attempted to describe these experimentally derived profiles by assuming D_p to be a function of the axial co-ordinate, z.

Barresi and Baldi then applied the Taylor theory for fluid diffusion to find the diffusion co-efficient of fluid turbulence (Hinze, 1975) valid for homogeneous turbulence and long diffusion time:

$$D_f = v'^2_{fz} \int_0^\infty R_L(\tau) d\tau = v'_{fz} \Lambda_L \qquad 2.4.17$$

where for isotropic turbulence

$$v'_{fz} = u'_{fz} \; ; \; \varepsilon = \frac{A_B u'^3_{fz}}{l_e} \qquad 2.4.18$$

and Λ_L is the Lagrangian integral length scale

where ε is the local dissipated power (per unit mass), and A_B is a co-efficient close to unity. l_e is the size of the energy containing eddies. If the local power is proportional to the total power dissipated by the impeller then:

$$\varepsilon \propto Po \; N^3 \; D^2 \qquad 2.4.19$$

Schwartzenberg and Treybal, 1968, noted that the fluctuating velocity is proportional to the impeller tip velocity, ND, so when N changes all fluctuating velocities and local dissipated powers, throughout the liquid, will increase by the same proportion.

Hinze, 1975, found that D_p was equal to D_f so:

$$Pe^* \propto \frac{u_t L^*}{D_f}$$

but $$D_f = u'_{fz} \Lambda_L$$

and $$u'_{fz} \propto \left(\frac{l_e \varepsilon}{A_B} \right)^{1/3} = \left(\frac{l_e P_o N^3 D^2}{A_B} \right)^{1/3}$$

so that $$Pe^* \propto \frac{u_t L^*}{P_o^{1/3} N (D^2 l_e)^{1/3} \Lambda_L} \qquad 2.4.20$$

As stated before, 2.4.20. would only be strictly valid for homogeneous isotropic turbulence where Pe^* would be constant for all positions within the tank. In reality, Barresi and Baldi acknowledge that Pe^* will vary but some averaged value for Pe^* may be useful for describing the average quality of suspension within the vessel. Taking l_e (Gunkel and Weber, 1975) and Λ_L (Lewins and Glastenbury, 1972) to be proportional to D, with D also as the characteristic length, L^*, then 2.4.20. reduces to:

$$Pe^* \propto \frac{u_t}{P_o^{1/3} ND} \qquad 2.4.21$$

The results of this analysis is shown in figures 2.4.4 to 2.4.6 . Each figure represents a type of impeller. Barresi and Baldi also used the experimental data of Bohnet and Niesmak, 1980, from a geometrically different tank, to find that their data was also well correlated to a σ vs K relationship.

However, the researchers concluded that the axial profiles cannot be described by a simple dispersion model with a constant turbulent diffusion co-efficient. They also speculated that the dispersion of the solids is strongly affected by large scale eddies or macroscopic turbulence.

Similar experimental results were obtained by Shamlou & Koutsakos, 1988; and Koutsakos, phD 1989. Instead of using an intrusive sampling technique, a He-Ne laser emitted light through the suspension to a photocell placed directly opposite, on the other side of the suspension.

Again a modified Péclet number is introduced as an important parameter.

$$Pe^{*} = \frac{u_s d_p}{\zeta_p} \qquad 2.4.21$$

where u_s is the relative settling velocity of the particles in suspension and ζ_p is the particle diffusion co-efficient.

The Péclet number is then related to the impeller tip speed and the terminal velocity of the particle in a still fluid.

$$\frac{U_s d_p}{\zeta_p} \propto \frac{u_t}{ND} \qquad 2.4.22$$

Figure 2.4.7 shows a semilogarithmic plot of local concentrations against height in the vessel at various impeller speeds. A perfectly homogeneous suspension would be represented by a vertical line. The slopes of the lines are a measure of the quality of suspension.

Aeschbach & Bourne, 1972, used the segregation co-efficient defined in equation 2.4.3 to investigate the optimization of tank design. The aim of this optimization was to improve the degree of suspension in a continuously stirred tank.The authors compared the S.C. values found for flat-bottomed vessels; flat-bottomed with draught tube; and profiled vessels (shown in figure 2.4.8).

These researchers were able to conclude that these profiled vessels produced the most homogeneous suspensions under the same experimental conditions. This type of vessel

was found by other investigators to be the most efficient for both solids uniformity (Bourne & Sharma, 1974; Chudacek, 1985), and for just suspension speeds (Cliff, Edwards, and Ohiaeri, 1980; Ohiaeri, 1981; Chudacek, 1985). However, the mechanical difficulties and cost in manufacturing such profiled vessels have hindered its application to industry. For the present study, this type of vessel was used to measure the solids distribution in agitated liquids.

All the experimental work into solids distribution has been conducted with low viscosity Newtonian liquids, typically water. Perhaps as a result of operating in high Reynolds numbers, the associated theoretical modeling has stressed the importance of turbulence and associated phenomena to explain the dispersion and resulting distribution of solids within the liquid phase. In the present study, the range of experimental data will be extended into the high viscosity/low Reynolds number régime using high viscosity Newtonian and non-Newtonian liquids.

Table 2.4.1 Solids Distribution Studies

Author(s)	Measurement Technique	ρ_s (kg/m^3)	liquid used	C_w (%WT)
Barresi & Baldi, 1987	side sampling	2600	water	0.5->5.1
Calderbank & MooYoung 1961	optical	2600	water	1 -> 5
Machon et al 1982	conductive probe	2548 -> 2650	water	4 -> 12
Musil & Vlk, 1978	conductive probe	<1900	water	11 -> 23
Nienow & Miles, 1978	photography	2150	water	50 NaCl crystals
Shamlou & Koutsakos 1989	optical	1513 -> 2800	water	< 10.0
This work 1990	optical	2900	glycerol & water; CMC	1.0

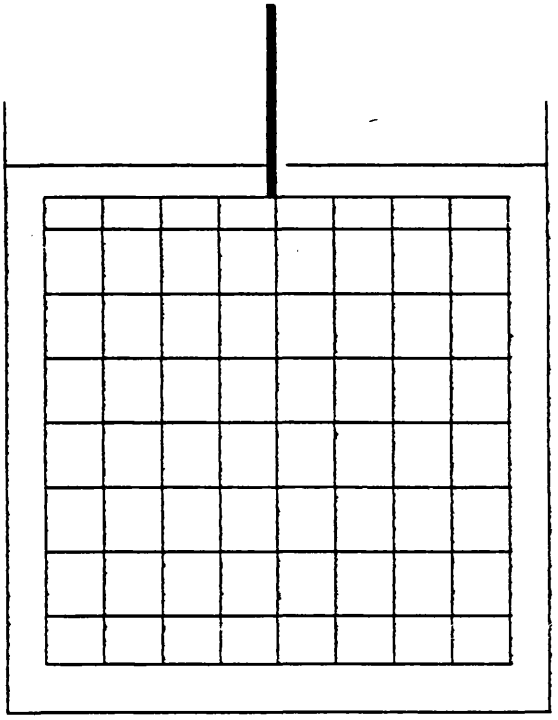

Figure 2.4.1

Vibratory agiatator made from wire mesh (Rouse, 1938)

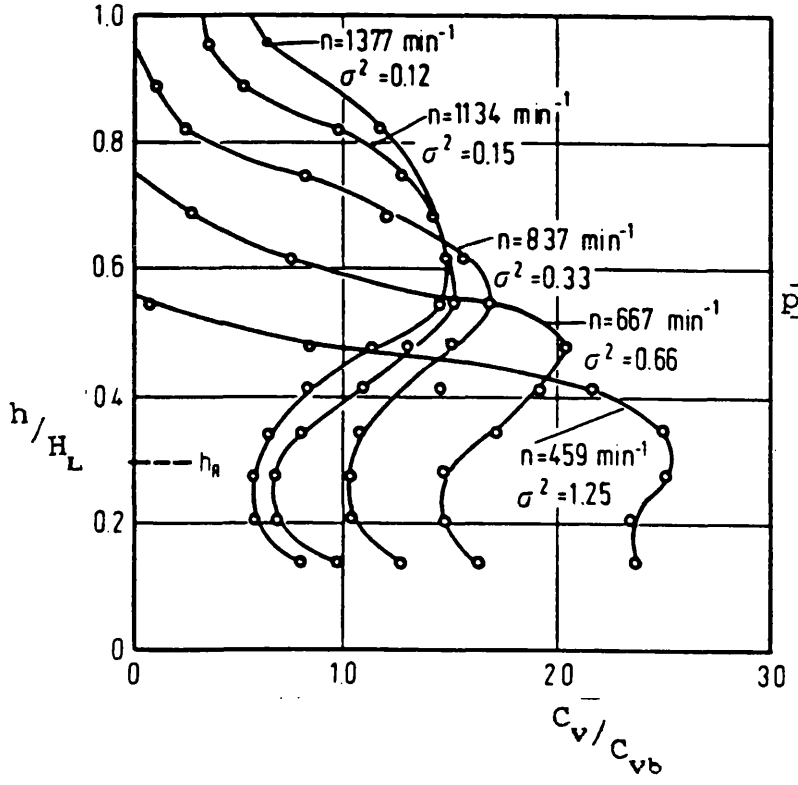

Figure 2.4.2

Effect of stirrer speed on concentration profile (Einenkel, 1980)

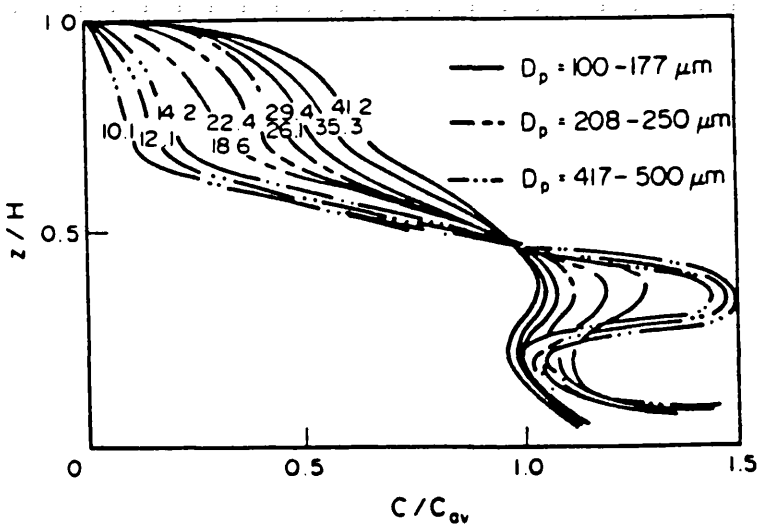

Figure 2.4.3 Axial concentration profiles with K as a parameter (Barresi & Baldi, 1987)

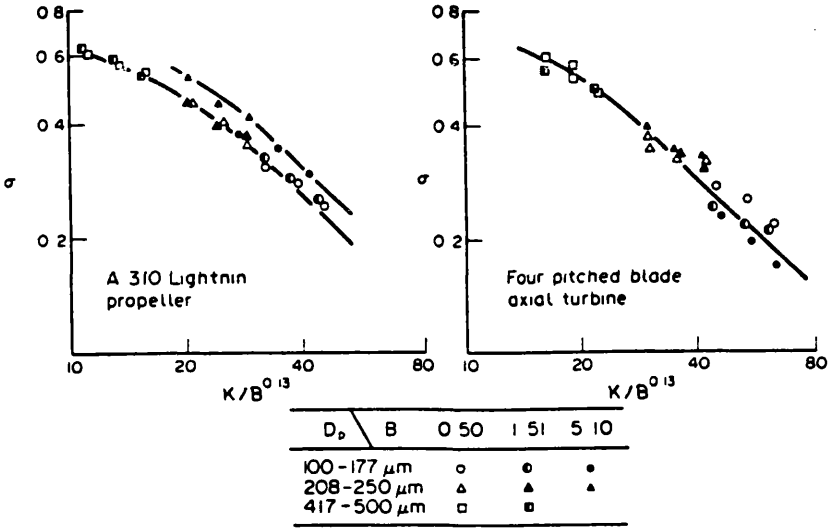

D_p \ B	0.50	1.51	5.10
100 - 177 μm	○	◐	●
208 - 250 μm	△	▲	▲
417 - 500 μm	□	◘	

Figure 2.4.4 A310 Lightning propeller

Figure 2.4.5 4-bladed pitched turbine

Figures 2.4.4 to 2.4.6

Distribution quality vs K (Barresi & Baldi, 1987)

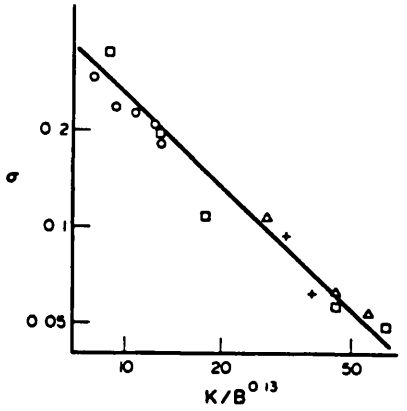

Key	Solid	D_p (mm)	ρ_p (kg/m³)	$u_t \times 10^2$ (m/s)	B (kg/kg %)
□	Styropor	1.125	1050	1.64	0.21
△	Glass	0.225	2480	2.24	0.744
+	Bronze	0.125	8850	3.49	1.77
○	Glass	0.715	2480	10.84	0.62

Figure 2.4.6 Data of Bohnet & Neismak, 1980

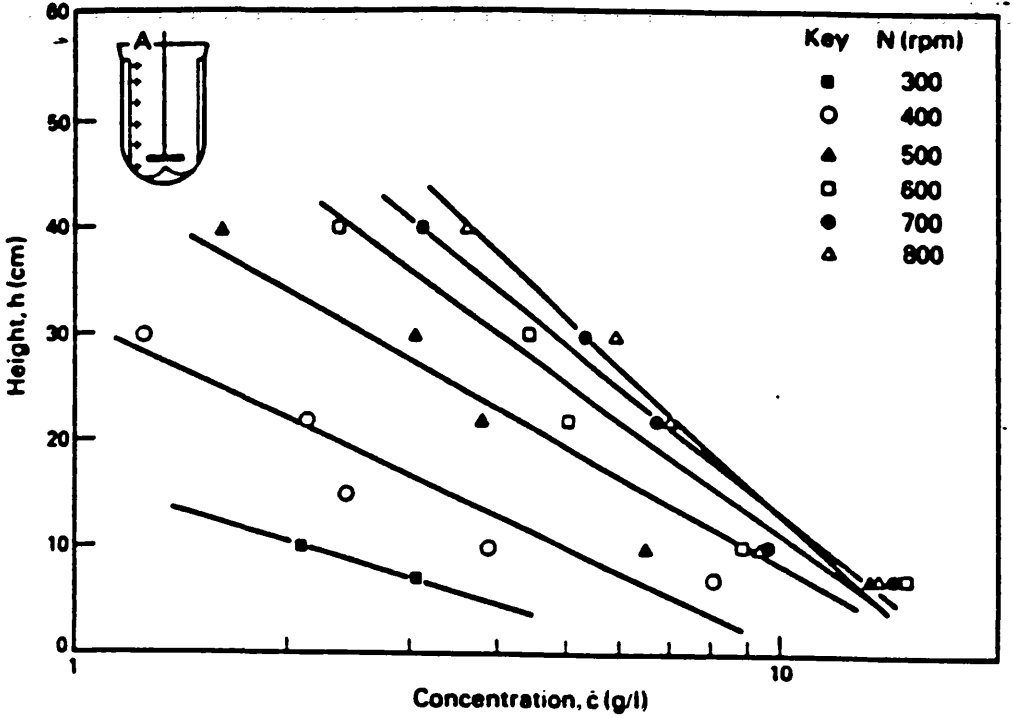

Figure 2.4.7 Semilog axial concentration profiles (Shamlou & Koutsakos, 1989)

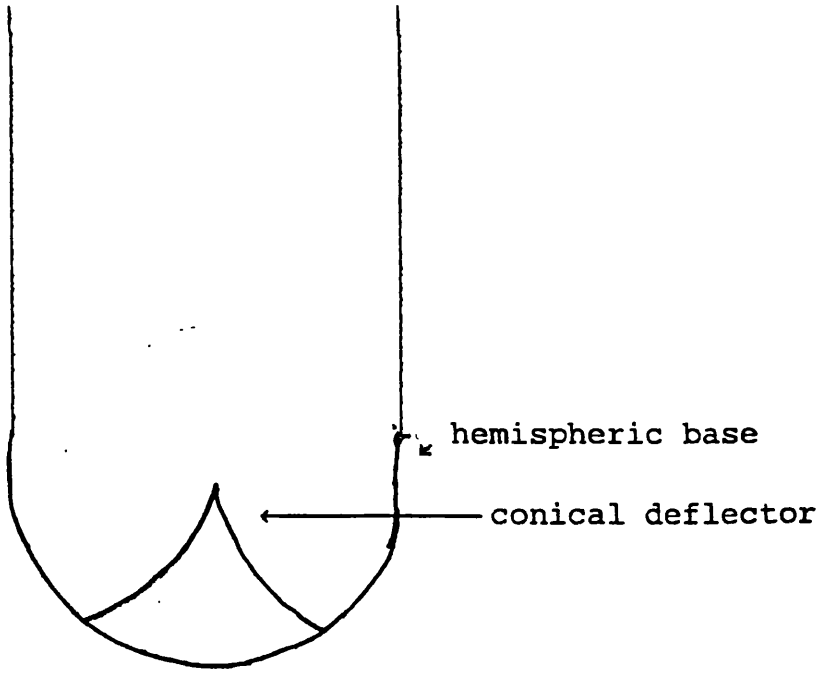

Figure 2.4.8 Diagram of Fully Profiled Vessel

CHAPTER THREE
MATHEMATICAL MODELING

The following model tries to relate the minimum impeller speed, N_{JS}, required to lift a solitary particle of diameter, d_p, and density, ρ_s, into suspension to other variables that previous empirical studies have shown to be pertinent. For the purposes of simplification the effect of particle concentration, although measurable, has been ignored for the purposes of this model. The effect of concentration can be taken into account and is discussed later in Appendix 5 and in chapter five.

In chapter four, the point at which the just suspension condition has been defined is that minimum impeller speed that lifts a particle from the base of the tank without requiring any neighbouring particles to assist in the process. In the viscous liquids considered in this study, the particles always migrated to the centre of the the base of the tank prior to suspension into the bulk of the liquid of absolute viscosity, μ, and density, ρ_f. For more detailed observations of the suspension process see Appendix 1.

This model is based on the hydrodynamic conditions caused by the mean (or time-averaged) liquid velocities found at the base of an agitated vessel. Unlike many previous models, it makes no use of the any turbulent properties of the liquid that may have generated by the impeller's rotation. With the viscous liquids used in this study, any model relying on turbulence to lift the particles into suspension cannot provide a satisfactory means of relating N_{JS} to other parameters.

Consider a spherical particle at the point of suspension at the centre of the flat base of an agitated vessel, directly below the impeller.(figures 3.1.a and b)

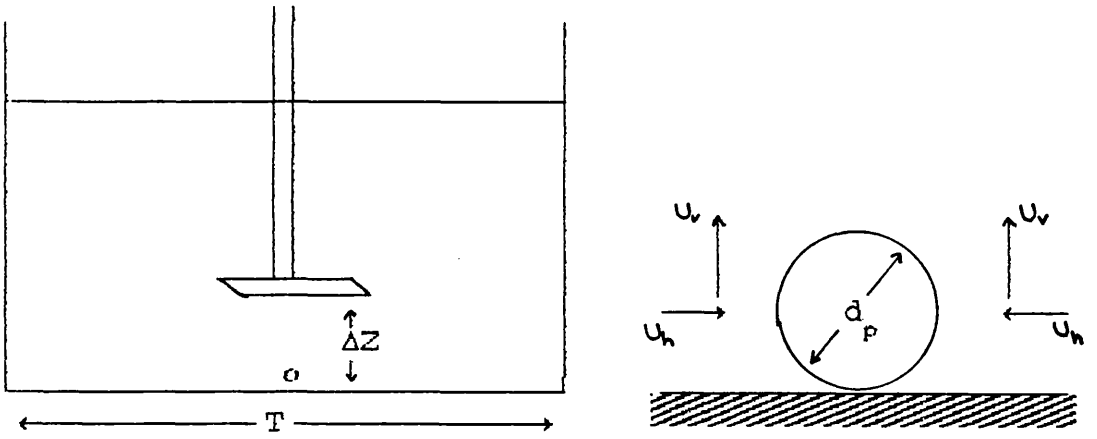

Figure 3.1 Solitary particle resting on the flat base of an agitated vessel

The liquid is swept out from the impeller to the walls of the tank and then flows down the walls before flowing radially inwards, close to the base of the tank. Concentrating on this liquid close to the base, the velocity of this liquid will be a complex function of the impeller speed and diameter, distance travelled since leaving the impeller and the physical properties of the liquid itself (viscosity and density). As the liquid approaches the immediate vicinity of the particle, the mean velocity of the liquid will have a vertical (axial) component as well as a horizontal (radial) component. In figure 3.1.b, u_h and u_v are the horizontal and vertical velocity components for the liquid flowing at one particle radius from the base of the tank, i.e. corresponding to the same axial position as the centre of gravity of the particle.

If the particle is a sphere of diameter d_p and density ρ_s, then the net downward force exerted on the particle will be :

$$F_G = 4/3\ \Pi\ (d_p/2)^3(\rho_s - \rho_f)g \qquad 3.1.1$$

The effect of u_h and u_v is to cause forces to act upon the particle. Each velocity component will give rise to a

lift force acting at 90° to that component, and a drag force acting in the same direction.

For the vertical component, u_v, the lift forces will cancel each other out because of the symmetry of the flow. For the same reason, the drag forces from the horizontal components will cancel each other out. This leaves a upward drag force from the vertical component and an upward lift force from the horizontal component. At the point of suspension the downward force will be equaled by these upward forces so that:

$$F_G = F_D + F_L \qquad 3.1.2$$

where F_D and F_L are the drag and lift forces, respectively on the particle.

F_D can be related to the mean liquid velocity in the following way:

$$F_D = 1/2\ \rho_f u_v^2\ \Pi\ (d_p/2)^2 C_D \qquad 3.1.3$$

and similarly for F_L :

$$F_L = 1/2\ \rho_f u_h^2\ \Pi\ (d_p/2)^2 C_L \qquad 3.1.4$$

where C_D and C_L are the drag and lift co-efficient, which are given their definitions by these two equations. In general, C_D and C_L are both functions of the particle Reynolds Number (Schlingting, 1968), although not the same function.

$$Re_p = \frac{\rho_f u\ d_p}{\mu} \qquad 3.1.5$$

Drag & Lift Co-efficients

From the point of view of the vertical velocity component the situation is similar to that encountered to a freely settling sphere, at its terminal settling velocity, in a motionless liquid. If this is the case then for the small

Re_p (<1) likely to be encountered when suspending solids in viscous liquids then:

$$C_D \propto \frac{1}{Re_p} \quad \text{or} \quad C_D = \frac{C_2}{Re_p} \qquad 3.1.6$$

This approximation is given further credence by the theoretical work of Goren & O'Neill, 1971.

Relating the lift co-efficient to liquid and particle properties requires a more profound analysis of the complex mechanisms which give rise to the lift force.

There are two mechanisms that may cause a particle to lift away from a plane surface:

(i) velocity gradient Bernouilli forces

(ii) stagnation point shift

(i) With the first of these, the plane (see figure 3.2) causes a velocity gradient. If the local flow is laminar, then there will be a linear velocity profile. In close proximity to a sphere, this velocity profile will give rise to a asymmetric pressure distribution, such that the pressure above the sphere is lower than the pressure below the sphere. This pressure difference causes a force on the particle away from the wall. Theoretical and empirical means of quantifying this lift force have been proposed (see table 3.1).

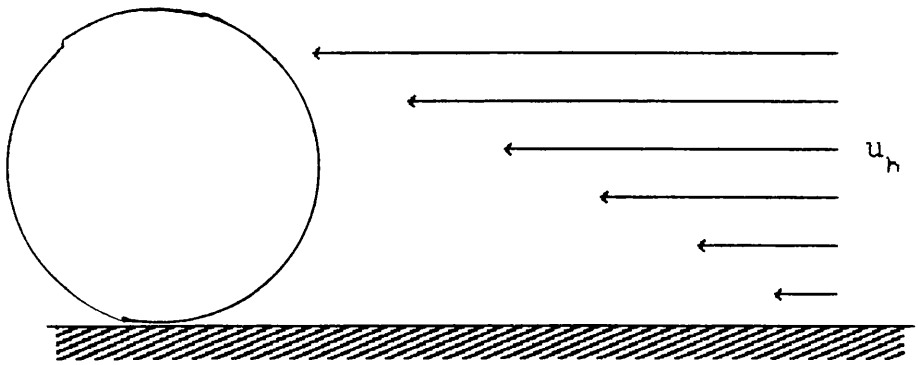

Figure 3.2 Undisturbed velocity profile for a liquid in laminar flow over a flat plate

Author	C_L
White, 1940	$C_D/4$
Thomas, 1961	~ 1
Saffman, 1964	$\propto 1/Re_p^{0.5}$
Leighton & Acrivos, 1985	~ 6

Table 3.1 Previous Estimates for the Lift Co-efficient

Unfortunately, these methods give conflicting results for C_L. Indeed, in a discussion of their mathematical analysis, Leighton & Acrivos, 1985, agreed that their approach did not give satisfactory results and acknowledged that "...the factors responsible for the observed resuspension remain, therefore, to be identified". Another problem is that these relationships for C_L only consider flow from one direction rather than the axisymmetric situation shown in figure 3.1b.

(ii) The mechanism that has been favoured in this study is that of a lift force caused by the shift in stagnation point. When there is flow around a symmetrical object, such as a sphere, then there will be no net lift force. However, by bringing the sphere next to a plane wall, this symmetry is absent. The stagnation point has been moved by angle θ_s from its original position S to S'. In any situation where the stagnation point has changed there must be a liquid circulation, (Massey, 1972).

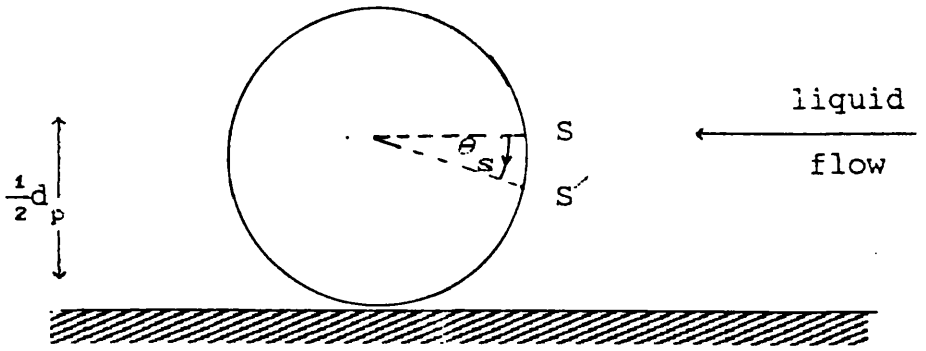

Figure 3.3 Stagnation point displacement in non-symetric flow

An analogous situation occurs with the Magnus Effect on a rotating cylinder in a moving liquid (S.W.Yuan, 1971; Massey, 1972). Although the particle on the point of suspension (in figure 3.1b) is not rotating, the analogy is made because the lift in both cases is caused by an angular shift in the stagnation point. By analyzing what determines the lift co-efficient for the Magnus Effect, one may be able to draw some useful conclusions on the lift co-efficient for a sphere on the point of suspension.

For an inviscid flow around a rotating cylinder, the Kutta-Joukowski theorem (Massey, 1972; Yuan, 1967) will predict the lift force per unit length of the cylinder (see figure 3.4).

$$L_F = \rho_f U \Gamma \qquad 3.1.7$$

where Γ is the circulation defined by:

$$\Gamma = \oint q_s ds \qquad 3.1.8$$

q_s being the component of velocity along an element of curve ds.

This implies a lift co-efficient given by:

$$C_L = 4\Pi \sin\theta_s \qquad 3.1.9$$

i.e. the greater θ_s, the greater C_L.

Examination of figures 3.4a and b reveal that for a fixed Γ/U_∞, then decreasing the cylinder radius from R_1 to R_2 increases θ_s hence $\sin\theta_s$ and C_L. For the case of a sphere resting on a plane, this would seem plausible. If the diameter of the particle is increased, then the distance between the centre-line of the particle, where the original stagnation point was situated, and the base would also increase. Since it is postulated that it is the proximity of the base that gives rise to the lift force, it would be expected that the influence of the base would lessen with an increased distance between the centre-line and the base. If this is the case, then there would be a smaller angular shift of the stagnation point, and hence smaller value of C_L for larger particles. Therefore, as a result of the above analysis it is proposed that:

$$C_L \propto d_p^{-n} \qquad n > 0 \qquad 3.1.10$$

This relationship has been the subject of experimental investigation in this study. The results of this investigation are discussed in Chapter 5 (section 3).

As stated before, in general C_L should be a function of the particle Reynolds Number, Re_p, and therefore also a function of viscosity. The Kutta-Joukowski equation is based on that pressure distribution arising from inviscid flow. In practice, for the Magnus Effect, a real liquid's viscosity acts in such a way that the lift force is diminished compared to equation 3.1.7.

This is because the viscosity of a real liquid alters the pressure distribution downstream of the projected area, i.e. to the right of the line AB in figure 3.5 such that $P_A - P_B$ is less than predicted by the inviscid flow analysis. The real liquid forms a boundary layer around the solid which under certain conditions will experience separation at a point on the downstream surface of the

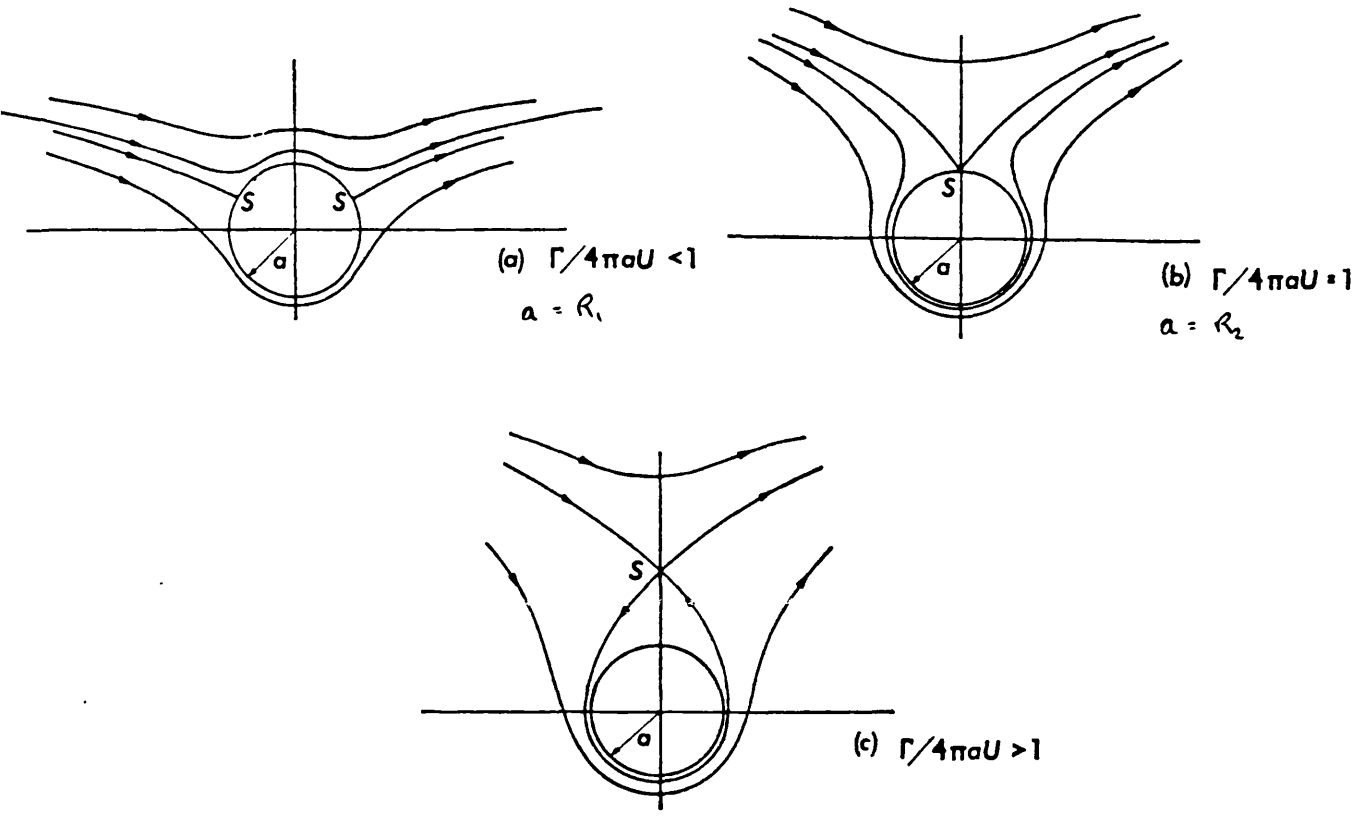

Figure 3.4 Flow around rotating cylinders in inviscid flow (Massey, 1972)

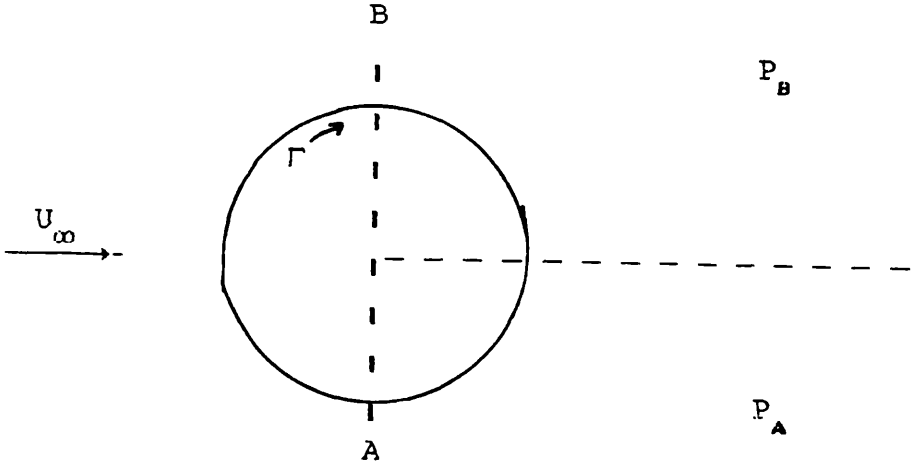

Figure 3.5 Flow around rotating cylinder in real fluid

solid (Schlingting, 1968). It is this boundary layer separation which, in this context, distinguishes the viscous from the inviscid pressure distributions. Preventing boundary separation will lead to the lift being increased to that predicted by the Kutta-Joukowski theorem.

The analogy with the Magnus Effect is significant since by means of "conformal transformation", a mathematical process invented by Joukowski, patterns of flow around a cylinder can be used to predict the pattern of flow for a body of different but mathematically related shape.

Referring back to the axisymmtric situation shown in figure 3.1b, the liquid impinges onto the sphere from all directions with equal horizontal velocity components, u_h. In such a situation, there can be no "downstream of the projected area", hence no boundary layer separation and no effect of viscosity or Re_p.

As a first approximation, the value of n in equation 3.1.9 has been taken as 1.

$$\text{i.e.} \quad C_L = \frac{c_1 T}{d_p} \qquad 3.1.11$$

where T, the tank diameter, is introduced as a characteristic length so that the constant of proportionality c_1 is dimensionless.Experiments have been performed to evaluate n and the results of these experiments are discussed in Chapter 5.3.

Substituting for C_L from 3.1.11 and C_D from 3.1.6 into equations 3.1.4 and 3.1.3 respectively and substituting for F_D, F_L, and F_G into 3.1.2

$$\frac{4}{3}\Pi(d_p/2)^3(\rho_s - \rho_f)g = \frac{1}{2}\rho_f\Pi(d_p/2)^2\frac{c_1 T}{d_p}u_h^2 + \frac{1}{2}\rho_f\Pi(d_p/2)^2\frac{c_2}{Re_p}u_v^2 \qquad 3.1.12$$

substituting for Re_p and after some re-arrangement:

$$\frac{4}{3}\left[\frac{\rho_s - \rho_f}{\rho_f}\right] g d_p = u_h^2 \frac{c_1 T}{d_p} + u_v \frac{c_2 \mu}{\rho_f d_p} \qquad 3.1.13$$

The work of Schwartzenburg & Treybal, 1968, as well that of Molerus & Latzel, 1987 indicates that u_h can be related to the impeller speed by a simple relationship such that:

$$u_h \propto ND(D/T) \qquad 3.1.14$$

if u_v is proportional to u_h then also

$$u_v \propto ND(D/T) \qquad 3.1.15$$

Since u_h is also determined by the velocity profile at the base of the tank, and if the local conditions are sufficiently laminar so that the profile is linear, then:

$$u_h \propto d_p \qquad 3.1.16.$$

hence

$$u_h \propto d_p ND(D/T) \qquad 3.1.17$$

or

$$u_h = A \frac{d_p}{T} ND(D/T) \qquad 3.1.18$$

and similarly

$$u_v = B \frac{d_p}{T} ND(D/T) \qquad 3.1.19$$

where A and B are dimensionless constants which depend on geometry, impeller type and also the properties of the liquid. It is expected that for a given geometry, at a fixed impeller speed, N, then an increase in viscosity will decrease u_h and u_v and hence A and B.

Substituting for u_h and u_v from equations 3.1.18 and 3.1.19 into 3.1.13 and re-arranging:

$$\frac{4}{3}\left[\frac{\rho_s - \rho_f}{\rho_f}\right]g = \frac{A^2 c_1}{T}(ND)^2(D/T)^2 + \frac{Bc_2}{T}\frac{ND}{d_p}(D/T)\upsilon \qquad 3.1.20$$

If the values for the composite constants A^2c_1 and Bc_2 were known, it would be a simple matter to solve for N from 3.1.20 as a quadratic (hence the term "quadratic mean flow" model)

$$N_{JS} = \frac{\frac{-Bc_2}{d_p}\left(\frac{D}{T}\right)^2\upsilon + \sqrt{\left(\frac{Bc_2}{d_p}\right)^2\left(\frac{D}{T}\right)^4\upsilon^2 + \frac{16}{3}\left(\frac{\rho_s - \rho_f}{\rho_f}\right)g\frac{A^2c_1}{T}D^2\left(\frac{D}{T}\right)^2}}{2\ \frac{A^2c_1}{T}D^2\left(\frac{D}{T}\right)^2} \qquad 3.1.21$$

Even without knowing values for the composite constants A^2c_1 and Bc_2, equation 3.1.20 can still be used to make some qualitative comparisons with the experimental data of other workers.

As the particle diameter, d_p, becomes larger, equation 3.1.20 predicts that the drag force component will become negligible compared to the lift force so that:

$$\frac{4}{3}\left[\frac{\rho_s - \rho_f}{\rho_f}\right]g \approx \frac{A^2c_1}{T}N_{JS}^2D^2\left(\frac{D}{T}\right)^2 \qquad 3.1.22$$

and the effect of d_p on N_{JS} has gone. This agrees with the experimental data provided by many researchers, even though they used low viscosity liquids (e.g. Baldi et al, 1978; Ditl & Reiger, 1985), where they have found that d_p has increasing influence only at lower d_p, giving the type of graph shown in figure 3.1.6.

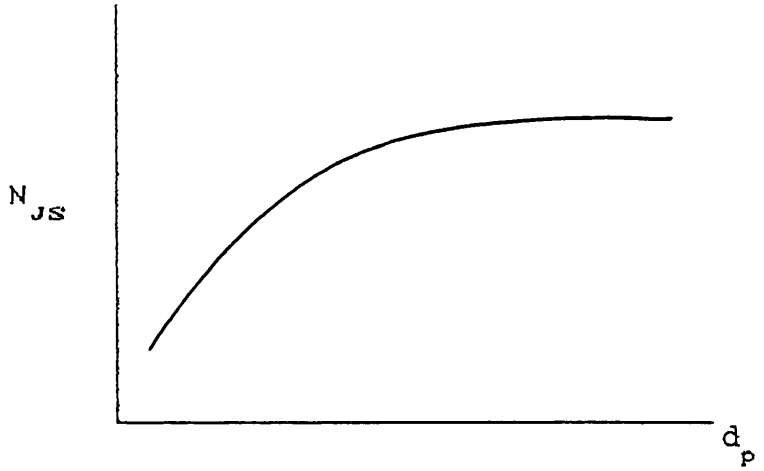

Figure 3.6 General effect of d_p on N_{JS}

The graphs presented by Ditl & Reiger, 1985, as well those of Baldi et al, 1978, show that, for the agitation systems they used, d_p has no measurable influence on N_{JS} after 1000 μm. In the correlation presented by Zweitering, 1958, equation 2.3.1, the exponent, or influence, of particle diameter on N_{JS} was 0.2. The particle diameter in Zweitering's experiments was only altered between 200 to 750 μm. When the experimental data is plotted on log/log paper, one straight line may well have given a satisfactory fit to the data. Therefore, the low value, 0.2, for the influence of d_p gives further support to the accuracy of the model. Indeed the various influences that d_p has on N_{JS} that have been recorded by different workers (table 2.3.1) may be accounted for by the different ranges of d_p that they investigated.

One of the problems associated with many of the purely empirical studies has been the presentation of results such that the influence of parameter, P, on N_{JS} is constant for all P. These correlations may be sufficient for design purposes within the range of experimental conditions considered, but can be highly misleading when trying to extrapolate to a different range of operating conditions, where P may have a different influence.

Referring to equation 3.1.22, the influence of gravity and buoyancy is given by:

$$N_{JS} \propto \left(\frac{\rho_s - \rho_f}{\rho_f}\right)^{0.5} g^{0.5} \qquad 3.1.23$$

which again is in good agreement with the value of 0.45 found by Zweitering, 1958. Although under different conditions when the drag force is no longer so small, the influence of gravity and buoyancy will also change.

The scale-up rule implied by 3.1.22 is:

$$N_{JS} \propto {}^{1}/_{D^{0.5}} \qquad 3.1.24$$

this too is likely to change for different systems, going some way to explain the wide disparities in scale-up rules suggested by previous workers (table 2.3.1).

Equation 3.1.21 can only be useful for quantitative predictions when values for the composite constants A^2c_1 and Bc_2 are known. As asserted before, these constants will be a function of the system geometry and the liquid's properties. The complex hydrodynamics associated with mechanical agitation means that finding theoretical predictions for A^2c_1 and Bc_2 is very difficult, and has so far proved elusive. Use of the PHOENICS code to solve the Navier-Stokes equations has been attempted (Pericleous & Patel, 1987) but has only proved to be of limited usefulness, predicting the velocity profiles in the bulk of the liquid away from the walls and base of the tank. The influence of viscosity was not investigated by their study.

However there are empirical ways to determine the values of A^2c_1 and then find a estimate for Bc_2. The constant A, at a given viscosity and agitation geometry, can be found by determining the velocity profile with different viscosity liquids at the base of the tank using an adjustable pitot tube (see Chapter Four). The reliance of C_L on d_p can be found by measuring the lift force on a stationary sphere with a symmetrical flow of liquid impinging on the sphere (see Chapter Four).

A more direct way of estimating A^2c_1 is to use experimental just suspension speed data for conditions where equation 3.1.22 is a good approximation, i.e. when d_p

is high and viscosity is low. (Use data such that the Archemedes Number is high). so that:

$$A^2c_1 = \frac{4}{3}\left[\frac{\rho_s - \rho_f}{\rho_f}\right]g\ \frac{T}{N_{JS}^2 D^2}\left[\frac{T}{D}\right]^2 \qquad 3.1.25$$

If the properties of the liquid are altered whilst keeping the geometry constant, then N_{JS} will change and also $\Delta\rho/\rho_f$ so A^2c_1 will change. A^2c_1 can then be plotted against the kinematic viscosity, μ/ρ_f, to find the relationship between them.

By using this method for υ from 4 x 10^{-5} to 2 x 10^{-3} m^2/s (see figure 5.1.22)

$$A^2c_1 \propto \upsilon^{-0.29} \qquad 3.1.26$$

Substituting for A^2c_1 into 3.1.25 and rearranging then it can shown that:

$$N_{JS} \propto \upsilon^{+0.115} \qquad 3.1.27$$

which is close to proportionality predicted by Zweitering, 1958 (equation 2.3.1)

Using the pitot tube experimental data for υ varying from 0.074 to 0.191 x 10^{-3} m^2/s (see figure 5.3.6)

$$A^2 \propto \upsilon^{-0.22} \qquad 3.1.28$$

The closeness of 3.1.26 to 3.1.28 gives further credence to the validity of the assumptions made in equations 3.1.10 and 3.1.11 that C_L is independent of viscosity and hence particle Reynolds Number. Therefore, c_1 is independent of liquid properties and is constant for the situation where the sphere lifts into suspension in the manner described in figures 3.1.1a and b. The pitot-tube measurements also confirmed the direct proportionality between u_h and N.

Knowing A^2c_1 one can then substitute these values in equation 3.1.20 to estimate values for the composite constant Bc_2 and its dependence on liquid properties. This

time, to enhance the accuracy of these estimates for Bc_2, experimental data should be chosen such that the drag force is at its most significant, i.e. at low Archemedes Numbers (low particle diameters and high viscosities).

Equation 3.1.20 relates the minimum impeller speed, N_{JS}, required to lift the last particle(s) to other pertinent design variables. However, it has not attempted to take the effect of solids concentration into account. The mean flow properties of the liquid in the immediate vicinity of the suspending particles can also be used to predict the small effect of solids concentration and show how even that small effect diminishes with increasing concentration. Appendix 5 shows a mathematical treatment of the problem based on the interchange of the liquid's kinetic energy and the particles' potential energy.

The Quadratic Mean Flow (QMF) model is based on the mean, or time-averaged, flow properties of the liquid that flows through the region immediately adjacent to those particles that rest on the tank prior to suspension. Although the geometry considered for the formulation of the QMF model is unique to radial flow in viscous liquids, it should still be possible to apply similar arguments, assumptions, approximations to different geometries and still achieve a relationship of the same form as equation 3.1.20. The composite constants A^2c_1 and Bc_2 will take into account the differing geometries so that the QMF model can be compared with the equations and data of other workers in Chapter Five. In the next chapter, a range of experiments has been devised to gain suspension speed data under different conditions. Further experiments have been developed in order to test out some of the assumptions made in this chapter. These are also explained in Chapter Four.

The main purpose of these series of experiments was to collect new data that will extend the range of suspension speed and distribution data from low viscosity Newtonian liquids to high viscosity Newtonian and non-Newtonian liquids.

The solids suspension experiments yielded data that can be used as for both qualitative and quantitative comparisons with previous work, as well as providing a means by which to test the "quadratic mean flow" model proposed in CHAPTER THREE.

The solids distribution data gathered in this study is completely novel, in so far as no previous quantitative work has been published with high viscosity liquids, Newtonian or otherwise. The resulting axial and radial concentration profiles can then be compared with that work that has been accomplished with low viscosity liquids to find any similarities and/or differences.

The suspension mechanism experiments were conducted in order to validate some of the assumptions made in CHAPTER THREE, and to give a better understanding of the hydrodynamic conditions at the base of a flat bottomed tank.

Further details and specifications of equipment used that have not been covered in this chapter may be found in Appendix 3.

4.1 Newtonian Liquids

These liquids were made either from various glycerol/water or corn syrup/water mixtures, prepared in situ. The composition of the glycerol/water mixture is checked by measuring the density, using a hydrometer, at the prevailing temperature. These measurements are then compared with a table of glycerol/water densities at different temperatures, Bosart & Snoddy, 1928, and the exact composition determined. Knowing the composition and temperature of the mixture, the dynamic viscosity can be found from a table produced from the findings of M.L.Sheeley, 1932. Some of these viscosities were checked by independent measurements. The various glycerol/water mixtures used are shown in table 4.1.1.

%wt glycerol	ρ_f (kg/m^3)	μ (Pas)	υ (m^2/s)x10^4
78.0	1202	0.049	0.408
82.5	1216	0.099	0.814
90.0	1235	0.200	1.62
93.0	1242	0.572	4.61
96.0*	1254	1.818	14.5
96.0*	1255	2.636	21.0

*different ambient temperatures

Table 4.1.1 Properties of selected glycerol/water mixtures at ambient conditions

For the corn syrup/water mixtures, a chart of composition (%wt corn syrup) vs refractive index was drawn up (see Appendix 2). At various (known) compositions, the

viscosity was measured so that by using a refractometer the composition and the viscosity at 20°C could be determined. However, the prevailing temperature was often below 20°C so the viscosity had to measured again either using a viscometer or by finding the terminal settling velocity of a sphere of known diameter and density. However, using the refractometer provided a quick means of checking to see if the viscosity of the syrup may have changed due a change of composition with time. With three independent means of measurement, it was possible to triple-check the viscosity of a mixture for any seemingly anomalous results. The properties of frequently used corn syrup/water mixtures are shown in table 4.1.2.

4.2 non-Newtonian Liquids

To prepare the non-Newtonian liquids, weighed amounts of 7H4C Carbonyl Methyl Cellulose, CMC, a white odourless powder, were added to a known quantity of distilled water. The solution is continuously agitated, at room temperature, until a uniform transparent liquid emerges.

%wt CMC	k	n
0.10	0.012	0.95
0.20	0.027	0.89
0.25	0.056	0.88
0.50	0.170	0.79
0.75	0.520	0.75
1.00	0.700	0.73

Table 4.2.1
Properties of CMC solutions at 20°C

The rheology of these various CMC solutions was found by testing each in a rheometer. The device chosen was a Contraves Rheomat 30, linked to a voltmeter to give a digital display of the torque. The samples of each solution were subjected to a co-axial cylinder geometry (Measuring System B). See Appendix 2 for more details of equipment and procedure.

Fitting the data to a power-law relationship, the values of the flow index, n, and intercept, k, were calculated and are shown in table 4.2.1.

4.3 Solids Distribution Experiments

4.3.1 Apparatus

For this series of experiments, the equipment used was originally built for E. Koutsakos, phD 1989.

Two geometrically similar tanks were used. Each is constructed of glass with a hemispheric base and cone deflector. A perspex box is fitted around each tank, filled with water to minimize optical distortions. Included with the tanks is a set of four detachable baffles, arranged symmetrically at 90 degrees to the adjacent baffle. Normally, baffles were not used. For further details of tank design see figure 4.3.1 and table 4.3.3.

Paramter	Specification
Classification	Class II
Maximu power output	0.5mW
Wavelegth	632.8nm
Initial beam diameter	0.83mm
Beam dvergence	1.3mRad
Stabilty	± 1 MHz
Polariation	Linear
Maximum operating temperature	60°C

Table 4.3.1 Specifications for laser

To measure the local solids concentration, a 5mW Barr & Stroud He-Ne laser was employed. The laser tube was connected to an assembly (see figure 4.3.3) which allowed movement in the vertical and horizontal planes. The laser beam has an initial diameter of 0.83mm. After passing through an expander, this diameter is increased by a factor of ten. Directly facing the laser, on the other side of the tank, is placed a silicon photocell (manufactured by R.S.). This cell is designed to receive light only of the same wavelength, 632.8nm, emitted by the laser. The photocell is connected to another assembly again allowing freedom of movement in the vertical and horizontal plane.

Parameter	Specification
Spectral range	350 -> 1150nm
Response	0.35 A/W at 650nm
Capacitance	350pF
Operating temperature	$-55^{o}C$ -> $70^{o}C$
Rise time (10% -> 90%)	50ns
Maximum power output	5mW
Maximum voltage	350mV

Table 4.3.2 Specifications for silicon photovoltaic cell

The output from the photocell is fed to an A/D converter which in turn is linked to a BBC Acorn computer with data acquisition software. When particles are in suspension, the amount of light that can pass through the tank from the laser to the photocell is a measure of the local solids concentration. The more light that can pass through, the less the concentration.

Different impellers were used but mainly 6-bladed 45 degree pitch turbines, details given in figure 4.3.4.

4.3.2. Materials

The solids distribution experiments were conducted with a variety of liquids both Newtonian and non-Newtonian.

The properties of these liquids are shown in table 4.3.4.

Glass beads of density 2900 kg/m^3 and diameters of 530μm and 1100μm were used for suspension.

4.3.3 Procedure

With a known volume of liquid in the tank together with a known weight of glass ballotini, the mean bulk solid concentration can be calculated.

The laser gun assembly is then manipulated so that the laser light shines through the tank at the desired axial and radial position. The photocell is then placed so that the light shines directly through the tank from the laser. To make sure that the laser and photocell are correctly aligned, the laser is switched on. A protective filter is placed immediately in front of the laser. This filter blocks out about 1/3 of the laser's power. If there is correct alignment, then the output from the cell, shown on the computer screen, will be about 200mV. When the filter is removed the output will be about 300mV. Protective curtains are then drawn together so that stray reflections from the laser do not cause any harm. Details of A/D converter, computer, and software are shown in Appendix.

The electric motor, details in 4.4, is then engaged and the speed control altered slowly to the desired impeller frequency. At the desired impeller speed, data is collected and stored on diskette by the computer, over a period of time, to determine the average output of the photocell. When the data acquisition has been completed, the impeller speed can be increased and the mixing system allowed to reach its new steady state before collecting more data. The more viscous or non-Newtonian the liquid, the more time should be allowed at each increment of speed for equilibrium to be reached.

The laser is switched off after all the distribution data at the desired impeller speeds has been collected. The laser gun assembly can then be safely maneuvered to the next position and the alignment procedure repeated as before.

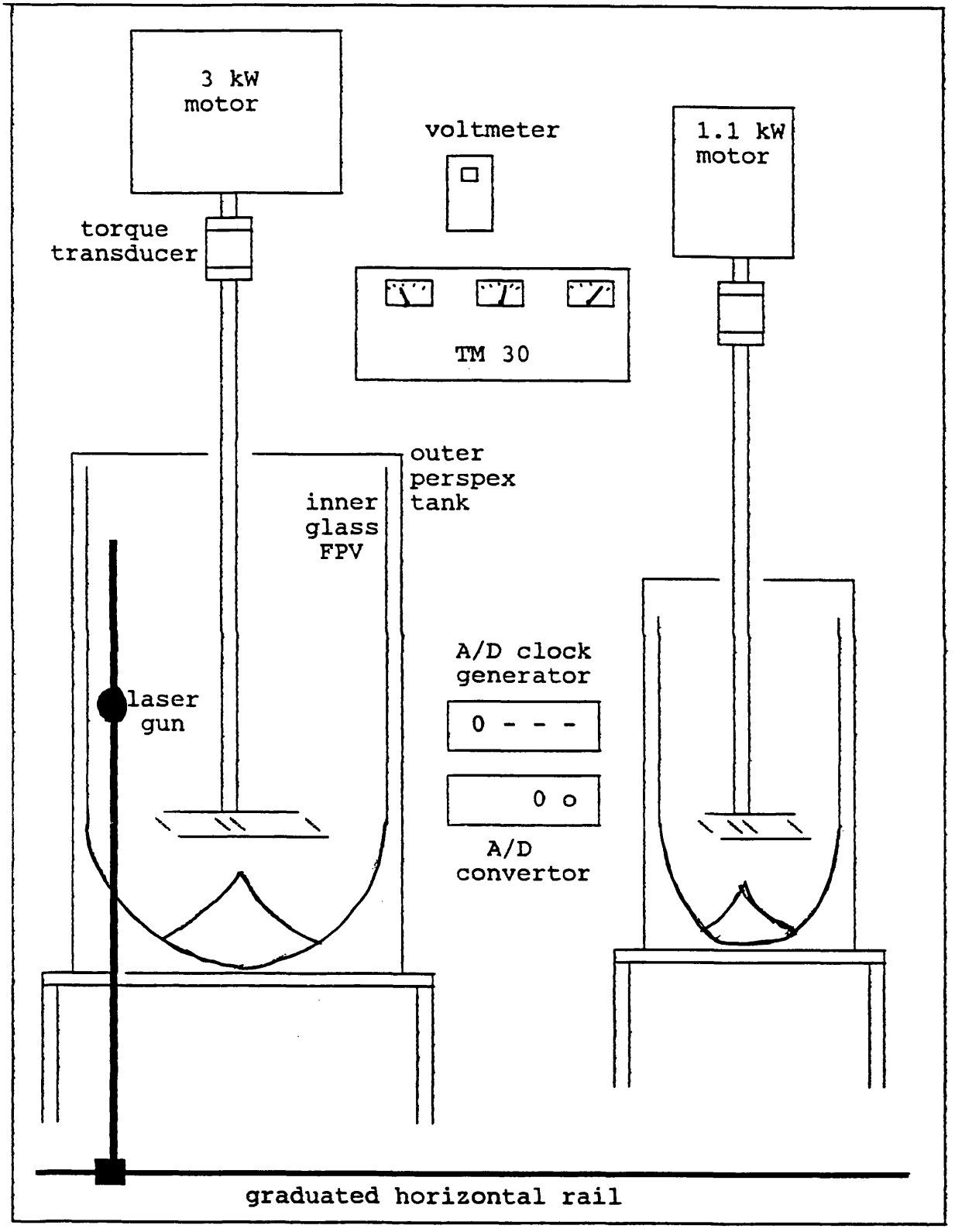

Figure 4.3.1 Schematic diagram of experimental apparatus

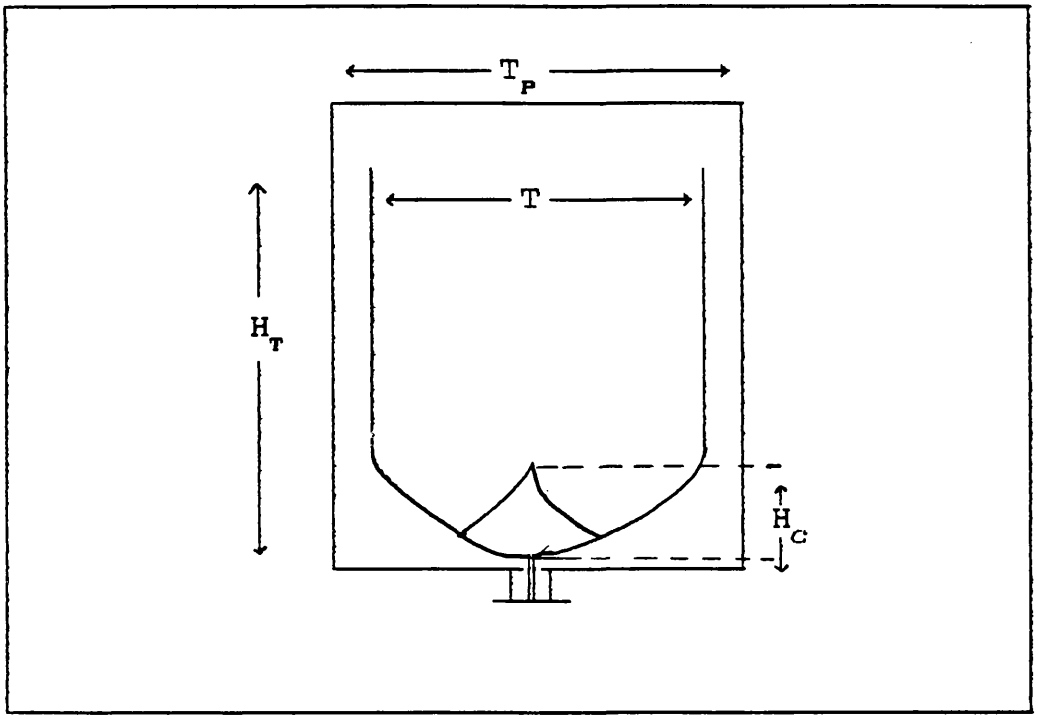

Figure 4.3.2 Diagram of Fully Profiled Vessel

dimension	15cm FPV	29cm FPV
T	15.0cm	29cm
H_C	3.7cm	7.3cm
H_T	40.2cm	86.0cm
T_P	30.0cm	34.0cm
Volume	$5.6dm^3$	$24dm^3$

Table 4.3.3 Dimensions of FPVs used

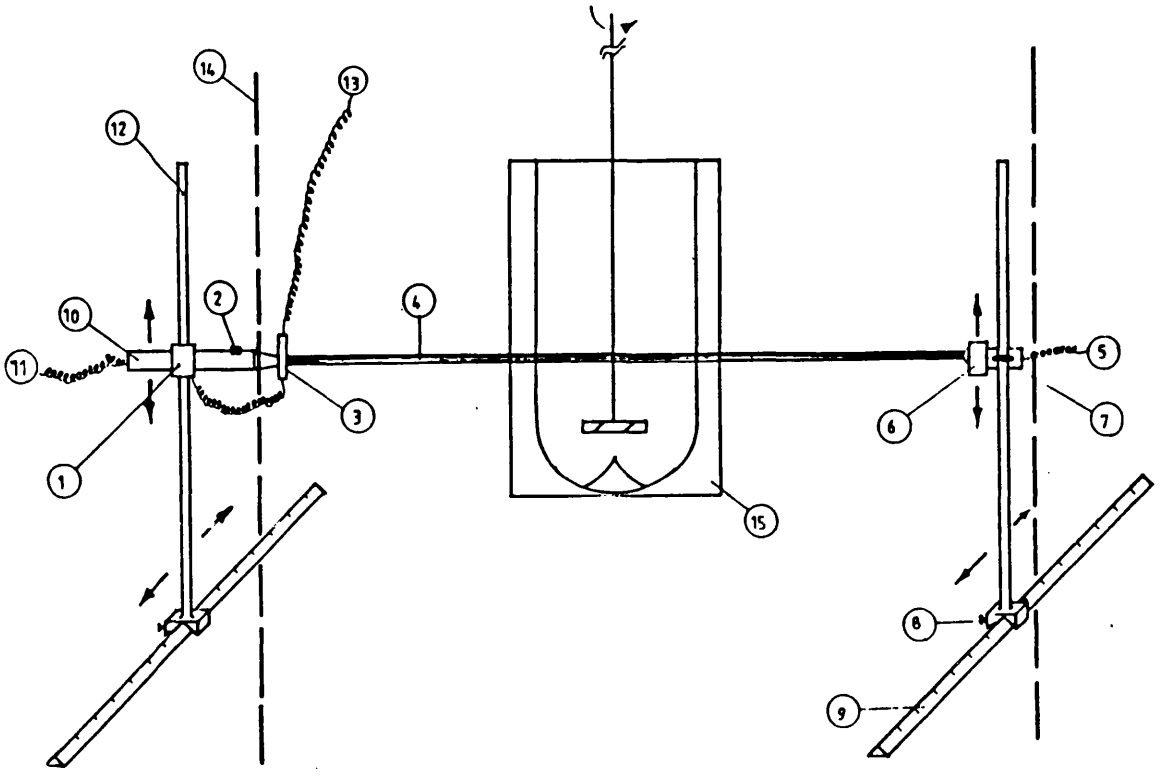

1. Micro switch cover (inc. Level adjusting screws, cut-off switch)
2. Intermediate on/off laser beam switch.
3. Light intensity reduction filter.
4. Laser beam.
5. To data acquisition system.
6. Photovoltaic cell
7. Level adjusting screws.
8. Horizontal position adjusting screws.
9. Horizontal rail bolted onto the floor.
10. Laser gun.
11. To on/off switch.
12. Vertical rail.
13. To mains supply.
14. Curtain.
15. Agitated vessel.

Figure 4.3.3 Diagram of equipment used for solids distribution experiments

(reproduced from E.Koutsakos, phD thesis, 1989)

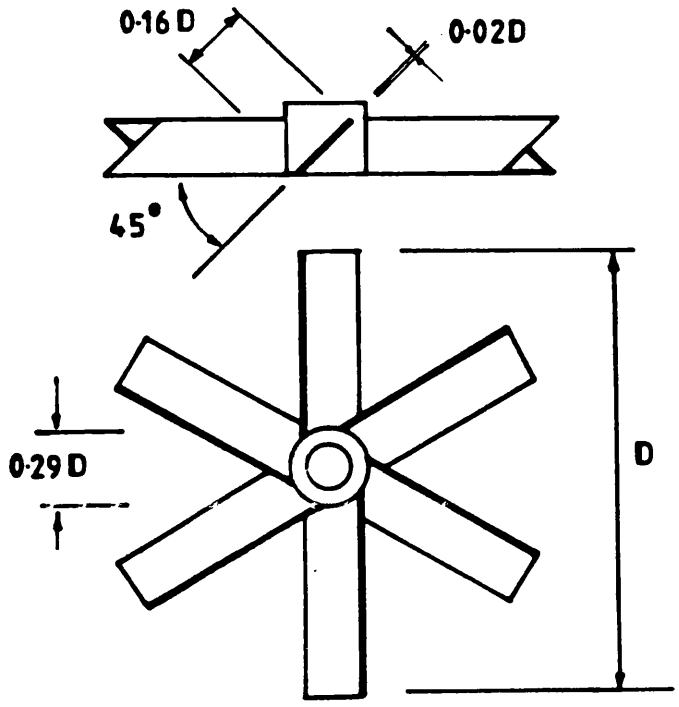

Figure 4.3.4 Geometry of six-bladed turbines used for both solids distribution and suspension speed experiments

4.4 Solids Suspension

4.4.1 Apparatus

The most important part of the equipment used is the Anyspeed electric motor and the associated EEL electronics designed to give information on the frequency of shaft rotation, the torque, and the resultant power consumption.(see figure 4.4.1).

The electric motor drives a shaft of 1" diameter and is infinitely variable between 0 to 2000 rpm, though at speeds below 90 rpm there is difficulty in maintaining a steady value. The motor can be used to drive the shaft either the clockwise or anticlockwise directions.

The vessels used for solids suspension were flat bottomed transparent cylinders made either from glass or perspex (details in table 4.4.1). Usually, there were no baffles.

diameter /cm	height /cm	capacity /cm^3
30.0	30.0	21200
24.0	28.0	12700
19.0	26.0	7370
16.3	20.0	4170
15.3	18.0	3310

Table 4.4.1
Dimensions of tanks used for suspension speed studies

The impellers used were all six-bladed 45 degree pitch turbines of various diameters, blade thicknesses and heights.(see table 4.4.2).

4.4.2 Materials

The solids used were always more dense than the surrounding liquid. The least dense were acetate spheres, 1270 kg/m^3, of diameters 2.0 to 5.0mm. The most dense were zirconium oxide spheres of density 3820 kg/m^3, of diameter 1.85 mm. Properties of all the solids (all assumed to be

spherical) used are shown in table 4.4.3. The PTFE and acetate spheres have been manufactured to a fine tolerance so that the diameters of these spheres has been very accurately determined (±0.5%). The diameters of the rest of the particles shown in table 4.4.3 are averages determined by sieve analysis. Typically, the range of particle diameters will vary ± 10% from the d_p value shown in table 4.4.3.

The Newtonian liquids used were either mixtures of glycerol and water or corn syrup and water. The non-Newtonian liquids were aqueous solutions of 7H4C CMC as described above in 4.2.

4.4.3 Procedure

The electronic EEL equipment was calibrated in accordance with the accompanying manual.(see Appendix 3 for details of calibration procedure). As a further check on the registered speed, a light sensitive tachometer was directed at the shaft to ensure that the digital display of the EEL equipment co-incided with that from the tachometer. Having prepared the liquid in situ, the temperature is recorded to ensure that the rheological properties do not differ markedly from those shown in tables 4.1.1 and 4.2.1.

A carefully weighed amount of solid is then poured into the tank, and care taken that all the trapped air that was entrained with these solids has been able to escape to the liquid surface.

The motor is then engaged and the speed raised incrementally. Between each increase in speed, a few minutes must elapse to ensure that the system is at equilibrium. The suspension of solids in such viscous liquids using 6-bladed 45 degree pitch impellers always causes the solids to be drawn in to the centre of the base directly below the impeller. This is true even when the impeller is rotating clockwise, i.e. "pumping downwards". This observation implies that this type of impeller is behaving more like a radial flow impeller rather than an axial flow impeller. With low viscosity liquids such as water, the opposite is true.

material	ρ_s /kg/m^3	d_p /mm
PTFE	2140	3.175
Zirconium oxide	3820	1.85
soda glass	2540	10.0
soda glass	2540	3.265
soda glass	2540	1.84
lead glass	2900	6.0
lead glass	2900	4.0
lead glass	2900	2.0
lead glass	2900	1.1
lead glass	2900	0.78
lead glass	2900	0.53
lead glass	2900	0.39
acetate	1270	5.0
acetate	1270	4.0
acetate	1270	2.0

Table 4.4.3
Properties of solids used for suspension studies

With some of the suspension studies the impeller speed at which the first particle is raised into suspension was recorded. More importantly, the speed at which the last particles go into suspension was recorded. At speeds well below N_{JS}, particles are lifted into suspension by climbing on top of other particles which have formed a mound at the centre of the base. There were occasions when this last speed could not be attained because the vortex had reached the impeller causing aeration. This last particle suspension speed corresponds to that minimum impeller speed

required to lift a particle from the base of the tank without needing any neighbouring particles to assist in the suspension process. With small particles this can be a subjective test and relies on good visibility. This visibility can be enhanced by using a bright light source focused at the base of the tank, and by colouring some of the glass ballotini to make individual particles easier to follow.

The resulting reproducibility of experimental results was within ± 4% The length of shaft that protrudes below the impeller should be kept to a minimum, especially in the more viscous liquids. 1 cm of excess shaft can cause the N_{JS} to be overestimated by about 10%.

When the experiments with a solid were completed, the contents of the tank were passed through a sieve to collect the particles and the liquid recycled for further use.

tank diameter (cm)	impeller diameter (cm)				
	6.5	8.0	10.0	13.0	16.5
15.3	X				
19.0	X	X	X		
24.0	X	X	X	X	
30.0	X	X	X	X	X

Table 4.4.2 Combinations of 6-bladed turbines and vessels investigated

4.5 Suspension Mechanism Experiments

These experiments were carried out to determine the influence of liquid properties, density, viscosity, and mean velocity, on particles resting at the centre of the flat bottomed tank. They divide into two distinct series of experiments; the first concerning the pressure and lift forces acting on a stationary spherical particle; and secondly, the effect of impeller speed and geometry on liquid velocities in the vicinity of the central part of the base of a flat-bottomed unbaffled vessel.

4.5.1 Lift Forces

The apparatus consisted of a rectangular transparent box (see figure 4.5.1) made from perspex. At either end of the box, are identical "snout-mouthed" nozzles connected via a T-junction to the outlet of a Stuart-Turner No.12 centrifugal pump. Liquid is ejected from the pump into tank through these nozzles and is recycled to the inlet of the pump through another T-junction.

At the centre of the base is 5.0mm hole with a pin projecting upwards. From this hole a flexible tube leads to one end of a Druck differential pressure transducer. In the lid of the box, another hole allows entry of a metal pressure probe which was connected to the other end of the transducer.

The pressure transducer is designed to operate in the range of 0 to 350 mBar, with the digital readout sensitive to 0.1 mBar. To increase the sensitivity of the pressure measurement, the transducer was linked to the same A/D converter and computer software described in 4.3.1. The screen of the computer is then able to give a real time display of the transducer output, which in turn gives a measure of the differential pressure. The software is able to take account of any pressure fluctuations encountered during the course of an experimental run and calculate an average value. The differential pressures encountered for these experiments were very low (in the order of 1cm of water) so that reproducibility could only be ensured to

within ±15%.

From this arrangement of hole and metal probe, the pressure difference, between the top and base of the sphere, could be measured. To measure the velocity of the liquid impinging on the sphere, the metal probe was replaced by a pitot probe.

The materials for the experiments consisted of a range of spheres, either made of wood or metal, each with a hole drilled at the base to allow the sphere to stay on the pin projecting upwards from the base of the tank. Also used were two mixtures of glycerol and water, one of 3.5 cP and the other of 6.0 cP. More viscous mixtures would have been desirable but the pump available would not have been able to force the liquid through the nozzles at a sufficient rate to give measurable pressure differences across the height of the sphere.

The most difficult part of the experiment is to determine the zero point of the transducer since this is apt to drift with time, the zero point being the transducer reading when the pump is off. The computer is used to collect data over a period of time to give an average mV reading that corresponds to the zero point of the transducer. The mBar reading of the transducer is also recorded. The centrifugal pump is switched on and the response of the transducer is displayed on the computer screen. After waiting for a steady state reading to emerge, the computer is then used to collect data. This whole process was repeated 3 or 4 times depending on the reproducibility of the results. Recording the mBar display of the transducer, at the zero point, and the corresponding mV reading gives a conversion of mV to mBar.

The same technique is applied to velocity measurement with the pitot probe which measures the impact pressure of the liquid forced through the nozzles, whilst the hole, still connected to the transducer, measures the static pressure. The liquid velocities are found at different heights from the base and at different positions along the longitudinal axis of symmetry of the box.

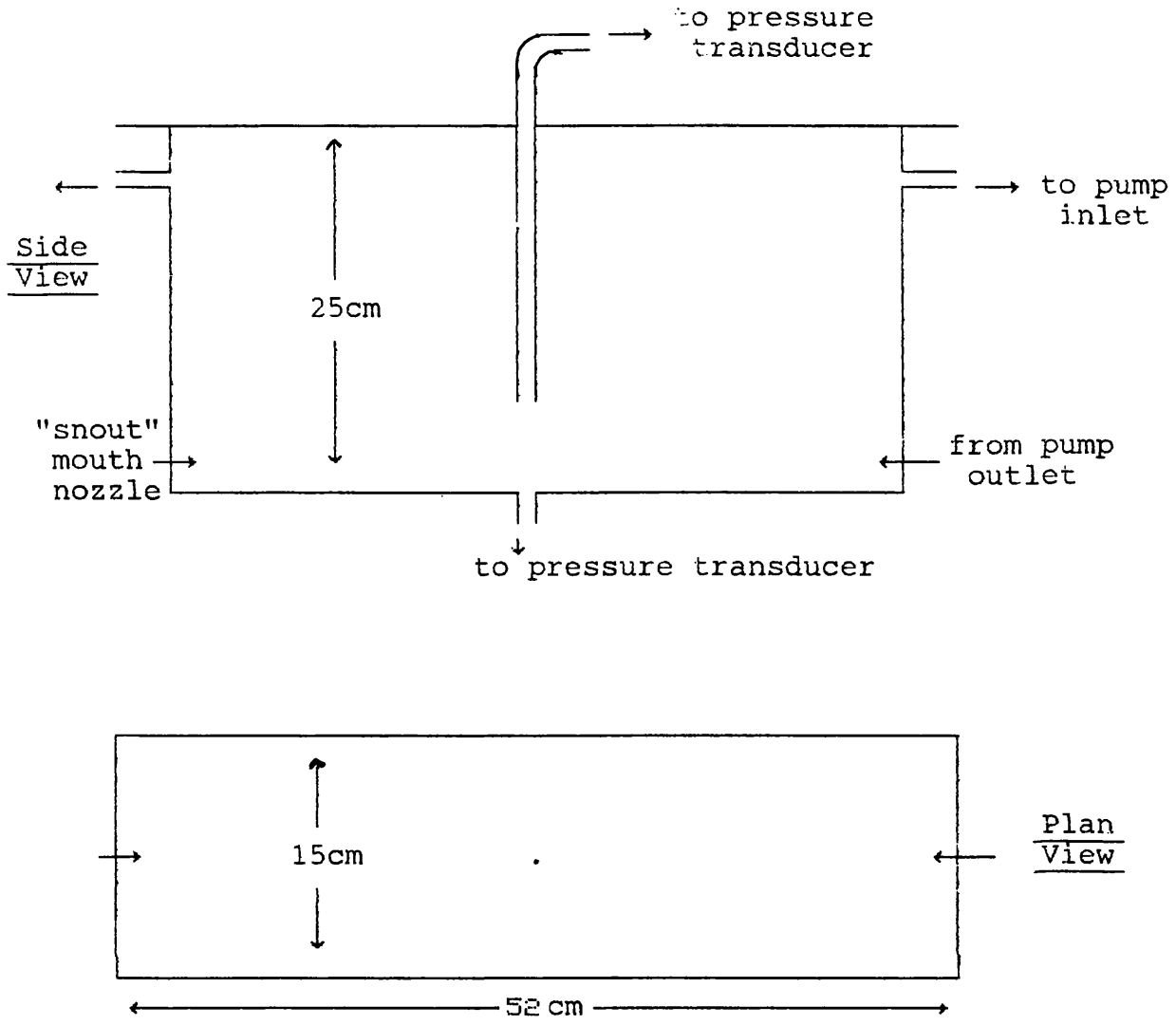

Figure 4.5.1 Diagram of "Water Tunnel" used for measurement of lift forces

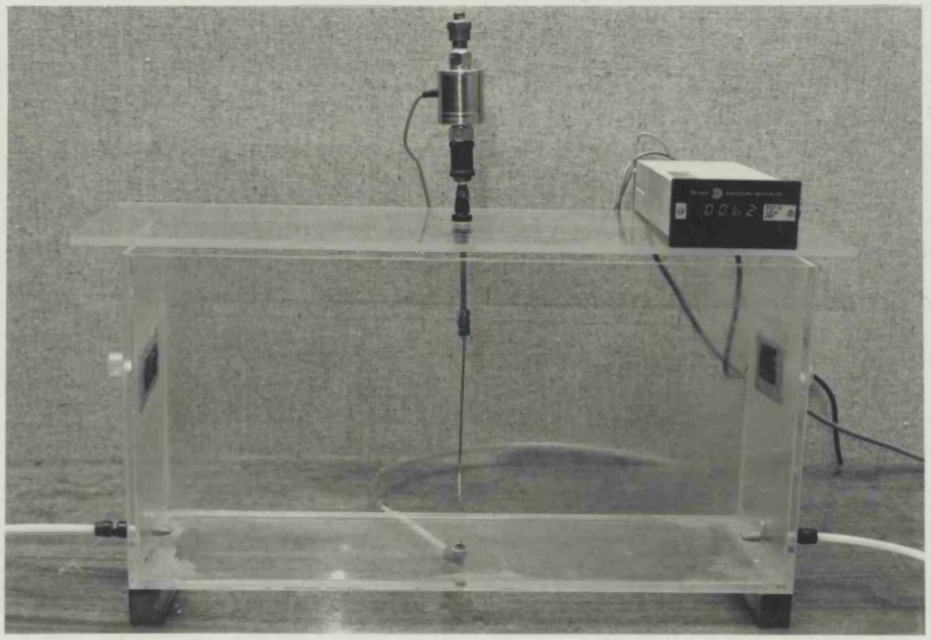

Figure 4.5.2 Apparatus for measuring lift forces

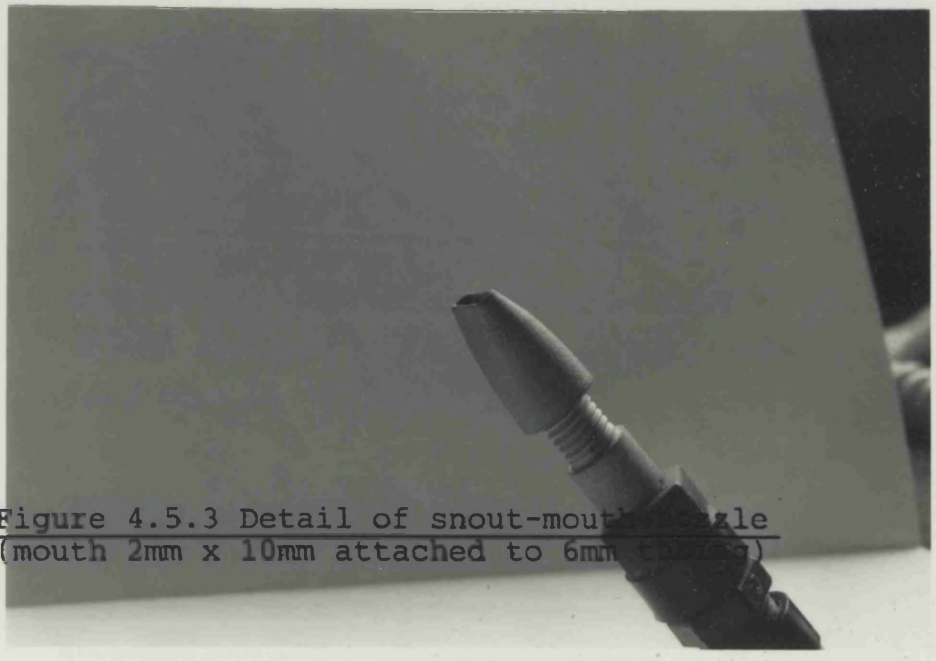

Figure 4.5.3 Detail of snout-mou[illegible]zle (mouth 2mm x 10mm attached to 6mm [illegible])

4.5.2 Effect of Impeller Speed on Liquid Velocities

The apparatus has much in common with that described in 4.4.1. The impeller is rotated by the same electric motor and the speed given by the same EEL equipment. The glass tank is cylindrical and unbaffled. The diameter is 29.0 cm and the height 28.0 cm. The base of the tank is made of perspex, through which a 3/8" hole has been drilled at the centre. Through this hole a pressure probe is inserted (see figures 4.5.3 and 4.5.4) which has freedom to move in the vertical/axial direction. Onto this probe a variety of specially designed attachments may be fitted which can either be exposed to the impact pressure of the radial component of the local liquid velocity, or the static pressure. By using the attachments in combination a variety of different radial positions can be sampled, from 6.6mm to 38.6mm. The pressure probe is linked one end of the same Druck pressure transducer described previously, which in turn is connected to the same A/D converter and BBC computer. Although the same arrangement is used for pressure measurement as described for 4.5.1, the reproducibility was improved because the differential pressures involved in 4.5.2 are generally greater. This means that the results are accurate to within ±10%

The impeller used is a 13.0 cm six-bladed 45 degree pitch turbine (described earlier in figure 4.4.2). The impeller is kept at a clearance of 9.1 cm.

Three glycerol/water mixtures were used whose properties are shown in table 4.5.1. The liquid level is always about 22.0 cm from the base.

%wt glycerol	μ Pa s	ρ_f kg/m^3
83	0.072	1218
87	0.150	1226
90	0.285	1235

Table 4.5.1
Properties of glycerol/water mixtures

The velocity, at a given axial and radial position, and impeller speed, is determined by finding the difference in the pressure recorded when the probe has type 1 (or type 2) attachments and when it has the static pressure attachment.

As before, the most difficult part of the experiment is ensure a reliable zero point reading for the transducer. Once this has been achieved, the electric motor is switched on and the impeller speed raised to the desired value. After allowing for steady state, the pressure transducer output is collected by the computer, and then the impeller speed raised again by some increment and more pressure measurements taken. The process is continued until the full range of impeller speeds has been investigated. This whole procedure was repeated 3 or 4 times to ensure reproducible results.

The data from the experiments described in this chapter are to be found in the Appendix. The presentation of discussion of the results that have emerged from the data can be found in the next chapter, Chapter Five.

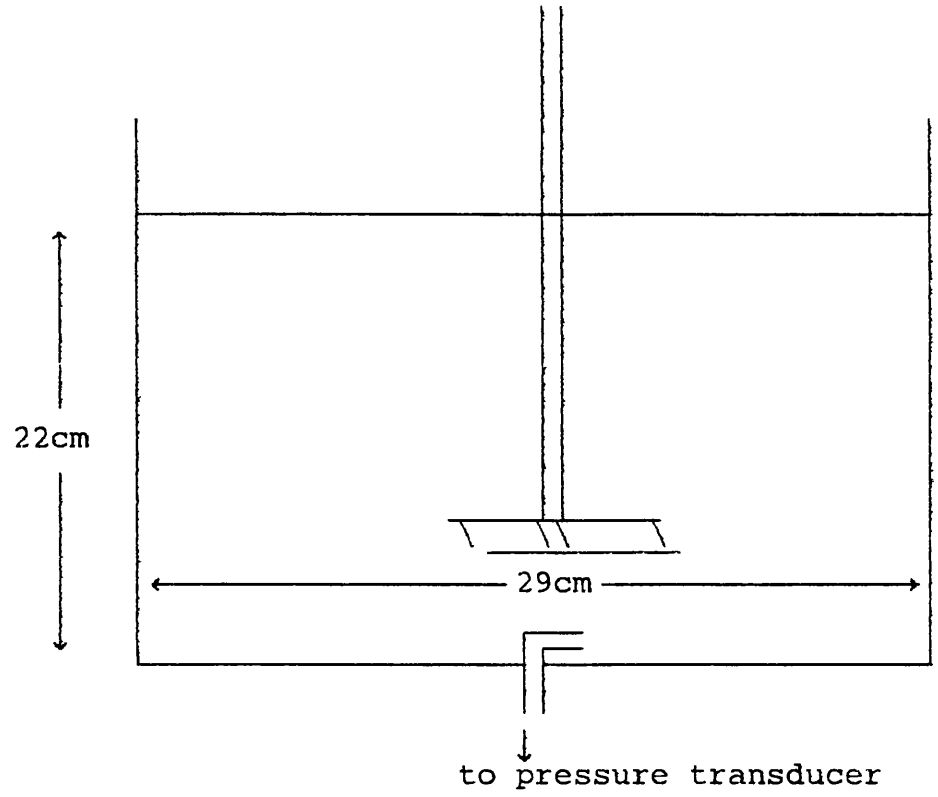

Figure 4.5.4 Equipment used for velocity profile experiments

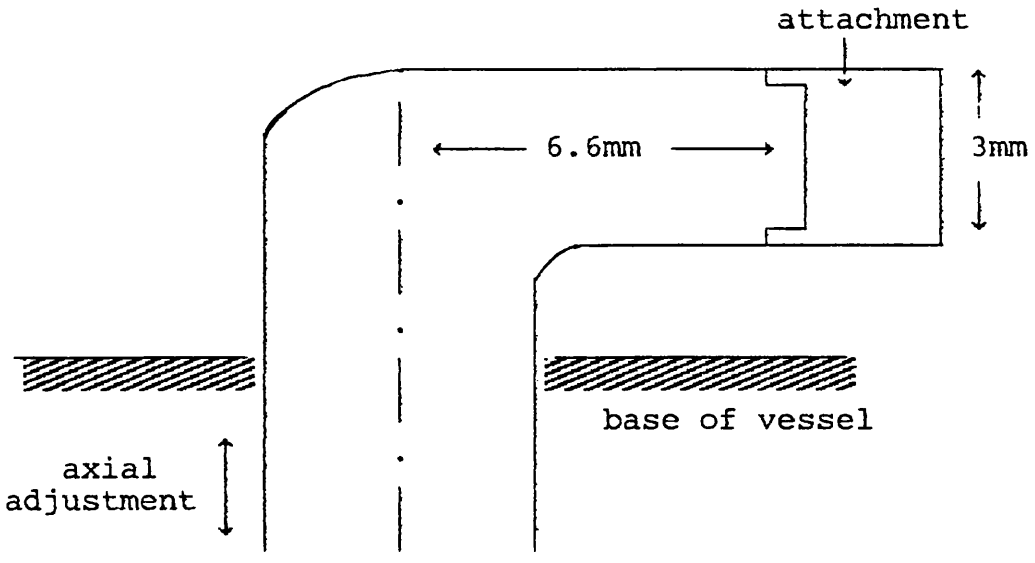

Figure 4.5.5 Detail of "telescopic" pitot probe

CHAPTER FIVE
Results and Discussion

This chapter is divided into five parts. In 5.1 the experimental results on solid suspension speeds and its variation with other design parameters are presented and discussed. Visual observations of the suspension process are noted in Appendix 1

In 5.2 the experimental data is presented to show how local solids concentrations vary with impeller speed under different agitation conditions. These local solid concentrations are then used to quantify the quality of mixing, and also used as a basis of comparison with other researchers' findings.

In 5.3 the data has been presented to show the behavior of a liquid at the centre of the base of a flat-bottomed agitated vessel as well as particle-liquid interactions.

5.4 contains calculations based on some of the results found from 5.1 and 5.3. These calculations are required to find constants used in the "quadratic mean flow" model developed in Chapter Three. Having evaluated these constants, the remaining results from 5.1 are compared with the model to test the accuracy of the proposed relationship.

In 5.5 the quadratic mean flow model is compared with other researchers and discussed with regard to the implications for design purposes and scale-up criteria.

5.1 Suspension Speed Experiments

a) Effect of Particle Diameter

The experimental data gathered in this study shows that, in general, particle diameter has little influence on the just suspension condition. For large diameter particles, above some critical size, this influence becomes so low that it cannot be measured. This critical diameter depends on the agitation system examined and especially on the viscosity of the liquid. It was found that the greater the viscosity, then the greater this critical diameter. For the experimental conditions covered in this study, the critical diameter varied in the range 1 to 2mm.

Figure 5.1.1. shows the influence of particle diameter on the just suspension speed, N_{JS}. For particle sizes below the critical diameter, the influence of particle diameter on N_{JS} is more interesting. The points on the graphs shown in figure 5.1.1 could be joined by one straight line for d_p less than d_{pc}. However, it would be more accurate to fit a curve which approaches an asymptotic value of N_{JS} as d_p tends to d_{pc}. By fitting a curve of ever decreasing slope, it can be seen that the effect of d_p on N_{JS} cannot be represented by a simple constant exponent proportionality of the form:

$$N_{JS} \propto d_p^a \qquad \text{for all } d_p \qquad 5.1.1$$

The data would seem to indicate that the exponent a is itself a function of d_p. For values of d_p above d_{pc}, a tends to 0; and for deceasing d_p, a increases so that d_p will have an increasing influence on N_{JS}. If the dimensionless group:

$$Ar = \frac{d_p^3 (\rho_s - \rho_f) g}{\upsilon^2 \rho_f} \qquad 5.1.2$$

is used to characterize the solid/liquid properties (Ar is the Archemedes Number), then as a general rule, it can be seen

that the lower the value of Ar, the greater will be the influence of d_p.

b) Effect of Solids Concentration

The influence of solids concentration on the just suspension speed, N_{JS}, was found to be small (see figures 5.1.2a and b). At high concentrations, even this small influence was found to diminish to such an extent that there was no measurable effect on N_{JS}.

Figure 5.1.2a shows typical plots of N_{JS} vs C_w, the weight percent concentration of particles added either to a glycerol/water mixture of viscosity, 0.049 Pas, or to a 0.5%wt CMC solution. A ten-fold increase in particle concentration results in increases for N_{JS} of less than 10%. Figure 5.1.2.b shows the effect of concentration in a corn syrup/water mixture for two sizes of glass ballotini. At low concentrations the N_{JS} values for the 4mm particles are, as expected, greater than for the 0.78mm particles. However, when the concentration is increased beyond 0.3%wt, the two curves cross each other. The 4mm particles are experiencing the hystersis effect (see 5.1.i) so that particle concentration will have even less effect on N_{JS} than described in figure 5.1.2a. The 0.78mm particles, being much lighter than the 4mm particles, will not experience the hysteresis effect (at least not to the same degree) and therefore particle concentration will have a greater influence on N_{JS}. If experiments had been carried out at concentrations close to 1%wt, without taking into account the hysteresis effect, it might have been concluded that increased particle diameter always led to a decrease in N_{JS} in highly viscous liquids. The effect of particle properties can, therefore, be confused when dealing with hystersis-inducing agitation systems. It was for this reason that many experiments were performed using only single particles (see Appendix 6 for results)

In a similar manner to that shown by the N_{JS} vs d_p (figure 5.1.1), the data points would be best fitted to a

smooth curve rather than 1 or more straight lines. As with the influence of particle diameter, concentration is more important at lower concentrations.

c) Effect of Impeller Clearance

In the relatively less viscous liquids (<0.2 Pas), using glycerol/water mixtures, the effect of impeller clearance would appear to be small so that for the impeller diameters used, the relationship between N_{JS} and the clearance, ΔZ, could be approximated by:

$$N_{JS} \propto \Delta Z^{0.1} \qquad 5.1.3$$

However, for the more viscous liquids examined, using corn syrup/water solutions, the effect of impeller clearance on N_{JS} is more complex (see figures 5.1.3 to 5.1.14).

Plots of N_{JS} vs ΔZ for different diameter impellers are shown in figures 5.1.3 to 5.1.14. Some of these plots show the existence of a minimum and therefore an optimum ΔZ for the lowest value of N_{JS}. This optimum position is dependant on the size of the impeller, D; the greater D, the greater the optimum ΔZ.

The interdependence of D and ΔZ is more complicated than might, at first, have been predicted. This relationship becomes more complex with agitated vessels containing liquids of high viscosity. For a given impeller diameter and clearance, rotating at speed N, then increasing the viscosity of the liquid will lower the the liquid velocities in all regions of the tank , but most importantly, the liquid's velocity in the immediate vicinity of the suspending particles, at the centre of the base of the tank, will be reduced.

The viscosity of the liquid has a damping effect on the liquid that emerges from the impeller region, and follows a pathlength, L, to the centre of the base. This damping effect will cause the liquid to lose energy and hence velocity as it proceeds along L. This pathlength, L,

is a function of the impeller clearance and diameter. The greater the diameter of the impeller and the smaller the clearance, then the smaller will be L. This may help to explain why such geometry has, generally, been found, by other researchers as well as this study, to lower N_{JS}. However, if L is lowered too much, then N_{JS} increases, which indicates that there is an optimum pathlength for a given agitation system.

As the pathlength is lowered, the curvature of the path becomes more pronounced. As with liquids flowing in a system of pipes and fittings (Nekrasov, 1969), the more rapid the change in direction, the greater the rate of change of momentum on the fluid elements, and hence the greater the forces on those elements resulting in greater pressure drops and energy losses. This would explain the existence of an optimum position, ΔZ, for an impeller of diameter, D, in a liquid of viscosity μ/ρ_f. To find the precise length of these pathlengths, L, more quantitative arguments would need to be used, perhaps employing some form of flow visualization technique; dye injection or radio-active tracer.

For the quadratic mean flow model, proposed in Chapter Three, the effect of clearance has not been considered theoretically. The results of this study show that impeller clearance can be an important design parameter for determining N_{JS}. Using some of the results obtained in this study, it might be possible to incorporate the effect of clearance, ΔZ, empirically.

However, the empirical relationship cannot be of a simple, constant exponent proportionality

$$N_{JS} \propto \Delta Z^{a} \qquad 5.1.4$$

but instead a should be a function of the kinematic viscosity, υ, and D.

In a paper presented by Conti and Baldi,1978, it was shown how the impeller clearance affected N_{JS} through its influence on their modified Re^{*} (see Chapter Two). Their analysis of the data indicated that the effect of impeller

clearance increases with increasing viscosity. Figure 5.1.15. shows the variation of Z_B as a function of Re^* for different impeller clearances. The range of viscosities examined by Conti and Baldi varied only from 0.645×10^{-3} to 7.8×10^{-3} Pas.

At constant D, one form of relationship suggested by the experimental data that would relate a to the viscosity is given by:

$$a = \left(1 - e\left\{\frac{-\beta\mu}{\rho_f}\right\}\right) + 0.1 \qquad 5.1.5$$

where β is a positive co-efficient. The value of 0.1 comes from the findings from data taken with low viscosity liquids so that when the viscosity is small then:

$$e\left\{\frac{-\beta\mu}{\rho_f}\right\} \text{ -> 1 and a -> 0.1} \qquad 5.1.6$$

and when the viscosity increases

$$1 - e\left\{\frac{-\beta\mu}{\rho_f}\right\} \text{ also increases}$$

hence the influence of ΔZ on N_{JS} increases. The coefficient β will take account of D.

The effect of impeller clearance was not investigated for non-Newtonian liquids. However, given the range of "effective" viscosities (0.01 to 0.1 Pas; as calculated from Metner & Otto, 1958) of the CMC solutions used, it might be assumed that the effect of clearance on N_{JS} would be similar that described by 5.1.3

d) Effect of Impeller Diameter (and Scale-up)

As with the effect of impeller clearance, the influence of impeller diameter seems to depend on the viscosity of the liquid. At low viscosities (i.e. when using glycerol/water mixtures), the effect of impeller diameter, D, is more straightforward so that:

$$N_{JS} \propto {}^{1}/_{D^2} \qquad 5.1.7$$

for the range of impeller diameters and clearances examined.

However, with the more viscous liquids, there is a more complex interaction between N_{JS} and the impeller diameter and clearance (as previously explained above 5.1.c), and the relationship shown in equation 5.1.5 no longer applies. Instead, for a given impeller clearance and tank diameter, there is usually a progressive flattening-out of the N_{JS} vs D curve (see figures 5.1.16 to 5.1.18). This will mean that a graph of impeller power consumption vs D at just suspension conditions will indicate an optimum impeller diameter. The results of Hirsekorn and Miller, 1953, showed that this optimum diameter corresponded to a D/T ratio of just over 0.6. However, they did not investigate how this optimum ratio would be affected by the impeller clearance.

Figure 5.1.19. shows the effect of scale-up on a corn syrup/water mixture of viscosity 4.7 Pa s at two different D/T ratios. Both ln/ln graphs are poorly represented by a straight line. At D/T = 0.33, the scale-up rule implied by figure 5.1.19. is:

$$N_{JS} \propto {}^{1}/_{D^{0.16}} \qquad 5.1.8$$

whilst for D/T = 0.42, the scale-up rule is:

$$N_{JS} \propto {}^{1}/_{D^{0.67}} \qquad 5.1.9$$

These wide variations in scale-up rule exemplify some of the problems encountered when dealing with such high

viscosity liquids.

e) Effect of Solid/Liquid Densities

Figure 5.1.20 shows how N_{JS} is influenced by the solid /liquid densities as characterized by the dimensionless group:

$$\left(\frac{\rho_s - \rho_f}{\rho_f}\right)$$

This shows that for all agitation conditions, N_{JS} is closely approximated by a simple (constant exponent proportionality such that

$$N_{JS} \propto \left(\frac{\rho_s - \rho_f}{\rho_f}\right)^{0.5} \qquad 5.1.10$$

This result is not surprising since many other researchers have also reported exponents of 0.5, or close to 0.5. Of all the particle properties, it is the the density of the particle that is the single most important parameter influencing N_{JS}. This is especially true at relatively low particle densities when ρ_s is only slightly greater than ρ_f.

f) Effect of Viscosity

Figure 5.1.21 shows how viscosity effects N_{JS} for a single glass particle of 6mm diameter at two different impeller clearances. The viscosity was varied by altering the relative %wt fractions of water and corn syrup to produce different Newtonian liquids. Changing the weight fractions also changes the density of the resulting liquid, and hence $\Delta\rho/\rho_f$. However, over the range of viscosities varied for figure 5.1.21, the density only changes from 1288 kg/m^3 to 1383 kg/m^3 causing a change in $\Delta\rho/\rho_f$ from 1.097 to 1.252; a change of less than 15%, whilst the kinematic viscosity has been altered from 1.25×10^{-4} to 7.23×10^{-3} m^2/s; a sixty fold variation. Given that N_{JS} is only proportional to $(\Delta\rho/\rho_f)^{0.5}$ then the effect of changing liquid density will have negligible impact on the shape of the graphs shown in figure 5.1.21.

From a kinematic viscosity of 1.25×10^{-4} to 1.1×10^{-3} m^2/s, the increase in viscosity also leads to an increasing N_{JS}, as might be expected. However, for the 3.6cm clearance, the rate at which N_{JS} increases is higher than the rate that would have been predicted by other workers. Taking the data points of 1.25×10^{-4} and 1.1×10^{-3} m^2/s and the corresponding N_{JS} values, there is a slope of 0.23 (cf Zweitering 0.1). This slope is also higher than that found from other experiments conducted in this study using glycerol/water mixtures at higher impeller clearances, when the experimental data agreed with the Zweitering exponent of 0.1.

At a clearance of 3.6cm, the graph shows a maximum at about 1×10^{-3} m^2/s (corresponding to an impeller Reynolds Number of about 60). If the viscosity is increased further, then there is a sharp fall in N_{JS} (slope = -1) until a viscosity of 3×10^{-3} m^2/s (Re = 10) after which the effect of increasing viscosity is very small. For a clearance of 4.4cm, the graph also shows a peak at a kinematic viscosity of 1×10^{-3} m^2/s, after which N_{JS} falls off even more rapidly with increasing viscosity than with the 3.6cm clearance. Indeed, the 4.4cm curve actually falls and continues

slightly below the 3.6cm curve as the viscosity is increased further. For viscosities below 1 x 10^{-3} m^2/s, the 4.4cm data shows a smaller effect of viscosity on N_{JS}, coming closer to the 0.1 influence.

The effect of viscosity upon N_{JS} is complicated because of the complex interaction between the impeller clearance and diameter at the higher viscosities associated with the corn syrup solutions.(See 5.1.c). Comparison of the graphs taken from data at 4.4cm and 3.6 cm, as shown in figure 5.1.20, gives a good illustration of the complex nature of these impeller clearance/viscosity interactions.

The model developed in Chapter Three has not been able to fully take account of the effect of viscosity on N_{JS} by purely theoretical means. As proposed at the end of Chapter Three, some of the results of this study can used in ways suggested by the modeling to find an expression for N_{JS} that takes viscosity into account. this means plotting (see equation 3.1.22)

$$A^2c_1 \text{ vs. } {}^{\mu}/_{\rho_f}$$

This plot is shown in figure 5.1.22, where the data has been taken from experiments using the moderate viscosity glycerol/water mixtures when impeller diameter/clearance/viscosity interactions are at their least significant. Under such circumstances, such a plot led to a simple correlation such that:

$$A^2c_1 \propto \left[{}^{\mu}/_{\rho_f}\right]^{-0.29} \qquad 5.1.11$$

Extending this simple analysis of the experimental data to the more viscous corn syrup solutions will not always yield the same relationship. What is required, is a relationship that predicts the effect of viscosity as shown in figure 5.1.21. but also reverts back to the simple correlation 5.1.11 .One possible form for this relationship has been proposed in 5.1.c.

Substitution of 5.1.11 for A^2c_1 into the quadratic mean flow model, equation 3.1.17, leads to result that

$$u_h \propto \left[\mu/\rho_f\right]^{-0.115} \frac{d_p}{T} ND\ (D/T) \qquad 5.1.12$$

This shows that that the main effect of viscosity is to cause energy losses between the impeller tip and the base of the tank and hence diminish the liquid velocities in the immediate vicinity of the suspending particles. This is corroborated by experimental data presented in the third section of this chapter. However, the way in which the geometry contributes to the rate of energy dissipation seems to become more complicated with higher viscosity systems.

g) Anticlockwise vs Clockwise Rotation
(and Effect of Baffles)

For all liquids and impeller diameters and clearances, that have been examined in this study, anticlockwise rotation of the impeller always led to a lower N_{JS} value than for clockwise rotation. The difference between the two may be small for the less viscous and less non-Newtonian liquids; but, as the either the degree of non-Newtonianness or viscosity of the Newtonian liquid increases, the the difference becomes more marked. In some cases, the N_{JS} obtained for clockwise rotation is twice as high as that found for anticlockwise.

The reason why there should be any difference between the two modes of rotation can be easily explained. The 45-degree pitch, 6-bladed turbine impeller used throughout these suspension speed studies, is regarded as a "mixed flow" impeller. This means that both radial and axial flow emerges from the impeller zone. With agitation in less viscous liquids, such as water, the impeller behaves more as an axial flow impeller rather than radial. However, with more viscous liquids, such as those used in this study, the flow was always radial (or at least more radial than axial), so that the particles were always drawn in from the periphery of the tank's base to the centre forming a mound of particles (see figure 5.1.23). This flow pattern is true of both clockwise and anticlockwise rotation.

The pitched turbines used for this study were all fabricated in such a way that anticlockwise rotation implied that the axial component would correspond to "pumping upwards", whereas for clockwise rotation, the axial component implied a "pumping downwards" action. Even in viscous liquids, these axial components do not completely disappear. Figures 5.1.23a and b show the different axial components superimposed onto the prevailing radial flow pattern for the two modes of rotation. In figure 5.1.23a, the axial component that remains acts in the opposite sense to the radial flow so that in the important central region, below the impeller, the radial

and axial components act against each other lowering the liquid velocities in the vicinity of the suspending particles. In figure 5.1.23b, the opposite is true; so that the axial component remaining may actually enhance the liquid velocities below the impeller.

In less viscous liquids, it has been common practice to install a set of baffles to promote solids suspension. However, with both the Newtonian and non-Newtonian liquids used in this study, baffles were found to inhibit the onset of the just suspension condition.

Baffles are thought to encourage axial flow at the expense of radial flow (as well as rotational flow), but since the predominant flow pattern in viscous liquids is still radial whether there are baffles in place or not, they act against (the flow and hence cause the system to be less efficient.

The circumstances which make baffles least efficient are when using larger diameter impellers or when trying to suspend solids in the more non-Newtonian liquids, when N_{JS} may be increased by a factor of two because of baffles.

h) Effect of non-Newtonianness

The non-Newtonian liquids used were all solutions of Carbonyl Methyl Cellulose (CMC) in distilled water. Rheological experiments showed that they behaved as pseudo-plastic power-law fluids such that:

$$\tau = k\dot{\gamma}^n \qquad 5.1.13$$

where n is the flow index (<1) and k is the consistency index. (See Chapter Four for properties of CMC solutions).

For such liquids the degree of non-Newtonianness can be thought of as the extent to which n varies from 1.(n=1 corresponds to a Newtonian rheometry).

Just as for the glycerol/water mixtures (see 5.1.h), the experimental data can be manipulated to show the effect of k and n on the just suspension condition. For Newtonian liquids, the dimensionless group, A^2c_1 was plotted against the kinematic viscosity, μ/ρ_f (or υ). For power-law fluids the nearest equivalent of μ is the consistency index k. It would be expected that for pseudo-plastic fluids the smaller n, the greater the local viscosity of the liquid at the walls and, in particular, at the base of the vessel away from the fast moving/high shear rate impeller region. Therefore, the group that might prove to be the nearest power-law equivalent of the kinematic viscosity is $k/\rho_f n$. Using N_{JS} data for large diameter glass and acetate particles a log/log graph of A^2c_1 vs $k/\rho_f n$ is plotted (figure 5.1.22), yielding a straight line such that:

$$A^2c_1 \propto \left[k/\rho_f n\right]^{-0.22} \qquad 5.1.19$$

Suspension of any type of solids in the same liquid should result in the same value for A^2c_1 as calculated from 3.1.22; the results for acetate and glass have a maximum deviation of about 15%. The exponent -0.22 is very similar to the value of -0.23 found for the Newtonian glycerol/water mixtures. Substituting for A^2c_1 from 5.1.19, means that the quadratic mean flow model can used to

predict N_{JS} for non-Newtonian liquids that display a power-law, pseudo-plastic rheology.

Altogether, six CMC solutions were prepared and used for suspension speed experiments. Although the two most concentrated solutions, 0.75 and 1.00%wt, seemed to display a simple power-law rheology (see Appendix for properties), agitation of larger samples in the 30cm tank showed thee two solutions to have discernible elastic properties. These were manifested by the "rod-climbing" or Weissenburg Effect at low impeller speeds as well as experiencing a recoil when agitation of the liquid is brought to sudden halt (more experimental observations made during the suspension process are to be found in Appendix 1). As a consequence, data from these solutions were not used to plot the graph shown in figure 5.1.22. For the acetate particles, there is a marked deviation from the straight line in figure 5.1.22. corresponding to suspension in the 0.5%wt CMC solution. There is no such deviation for the glass particles. This may be evidence that even the 0.5%wt solution may have elastic properties which may hinder the the acetate more than the glass because of the lower speeds associated with suspending the much less dense acetate, whereas the glass requires much higher speeds when the elastic effects become less significant. See Appendix 2 for more information on rheology and rheometry of non-Newtonian fluids.

i) Hysteresis Effect

For the less viscous liquids, below 2.0 Pas, there is no sign of any hysteresis for any of the particles thus far tested for suspension studies. This means that it should make no difference to X (see figure 5.1.24) whether the impeller speed, N, is increased or decreased to some value, N_X, then X_N will always be the same if enough time is is given for equilibrium to be established. However, when the liquid is viscous enough and the particles are of sufficient mass, then a hysteresis develops.

When the impeller speed is increased from zero, then X as a function of N will follow a similar curve to that solid line shown in figure 5.1.24 until all the particles have been suspended. During this process any particles that become suspended never fall back to the base and an equilibrium is never achieved between the rate at which particles drop out of suspension and rise into suspension.

Once a particle is suspended, it is always to be found close to the plane of the impeller, rotating just beyond the tips of the impeller. When all the the particles are in suspension, subsequent lowering of the impeller speed below N_L will not cause any particles to drop out of suspension, no matter how much time is allowed, until N is lowered to N_D when the first particles drop out of suspension. In some cases, N_D/N_L can be as low as 0.25. N_D/N_L is a function of both particle mass and concentration. The higher the concentration, and/or the lower the particle mass, the higher will be N_D/N_L.

Even at N_D, those particles that are still in suspension will remain indefinitely, still at the impeller plane. Eventually, if the impeller speed is lowered enough, to N_P, the impeller can no longer support any particles in suspension. In some cases, N_P can be as low as 50 rpm.

In cases where there is a hysteresis, the speed at which the last particle is lifted into suspension, N_L (i.e N_{JS}), is not a function of particle concentration. This should not be not unexpected since suspended particles do not fall back and "hinder" the remaining particles from

taking off as would normally be the case for non-hysteresis suspension conditions. This would tend to support the analysis presented in Appendix 5 explaining the effect of solids concentration on the just suspension condition. Because the hysteresis effect is less important for lighter particles, concentration will still have an effect on N_{JS}. This means that whilst N_{JS} may stay constant for heavier particles, over a range of concentrations, the N_{JS} values for lighter particles will increase over the same range of concentration. The experimental data presented in Appendix 6 shows that this can mean that, for example, 0.1%wt of 0.78mm glass ballotini has a N_{JS} value of 294rpm whilst 6mm glass ballotini, experiencing the hysteresis effect, has a N_{JS} value of 231rpm. For those particles heavy enough to exhibit the hysteresis, the N_{JS} value is the same as though there were only one particle in the tank.

A priori, it may have been expected that the lighter, smaller particles, which have smaller terminal settling velocities, would have the the greatest chance of exhibiting a hysteresis. However, from the suspension studies conducted with nine different particle masses, the opposite is observed. Another experimental finding is that increasing the impeller diameter increases N_D/N_L thereby diminishing the hysteresis effect.

An interesting analogy that may help to understand the hysteresis effect can be found from visualizing a length of string attached to a stone. When the string, and the stone at the end of it, is made to rotate above a critical frequency the stone will describe a circular motion. If the stone were to be replaced by a much lighter object such as a table tennis ball, it would prove much more difficult to keep the ball aloft, and would certainly require a much higher frequency of rotation. This type of analogy may suggest that the key to understanding, and therefore predicting the hysteresis effect, is the extent to which the mass of the particle allows for the storage of angular momentum.

Figure 5.1.1a
Effect of Particle Diameter

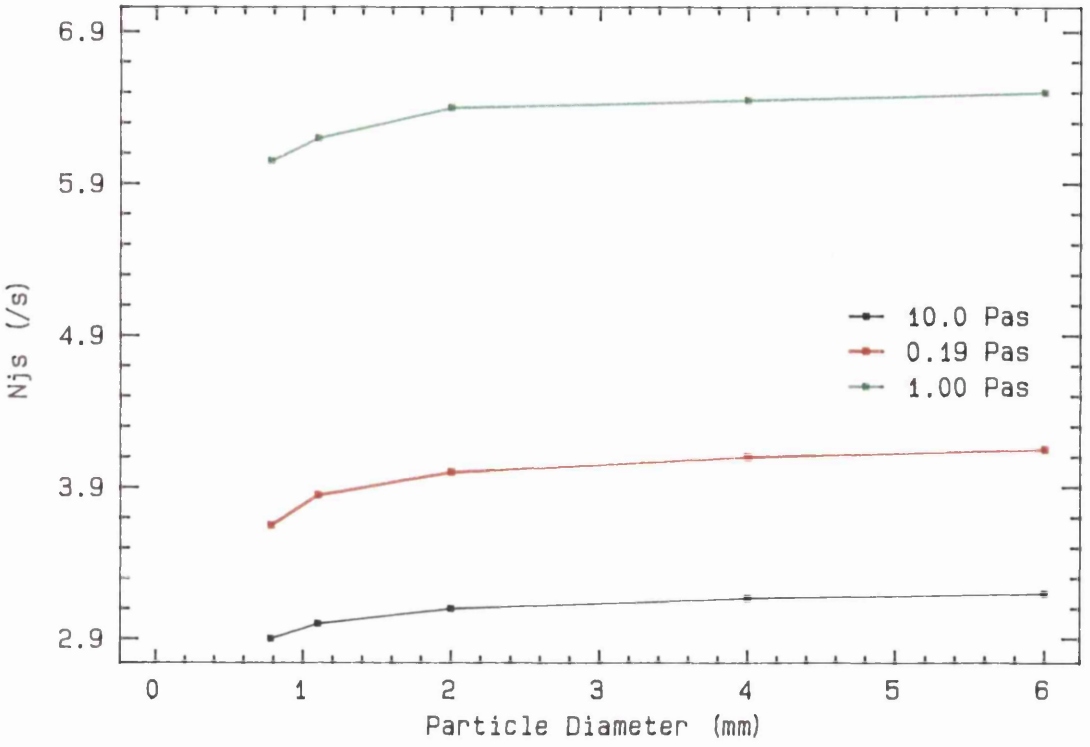

D = 10cm;T = 30cm;ΔZ = 3.6cm; ρ_s = 2900kg/m^3

Figure 5.1.1a
Effect of Particle Diameter
(log/log scales)

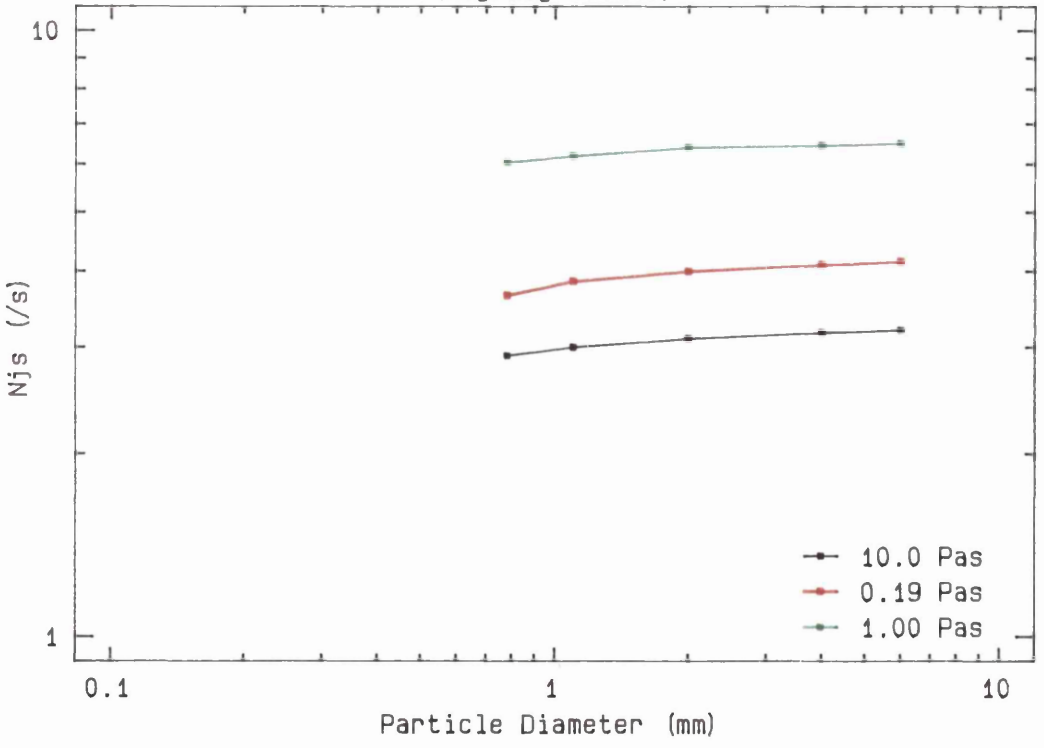

Figure 5.1.2a Effect of Concentration
with CMC & Glycerol/water

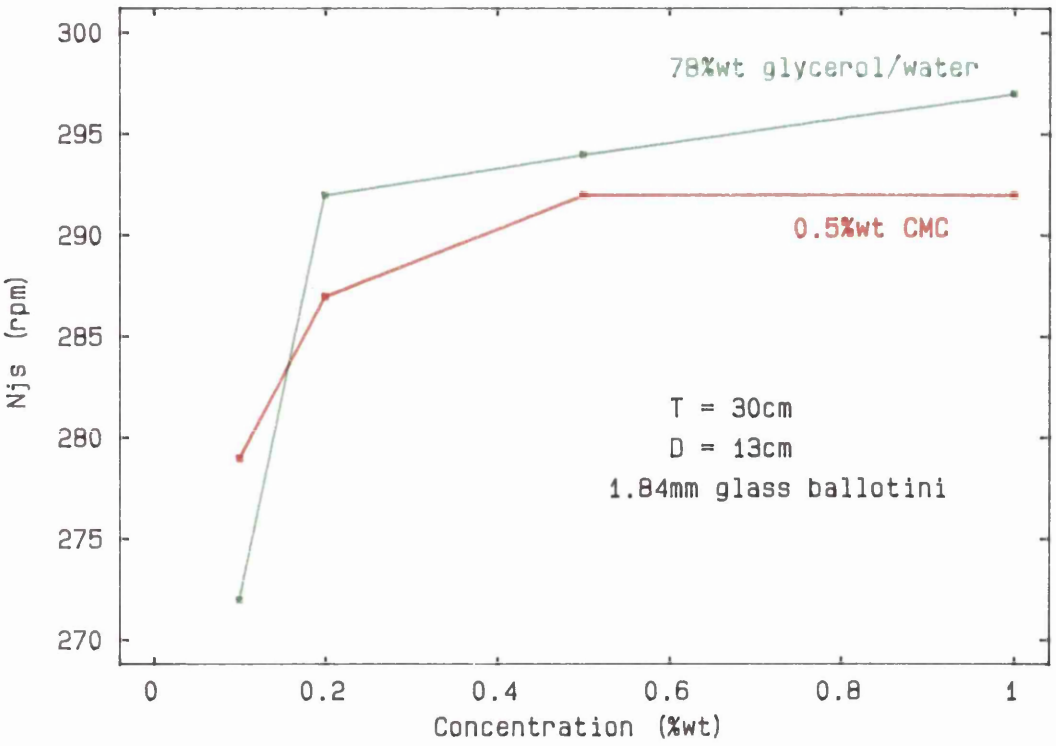

Figure 5.1.2b Effect of Concentration
with Corn Syrup/water Mixture

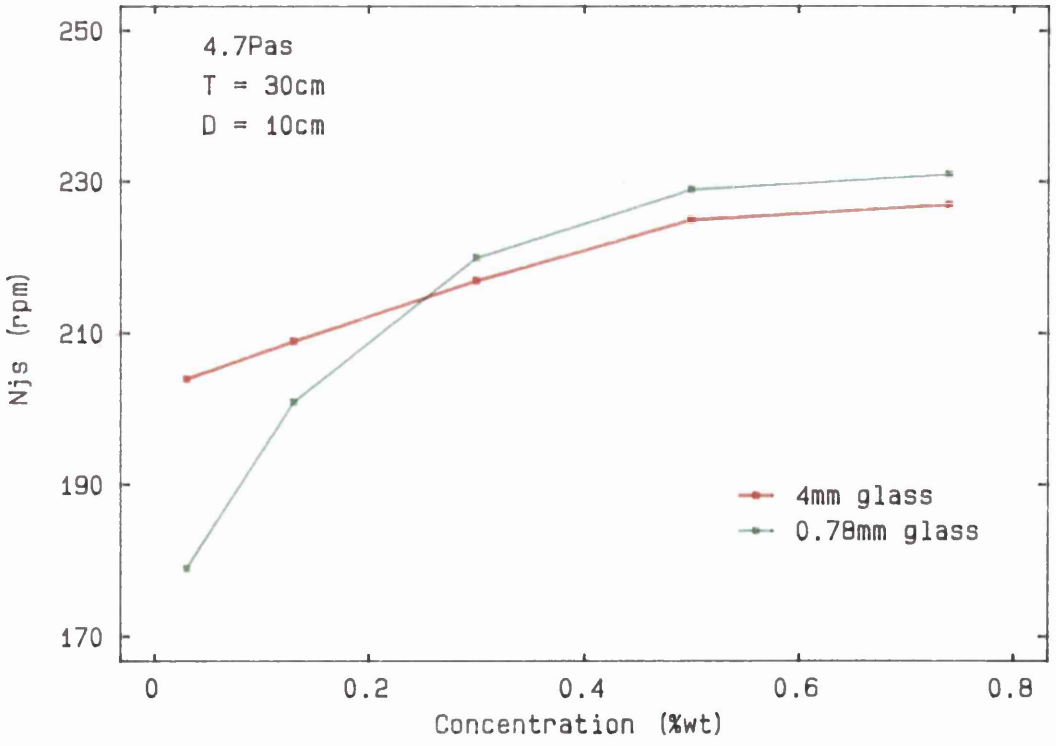

Figure 5.1.3
Effect of Clearance
D=8cm

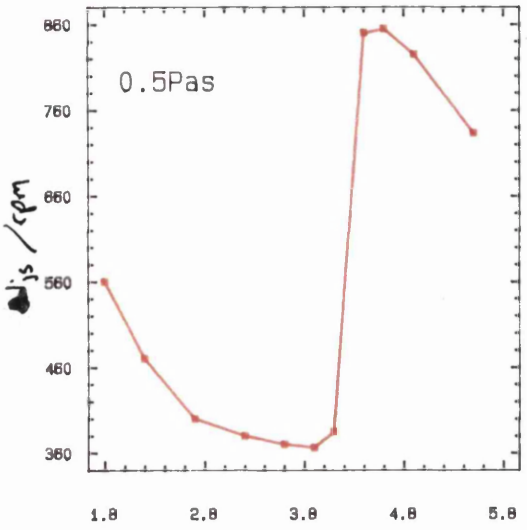

Impeller Clearance/cm

Figure 5.1.4
Effect of Clearance
D=10cm

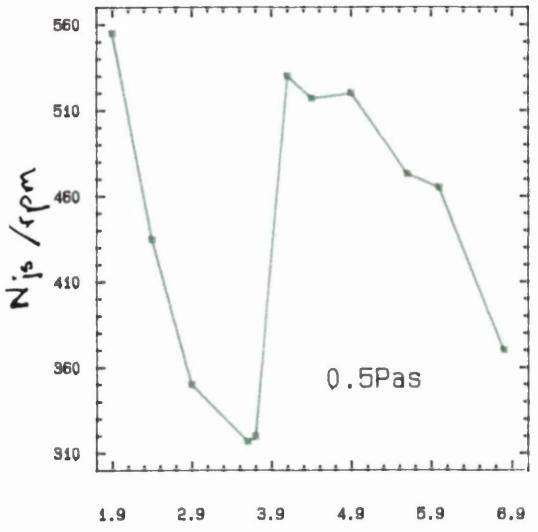

Impeller Clearance/cm

T = 30cm; using a single 6mm glass sphere

Figure 5.1.5
Effect of Clearance
D=13cm

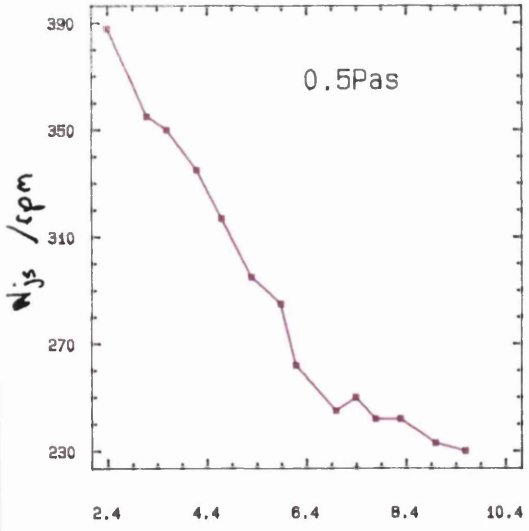

Impeller clearance/cm

Figure 5.1.6
Effect of Clearance
D=16cm

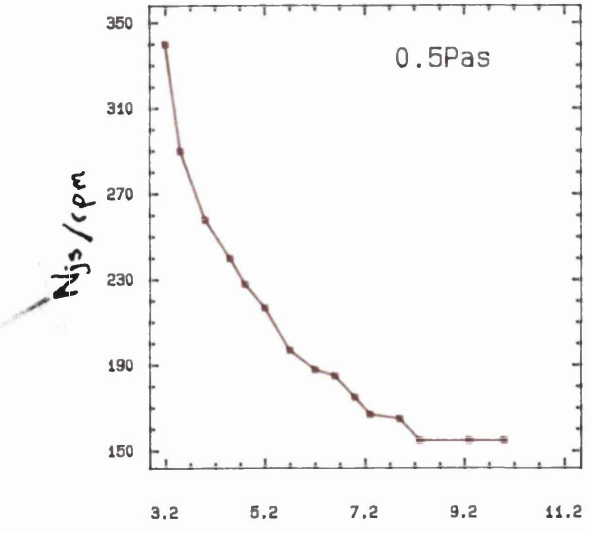

Impeller Clearance/cm

Figure 5.1.7
Effect of Clearance
D=8cm

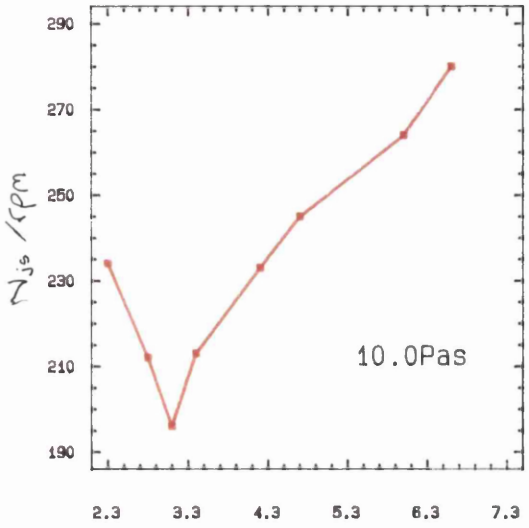

Figure 5.1.8
Effect of Clearance
D=10cm

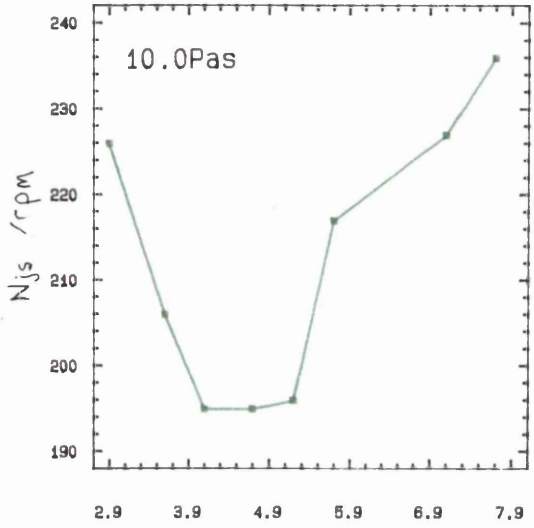

T = 30cm; using a single 6mm glass sphere

Figure 5.1.9
Effect of Clearance
D=13cm

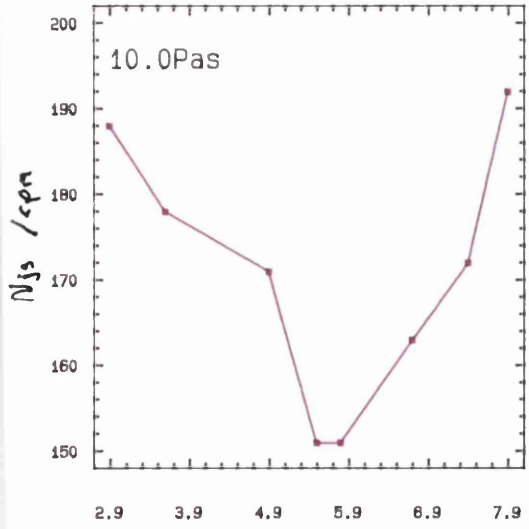

Figure 5.1.10
Effect of Clearance
D=16cm

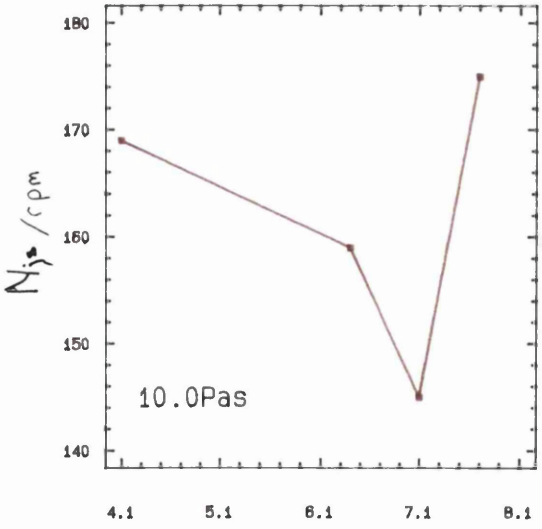

Figure 5.1.11
Effect of Clearance
D=8cm

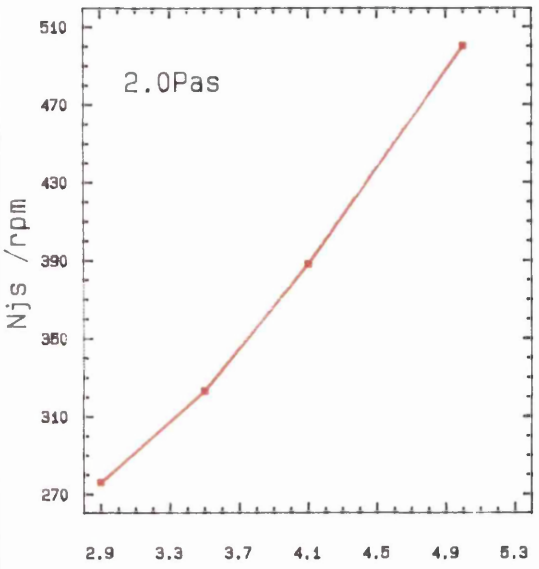

Figure 5.1.12
Effect of Clearance
D=10cm

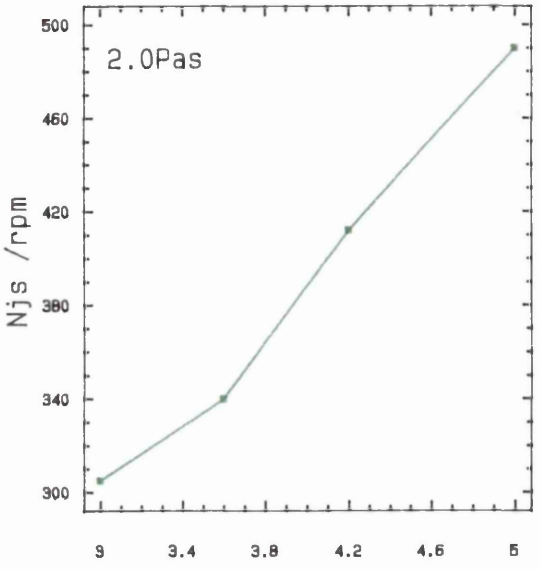

T = 30cm; using a single 6mm glass sphere

Figure 5.1.13
Effect of Clearance
D=13cm

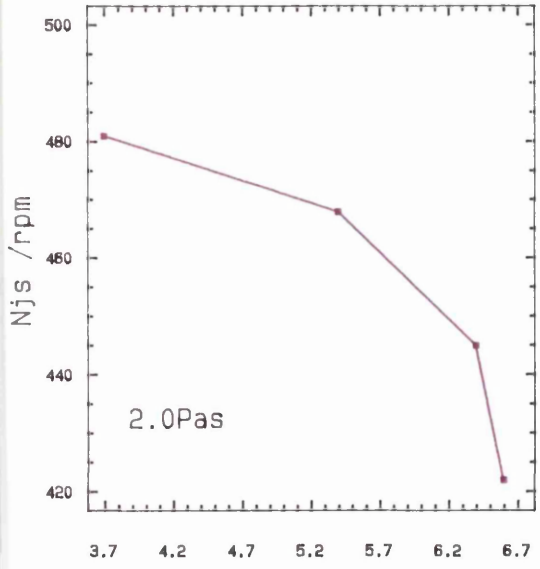

Figure 5.1.14
Effect of Clearance
D=16cm

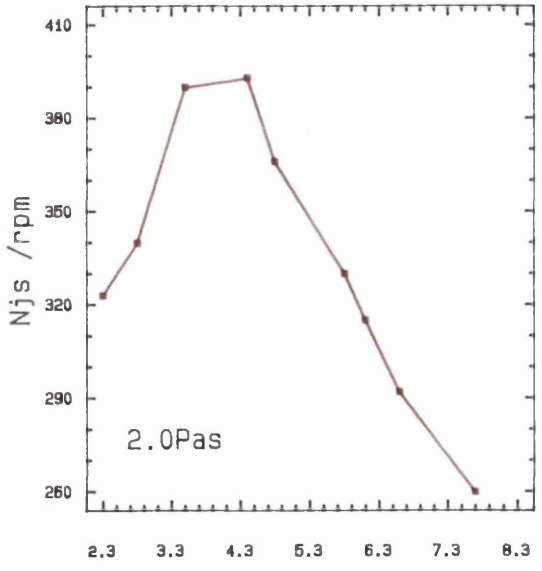

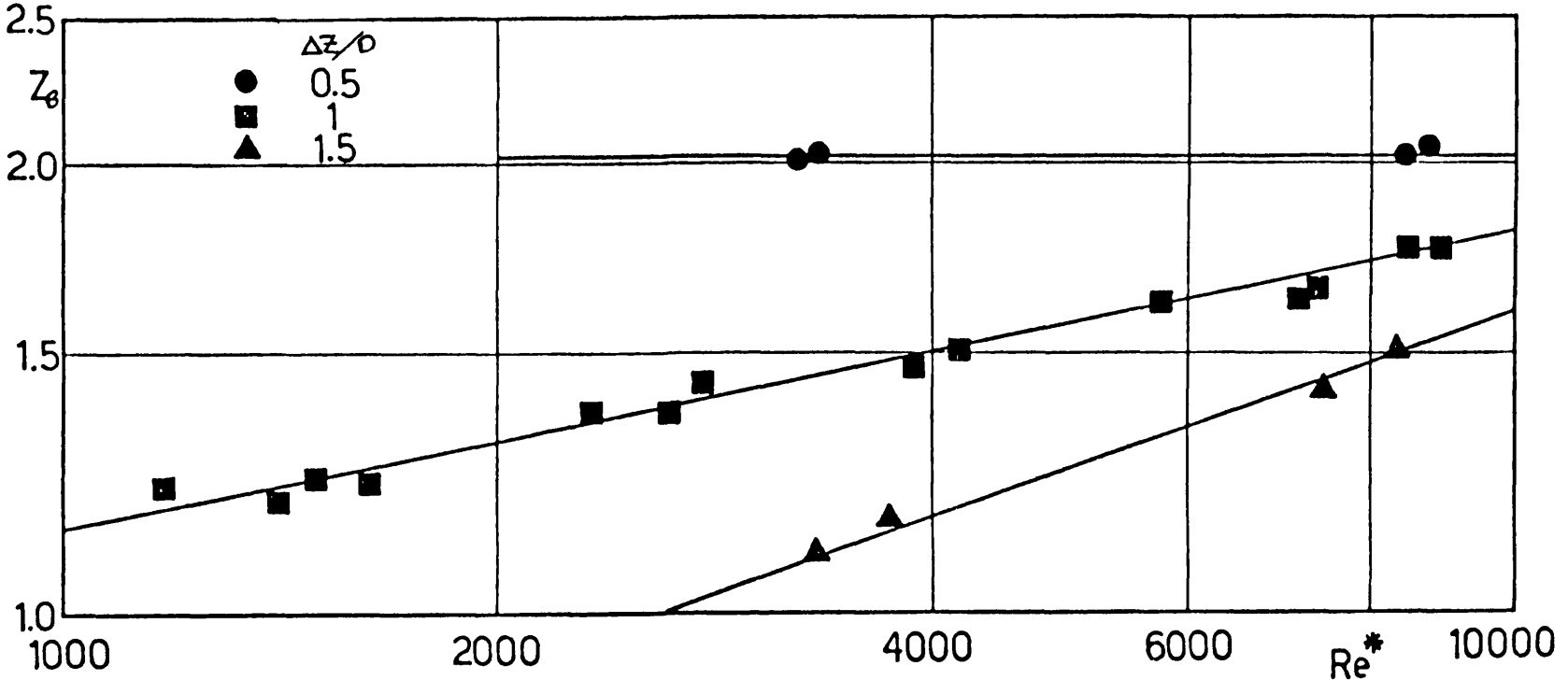

Figure 5.1.15 Variation of Z_B with Re^* at different clearances
(Conti & Baldi, 1978)

Figure 5.1.16a
Interaction of Impeller
Diameter and Clearance

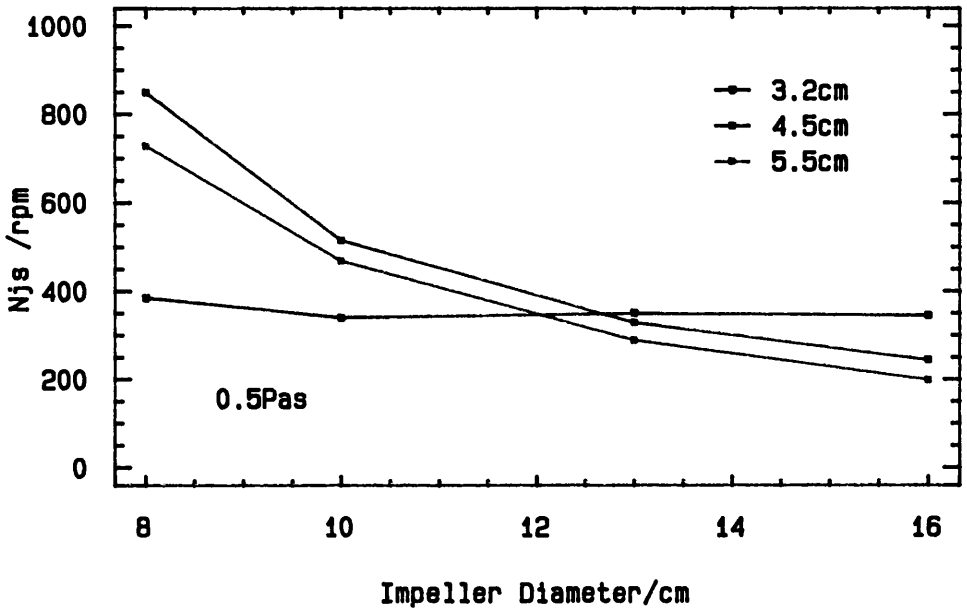

T = 30cm; using a 6mm glass sphere

Figure 5.1.16b
Interaction of Impeller
Diameter and Clearance

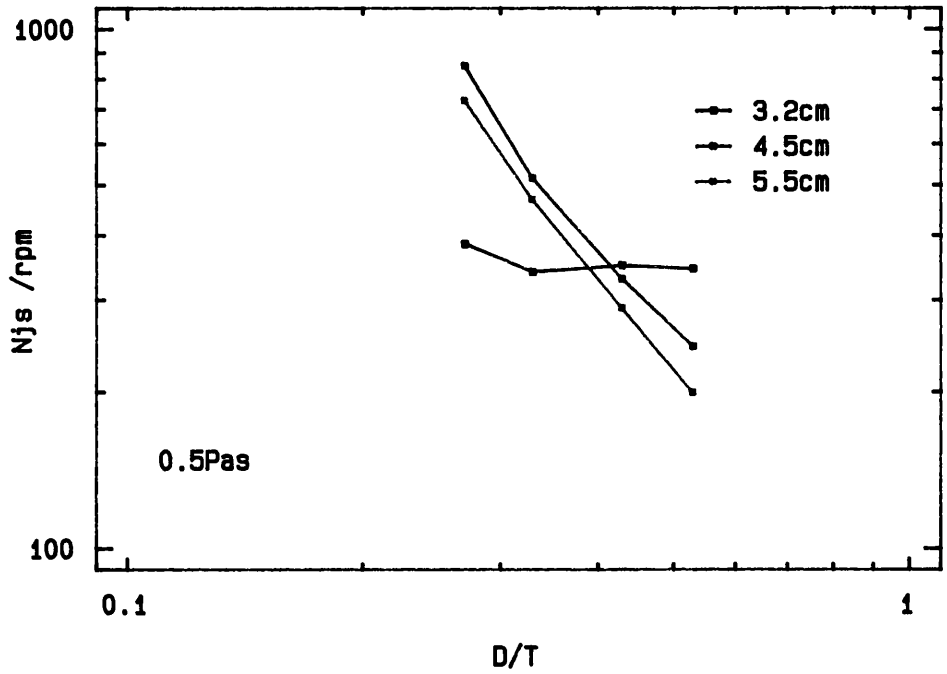

Figure 5.1.17a
Interaction of Impeller
Diameter and Clearance

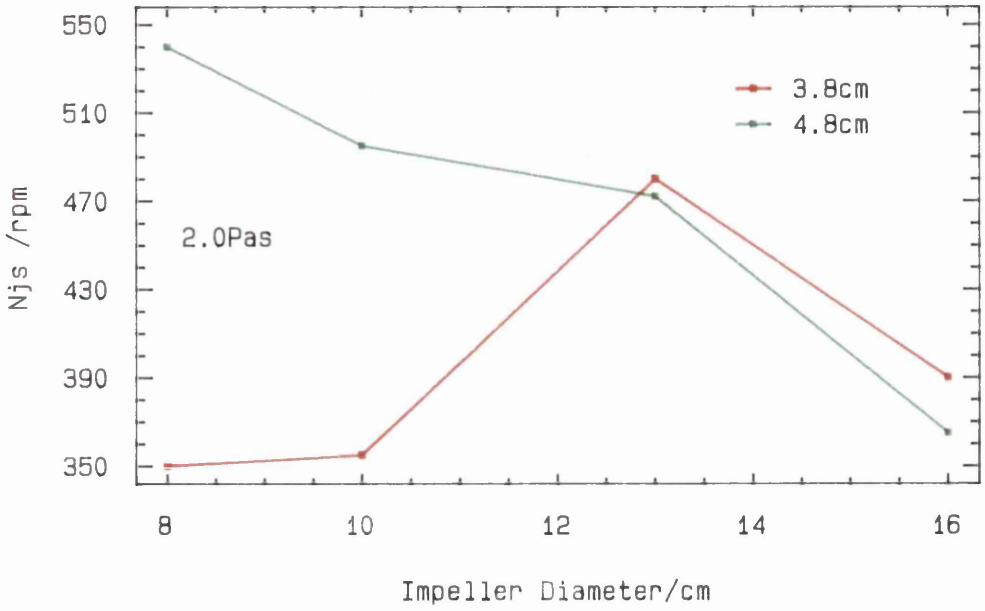

T = 30cm; using a single 6mm glass sphere

Figure 5.1.17b
Interaction of Impeller
Diameter and Clearance

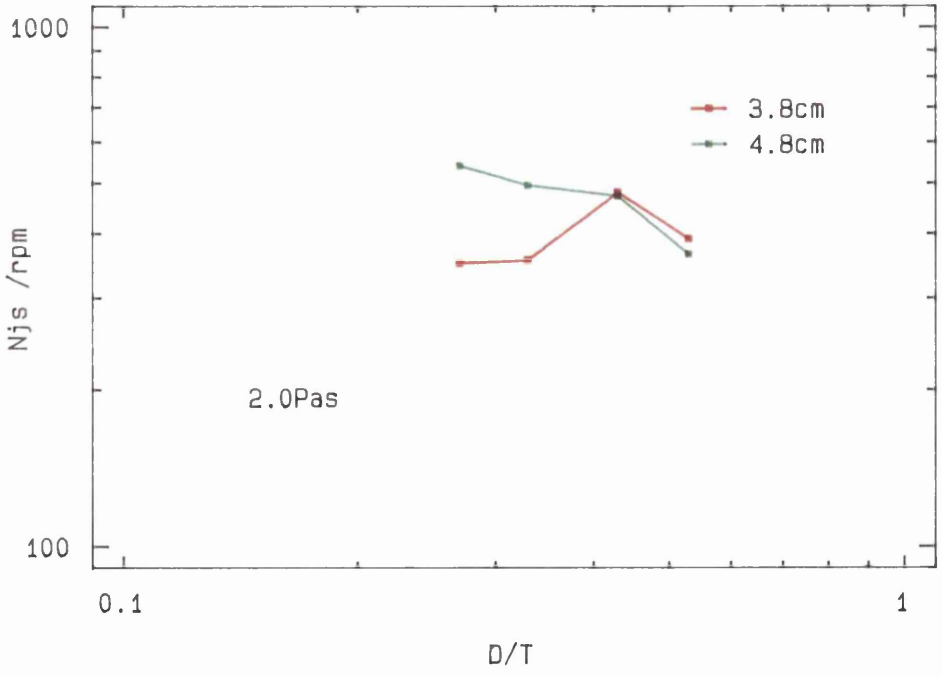

Figure 5.1.18
Interaction of Impeller
Diameter and Clearance

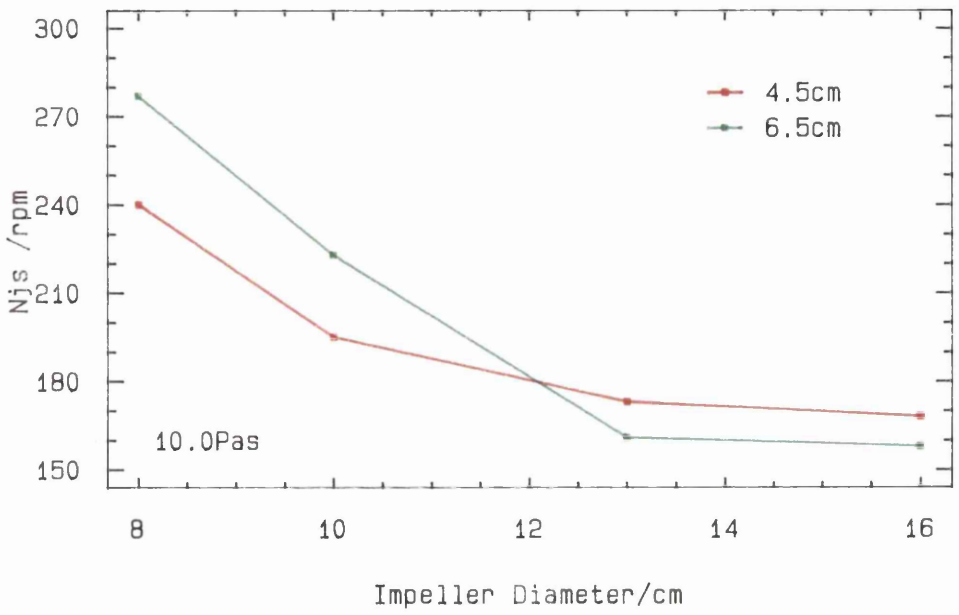

T = 30cm; using a single 6mm glass sphere

Figure 5.1.18
Interaction of Impeller
Diameter and Clearance

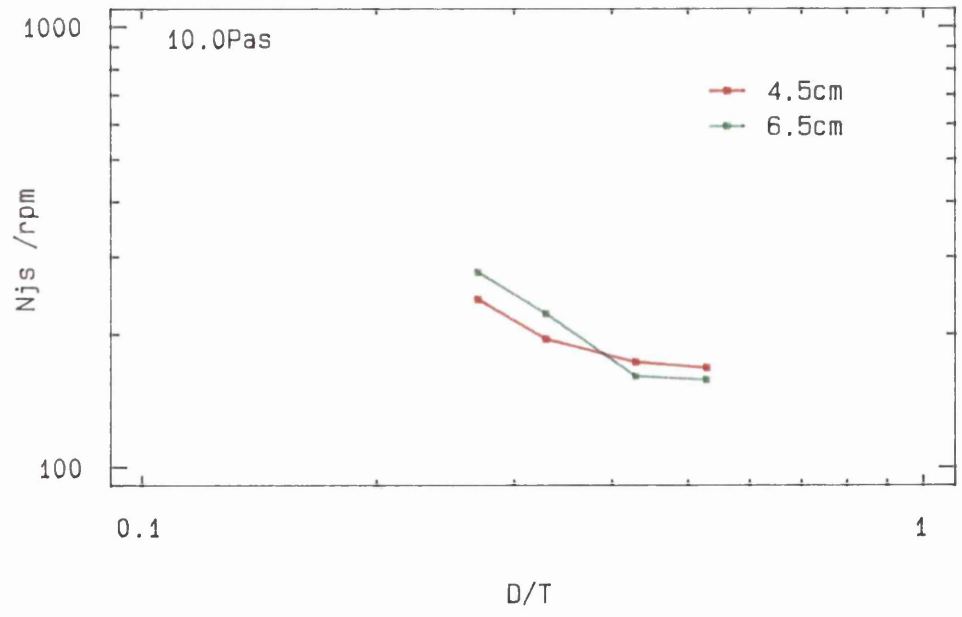

Figure 5.1.19

Plots of Njs vs Impeller Diameter at constant D/T

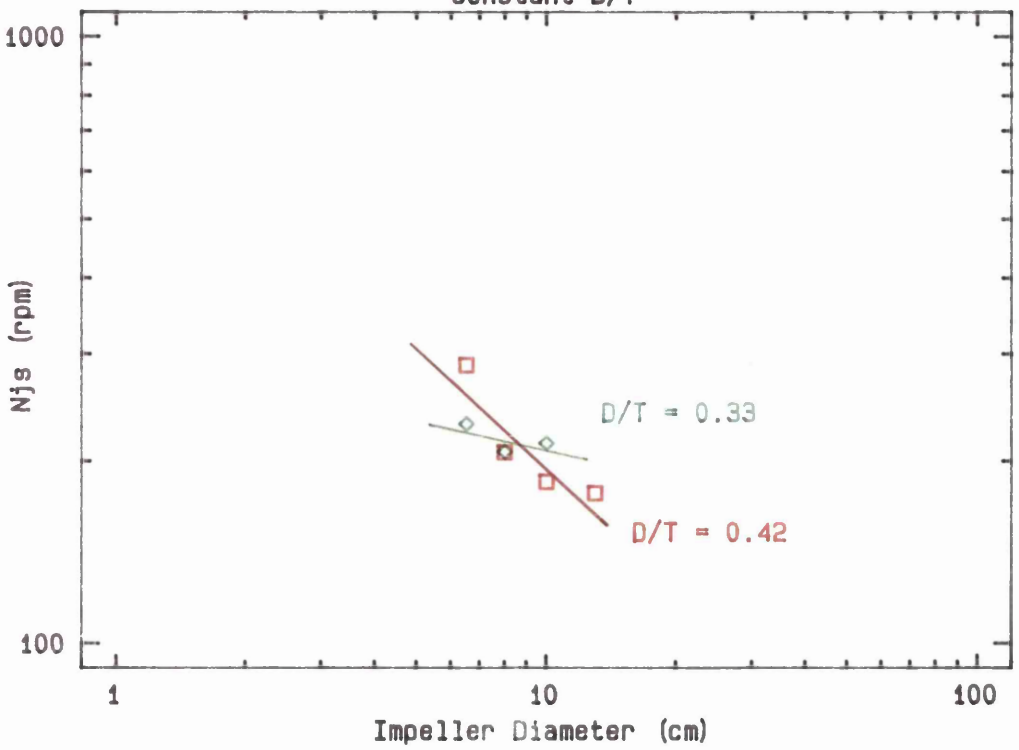

Figure 5.1.20

Plot of Njs vs Density Ratio

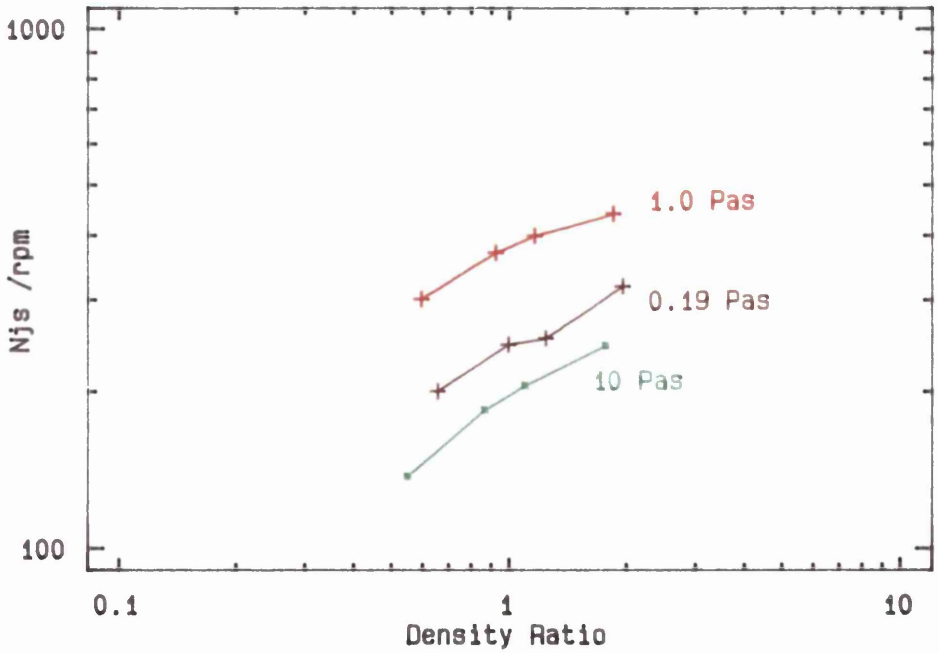

Figure 5.1.21

Effect of Viscosity

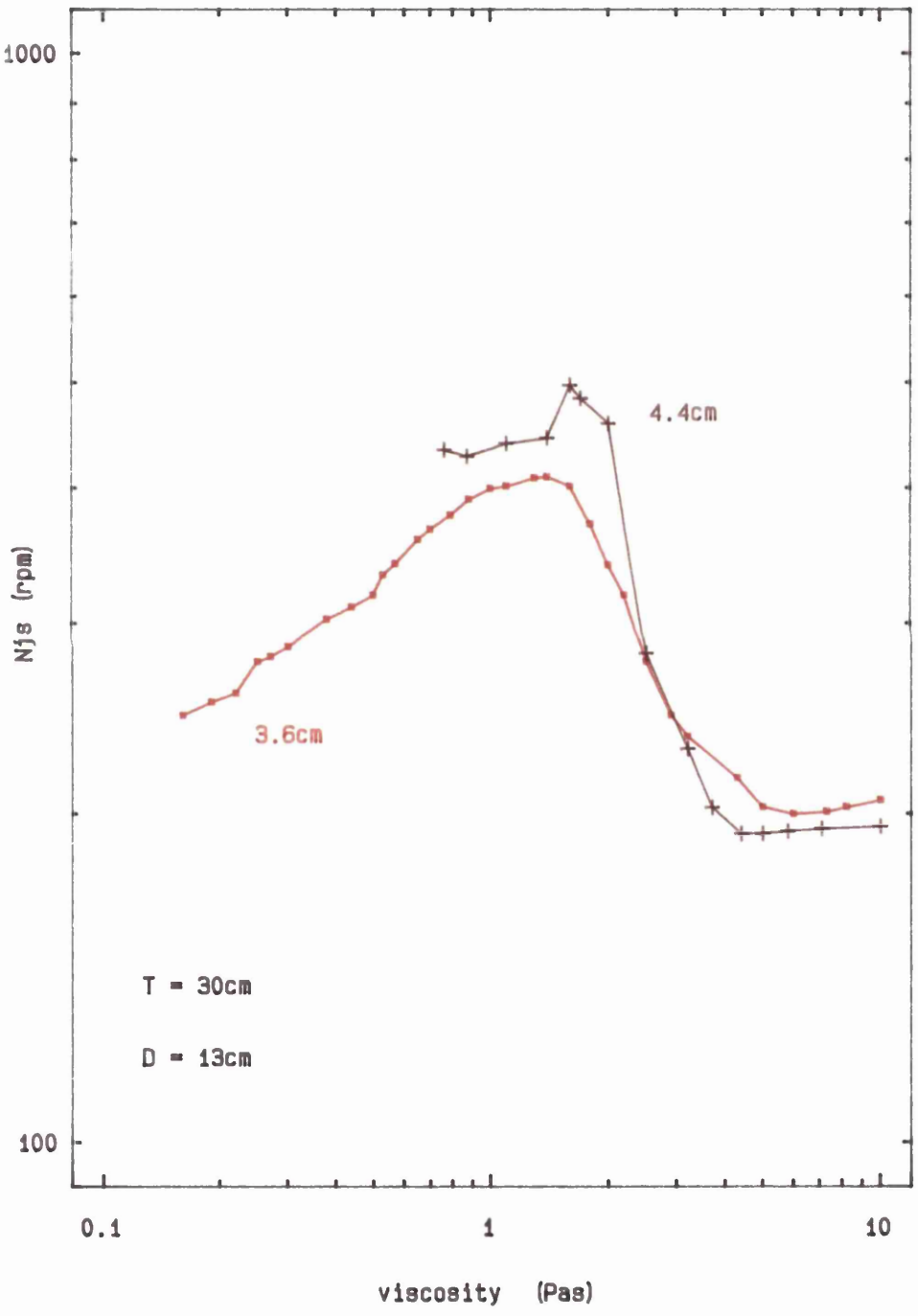

Figure 5.1.22

Plot of $A^2 c_i$ vs (Equivilent) Viscosity

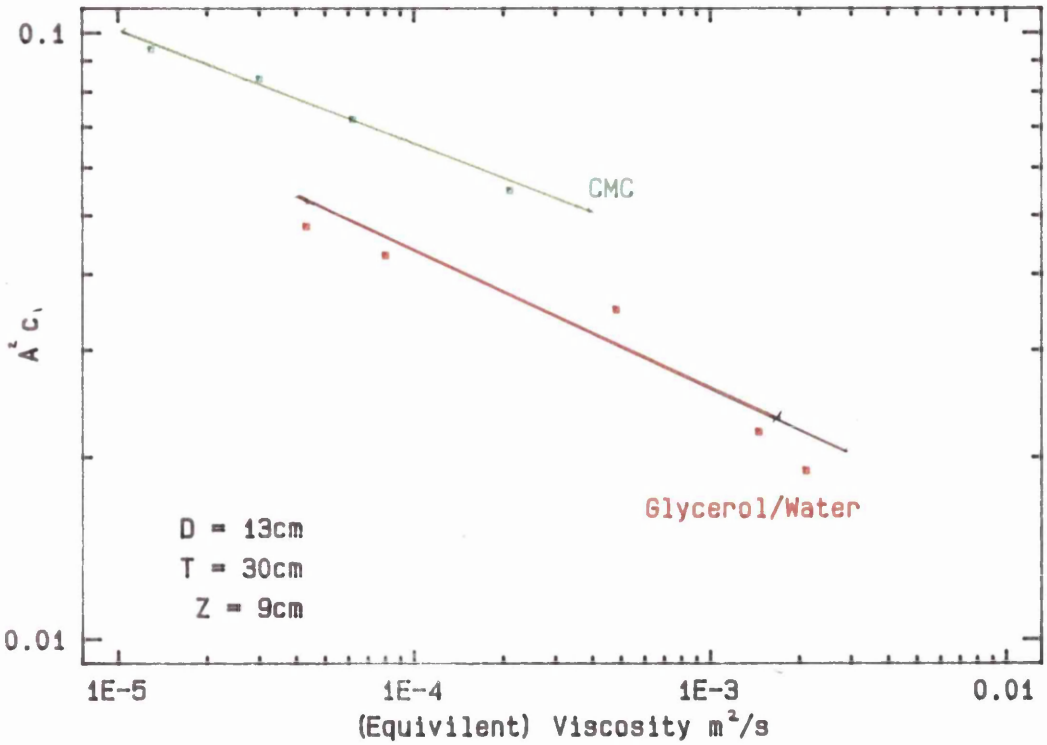

d_p = 1.84mm; C_w = 1.0%wt; ρ_s = 2580kg/m^3

correlation co-efficients:

CMC = 0.972

Glycerol/water = 0.958

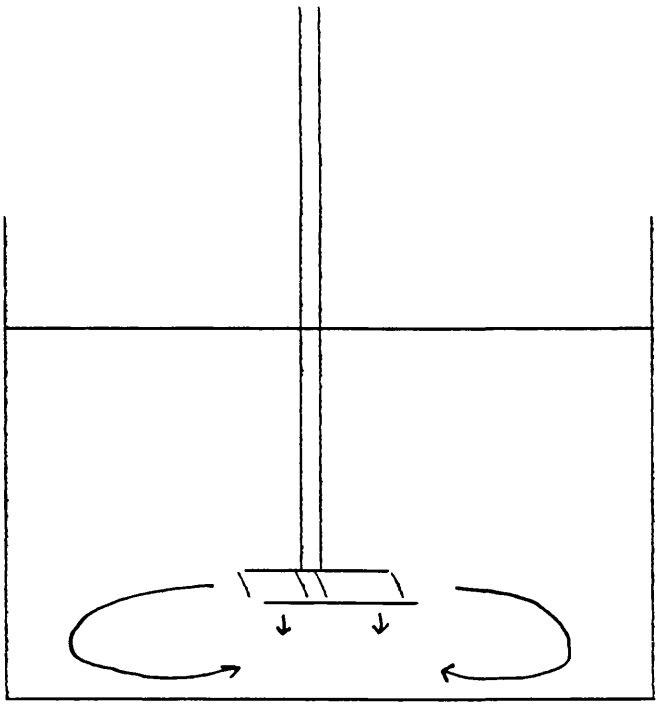

(a)
clockwise
rotation
leading to
"downward"
pumping

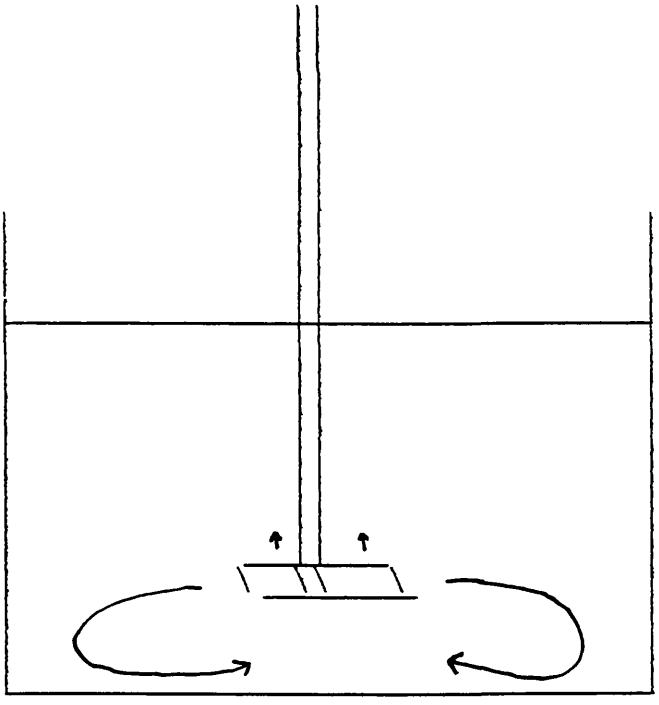

(b)
anticlockwise
rotation
leading to
"upward"
pumping

Figure 5.1.23 Schematic representations of observed flow patterns in viscous liquids

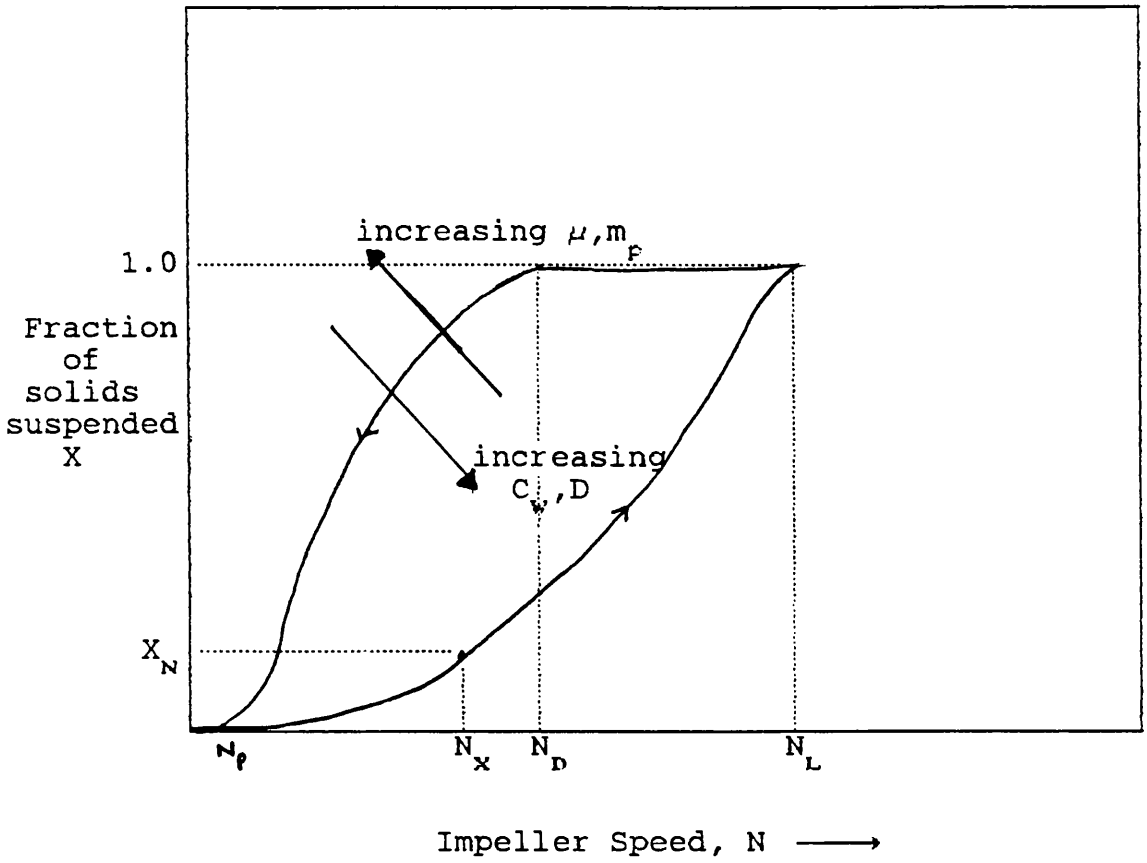

Figure 5.1.24 Graphical representation of hysteresis effect

5.2 Solids Distribution Experiments

a) Local Concentration Profiles

The local solids concentrations were sampled using the laser/photocell arrangement described in Chapter Four. These are average concentrations in an "optical pathlength" described by the beam of the laser light shining from one side of the tank to the photocell on the other side. These concentrations of solids were investigated for different axial and radial positions for a range of impeller speeds. The most significant changes in local concentration, in the bulk of the liquid, were observed to occur in the axial direction, and typically, the laser/photocell assembly is directed so that the beam shines at axial positions halfway between the axis of the tank and the inner wall; the midradial position. Some experiments have been conducted at different radial positions; midradial + or - Δr.

The means by which the voltage output of the photocell was used to calculate the local solids concentration is explained in Appendix 7. All the experimental readings are to be found in Appendix 6.

Some typical concentration vs impeller speed graphs are presented in figures 5.2.1 and 5.2.2. for both the Newtonian glycerol/water mixtures and the non-Newtonian CMC (Carbonyl Methyl Cellulose) solutions.

These graphs all have the same general pattern, see figure 5.2.3. At low speeds (A -> B), hardly any particles are lifted into suspension, but as the impeller speed is increased beyond B, the rate at which particles are suspended rapidly increases. This corresponds to the topmost particles (those resting on top of other particles) being lifted off because of the higher liquid velocities found with increasing distance from the base of the tank. These increased liquid velocities give rise to increased hydrodynamic forces on the particles as described in Chapter Three.

Between B and C, even small increments in impeller speed, N, will lift increasing numbers of particles into

suspension, and also lift them into higher axial positions. At C, there is a rapid falling off in the rate at which the local concentration, C_w, increases with N, especially marked in the case of axial positions below the plane of the impeller. At such axial positions, some researchers (eg. Koutsakos, phD thesis, 1989) reported that at C, there is a small local peak in the concentration, which in turn corresponds to the just suspension condition. Others have also used this point, although not necessarily as a peak, to determine N_{JS} and has been termed the "c-break" criterion (see Chapter Two). However, using this technique for this study usually led to underestimating N_{JS} by about 10 to 15% as compared with visual methods. For most systems investigated, increasing N (to D) beyond N_{JS} did little to increase solids concentrations in the bottom half of the tank, but can cause significant increases in the local concentrations nearer the surface of the liquid and hence improve the overall distribution of solids. Figure 5.2.1. shows local concentration vs impeller speed, N, for a 70%wt glycerol/water mixture of viscosity 0.022 Pa s (about 20 times the viscosity of water). This represents the least viscous of the Newtonian liquids investigated, and the graphs, at different axial positions, conform to "S-curve" described in figure 5.2.3. For axial positions below the impeller, 3 and 7 cm, there is little change in concentration as N is increased beyond N_{JS}. Below the impeller, the local concentrations are above the bulk hold-up concentration of 1%wt. It is interesting to note that that the local concentration goes through a minimum just above the impeller (at 11cm). This must be due to the complex hydrodynamics of the liquid motion, especially at close proximity to the impeller region.

Increasing the viscosity of the liquids leads to a more complex set of concentration vs impeller speed curves. Figures 5.2.4. and 5.2.5. show concentration curves for the same geometry as used for the 70%wt glycerol/water, but this time containing 77%wt and 82%wt glycerol/water mixtures respectively. As the viscosity is increased to 0.044 Pa s, and then 0.077 Pa s, the differences between

the maximum and minimum local concentrations also increase, with the local concentration at 3cm (the maximum) being much higher than the local concentration at 11cm, representing the minimum in the case of 77%wt, and much higher than the concentration at 7cm, representing the minimum for 82%wt glycerol/water. It is interesting to note that the in the case of the 82%wt glycerol/water system, after reaching a minimum at 7cm, the local concentration increases with height so that at 23cm, the local concentration is coming close to reaching the peak concentration recorded at 3cm (see figure 5.2.5.).

For solids suspension in the non-Newtonian liquids, the profiles show greater discontinuities and extremes. Figures 5.2.6. and 5.2.7. show concentration vs impeller speed for CMC solutions (0.25 and 0.50%wt) in the 15cm fully profiled tank, using 1.0%wt 530 μm glass ballotini. Figure 5.2.7. shows concentration vs impeller speed for 0.5%wt CMC, the most non-Newtonian of the three liquids. The data at a height of 14cm is particularly interesting because of the very high concentrations recorded, peaking at 400rpm, at almost twice the average bulk holdup concentration of 1.0%wt. As the impeller speed is increased to N_{JS}, at 440rpm, there is a slight fall in concentration, but when N is increased further to about 500rpm, the local concentration falls dramatically from over 1.6%wt to 0.8%wt. This phenomenon is explained by the formation of a ring of particles which circulate slowly at the periphery of the vessel at a distinct height, between the plane of the impeller and the free surface of the liquid. The ring formation is most accentuated for smaller particles in liquids of increasing pseudo-plastic rheology (see Appendix 1 for more detailed experimental observations).

This ring is a region of very high solids concentration, which increases the average local concentration detected by the photocell along the optical pathlength of the laser. Typically, the ring (see figure 5.2.8). is about 20 particle diameters high and 1 or 2 diameters thick (radially). Referring back to the 14cm curve, the high concentration recorded, with a peak of

1.85%wt at 400rpm, corresponds to the full 9mm width of the laser beam passing through the ring. As the speed is increased above 400rpm, two factors cause the local concentration, at 14cm, to fall. The first is that the plane of the ring rises up the vessel away from the impeller and closer to the liquid surface. Secondly, the increasing speed of the impeller causes the shear rate everywhere in the tank, even at the periphery, to increase, leading to the breaking-up of the ring so that fewer particles are caught within the ring, and those that remain are more widely spaced. This explains the shape of the data collected for the 19cm curve (the next sampling point up) where, at a speed of 580rpm, there is a peak concentration of 1.1%wt. This corresponds to the ring having been raised to that height at 580rpm. However, the peak is much less than before because of the consequence of increasing the impeller speed. Instead of so many particles being trapped in the ring, they are better distributed within the bulk of the liquid.

Figures 5.2.2. and 5.2.6. show the concentration vs impeller speed for 0.20 and 0.25%wt CMC solutions respectively. A similar pattern of peaks is also shown by these graphs, but they are less pronounced than in figure 5.2.7.

Figure 5.2.9. shows the concentration profiles for the three non-Newtonian liquids at just suspension speed conditions. There is a marked contrast between these profiles and those for the Newtonian liquids, shown in figure 5.2.10. Whereas the Newtonian profiles are characterized by troughs, at either 7 or 11 cm; the non-Newtonian profile are characterized by sharp peaks at either 11 or 14 cm.

As mentioned before, these peaks diminish as the impeller speed is increased beyond N_{JS}. Figure 5.2.11. shows the CMC concentration profiles at (about) 1.5 N_{JS}. The most obvious difference between the two sets of profiles (figures 5.2.11 and 5.2.9) is the lack of such sharp peaks at the higher speeds, and the more even distribution of solids with height, especially between 3 to

19cm. The maximum concentrations appear near the top of the liquid.

For the Newtonian liquids at $1.5N_{JS}$, comparison of figures 5.2.12 with 5.2.10. at N_{JS} show little in the way of obvious qualitative differences, although quantitatively, the profiles have become more uniform and closer to the bulk average concentration of 1.0%wt. Inspection of figure 5.2.11., for the CMC solutions, shows that nearly all the local concentrations are below 1.0%wt so that the average appears to be about 0.75%wt instead of the expected average of 1.0%wt. This can be explained by the large numbers of particles that are to be found on the sides of the cone, even at high impeller speeds. In the pseudo-plastic CMC solutions, the liquid velocities are likely to be low near the cone so that the particles will also be moving slowly. Whereas for the glycerol/water mixtures, the particles move more quickly at the base. It should be remembered that the just suspension speed is defined in this study as the minimum impeller speed required to lift a particle directly from the base without that particle requiring the aid of other particles on which to climb on to prior to lift off.

b) Quality of Mixing for Suspensions - the Mixing Co-efficient

Previous discussion 5.2.a has dealt with the variation of local solids concentration at different positions within a fully profiled vessel at a range of impeller speeds for different Newtonian and non-Newtonian liquids. Examination of the concentration profiles in figures 5.2.9. to 5.2.12 can give a qualitative indication of how uniform (or how close to homogeneity) the solids distribution is in different parts of the tank. Unfortunately, a generally agreed means of quantifying the degree of homogeneity does not exist (see Chapter Two).

However, for the purposes of this study, a modified version of the mixing co-efficient proposed by Bohnet & Niesmak, 1980, has been employed to compare one system with another in order to discuss the performance of that system with regard to how well distributed the solids are. Bohnet & Niesmak, and more recently Barresi & Baldi, 1987, used the standard deviation, σ , of the concentration profile to determine the quality of the suspension:

$$\sigma = \frac{1}{n}\sum_{h=1}^{h=n} \sqrt{\left(\frac{C_h - C_w}{C_w}\right)^2} \qquad 5.2.1$$

so that if the suspension were perfectly uniform (a situation which almost impossible to achieve), then $\sigma = 0$, since for all i, $C_h = C_w$. This means that $1-\sigma$ can be defined as the mixing co-efficient, M_c, on a scale of 0, when all the solids are at rest at the bottom of the tank, to 1, representing the ideal case of homogeneity.

The geometry of the fully profiled vessel, together with the laser/photocell sampling technique means that equation 5.2.1. has to be modified so that local concentration measurements in the hemispheric base section of the vessel are given less weighting than measurements in the cylindrical section. This is because the optical pathlength, OPL, is shorter in the hemisphere than in the

cylinder, and correspondingly the "optical pathvolume", OPV, will be less.

$$OPV = \frac{\Pi\, d_b^2}{4} OPL \qquad 5.2.2$$

where d_b is the diameter of the laser beam (9mm). If the OPV is smaller, then the corresponding concentration sample will be less representative than samples taken when the OPV is larger, and should therefore be given less weighting. This argument applies to different radial as well as axial positions through which the laser beam is directed.

For a given radial position (typically mid-radial), the different axial sampling points describe a "slice" through the tank d_b wide. This slice is itself divided by the optical pathlengths and volumes as shown in figure 5.2.13. The average local concentrations at h_1 to h_6 (or h_7) have been measured by the laser/photocell arrangement. The average concentration in volume (1), C_{V1} can be estimated by:

$$\frac{C_{h1} OPV_{h1} + \left(\hat{C}_{h1} OPV_{h1} + \hat{C}_{h2} OPV_{h2}\right)}{\left(OPV_{h1} + OPV_{h2}\right)} = C_{V1} \qquad 5.2.3$$

where C_{V1} is calculated from a volume weighted average of the local concentrations that bound volume (1); i.e. from C_{h1} and C_{h2}. This process can be continued up the vessel to the liquid surface, at h_L, where the particle concentration is assumed to be zero. Each of these 7 weighted average concentrations within the slice cover different volumes, V_i, depending on the spacing of the sampling heights and the local geometry.

The standard deviation, σ, can now be calculated from:

$$\sigma = \frac{1}{nV_T}\sum_{i=1}^{i=n} \sqrt{\left(\frac{C_{wi} - C_w}{C_w}\right)^2}\ V_i \qquad 5.2.4$$

where V_T is the total volume of the slice

To facilitate the calculation of σ and hence M_c, a BASIC computer program, MYMIX, has been written which calculates σ for a fully profiled vessel, after inputting the dimensions of the tank and the sampling heights, with the corresponding local concentrations (see Appendix 8 for algorithm and program listing). The following results and discussion in 5.2.c to f are based on comparisons of M_c vs an independent parameter such as impeller speed or power consumption, to show quantitatively, as well as qualitatively, the effects described in the subsection titles 5.2.c to f.

Figures 5.2.14. and 5.2.15. show concentration vs impeller speed, and concentration profiles respectively for 530 μm glass ballotini in 77%wt glycerol/water. The three curves in each figure represent the effect of the radial variation in sampling position. At a position signified by midradial -3.5cm, the laser is directed 3.5cm closer to the central axis of the tank, and at midradial +3.5cm, the beam is directed 3.5cm closer to the walls of the tank. These figures show that, at a given axial position, there is a distinct radial variation in concentration. The local concentration increases with radial distance from the central axis of the tank. The midradial curve comes closer to the midradial -3.5cm values than +3.5cm. Since the volume of the -3.5cm slice will be greater than the +3.5cm slice, a volume-weighted average of these two curves will co-incide very closely to the midradial curve. This gives the the justification for using the midradial position as being sufficiently representative of the radially averaged concentration at any given axial position (see Appendix 6 for more data at different radial positions).

For greater accuracy in calculating M_c for a given agitation system, data at all three radial positions should

be used. Each radial position has six sampling heights which describe the "slice". The M_c values from each of the three slices can then be given a volumetric weighting to give a M_c value for the whole tank. Just as when conducting any statistical survey, if more samples are taken, then a more accurate value of M_c will emerge.

c) Effect of Viscosity and non-Newtonianness

One way to show the effect of viscosity (and non-Newtonianness) on the solids distribution is to plot the Mixing Co-efficient, M_c, against impeller speed, N. Figures 5.2.16. and 5.2.17 show such a plot for six liquids containing the same bulk hold-up concentrations, C_w, of 530 μm glass ballotini (1%wt), in a 15cm diameter Fully Profiled Vessel (FPV). Comparison of the graphs shows that the more viscous the liquid, then the worse will be the distribution of solids.

All six plots show the same general trend; at speeds of about 0.75 N_{JS}, M_c suddenly begins to improve with increasing N. This increase in M_c continues slightly beyond N_{JS} before reaching an almost constant plateau value. As might be expected, the N_{JS} values increase with viscosity of liquid.

The 0.5%wt CMC data shows a more erratic plot than the others. This can be explained by the more significant presence of a ring of particles at a distinct level between the the plane of the impeller and the liquid surface (as previously discussed in 5.2.a). The other two CMC plots show less erratic behavior because they contain less CMC and are therefore less pseudo-plastic, although they still display ring formation.

Another way in which to examine the effect of viscosity is to plot M_c as a function of the power consumption of the impeller. Although the power was not measured at the time of these particular experiments, the power consumption can still be accurately estimated from an appropriate Power Number vs. Reynolds Number curve. For

both FPVs used (of diameters 15cm or 29cm), the ratio of impeller to tank diameter, D/T, was kept at 0.57. Power curves have been found for a 30cm flat-bottomed unbaffled tank with 8, 10, 13, and 16.5cm six-bladed pitched turbines (figure A2.4). Assuming that the 16.5cm power curve can be used as a close approximation, where D/T = 0.55, then at a given Re, Po can be determined and the power consumption calculated. For the non-Newtonian liquids, the Reynolds Number can be estimated by using the method suggested by Metzner & Otto, 1958. The average (or effective) shear rate, $\dot{\gamma}_{av}$, is assumed to be proportional to the impeller speed

$$\text{i.e.} \quad \dot{\gamma}_{av} = k_s N \qquad 5.2.6$$

For "small" impellers, k_s can be taken to be 13. Knowing $\dot{\gamma}_{av}$, the average (or effective) viscosity can be calculated for a power law fluid.

$$\mu_{av} = k\,\dot{\gamma}_{av}^{n-1} \qquad 5.2.7$$

substituting for $\dot{\gamma}_{av}$ from 5.2.6. then

$$\mu_{av} = k(k_s N)^{n-1} \qquad 5.2.8$$

This value of μ_{av} can then be used to calculate the Reynolds Number.

$$Re = \frac{\rho_f D^2 N}{k(k_s N)^{n-1}} = \frac{\rho_f D^2 N^{2-n}}{k\,13^{n-1}} \qquad 5.2.9$$

When the liquid is Newtonian, n = 1 and equation 5.2.9. reverts back to the usual expression for Re.

The graphs shown in figures 5.2.18. and 5.2.19 show M_c as a function of power consumed by the impeller for the same six liquids used for the graphs presented in figures 5.2.16 and 5.2.17. The shape of the graphs in figures 5.2.16 and 5.2.17 are similar to those shown in figures 5.2.18 and 5.2.19. Again the 0.50%wt CMC plot shows the most erratic curve, but generally it can be seen that as

the power consumption is increased (by increasing the impeller speed), the quality of mixing improves rapidly at first, then settles at a nearly constant value. Taking the Newtonian liquids as a group, the plateau value for the 70%wt glycerol/water is higher than the 77%wt which in turn is higher than the 82%wt. All the plateaux for the Newtonian liquids are higher than all of the non-Newtonian liquids. This is in spite of average viscosities for the 0.20 and 0.25%wt CMC solutions being lower, at this range of impeller speeds, than the 77%wt and 82%wt glycerol/water mixtures. Figure 5.2.20 shows plots of the plateau values for M_c against viscosity, or effective viscosity. For the non-Newtonian liquids, the viscosity is calculated at an average shear rate corresponding to the impeller speed when the plateau is first attained (taken to be at or sufficiently close to N_{JS}).

It can be seen that even at the same "effective" viscosity, the solids distributions in the CMC solutions are poorer than in the corresponding Newtonian liquids. The difference may be partially explained by the higher density differences for the non-Newtonian liquids (between the glass and the surrounding liquid), but it seems clear that the most important difference is the "non-Newtonianness" of the fluid, and in particular, by the effect of the local shear rate on the local viscosity. The concept of the effective viscosity may only have validity in the immediate vicinity of the fast moving impeller region. However, with pseudo-plastic fluids such as CMC, the viscosity at the peripheral regions of the tank will be greater because the local shear rates will be considerably lower than at the impeller. The rings of suspended solids, mentioned earlier, are trapped within such a slow moving region of the tank where the viscosity is high leading to slow terminal settling velocities. This combined with upward motion of liquid at the walls above the plane of the impeller will counteract the downward force of gravity on the particles. The force of gravity is not completely balanced and some particles do settle from the ring back to the base of the tank, and are subsequently resuspended.

However, some particles from the bulk of the liquid are thrown outwards to the walls of the tank and join the ring. At steady state, an equilibrium is set up between the rate at which particles drop out of suspension and the rate at which particles join the ring from the bulk. For more detailed experimental observations concerning ring formation see Appendix 1.

d) Effect of Particle Size

Experiments were only conducted with glass ballotini of two diameters, 530μm and 1100μm. The densities of the two are identical; 2900kg/m^3.

Figure 5.2.21 shows a graph of mixing co-efficient, M_c, vs impeller speed, N, for the two sizes of ballotini in the 15cm FPV containing 77%wt glycerol. Although the just suspension speed, N_{JS}, for the 1100 μm ballotini is only slightly higher (280rpm) than for the 530 μm (240rpm), there is a significant difference in the quality of mixing. At these N_{JS} values, the M_c values for the 530 μm ballotini at the just suspension condition is about 0.84 whilst for the 1100 μm, the corresponding M_c is only about 0.48. Thereafter, the difference between the two curves narrows, but at their respective plateau values, the 530 μm particles have a value of 0.86 and for the 1100 μm, a value of 0.64.

This difference in the quality of mixing is not unexpected since the effect of increasing the particle diameter is to also increase the the mass of the particle and hence the settling velocity of the suspended solids. For the 0.25%wt CMC solution (figure 5.2.22), the 530 μm curve is initially higher but then at 400 rpm, the two curves merge together. The most plausible explanation for the narrower differences found in the CMC system maybe connected to the ring formation reported earlier. These rings distort the local concentrations of particles, causing sharp peaks and troughs in the concentration profile, which in turn lead to poorer solids distribution. When the size of the particles is increased,

the settling velocity of the particles increases so that particles sink back to the bottom more readily, but also fewer particles are entrained with the ring. The diminishing of ring formation helps to mitigate the effect of increased settling velocity. In the case of the 15cm FPV, the two effects seem to exactly balance each other. This would agree with the observation that ring formation is more important in smaller vessels.

e) Effect of Impeller Type and Clearance

For most of the solids suspension and distribution experiments, the agitation was provided by a six-bladed 45 degree pitched turbine. However, for the purposes of comparison, a 15cm three-bladed propeller (pumping upwards) was used to provide agitation in the 29cm FPV. This was done for 1100 μm ballotini in 77%wt glycerol/water and then in 0.25%wt CMC. (Pumping downwards still gave rise to particles migrating to the central cone prior to suspension).

Figure 5.2.23. shows a graph of M_c vs N for the two impeller types. The just suspension speed for the 16.5cm six-bladed turbine is 200 rpm, which is lower than than that for the propeller, 260 rpm. This does not mean that the pitched turbine is more efficient than the propeller since the power number and hence the power consumption is higher than that of a propeller at a given Reynolds Number.

For the range of impeller speeds considered, the six-bladed turbine has a better distribution of solids. At the N_{JS} values, the corresponding M_c for the turbine is about 0.5, whilst for the propeller, about 0.35. As the speed is increased further beyond N_{JS}, the M_c curve for the turbine appears to improve only slightly reaching a plateau of about 0.55-0.60, whilst the M_c curve for the propeller shows a faster rate of improvement with increasing N; and may well overtake the turbine's M_c curve if the speed is increased sufficiently (somewhere around 400 rpm).

Unfortunately, with the (mainly) unbaffled systems

considered for experimentation, increasing the impeller speed beyond those shown on the graph would have resulted in an unacceptably high degree of vortexing, leading to possible aeration as the nadir of the vortex reaches to the plane of the impeller. Vortexing also causes distortions near to the free surface of the liquid so that the laser/photocell cannot be used to gather local solids concentrations near to the top of the liquid.

Figure 5.2.24. shows the quality of mixing for a non-Newtonian liquid, 0.25%wt CMC. As before, with the glycerol/water mixture, agitation with the turbine leads to a lower N_{JS} value (200 rpm vs 240rpm) and a higher M_c value of about 0.51 compared with 0.44 for the propeller. The gap between the two curves is narrower than for a Newtonian liquid and this can be explained by the observation that ring formation is more inhibited with the propeller compared with the turbine. As previously explained, the formation of rings is associated with poorer solids distribution.

Figure 5.2.25. shows a comparison of M_c vs N for two impeller clearances in 0.25%wt CMC using the 16.5cm turbine. The N_{JS} value for the lower clearance of 9.0cm is less than that of the 15.5cm clearance; 180 vs 220 rpm. At these conditions, there is little difference in the solids distribution, even beyond the just suspension condition the difference between the two curves is small.

f) Effect of Baffles and Tank Size

Figure 5.2.26 shows graphs of the mixing co-efficient, M_c, vs impeller speed, N, for unbaffled and baffled agitation in a FPV containing 77%wt glycerol/water and 1%wt of 530 μm glass ballotini. The just suspension speed, N_{JS}, for the unbaffled system is only 180 rpm compared with 280 rpm for the baffled vessel. This represents a 56% increase in N_{JS} because of the baffles. At the N_{JS} conditions for the two systems, M_c for the unbaffled vessel is better, about 0.70, than the baffled, 0.63. At higher speeds, it may be that the M_c for the baffled system will approach the M_c curve for the unbaffled system. However, for the range of impeller speeds covered, the data collected would seem to show that adding baffles not only hinders the just suspension speed (as discussed earlier in 5.1.g), but also leads to a poorer solids distribution in such liquids as 77%wt glycerol/water, over one order of magnitude more viscous than water (0.044 Pas compared to 0.001 Pas). This is in direct contrast with the situation for liquids with similar viscosities to water, where the addition of baffles is always recommended both to lower N_{JS} and to improve solids distribution. However, such recommendations do not seem based on any systematic comparison of baffled and unbaffled systems. From the point of view of practicality, it is often very difficult to perform suspension experiments with unbaffled vessels containing water because agitation causes such a high degree of vortexing that the nadir of the vortex reaches the plane of the impeller before the impeller speed has been increased to N_{JS}, so that N_{JS} cannot be determined. When the vortex reaches down to the plane of the impeller, there are two problems; one is that any aeration of the liquid will change the nature of the liquid, and secondly, the impeller may experience violent vibration resulting in serious damage for the electric motor. It may be for these reasons, that baffles should be recommended for agitation with the less viscous liquids like water.

Figures 5.2.27 and 5.2.28. show graphs of M_c vs N for

the 29 and 15cm FPVs containing 0.25%wt CMC and 77%wt glycerol/water. In all cases, the solids suspended were 530 μm glass ballotini. For the 15cm vessel, the ratio of impeller to tank diameter, D/T, was 8.5/15 = 0.57; and for the 29cm vessel D/T was 16.5/29 = 0.57. This means that correct scale-up was observed. For the Newtonian system, the ratio of N_{JS} values for the two tanks was 180/240, whilst for the corresponding ratio of impeller diameters was 16.5/8.5 so that if:

$$N_{JS} = {}^{1}/_{D^{a}}$$

then $a = 0.43$

(The QMF model would have predicted a value slightly less than 0.5)

For the non-Newtonian CMC liquid the same analysis can be performed. This time a is 0.56, about 0.1 higher than predicted by the model.

Considering first the Newtonian systems, the graphs presented in figure 5.2.27 show that initially, for low impeller speeds, the 29cm tank has a better distribution. However, as the just suspension condition is approached, M_c in the 15cm vessel improves dramatically so that at N_{JS}, M_c in the 15cm vessel has reached 0.84. Increasing N beyond N_{JS} only results in a slight improvement so that M_c has a plateau value of 0.86. For the 29cm vessel at N_{JS}, M_c is about 0.7 and eventually reaches a plateau value of about 0.76.

With the non-Newtonian liquid, CMC, at low impeller speeds, again the solids distribution in the larger vessel is better than the 15cm vessel.

Another way of comparing the two sizes of tank, for each liquid, is to use the experimental data to plot graphs of M_c vs specific power consumption (power consumed by the impeller per unit mass of liquid being agitated). At a given Reynolds Number, the Power Number, and hence the power consumption, can be estimated from the Po vs Re curves found in Appendix 2 for six-bladed turbines. Since in every case the volume and density of liquid was recorded, the specific power can easily be calculated.

Figure 5.2.29 shows graphs of M_c vs specific power for the 29 and 15cm tanks using 77%wt glycerol/water. The specific power consumption, P_M, at the just suspension condition is higher for the larger diameter tank; 0.138 W/kg compared with 0.055 W/kg. At these N_{JS} conditions, the M_c value for the smaller tank is higher 0.84 than the larger tank, 0.70.

For a non-Newtonian system, graphs of M_c vs P_M are presented in figure 5.2.30. As with the Newtonian system, the larger tank has the higher value of P_M at N_{JS}, although the difference in mixing co-efficient is much smaller; 0.64 compared to 0.62. After the N_{JS} condition, the M_c curves almost merge together to reach a plateau value of 0.64. From the results presented in this figure, it would appear that at a given P_M, the mixing co-efficient is almost the same for both sizes of vessel. This means that scale-up had no effect on the quality of mixing in 0.25%wt CMC.

g) Comparison with other work

In Chapter Two, different methods of assessing the quality of mixing have been examined by other researchers. One of the consequences of the different approaches to the problem is the lack of a generally agreed quantitative measure of how well distributed the solids are, and how close the agitation system is to homogeneity. As well as the difficulty of comparing quantitative data from one set of experiments performed by one worker with those of another, there has been no data collected (or at least not yet reported in the literature) for agitation systems where the viscosity of the liquid differs markedly from that of water, whether the liquids are viscous Newtonian or pseudo-plastic non-Newtonian.

Since previous research has concerned itself with the solids distribution in liquids of viscosity in the order of 0.001 Pas (the viscosity of water), it may not be surprising that any theoretical work and modeling has relied on the properties associated with liquid turbulence to explain the concentration profiles determined from their measurements.

Although none of the data collected for this study has used liquids sufficiently low in viscosity for fully turbulent agitation, it may prove useful to plot the data in ways suggested by the theoretical work of others in order as a means of comparing the distribution of solids in the viscous Newtonian and non-Newtonian liquids with those low viscosity/high Reynolds Number systems examined by others.

There are two teams of workers with whom comparison may prove most useful; Shamlou and Koutsakos, 1986 and 1989 (and Koutsakos, phD 1989), and Barresi and Baldi, 1987. The approaches of both of these sets of workers have been introduced in Chapter Two.

Shamlou and Koutsakos have based their theoretical work on a one-dimensional turbulent diffusion model (as have Barresi and Baldi). By plotting their concentration profile data on semi-log graph paper, they found that their

data points lay on straight lines (see figure 5.2.31). The slope of these lines are determined by the properties of the liquid and the solid. Those points that did not lie on the straight line were usually to be found near the impeller region, where the fluid hydrodynamics is at its most complex. For a perfectly mixed suspension, the line would be perfectly vertical, of infinite slope, so that the concentration is constant for all h. In practice, this is difficult to achieve and so the deviation of the slope of the semi-log plot from the vertical can be taken as a measure of the quality of mixing for the suspension. The slope of the line is given by $-\zeta/u_s$.

Figure 5.2.32. shows a semi-log concentration profile for 70%wt glycerol/water. This mixture represents the least viscous of the glycerol/water mixtures examined in this study. At impeller speeds at or above the just suspension speed, N_{JS}, the points lie on a straight line of negative slope. Under these conditions, the impeller Reynolds Number is above 1400, when the the system although not fully turbulent, may be sufficiently turbulent for the model to have some applicability. At 360 rpm (about 1.6 N_{JS}), the slope is very close to the ideal homogeneous condition. The Re is above 2300. At N_{JS}, the slope of the semi-log lot is approximately -30cm and at 360 rpm, about -50cm. A plot of $\zeta/u_s d_p$ vs N on log/log graph paper should yield a straight line graph of slope 1 ($\zeta/u_s d_p$ being the reciprocal of the Péclet Number). Using the UNISTAT software package, the data was processed to calculate the slopes of the semi-log plots at each impeller speed for the 70%wt glycerol/water mixture . It should be noted that the fits for the semi-log "straight lines" were generally very poor, especially at low impeller speeds. Having calculated these slopes, they must divided by the particle diameter, in this case 0.053cm, in order to determine 1/Pe.

There are two obvious differences between the graphs in figure 5.2.33. The first is the shape of the graphs. The Shamlou & Kousakos graph in figure 5.2.33. show straight lines of constant slope, whilst the 70%wt glycerol/water data shows a straight line initially but then at 320 rpm

(5.33 /s), the 1/Pe reaches a peak of just over 1000. This probably signifies the beginning of a flat plateau in the graph when increasing N no longer influences the quality of mixing and hence 1/Pe. Secondly, the slope of the initial straight-line section between 180 and 300 rpm is much higher than 1, approximately 2.5. This would indicate that there is a much higher rate of improvement in solids distribution with increasing speed using 70%wt glycerol/water as compared with the water used by Shamlou and Koutaskos. Even with water, however, it would have been expected that the slope of the graph shown in figure 5.2.33 would lessen as the speed is increased beyond N_{JS}. Only under ideal conditions, with small particle diameters and small solid/liquid density differences, would it be expected that 1/Pe would continue to increase until at some at some critical impeller speed, the distribution of particles had become sufficiently homogeneous that 1/Pe approached infinity.

Figures 5.2.34 and 5.2.35 show semilog plots for 82%wt glycerol/water and 0.25%wt CMC respectively. These show a marked divergence from a simple straight line.

The significance of the Péclet Number features in the work of Barresi and Baldi, 1987. This Péclet Number can, by appropriate substitutions (see Chapter Two), be shown to be related to the Power Number, Po, and the impeller tip speed ND, and the solid/liquid properties so that

$$Pe^{*} = \frac{u_t}{Po^{1/3}ND} \qquad 5.2.10$$

The reciprocal of this modified Péclet Number is termed the K-parameter.

$$\text{i.e.} \qquad K = \frac{Po^{1/3}ND}{u_t} \qquad 5.2.11$$

Figure 5.2.36 shows some axial concentration profiles that Barresi and Baldi presented in their 1987 paper. Increasing the K-parameter increases the quality of the suspension. It should be noted that Barresi and Baldi only conducted their experiments with water at 20°C. Barresi and Baldi found

that the axial variation of solids concentration was always greater than the radial variation. Only for radial flow impellers did they find any significant radial profiles, which were found to be limited to the region immediately below the impeller.

As explained earlier (5.2.b), Barresi and Baldi adopted the standard deviation of the concentration profile to give a quantitative measure of the quality of the suspension. This standard deviation, σ, was then plotted against the product of K and $B_c^{0.19}$, where $B_c^{0.19}$ is a correction (taken empirically from Zweitering, 1958) to take account of the mean concentration of solids, C_w, for dilute suspensions. Figure 5.2.37 shows such a plot for a six-bladed pitched blade disc impeller. The values of K are always determined for N equal or greater than N_{JS}. For low mean concentrations, upto 1.51%wt the points are well described by one straight line, but at the highest concentration, 5.10%wt, the data deviates from the straight line, and instead σ is higher than expected. Although it may be true that empirically:

$$N_{JS} \propto B_c^{0.19} \qquad 5.2.12$$

Barresi and Baldi do not make clear why they have chosen to correct their K-parameters to take account of the mean concentration. The mean solids concentration has already been taken into account when calculating the standard deviation. However, since for dilute concentrations the correction factor is quite close to unity, this has a negligible factor of the graphs presented by Barresi and Baldi. Graphs for other types of impellers investigated by Barresi and Baldi are presented in Chapter Two.

Figures 5.2.38 and 5.2.39 show σ vs K for the glycerol/water mixtures and the pseudo-plastic CMC solutions. The correction factor of $B_c^{0.19}$ does not need to be included since all the experiments were conducted with a mean solids concentration of 1.0%wt. For each of the graphs presented in figure 5.2.39, the terminal velocity has been assumed to correspond with the average viscosity, which in

turn depends on the average shear rate being proportional to the impeller speed (Metzner & Otto, 1958). σ has been modified to take account of the Fully Profiled Vessel (FPV) used for the solids distribution experiments in this study (see 5.2.b).

For figure 5.2.38, showing the Newtonian data, the graphs show that increasing K for each system does indeed correspond to a lowering in the standard deviation, σ , and hence an improvement in the quality of suspension; $\sigma = 0$ being perfectly homogeneous. However, if the analysis presented by Barresi and Baldi were to hold at this range of viscosities and Re, the three curves should co-incide. Since they do not co-incide, or even come close, then it is clear that Barresi and Baldi's analysis cannot be extrapolated from the fully turbulent regime even into the transition regime. It is interesting to note that Barresi and Baldi did not test their K-parameters at different liquid viscosities. The liquid viscosity not only determines the terminal settling velocities of the solid particles, u_t, in still liquids but may also determine the degree to which u_t is diminished in agitated liquids (see Chapter Two). Because of an acknowledged lack of information, Barresi and Baldi calculated the K parameter using the still fluid values for u_t, over estimating these u_t and hence underestimating K. As the conditions become less turbulent, the u_t used for K-parameter and the actual u_t will come closer together so that it may be possible that the curves for less viscous liquids should be shifted to the right to an extent inversely proportional to their viscosity so that they might overlap. However, this is only conjecture, since the degree to which u_t for agitated liquids differs from still liquids still not known with any degree of precision. Even if these curves could be made to overlap, each viscosity of liquid appears to have a minimum value of the standard deviation at which the quality of mixing remains constant no matter how much the value of the K-parameter is increased. These minimum values of σ , corresponding to the plateau values for M_c, remain unexplained by theories that rely only on isotropic

turbulence.

For given liquid and particle properties, K is proportional to N, and since σ is simply 1 - Mc, it should not be surprising that the graphs in figures 5.2.38 and 5.2.39 resemble the "mirror image" of graphs of M_c vs N presented earlier in this chapter, figures 5.2.18 and 5.2.19. These graphs all reached plateau values for M_c so that increasing N would not improve the quality of suspension. These plateaux correspond to the leveling out of the σ vs K graphs. If N were increased to a high enough value, then the graphs presented by Barresi and Baldi, e.g. figure 5.2.37, should also show a leveling out with K (or N).

Graphs of σ vs K for the non-Newtonian CMC liquids are presented in figure 5.2.39 A similar pattern in this figure as compared with figure 5.2.38 except that σ does not fall smoothly with K, but instead declines in a series of peaks and troughs. These correspond to the formation of rings discussed earlier in this chapter.

As a result of analyzing the solids distribution data gathered from this study, it may be concluded that there are, as yet, no satisfactory quantitative or qualitative means of explaining or predicting the distribution of suspended solids in liquids which experience agitation in the laminar or transition régimes that have reported in the literature. This corresponds to the scarcity of any type of work reported on non-turbulent solids suspension (see Chapter Two). It should also be remembered that those models that have been applied to the fully turbulent systems do not always lead to satisfactory descriptions of the solids distribution. Indeed Barresi and Baldi make some interesting comments in the conclusions of their 1987 paper, where they admit that the axial concentration profiles cannot be described by simple dispersion model and speculate that the distribution of the solid particles may be "...strongly affected by large-scale eddies or macroscopic turbulence which is not easy to describe with a model".(See Appendix 6 for more data at different radial positions).

Figure 5.2.1

Local Concentration vs Impeller Speed
(at midradial position)

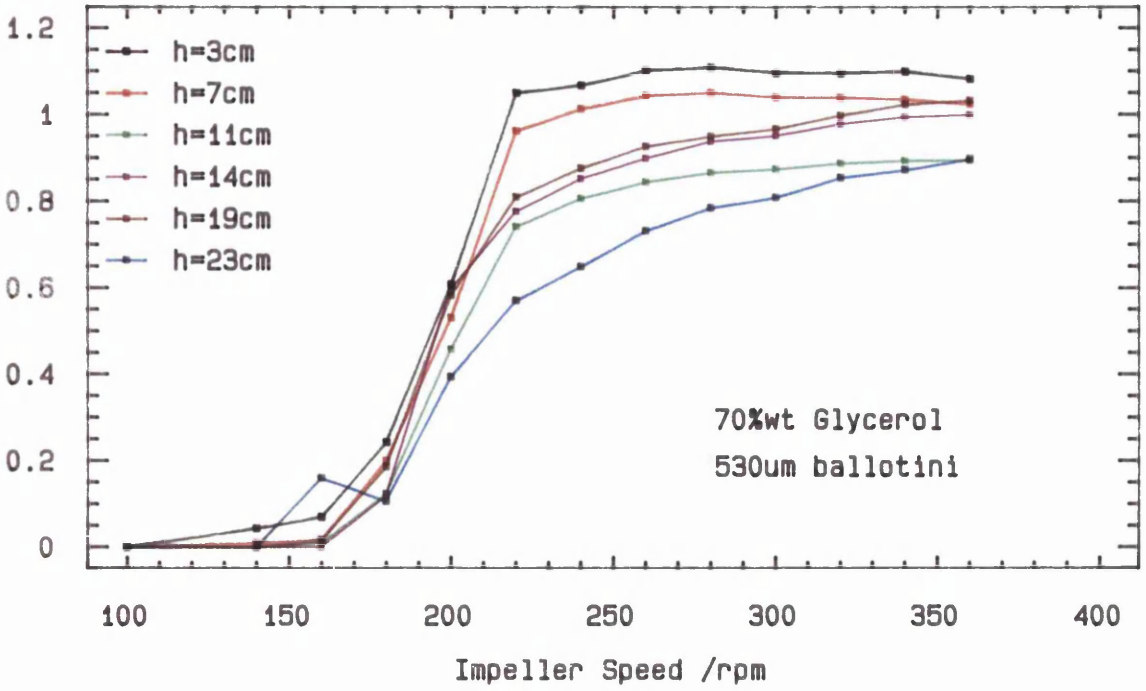

Figure 5.2.2

Local Concentration vs Impeller Speed
(at midradial position)

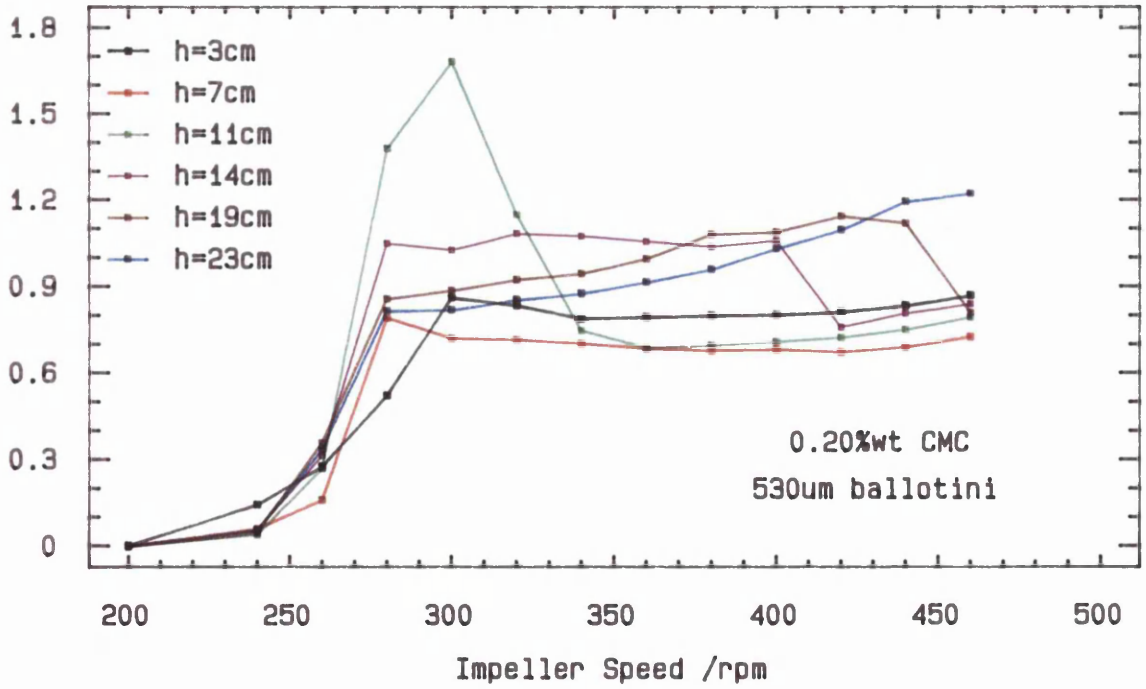

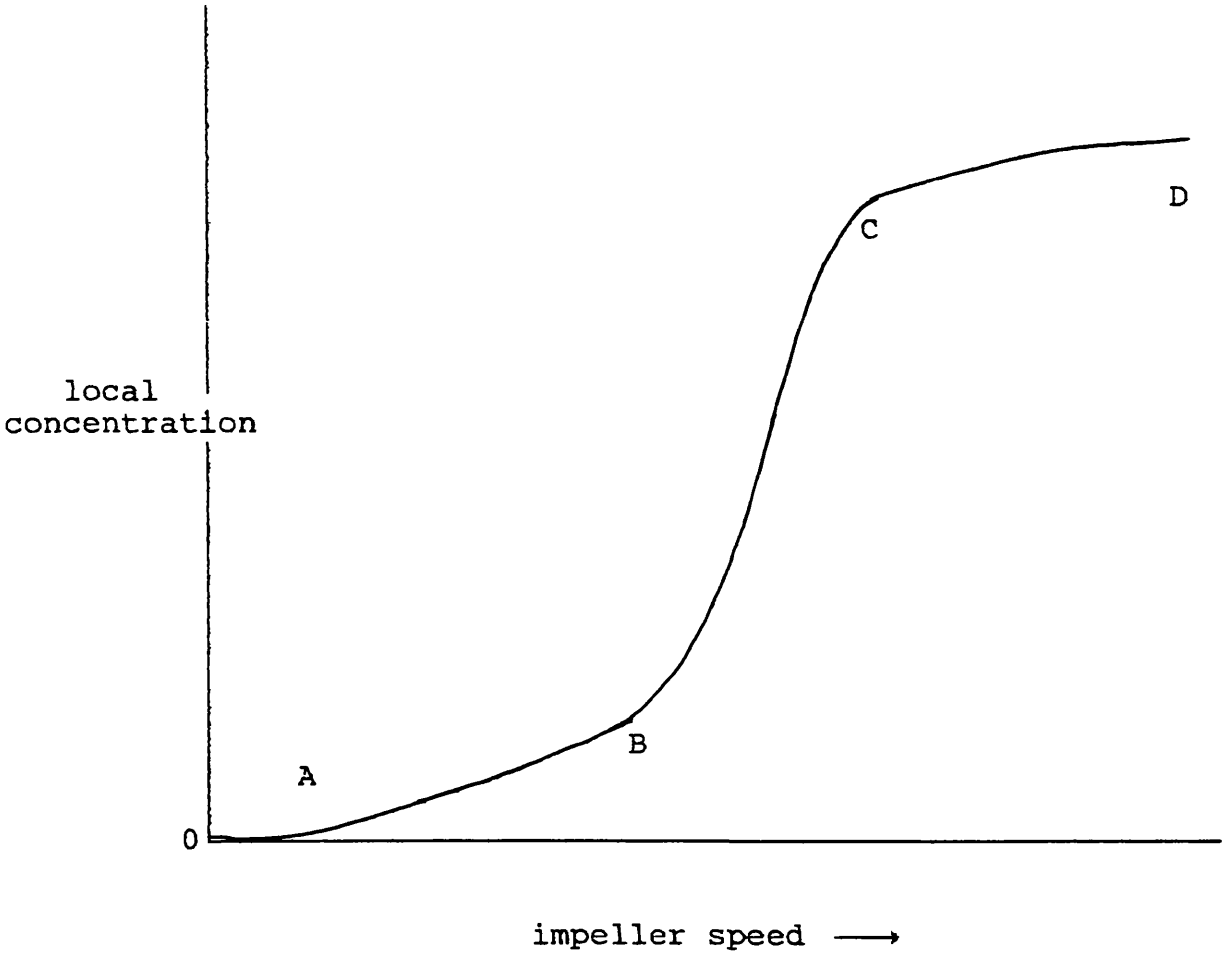

Figure 5.2.3 Sketch graph of the typical variation of local solids concentration with increasing impeller speed

Figure 5.2.4

Local Concentrations vs. Impeller Speed
(at midradial position)

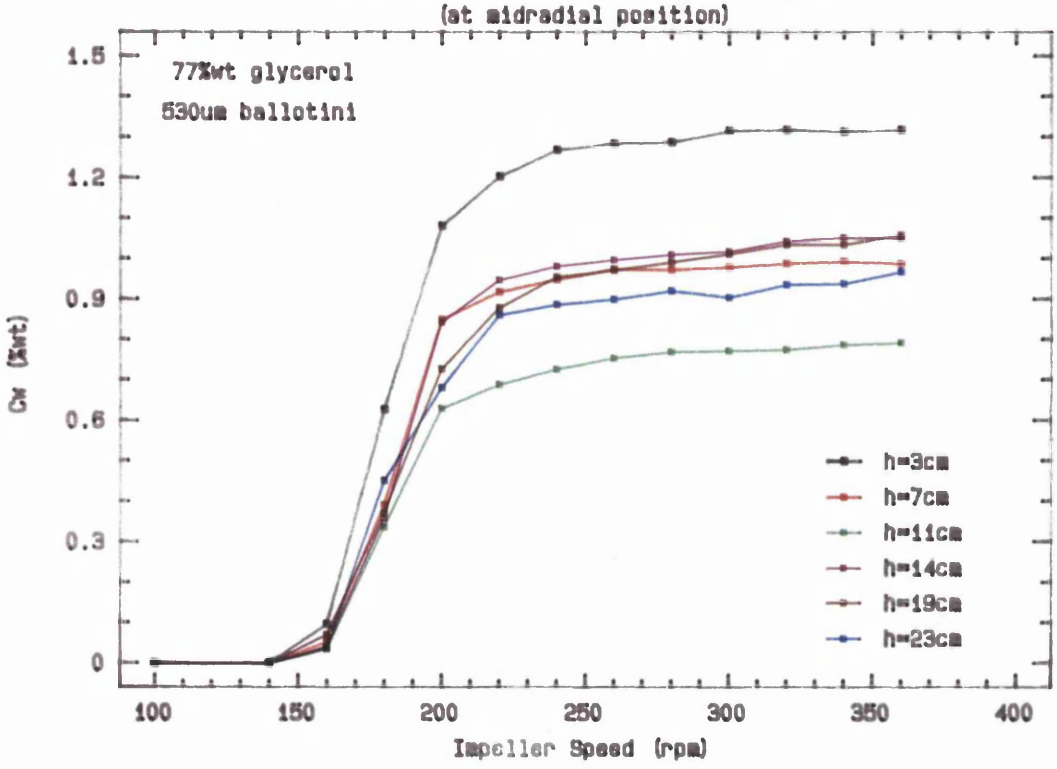

Figure 5.2.5

Local Concentrations vs Impeller Speed
(at midradial position)

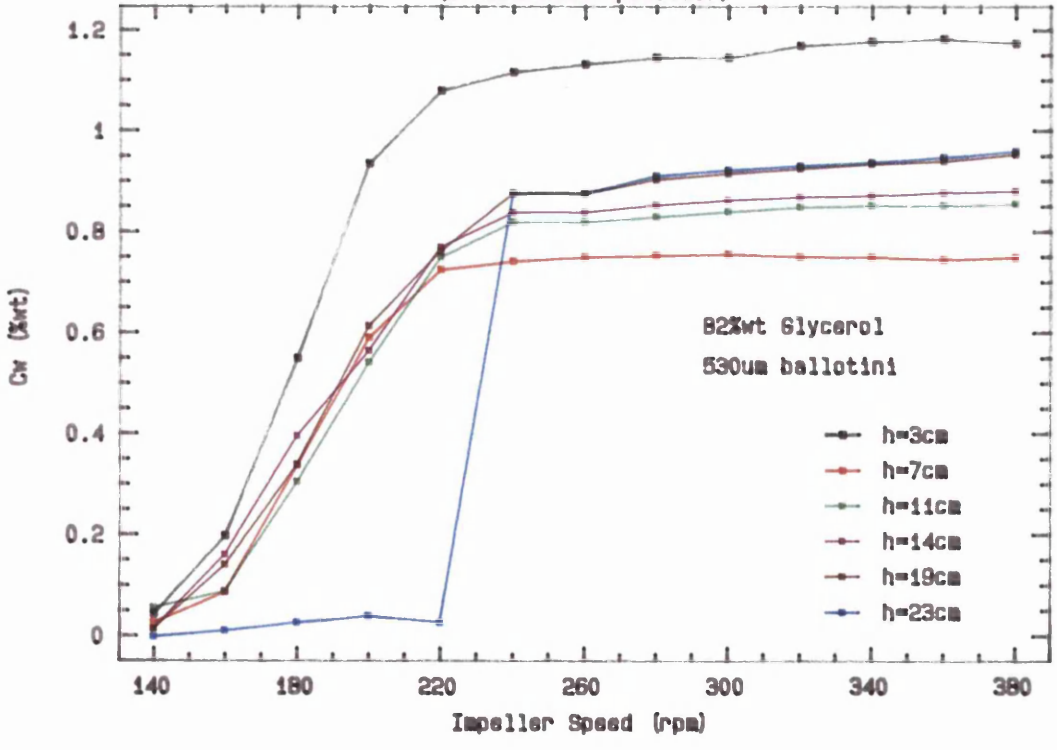

Figure 5.2.6

Local Concentrations vs Impeller Speed
(at midradial position)

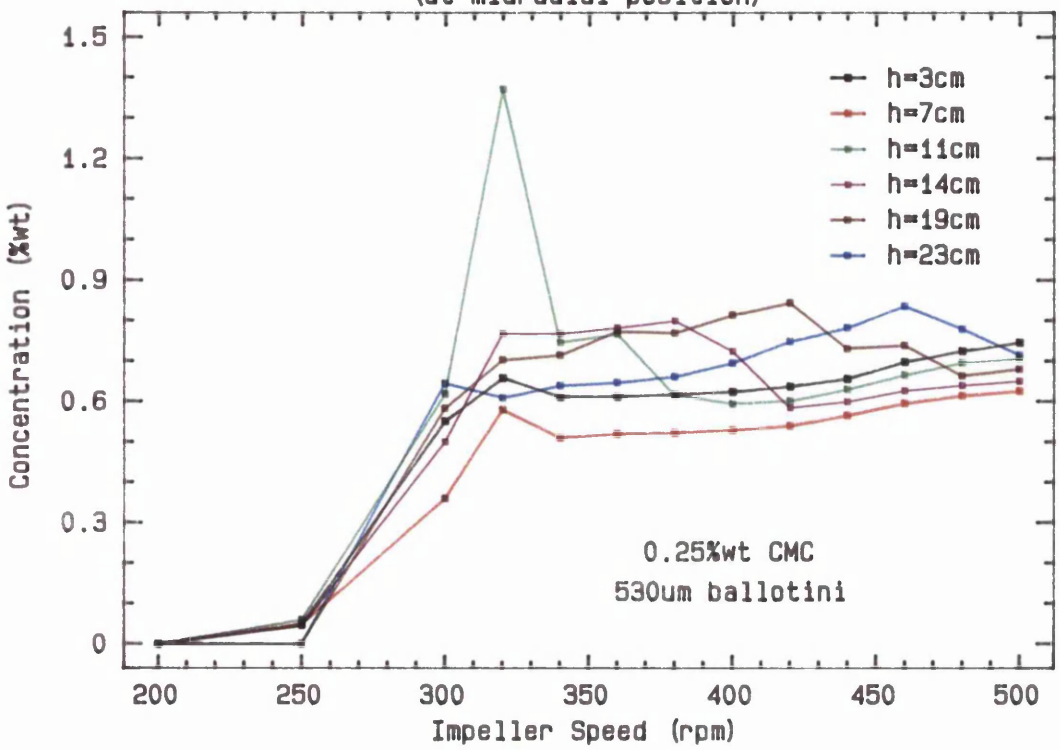

Figure 5.2.7

Local Concentration vs Impeller Speed
(at midradial position)

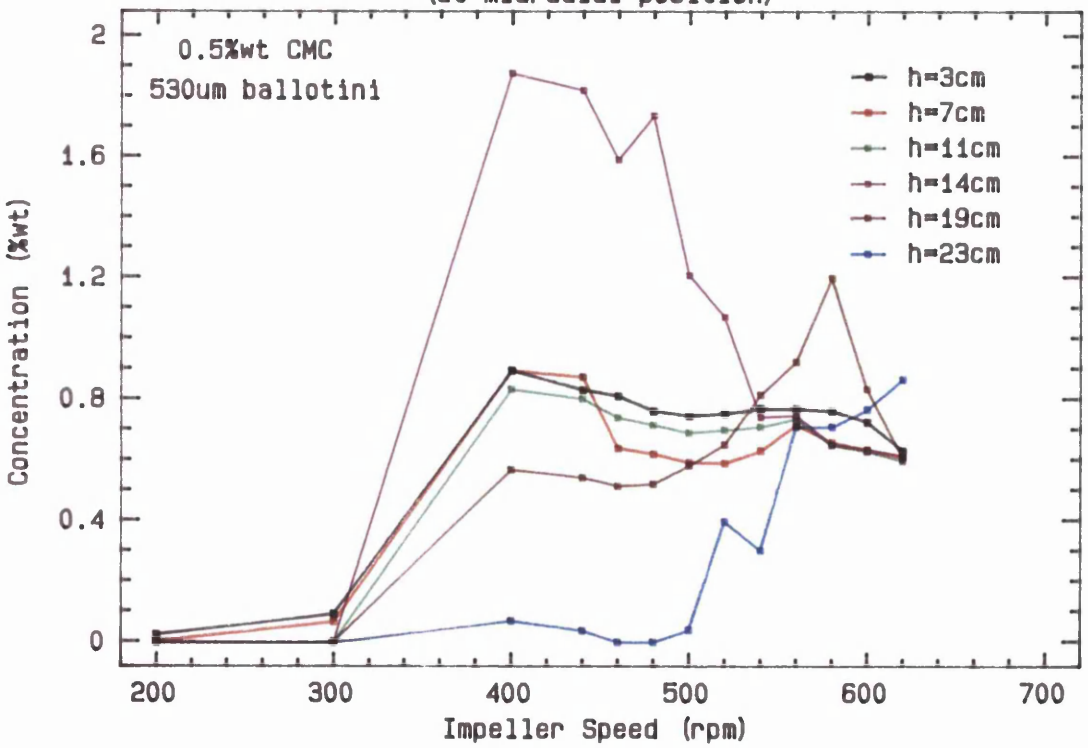

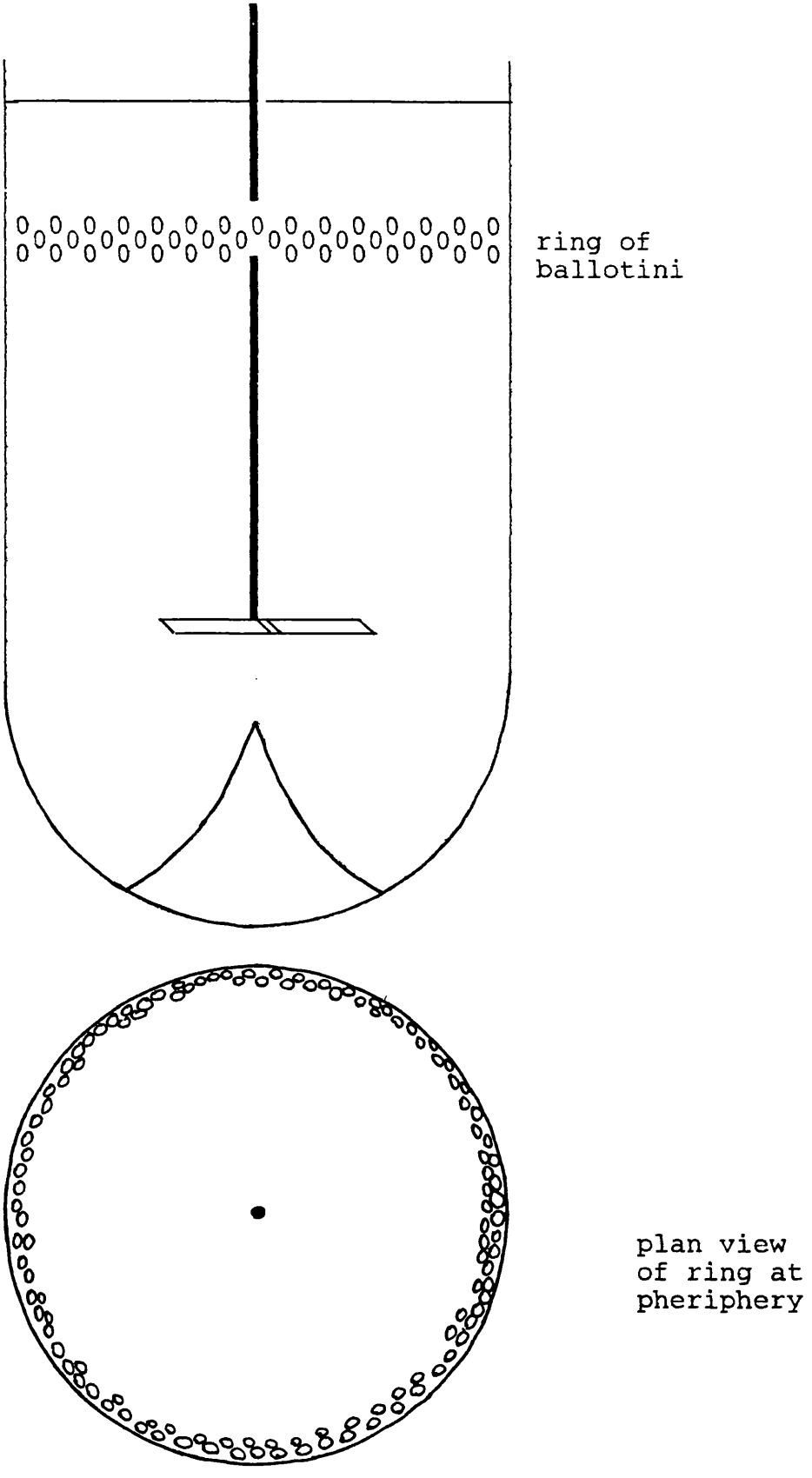

Figure 5.2.8 Ring formation in CMC solutions

Figure 5.2.9

Axial Concentration Profiles
(midradial, Njs)

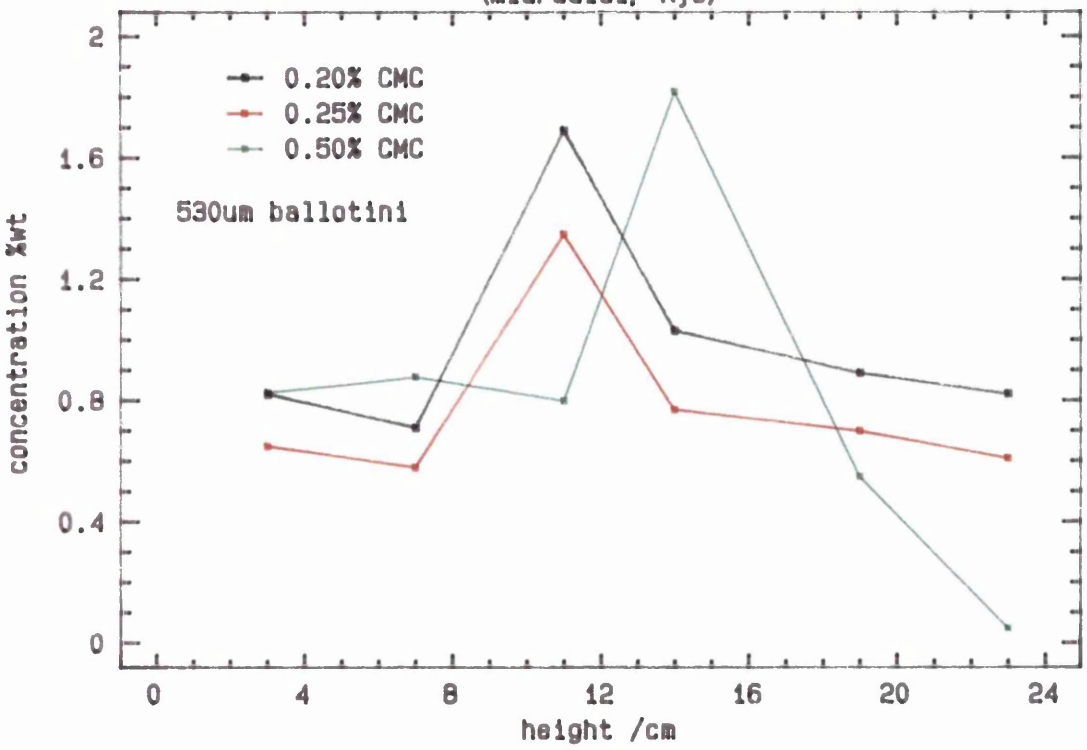

Figure 5.2.10

Axial Concentration Profiles
(midradial, Njs)

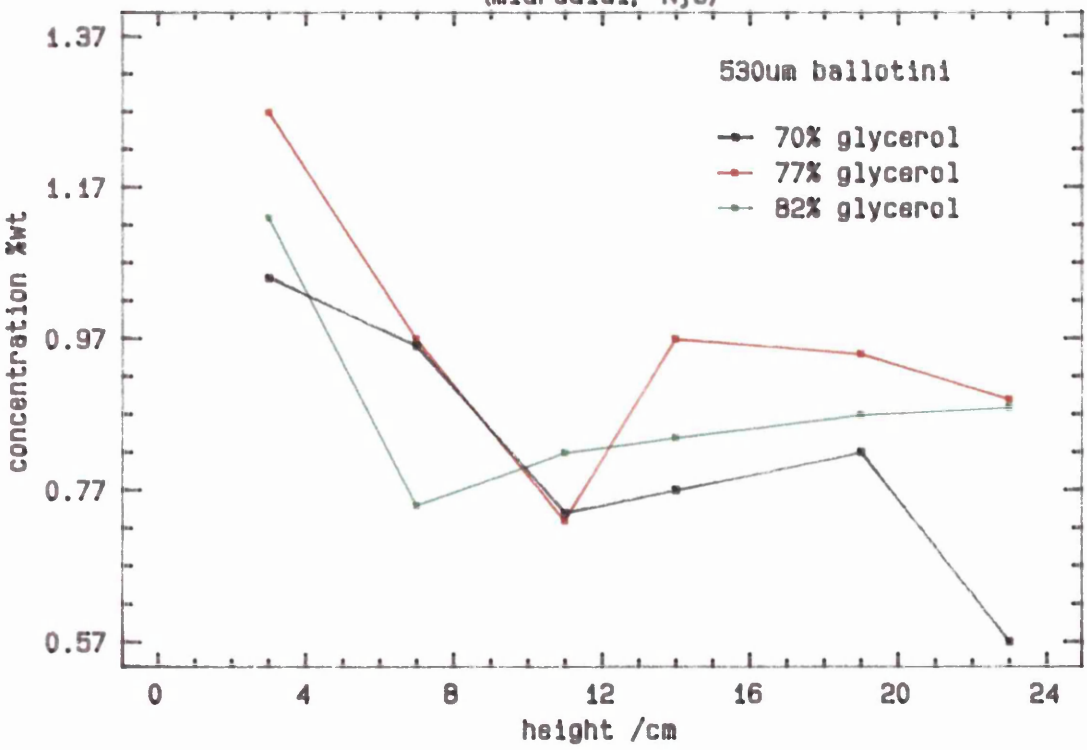

Figure 5.2.11

Axial Concentration Profiles
(midradial, 1.5Njs)

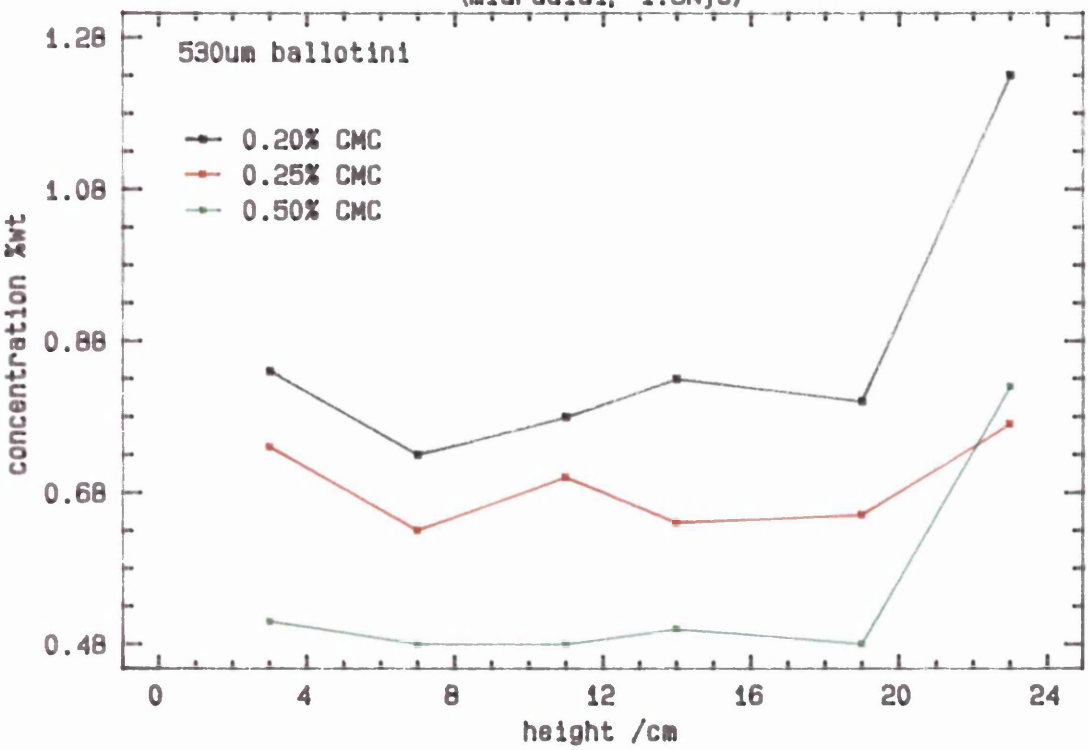

Figure 5.2.12

Axial Concentration Profiles
(midradial, 1.5Njs)

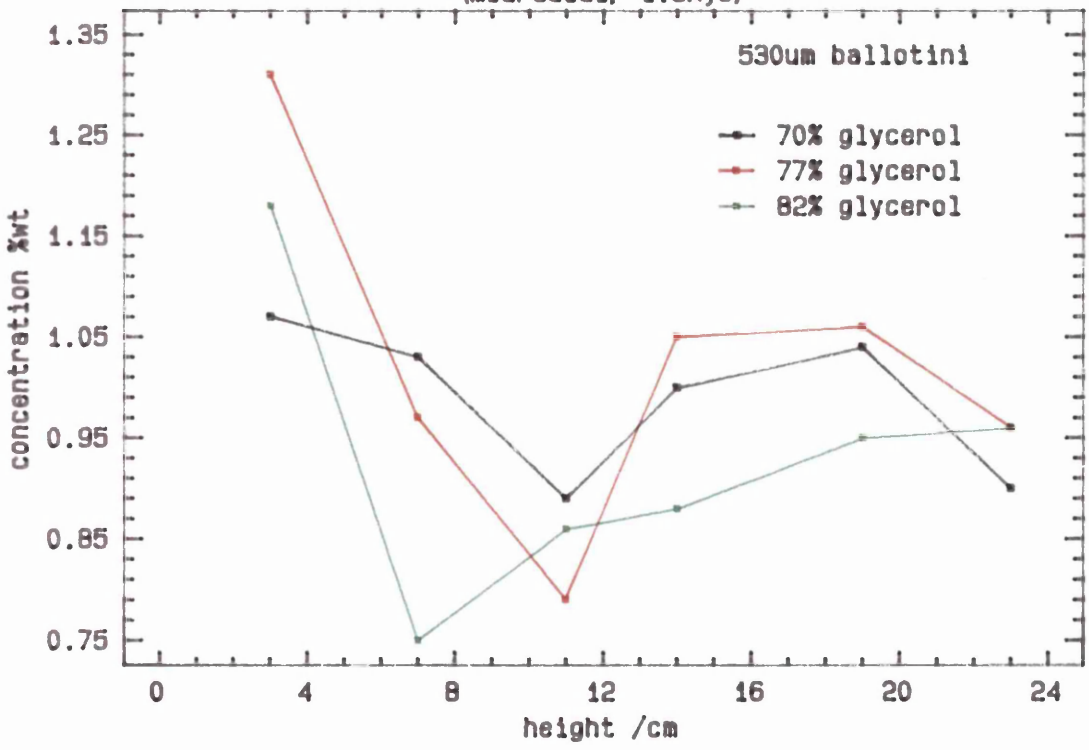

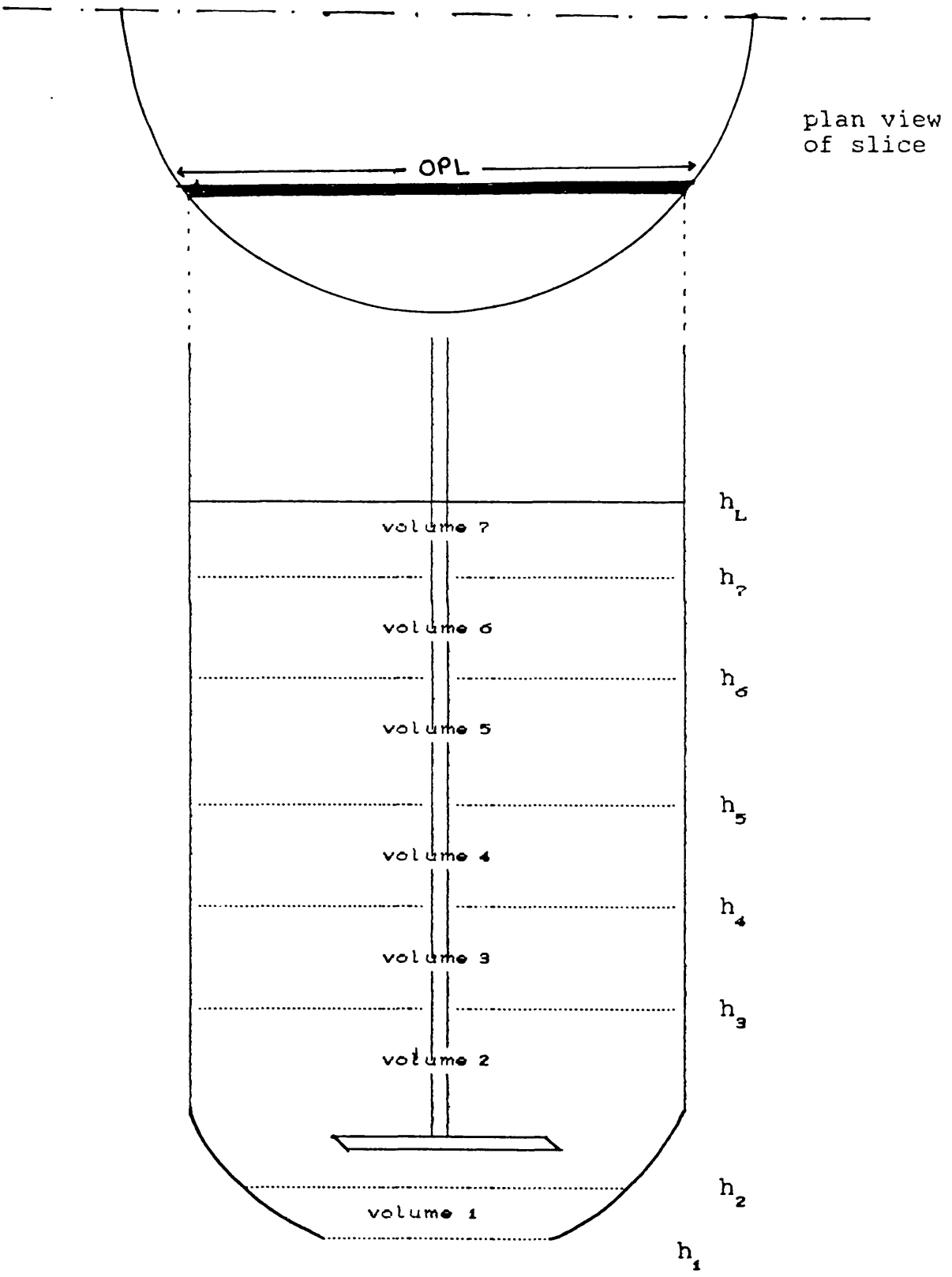

Figure 5.2.13 Division of a "slice" into volumes

Figure 5.2.14

Concentration vs Impeller Speed
(axial height 19cm)

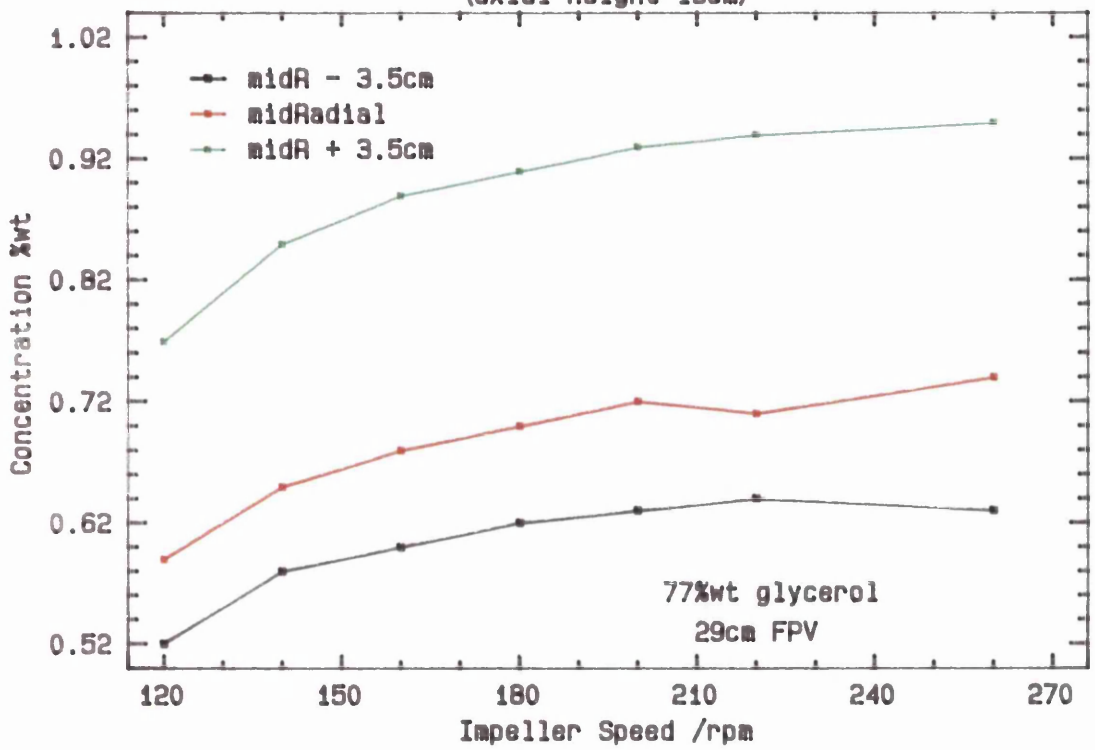

Figure 5.2.15

Axial Concentration Profiles
(Njs conditions)

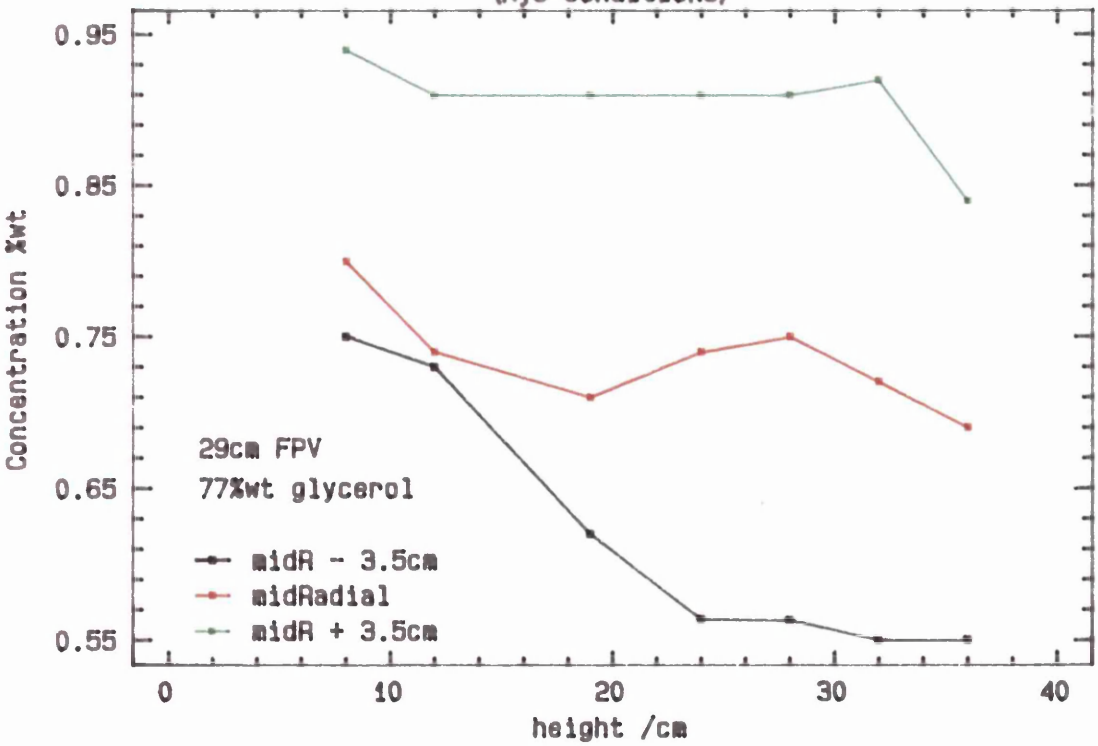

Figure 5.2.16 Mc vs N for glycerol/water mixtures

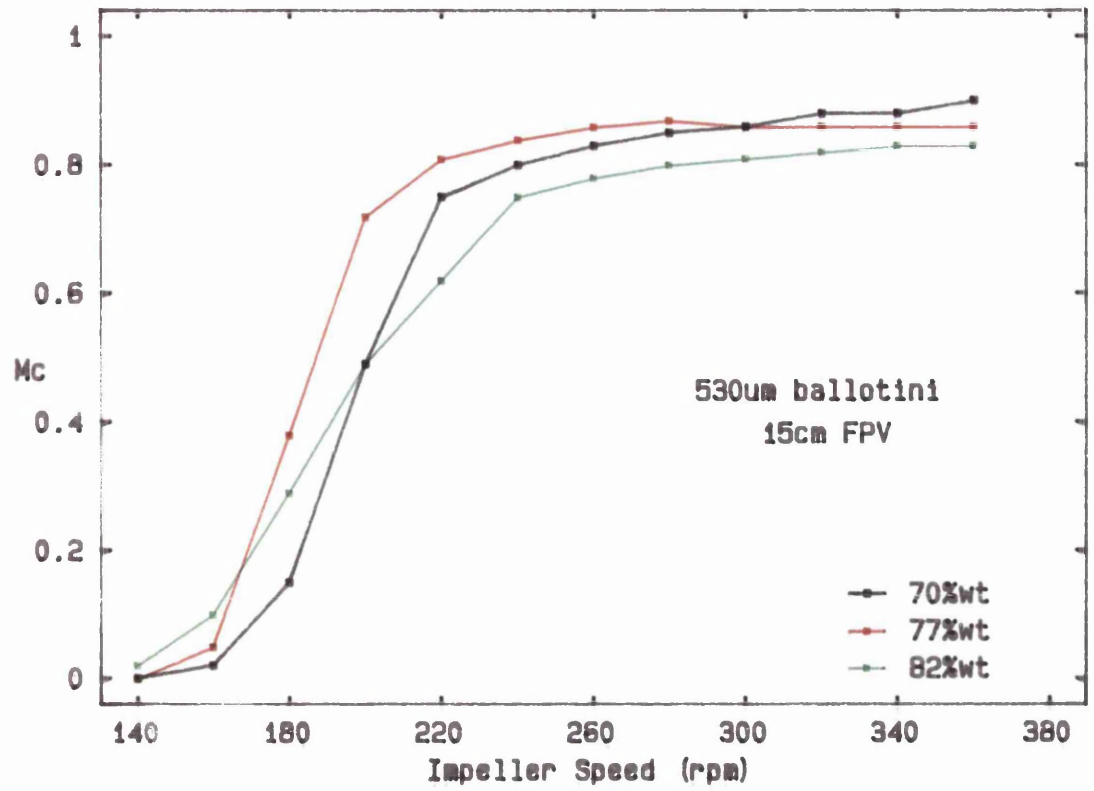

Figure 5.2.17 Mc vs N for CMC solutions

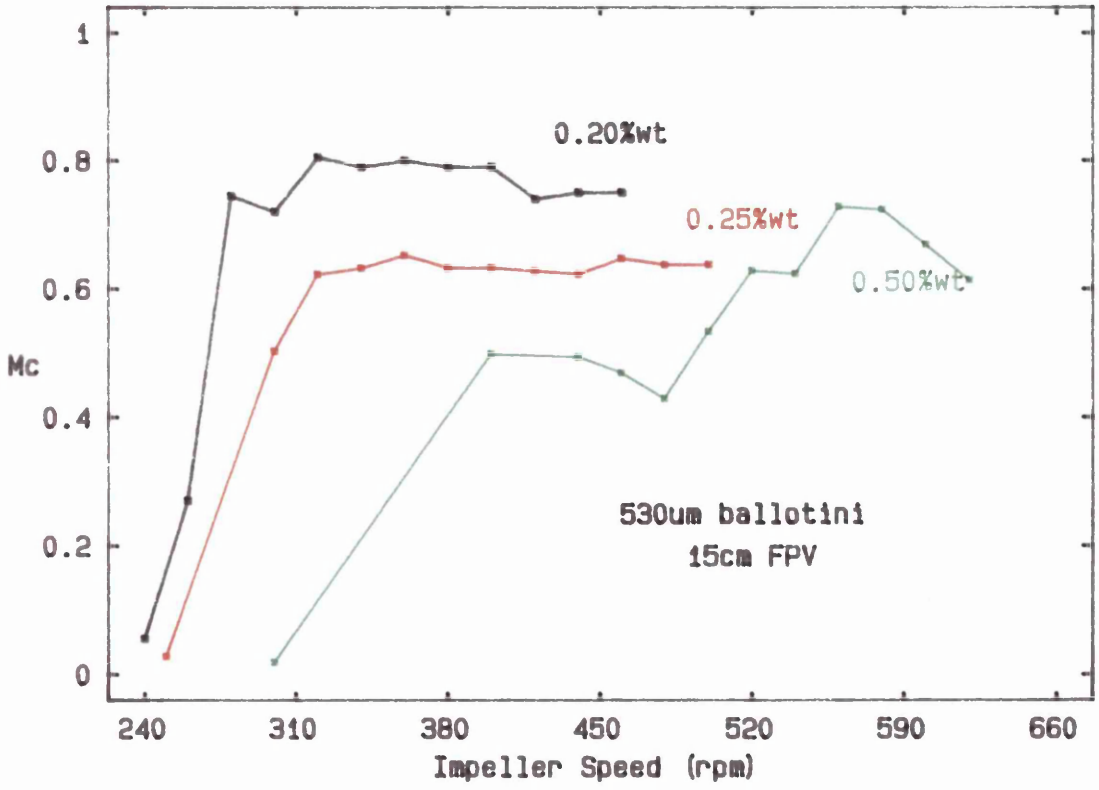

Figure 5.2.18 Mc vs Power consumption
for glycerol/water mixtures

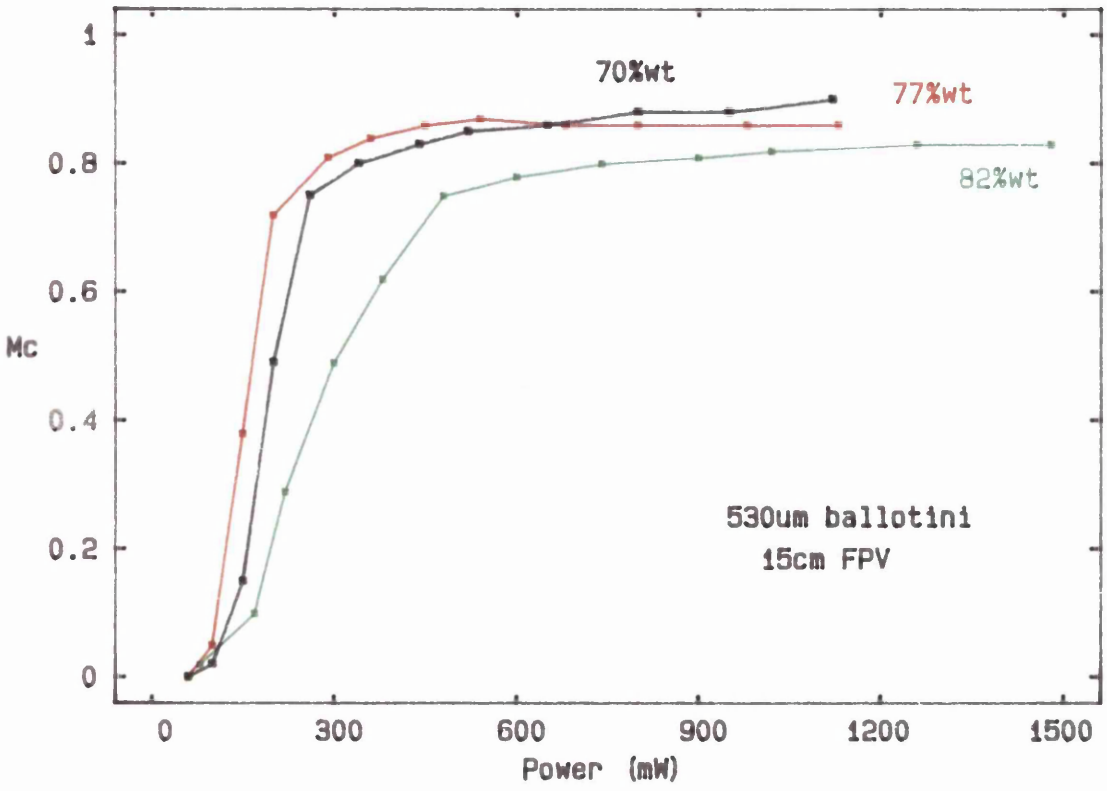

Figure 5.2.19 Mc vs Power Consumption
for CMC solutions

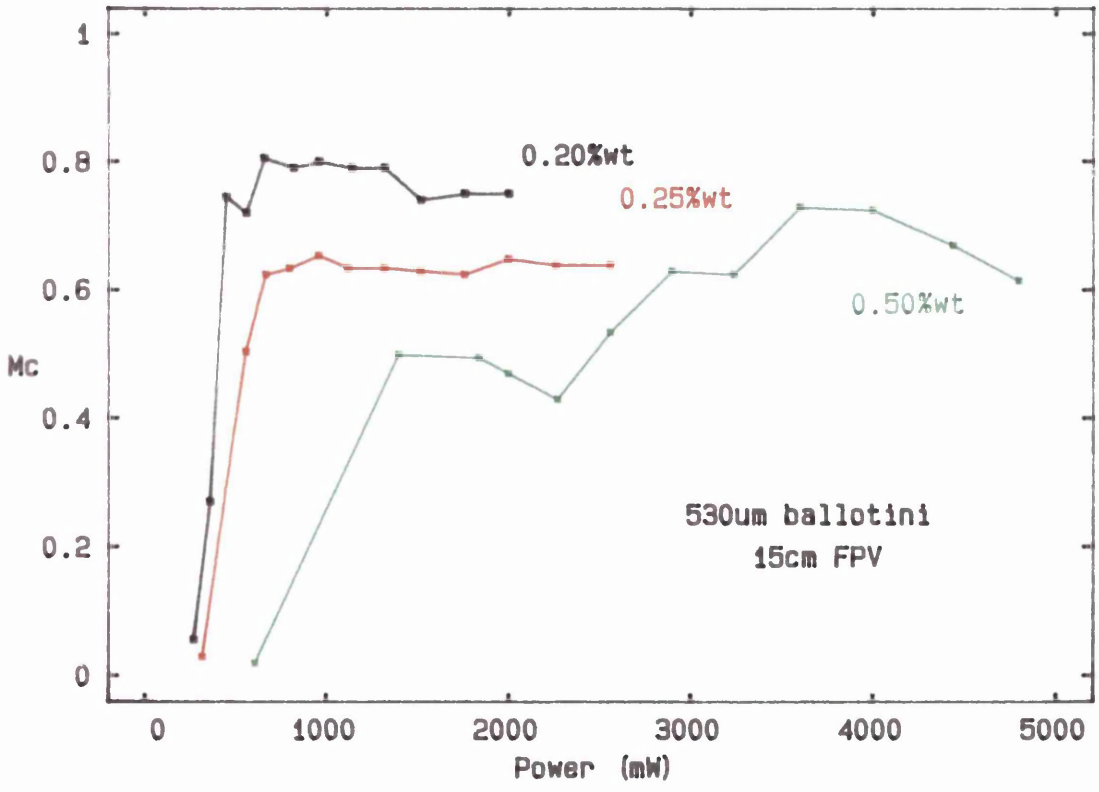

Figure 5.2.20

Plot of Plateau Mc vs (Effective) Kinematic Viscosity

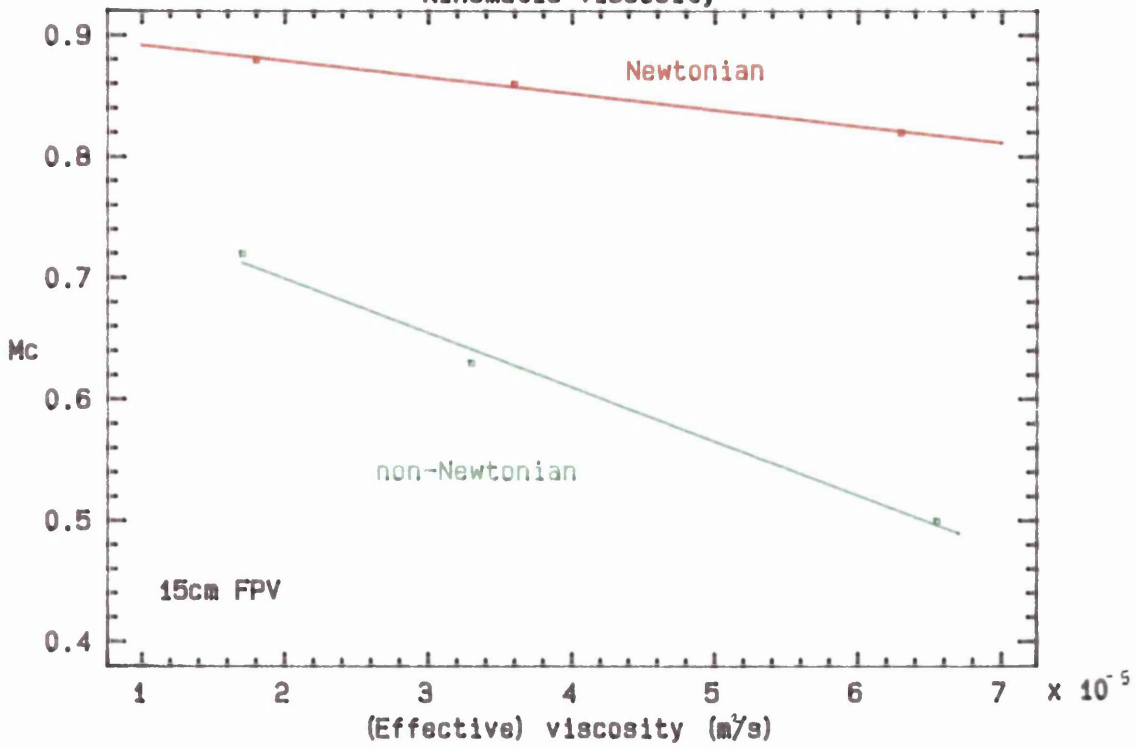

Figure 5.2.21

Plot of Mc vs N using
77%wt glycerol/water

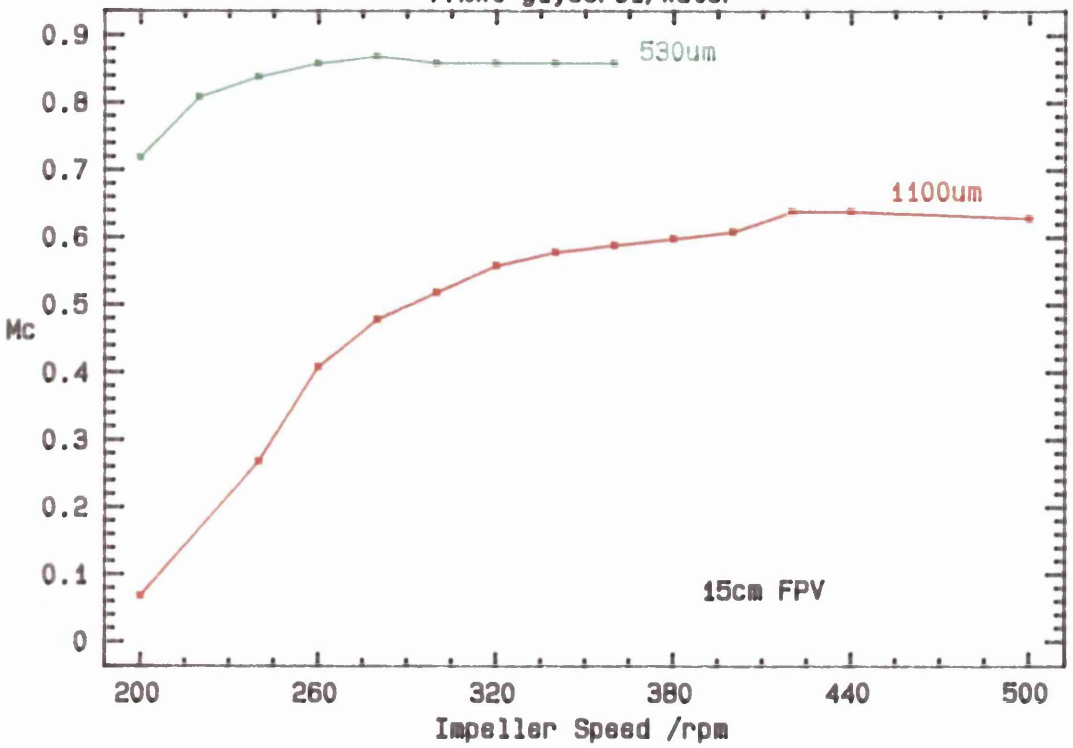

Figure 5.2.22

Plot of Mc vsing
0.25%wt CMC

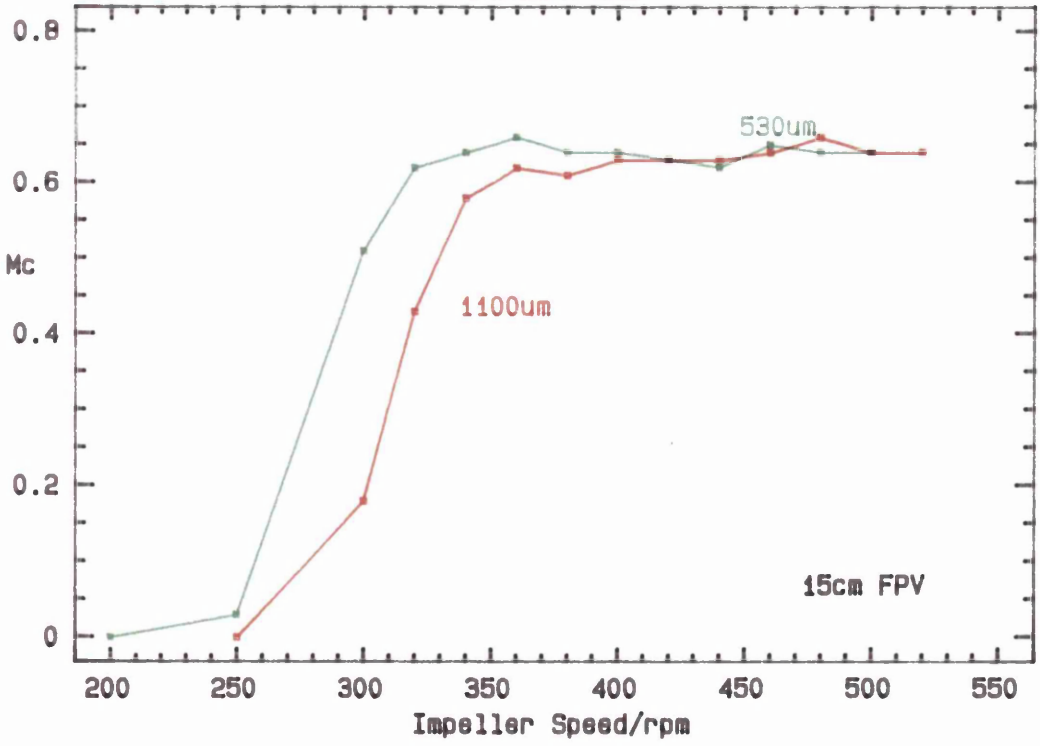

Figure 5.2.23

Plot of Mc vs N for Different Impellers

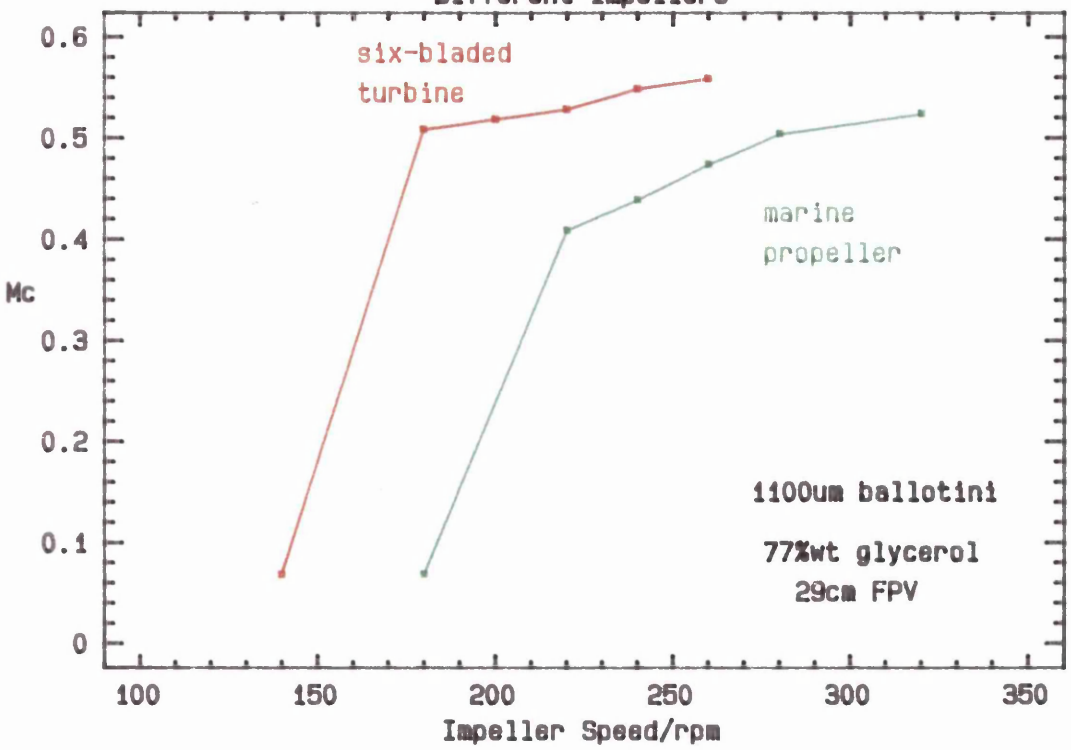

Figure 5.2.24

Plot of Mc vs N for Different Impellers

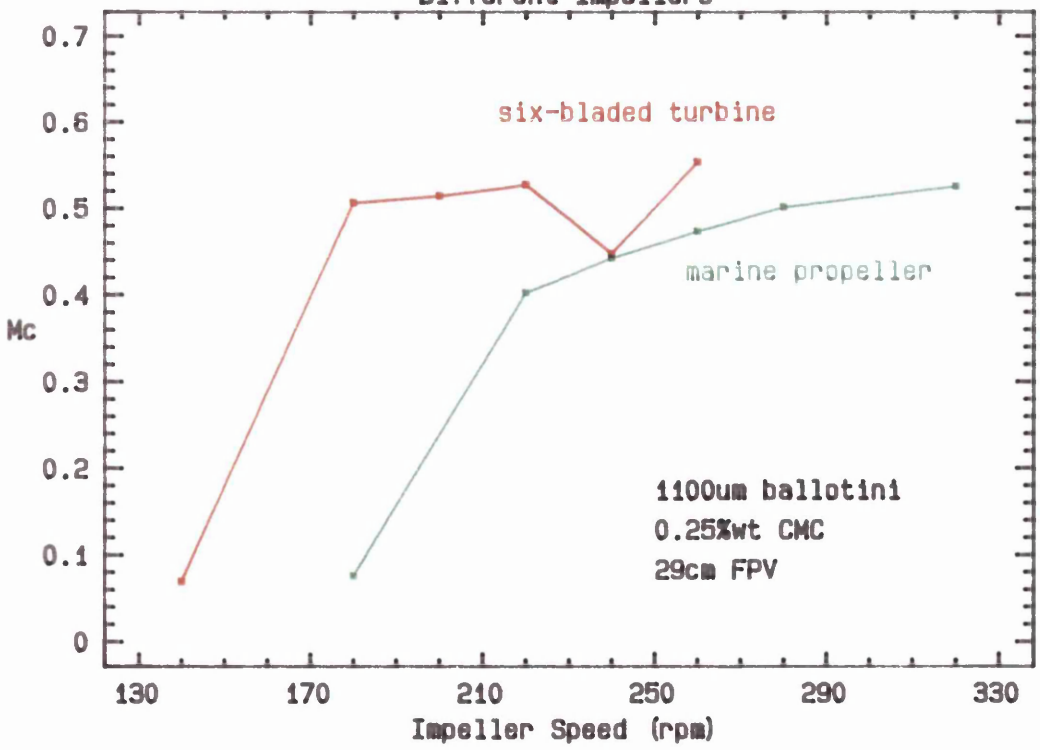

Figure 5.2.25 Mc vs
Effect of Impeller Clearance

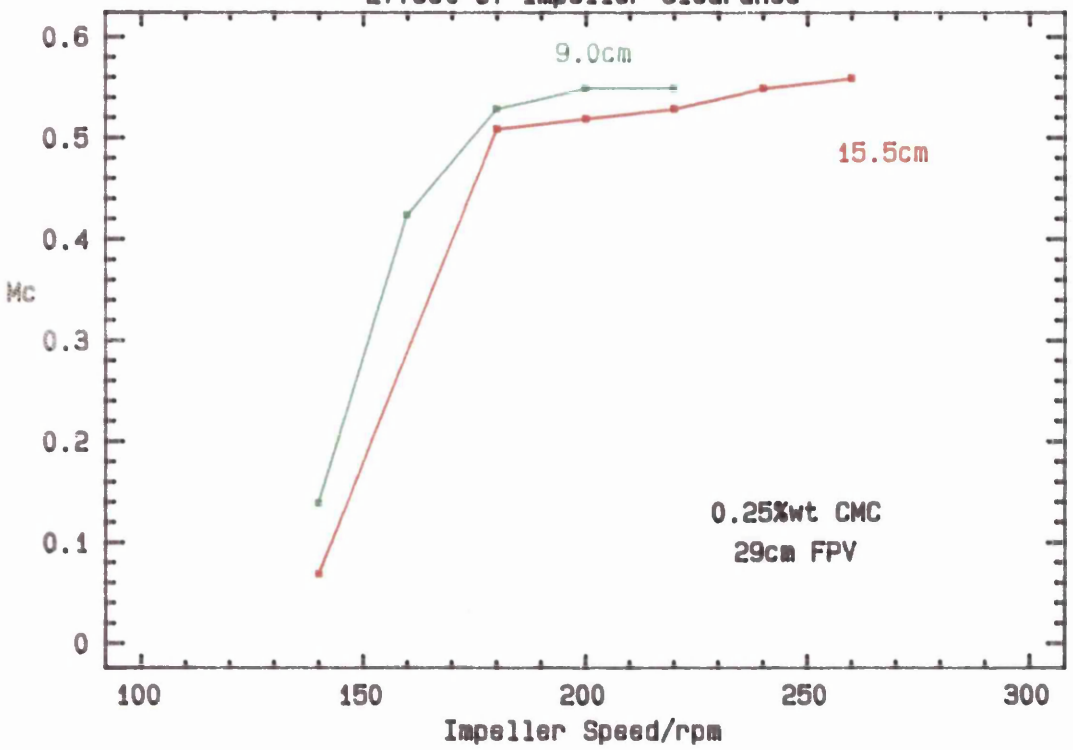

Figure 5.2.26 Mc vs N
Effect of Baffles

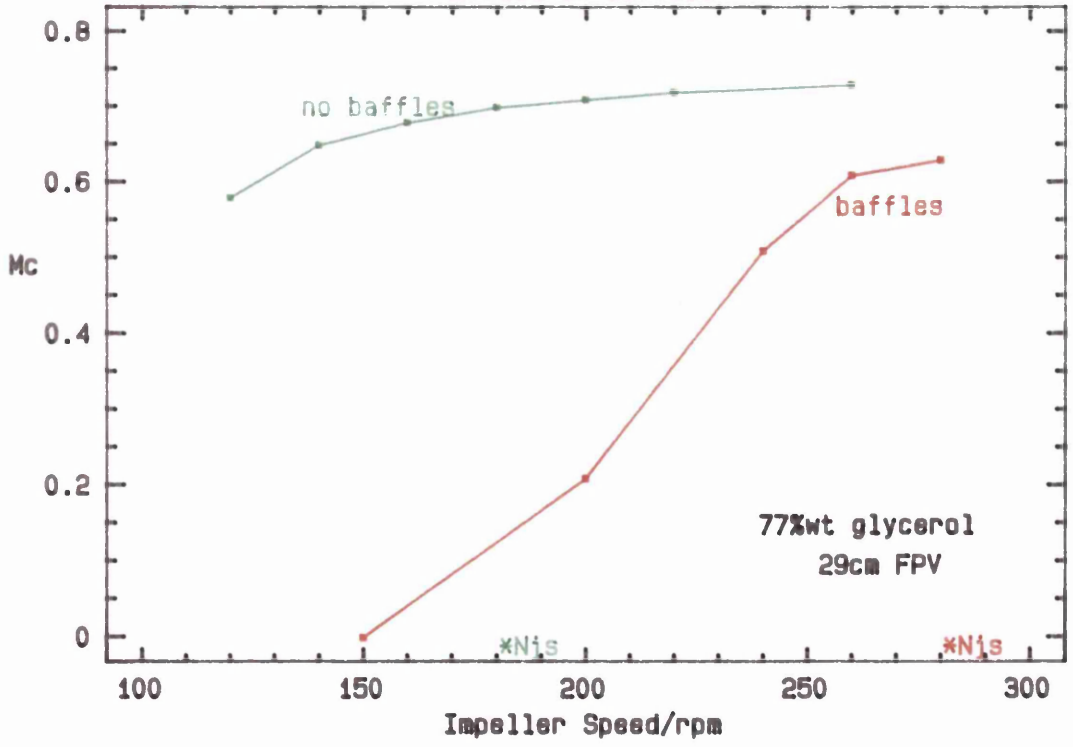

Figure 5.2.27

Plot of Mc vs N
Effect of Tank Size

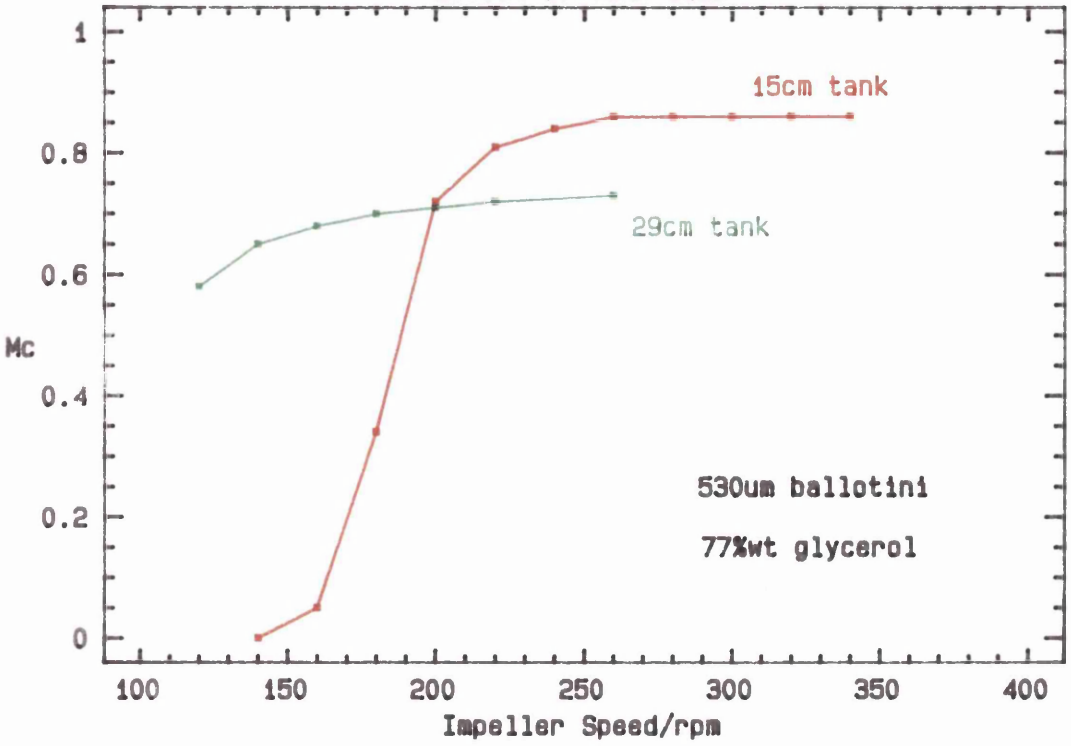

Figure 5.2.28

Plot of Mc vs N
Effect of Tank Size

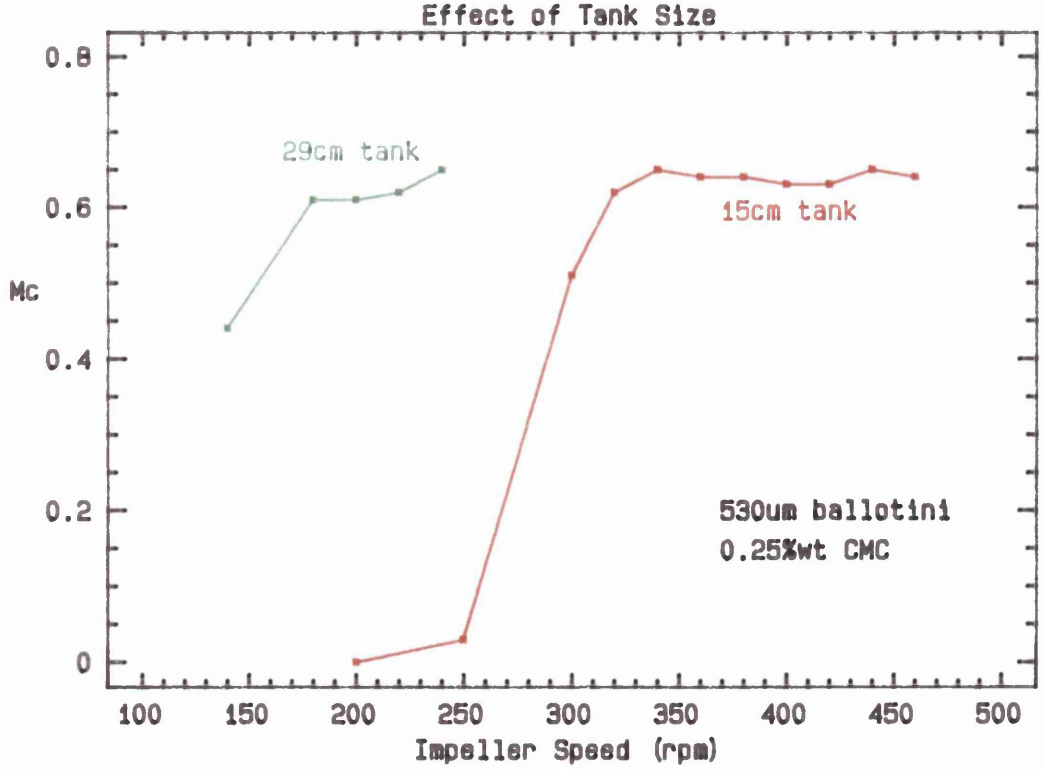

Figure 5.2.29

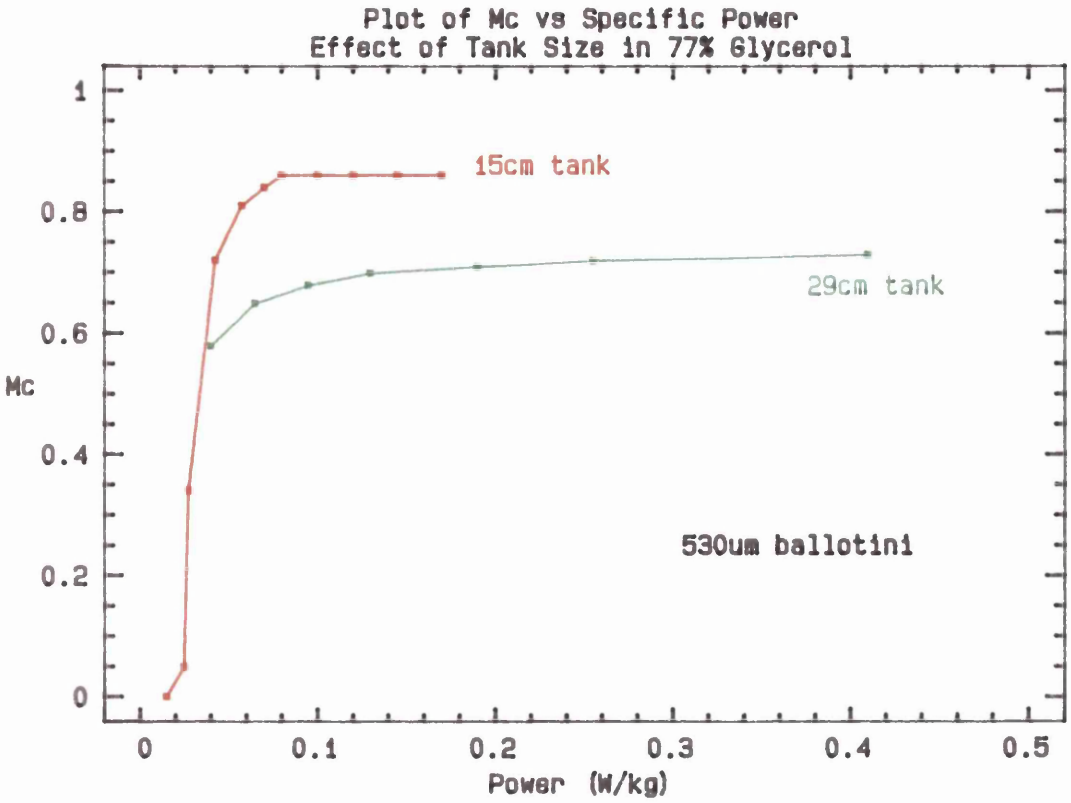

Figure 5.2.30

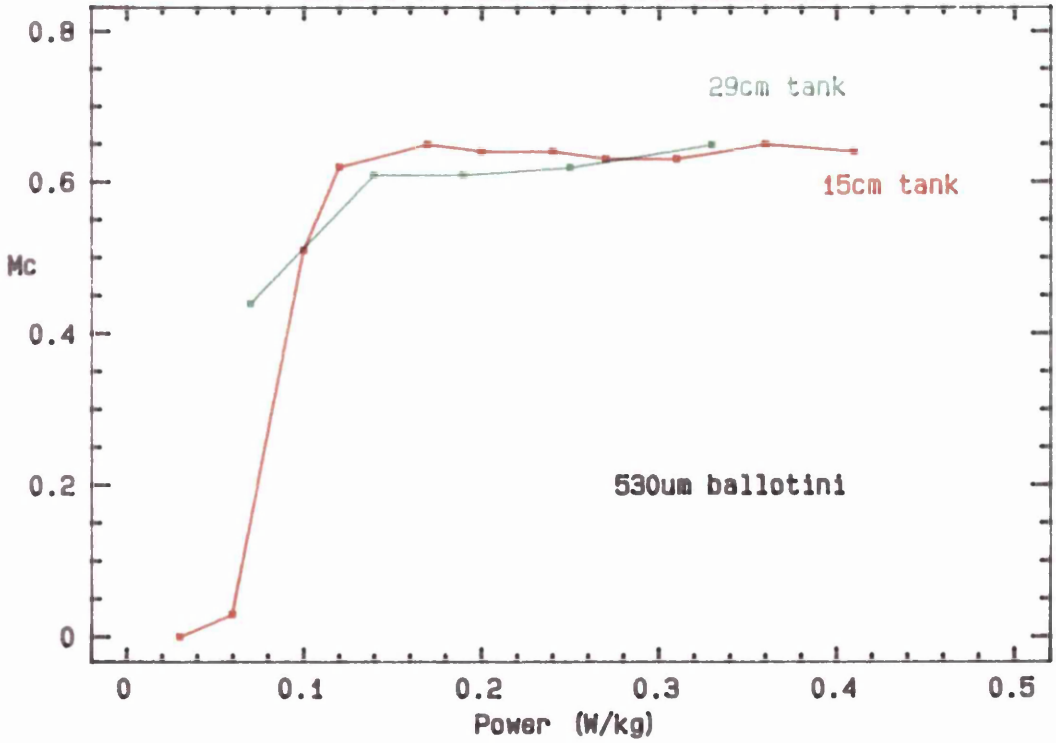

Figure 5.2.31

Semilog Axial Concentration Profiles
(in Water)

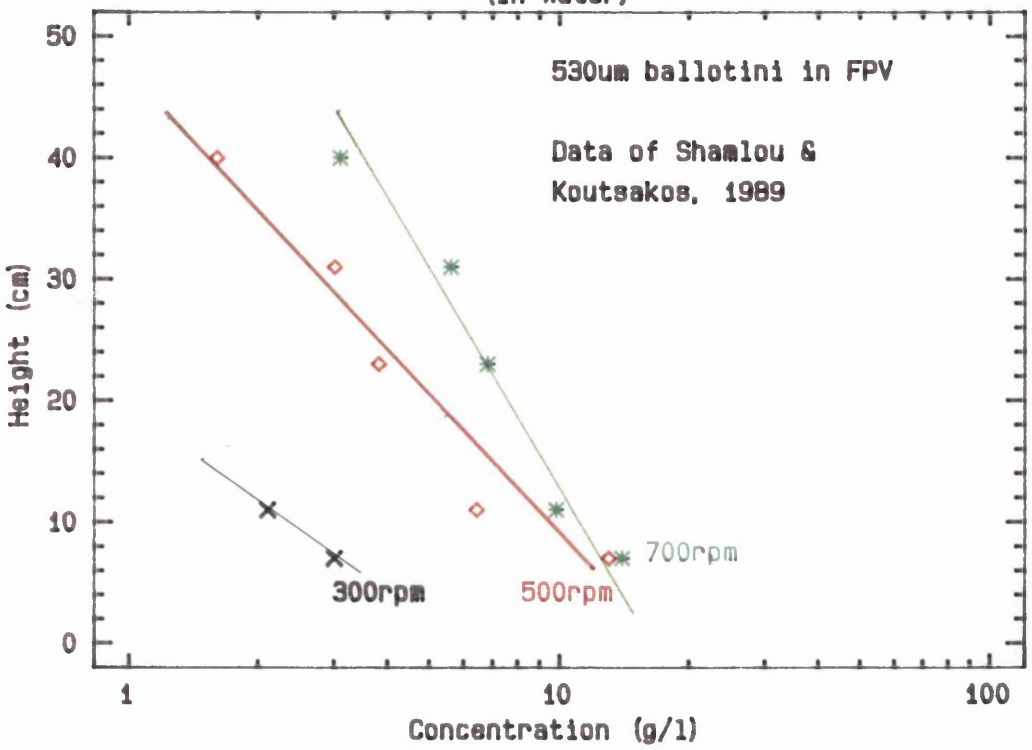

Figure 5.2.32

Semi-log Axial Concentration Profile
for 70%wt Glycerol/Water

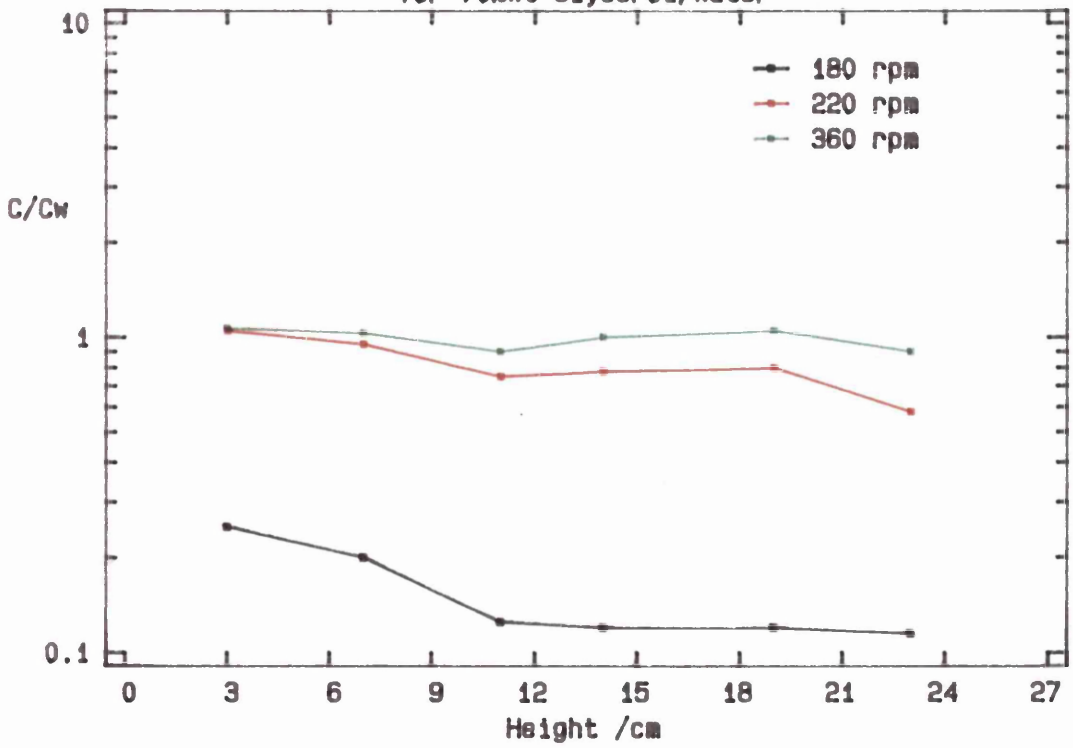

Figure 5.2.33
Plot of 1/Pe vs Impeller Speed

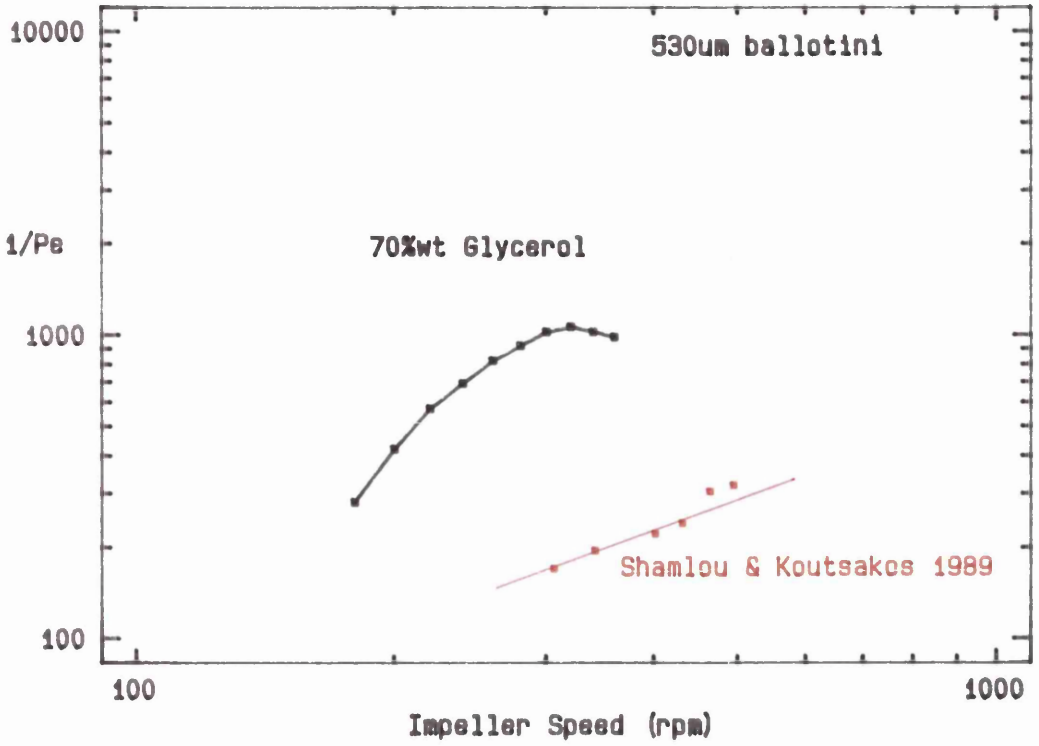

Figure 5.2.34

Semi-log Axial Concentration Profile
for 82%wt Glycerol/Water

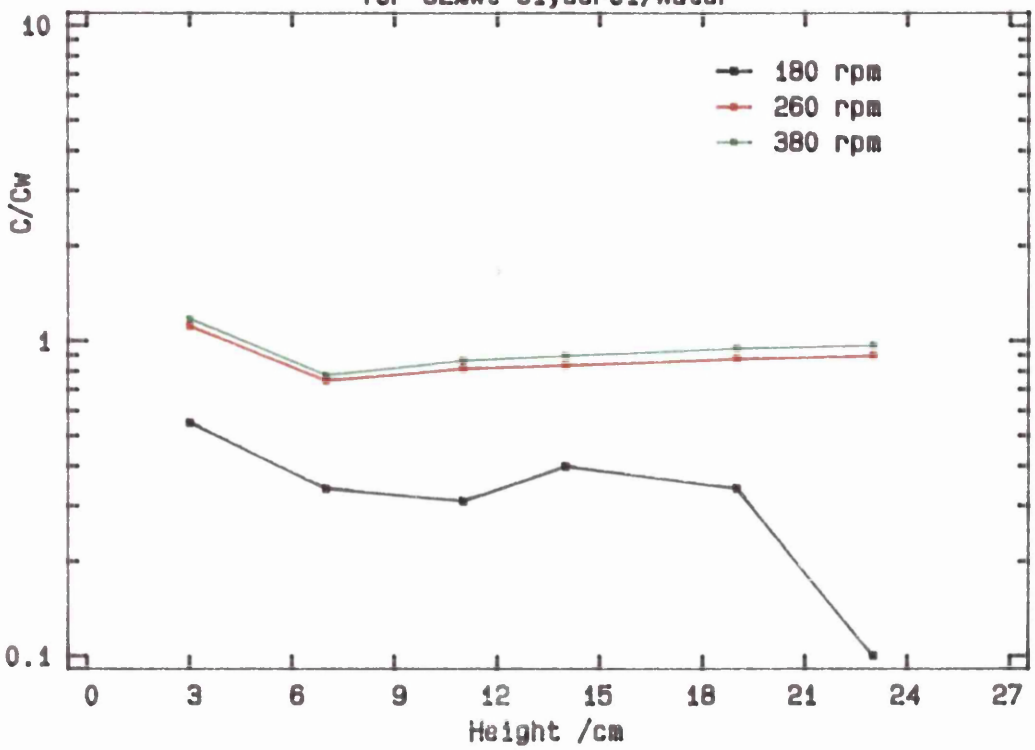

Figure 5.2.35

Semi-log Axial Concentration Profile
for 0.25%wt CMC

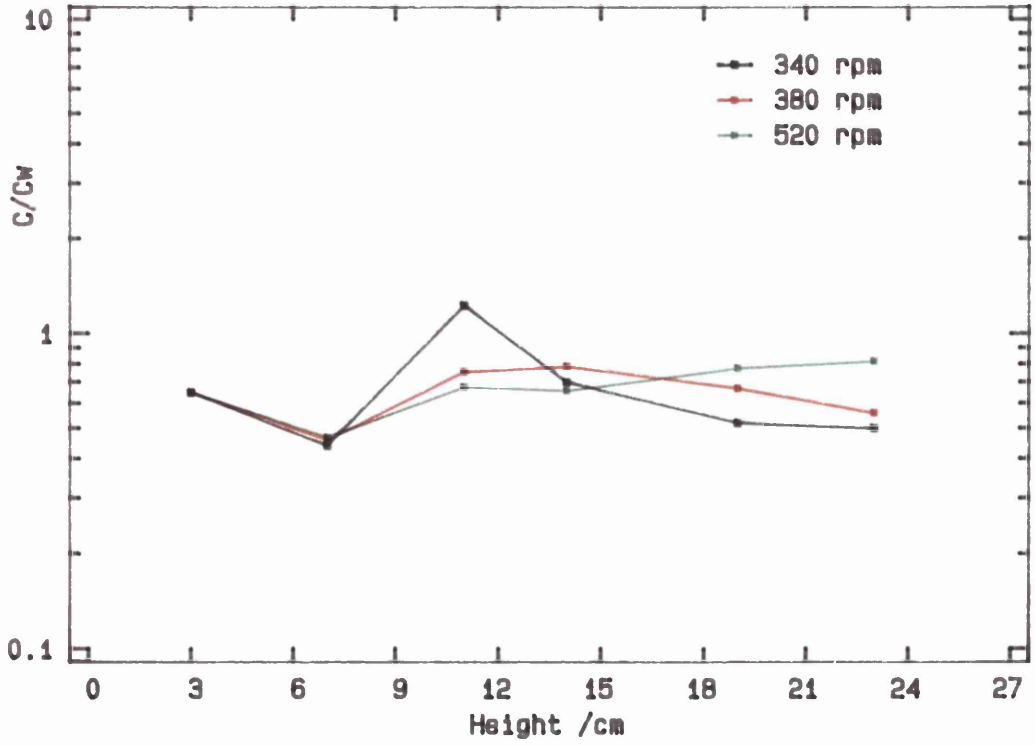

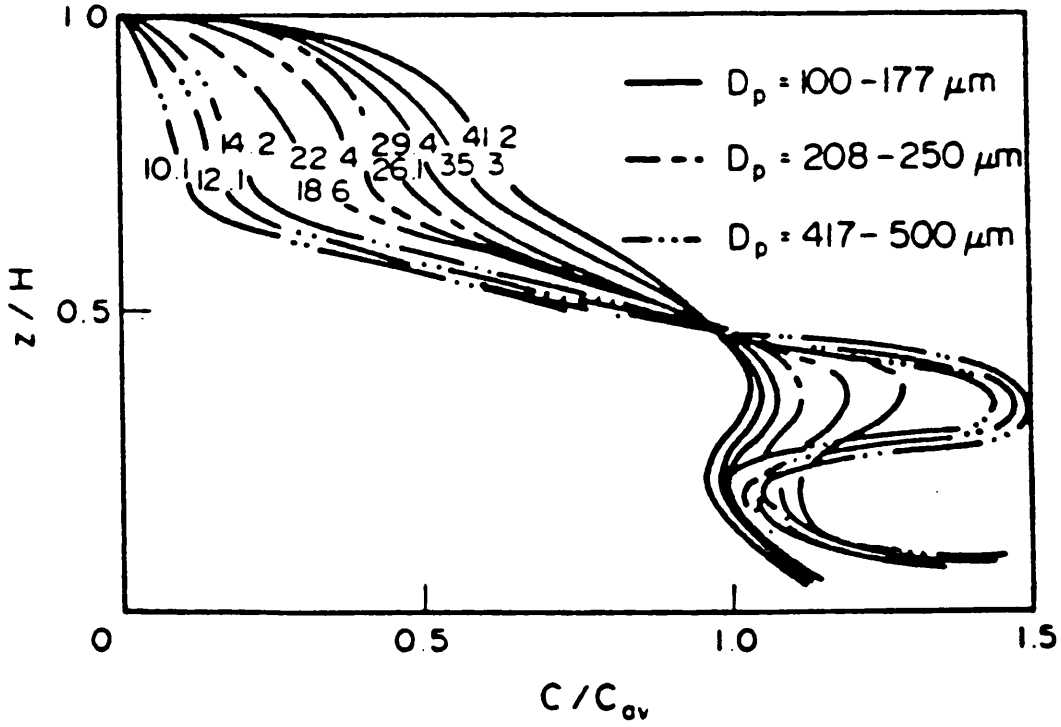

Figure 5.2.36 Axial concentration profiles with K as a parameter (Baressi & Baldi, 1987)

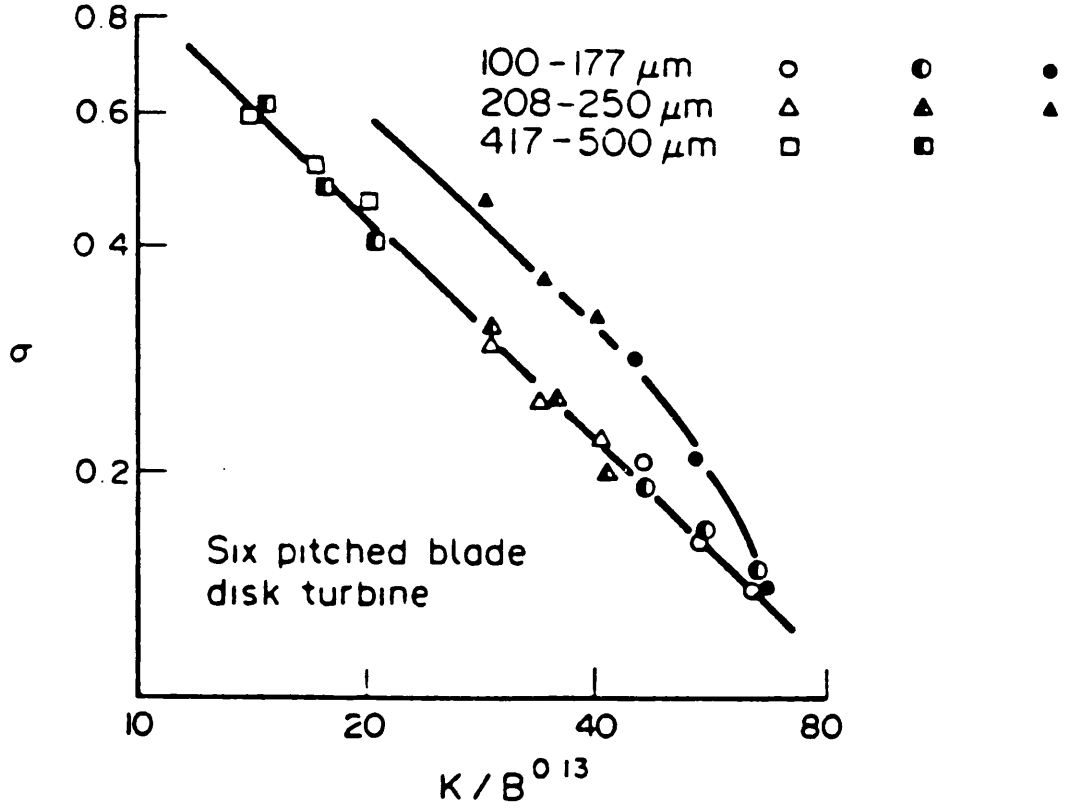

Figure 5.2.37 Distribution quality vs K (Barresi & Baldi, 1987)

Figure 5.2.38
Plots of Local Concentration Variance vs K-Parameter

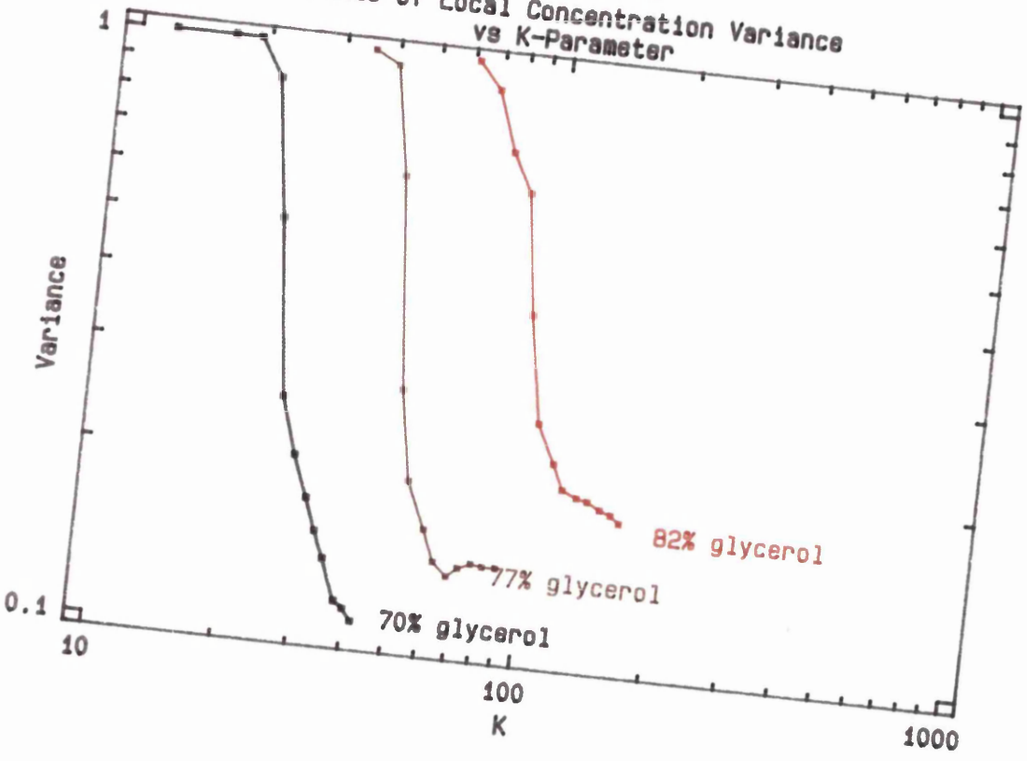

Figure 5.2.39
Plots of Local Concentration Variance vs K-Parameter

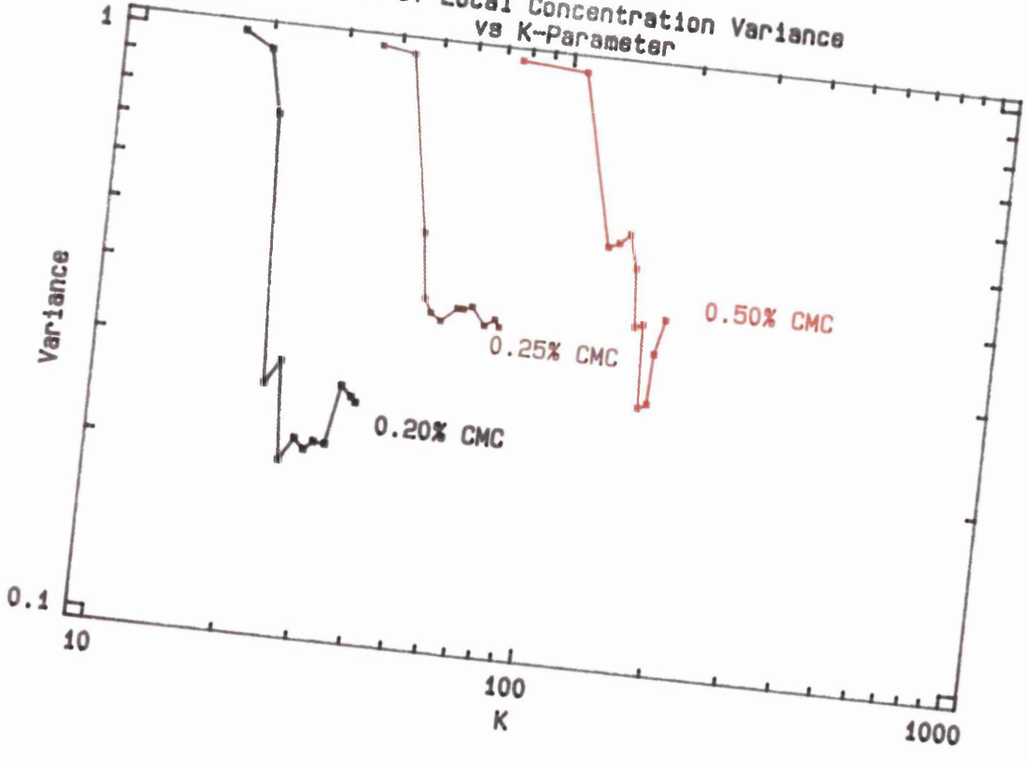

a) Lift-force measurements - determination of C_L

In Chapter Three, a mathematical model has been developed in order to relate N_{JS} to the other design parameters that define the agitation system. This model relies on a force balance between the effective weight of the particles (gravity - buoyancy) and the hydrodynamic forces on the particles that arise from the mean (or time-averaged) flow of liquid immediately adjacent to those particles resting at the base of the vessel.

$$F_G = F_L + F_D \qquad 5.3.1$$

where F_L is the lift force on the particle

F_D is the upward component of the drag force on the particle

and F_G is the effective weight of the particle.

As has been discussed in Chapter Three, relating F_G and F_L to particle and liquid properties is relatively straight forward. Unfortunately, the determination of F_L and the associated co-efficient, C_L, is more problematic because there is very little theoretical or experimental work that can easily be applied to the prediction of C_L for a sphere resting on a plane with axisymmetric flow and for intermediate particle Reynolds Numbers ($10^{-2} < Re_p < 10^{1}$) .

In Chapter Three, an analysis of existing knowledge on boundary layer theory and the effect of liquid circulations in the vicinity of a sphere has led to a relationship between the lift co-efficient and the particle such that:

$$C_L \propto {}^{1}/_{d_p^n} \qquad n > 0 \qquad 5.3.2$$

This means that no matter what the viscosity or density of the liquid, or its relative velocity, only the diameter of the particle will decide the magnitude of the lift

co-efficient. This does not mean that the liquid properties just mentioned are not important in deciding the magnitude of the lift force:

$$F_L = \frac{1}{2}\rho_f \pi \left(d_{p/2}\right)^2 u_h^2 C_L \qquad 5.3.3$$

where u_h is a function of liquid viscosity as well as other variables.

In order to show that C_L is dependent only on the particle diameter, a series of experiments were conducted in which the pressure difference between the base and the top of the sphere was measured for a range of different diameter spheres in two viscosities of liquid (see Chapter Four for more detail of equipment and procedures).

Figures 5.3.1. and 5.3.2. show the resulting velocity profiles of the axial component of the liquid's velocity at three different axial distances from the centre of the "water tunnel". For each profile, the velocity, at first, increases with distance from the base. The velocity then reaches a peak before falling off. For the more viscous of the two glycerol/water mixtures, these peaks all occur at about 4mm from the base, whilst at a viscosity of 0.0035 Pas, the peak depends on the axial position of the profile. As the measurements are taken closer to the centre, the axis of the jet of liquid is being forced from the horizontal to the vertical. This causes the peak velocity to be shifted upwards away from the base. At higher viscosities, the jet will not remain so distinct since much of the initial energy of the jet emerging from the mouth of the two nozzles will have been dissipated into the almost stagnant liquid that constitutes the bulk of the liquid in the water tunnel. This explains why the profile peak does not rise significantly higher from the base, and also why the liquid velocities are generally less in the 0.006 Pas liquid compared to the 0.0035 Pas mixture.

These velocity profiles are not the same as those profiles expected in the vicinity of a sphere at the base of an agitated tank with a radial flow pattern. However, this should not interfere with the proposed relationship

between C_L and d_p. The positioning of the two nozzles ensures that the sphere still experiences axisymmetric flow (although in this case only along one axis of symmetry), and so the analysis presented in Chapter Three should be equally applicable. The nozzle dimensions and the geometry of the water tunnel should only effect the relationship between C_L and d_p in so much as the constant of proportionality, c_1^* may differ from the actual value of c_1 applicable to the conventional agitation systems used for this study.

Table 5.3.1. shows the measured differential pressures for each size of sphere in both viscosities of liquid. Ideally more viscous mixtures of glycerol and water should be used, together with smaller diameter spheres, but the limitations of the centrifugal pump and pressure measurement equipment meant that this was impracticable.

If the pressure differential across the sphere is known, the lift force on the particle can be determined by equation 5.3.4. (D.G.Thomas, 1961):

$$F_L = \frac{3}{2}\,\frac{4}{3}\,\Pi\left(d_{p/2}\right)^3 \frac{\Delta P}{d_p} \qquad 5.3.4$$

by definition

$$F_L = \frac{1}{2}\,\rho_f \Pi\left(d_{p/2}\right)^2 u_h^2\, C_L \qquad 5.3.5$$

then equating 5.3.4. to 5.3.5. and after some rearrangement

$$C_L = \frac{2\Delta P}{\rho_f u_h^2} \qquad 5.3.6$$

u_h is taken to be the averaged, undisturbed velocity, u_{CL}, of the liquid acting at the centre-line of the particle, one particle radius from the the centre of the vessel. The value of u_{CL} can be calculated from:

$$u_{CL} = \frac{1}{d_p}\int_0^{d_p} u(z)\,dz \qquad 5.3.7$$

The integral can be evaluated numerically from the area under the velocity profile. If the required velocity, u_{CL},

does not co-incide with one of the velocity profiles, then u_{CL} was approximated by linear interpolation.

The following example shows how C_L was calculated for a 16mm sphere. Using the 1096 glycerol/water mixture

$$u_{CL} = \frac{1}{16}\int_0^{16} u(z)dz = 12.6\text{cm/s} \qquad 5.3.8$$

where the integral has been evaluated by integrating the velocity profile 1.5cm from the centre of the vessel. However, the pertinent value of u_{CL} has to be found at a distance of 0.8cm ($d_p/2$) from the vessel centre. Assuming that there is perfect symmetry, the horizontal velocity component must be zero for all heights, z, at the centre of the vessel,, so that

$$u_{CL} = \frac{8}{15} \times 12.6 = 6.72\text{cm/s} \qquad 5.3.9$$

The measured value of ΔP was 7.2 Pa

$$\therefore\ C_L = \frac{2 \times 7.2}{1096 \times (0.0672)^2} = 2.91 \qquad 5.3.10$$

Figure 5.3.3. shows a ln/ln plot of C_L vs d_p using data from both viscosities. The data is well correlated by a straight line with a random scatter of points about the line of best fit (correlation co-efficient = 0.964).

The Unistat plot indicates that

$$C_L \propto {}^1/_{d_p^{0.71}} \qquad 5.3.11$$

whilst for the purposes of the model, it was assumed that

$$C_L \propto {}^1/_{d_p^{1.0}} \qquad 5.3.12$$

Substitution of 5.3.11. into the Q.M.F. model so that

$$C_L = c_1 \left[T/d_p \right]^{0.71} \qquad 5.3.13$$

would alter the first R.H.S. term of 3.1.20:

$$1^{st} \text{ R.H.S. term} = A^2 c_1 \left[d_p/T \right]^2 N_{JS}^2 D^2 (D/T)^2 \left[T/d_p \right]^{0.71} \qquad 5.3.14$$

However, this would mean that N_{JS} is no longer independent of the particle diameter, even at high d_p. Instead, when the first R.H.S. term dominates the second term,

$$N_{JS}^2 \propto 1/d_p^{0.29} \qquad 5.3.15$$

and therefore, N_{JS} would peak at some value of d_p before declining gradually with increasing d_p. Although some experimental evidence has shown that this may be the case (Shamlou & Zolfagharian, 1987), the experimental data gathered in this study, as well as others, does not indicate such a peak. (see 5.3.b for further discussion of the possible implications of equation 5.3.13 for the Q.M.F. model).

The lift force measurements were conducted in a rectangular vessel, rather than a cylinder. As a consequence, the relationship described by 5.3.13 can only crudely approximate to the real situation of particle suspension in a cylindrical vessel. Although the value of the exponent, 0.71, is unlikely to be affected by the geometrical differences, the value of the constant of proportionality, c_1, is. In order to come more closely to this value of c_1, a means would have to be found of measuring the differential pressure across the height of the sphere fixed to the base of a flat-bottomed tank with a suitable impeller to provide a radial flow pattern. This may prove difficult to achieve accurately because the introduction of any pressure probes would be even more intrusive than when taking measurements with the water tunnel apparatus.

Experiments have been conducted by other researchers investigating the lateral migration of rigid spheres, which

was first investigated by Segre and Silverberg, 1962. However, these studies have concentrated on determining particle trajectories. An experimental paper by Eichhorn and Small, 1964, in which spheres were suspended in Poiseuille flow, tentatively concluded that "...C_L decreases with increasing Re_p and increases with decreasing diameter ratio". (The diameter ratio defined as particle diameter divided by tube diameter). The second half of this conclusion is in agreement with the experimental results shown in figure 5.3.3. The lack of any effect of Re_p on C_L in this study can be explained by the arguments of symmetry discussed in Chapter 3.

Table 5.3.1

Experiments to determine the Lift Co-efficient

d_p/mm	μ/Pas	u_{cl}/ms^{-1}	Re_p	ΔP/Pa	c_L
12.5	0.0035	0.0508	199	5.0	3.51
16.0	0.0035	0.0672	337	7.2	2.91
20.5	0.0035	0.0834	535	9.2	2.42
24.0	0.0035	0.0968	727	11.1	2.16
39.0	0.0035	0.1200	1466	13.0	1.65
12.5	0.0060	0.0470	110	5.0	4.03
16.0	0.0060	0.0632	189	6.5	2.90
20.5	0.0060	0.0803	308	7.5	2.07
24.0	0.0060	0.0928	416	11.0	2.28
39.0	0.0060	0.1110	802	11.1	1.63

Figure 5.3.1

Velocity Profiles in Water Tunnel
with 1096 Glycerol

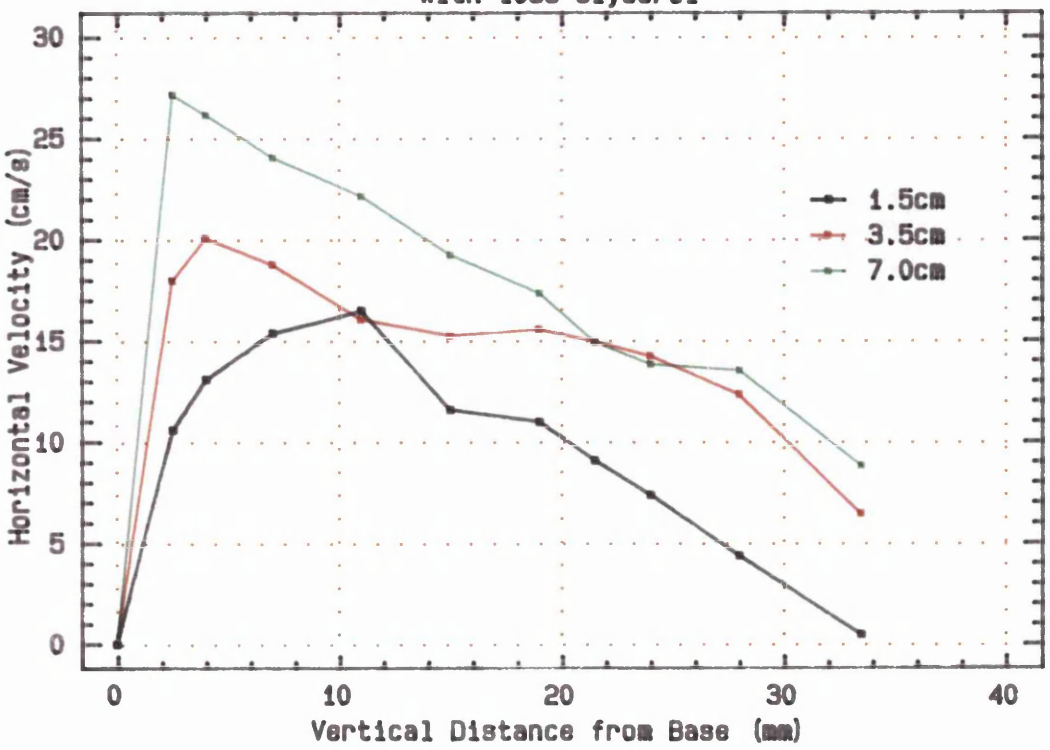

Figure 5.3.2

Velocity Profiles in Water Tunnel
with 1122 Glycerol

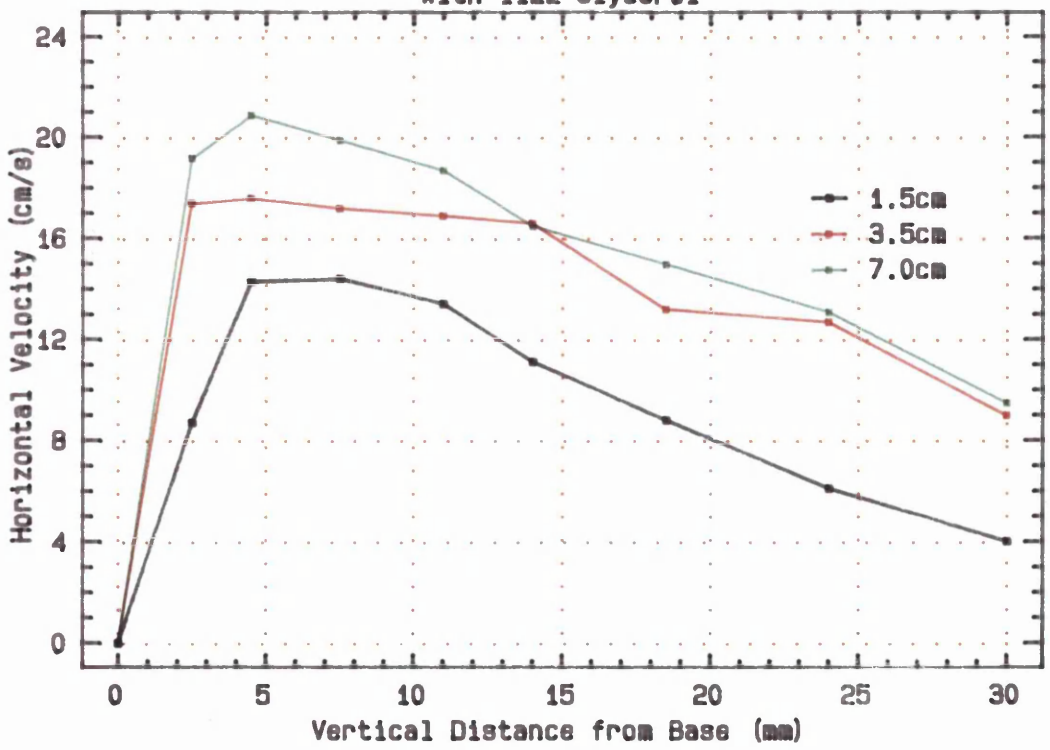

Figure 5.3.3
Lift co-efficient vs particle diameter

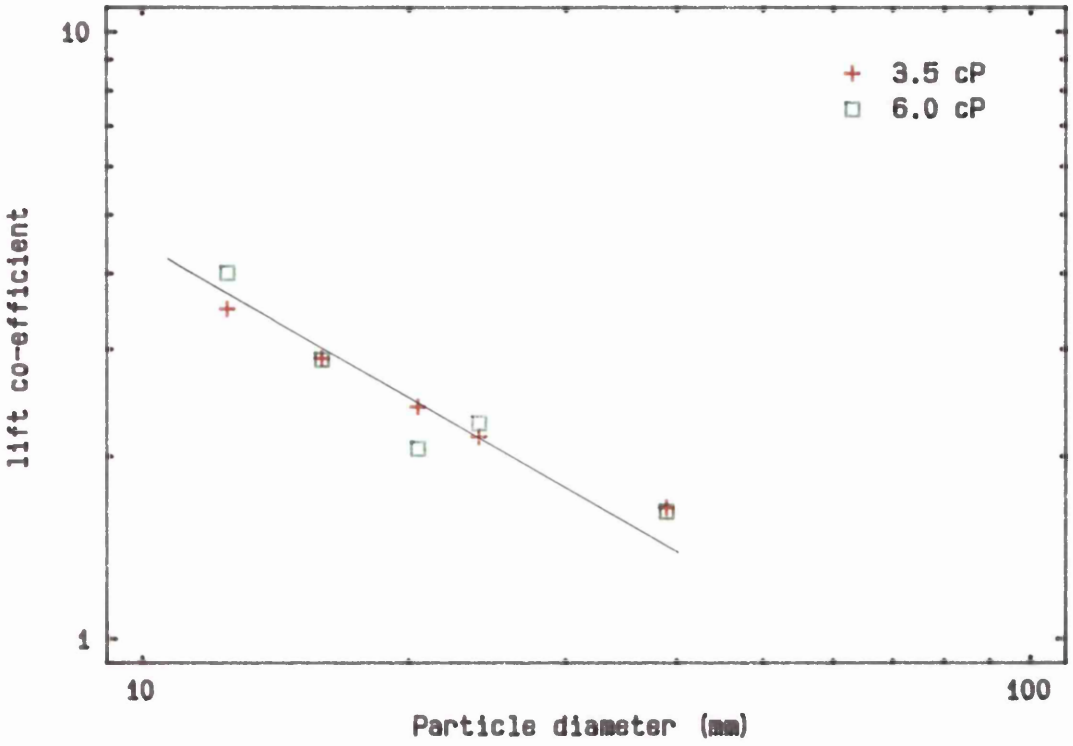

b) Velocity profile measurements

The purpose of these velocity measurements is to determine the velocity profile at the base of a flat bottomed cylindrical vessel. These profiles have been measured in a variety of glycerol/water mixtures with differing physical properties, most importantly viscosity (see Chapter Four for more detail of equipment and procedures). These profiles have also been measured at a variety of radial positions close to the centre of the flat base of the tank.

Following the work of Molerus & Latzel, 1987, it was important to confirm, at a given r and z close to the area where the last particles would lift into suspension, that the horizontal (radial) component of the liquid's velocity is proportional to the impeller tip speed, ND.

Figure 5.3.4. shows a typical plot of u_h against N for the impeller and tank used. The UNISTAT software shows that the data is well fitted to the a straight line passing through the origin so that:

$$u_h \propto N \qquad 5.3.16$$

Other plots of u_h vs N are presented in Appendix 6. Figure 5.3.5. shows velocity profiles obtained at various impeller speeds in a 83%wt glycerol/water mixture. These can be contrasted with the velocity profiles presented in 5.3.a. The closest that the centre-line of the pitot tube comes to the base of the tank is 1.5mm. Lacking any other information, the points have been connected with a straight line, as indeed have all adjacent points. It should be remembered that these velocities are probably overestimates of the actual u_h because the presence of the pitot tube acts to shield the liquid from opposing liquid components. Although for the suspension of large particles, 6 to 10mm in diameter, the degree of shielding afforded by the pitot tube and the spherical particle will be very close.

Curiously, the flattest profiles are found for the lowest impeller speeds (95-97 rpm), even though this should

correspond to when conditions are most laminar (or at the least turbulent). At higher speeds, there is greater variation with distance from the base, z, especially with the more viscous glycerol/water mixtures. When the local conditions are turbulent, it is expected that velocity profile will be flatter, whereas for laminar conditions, a linear velocity profile might have been expected. This can only be consistent with the conclusion that the data gathered at 95-97 rpm is unreliable because of the limitations of the pressure recording equipment. These pressures, in turn, are used to determine the horizontal component of the liquid's velocity. The velocities calculated at higher impeller speeds, where the experimental data seems more reliable, show that between 1.5 and 6.5mm, the velocity profile is neither flat nor laminar, i.e. in some intermediate régime.

In the development of the "quadratic mean flow" model (see Chapter Three), an assumption is made that the local conditions are sufficiently laminar at the base of the tank so that the velocity profile in the proximity of the suspending spheres is linear and as a consequence

$$u_h \propto d_p \qquad 5.3.17$$

The effective velocity component that is assumed to determine the hydrodynamic forces, lift and drag, on the particle is taken to be an averaged velocity across the diameter of the particle. In the case of a linear velocity profile, this average will occur at the centre-line of the particle, $d_p/2$ from the base. This still seems to be a good assumption for particles of diameter less than 1.5mm, but for larger particles, the profile will not be linear. However, as long as the velocity still increases with z, then the assumption will still be a good approximation for particles upto about 10mm in diameter.

The velocity profiles were determined for each liquid at three radial distances from the centre; 6.6, 10.6, and 15.6mm. At a radial distance of 10.6mm, the horizontal velocity component is at its highest. At any given height

from the base, the horizontal component will be zero at the centre of the tank and at the periphery of the tank. In between these two points, assuming a radial flow pattern, the liquid must accelerate inwards from the periphery and reach some peak velocity before decelerating as it approaches the centre. From the experimental data gathered for this impeller and tank, these peak horizontal velocities are to be found close to 10.6mm from the centre of the tank.

The results from this set of velocity profile experiments can be used to prove the relationship described by equation 5.3.16. Experiments were not conducted with different impeller diameters or clearances or tank sizes. This means that it has not been verified that for all D, ΔZ, and T, that:

$$u_h \propto ND(D/T) \qquad 5.3.18$$

only that for a given ΔZ, D, and T, u_h is directly proportional to N.

As explained in 5.1. there is a complex interaction between ΔZ and D in highly viscous liquids. This interaction would mean that altering the tip speed by changing D rather than N would not necessarily lead to the same u_h. The constant of proportionality, A, is a function of viscosity and clearance (amongst other variables). Changing D, even for the same viscosity of liquid may change the way that the impeller clearance influences A and hence u_h, so that u_h will no longer be proportional to ND.

Unfortunately, investigation of the relationship between the impeller clearance/diameter interaction and the consequent u_h did not prove possible with the equipment available. As the liquid increases in viscosity (above 0.25 Pas), the liquid velocities become so low that the pressure transducer is unable to reliably detect the difference between the impact and static pressures.

If u_h is proportional to N, then the slope of the UNISTAT plots will give the constant of proportionality, A^*.

$$u_h = A^*N \qquad 5.3.19$$

where A^* is equivalent to AD(D/T)

If the geometry is kept constant, and only the kinematic viscosity varied, then the variation of A^* as a function of υ can be empirically determined. Using the data from all radial and axial positions used to measure the horizontal velocity component, an averaged value for A^* can be calculated for each glycerol/water mixture. Table 5.3.2. shows the averaged A^* in each mixture.

$\frac{\mu}{\rho_f}$ (m^2/s)	A^*
0.000231	0.1425
0.000122	0.1469
0.000059	0.1650

Table 5.3.2
Effect of Viscosity on Velocity Profile

Using these three points to plot ln A vs ln(υ), an empirical relationship is found such that for this range of viscosities

$$A^* \propto \upsilon^{-0.11} \qquad 5.3.20$$

For a constant geometry and liquid, the constant of proportionality, A, introduced in equation 3.1.17 will in turn be proportional to A^*. In 5.1.f a graph is presented showing that:

$$A^2C_1 \propto \upsilon^{-0.23}$$

From the results of these velocity measurements, admittedly with a narrow range of data, it has been found that:

$$A^2 \propto A^{*2} \propto \upsilon^{-0.22} \qquad 5.3.22$$

This gives an independent confirmation of the role played by the liquid viscosity in determining u_h and C_L that had been assumed in Chapter Three. This means that the

primary influence of viscosity, in the suspension process, is to dampen the liquid's horizontal velocity (as well as vertical) component as a fraction of the impeller tip speed. Although the viscosity of the liquid will effect the magnitude of the lift-force on the suspending particles, by influencing u_h, it will have no influence on the magnitude of the co-efficient of lift.

Following on from the discussion of equation 5.3.15, in 5.3.a, it is possible to use the data gathered in 5.3.b to explain how the Q.M.F. model can be consistent with the experimental observation that N_{js} becomes independent of particle diameter at high d_p.

The modified R.H.S. term (equation 5.3.14) is proportional to $d_p^{1.29}$. However, in order for N_{JS} to become independent of d_p, the R.H.S. term should be proportional to $d_p^{1.0}$.

The velocity profiles shown in figure 5.3.5 indicate that the assumption of a linear velocity profile at the base of the tank is only an approximation, so that:

$$u_h \propto d_p^n \quad 0 < n < 1 \qquad 5.3.23$$

If n were such that:

$$u_h^2 \propto d_p^{1.71} \qquad 5.3.24$$

then the condition for the first R.H.S term to be proportional to d_p^1 would be satisfied. This would imply a value of n of 0.855.

Equations 3.1.17 and 3.1.18 would then be modified to:

$$u_h = A\left[d_p/_T\right]^{0.855} ND(D/T) \qquad 5.3.25$$

and

$$u_h = B\left[d_p/_T\right]^{0.855} ND(D/T) \qquad 5.3.26$$

Figure 5.3.7. shows a typical velocity profile replotted on ln/ln co-ordinates. This confirms that n < 1, but also indicates that n is closer to 0.7 rather than 0.85.

However, for the purposes of the discussion that follows in 5.4, the original model described in Chapter Three is compared with the experimental data gathered in this study as well as the findings of other workers.

Figure 5.3.4
Plot of Horizontal Liquid Velocity vs Impeller Speed

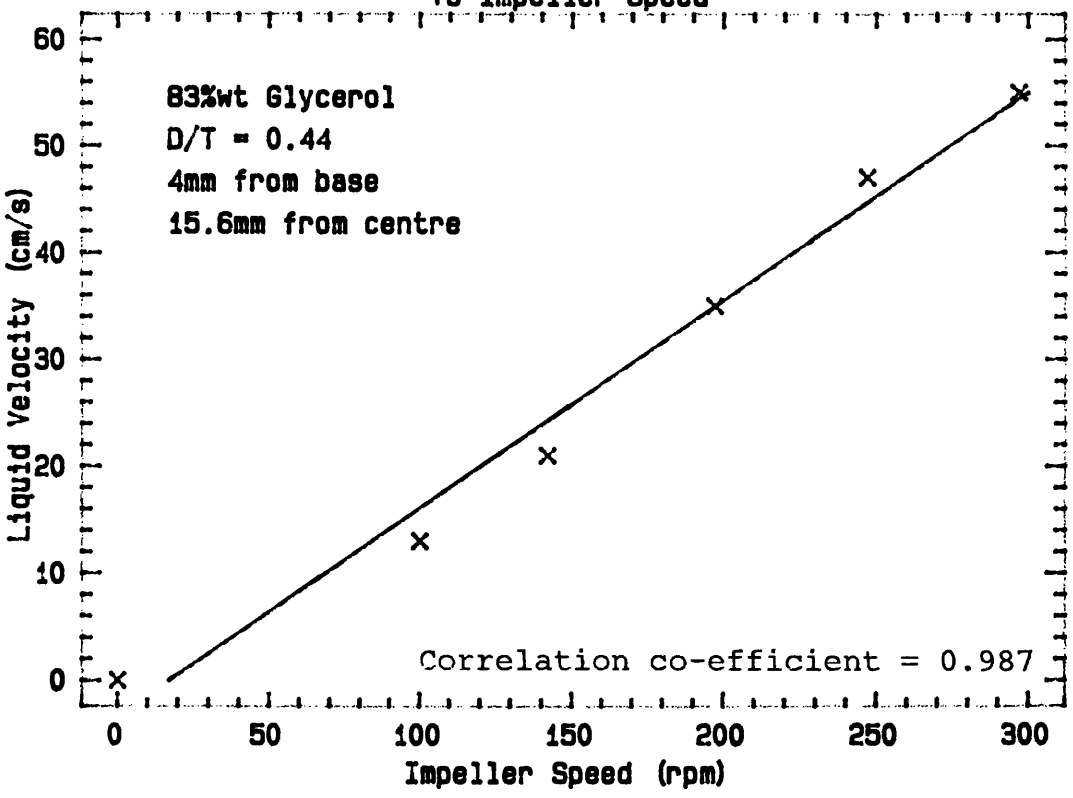

Figure 5.3.5

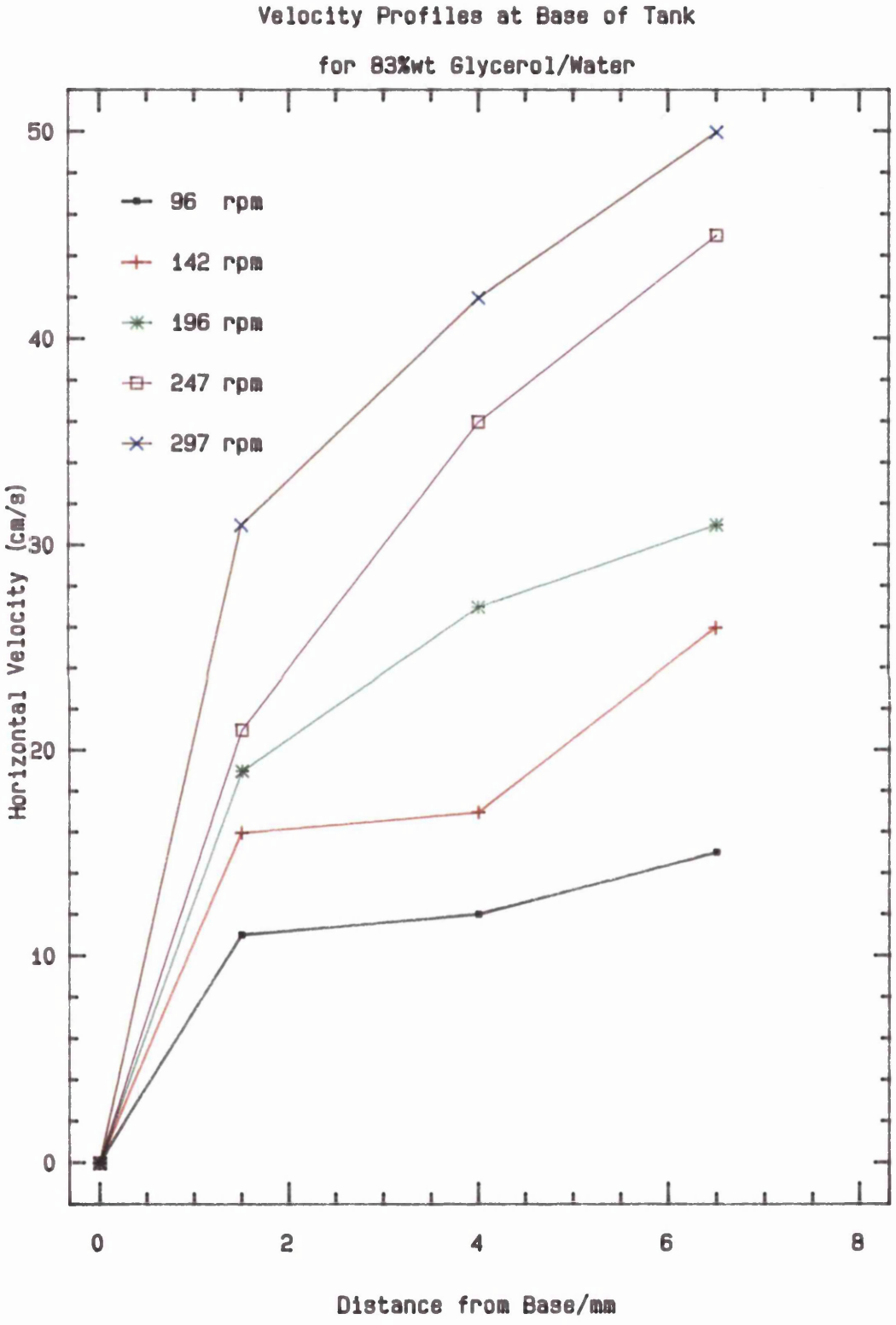
Velocity Profiles at Base of Tank
for 83%wt Glycerol/Water
96 rpm
142 rpm
196 rpm
247 rpm
297 rpm
Horizontal Velocity (cm/s)
0
10
20
30
40
50
0
2
4
6
8
Distance from Base/mm

Figure 5.3.6
Plot of A* vs Kinematic Viscosity

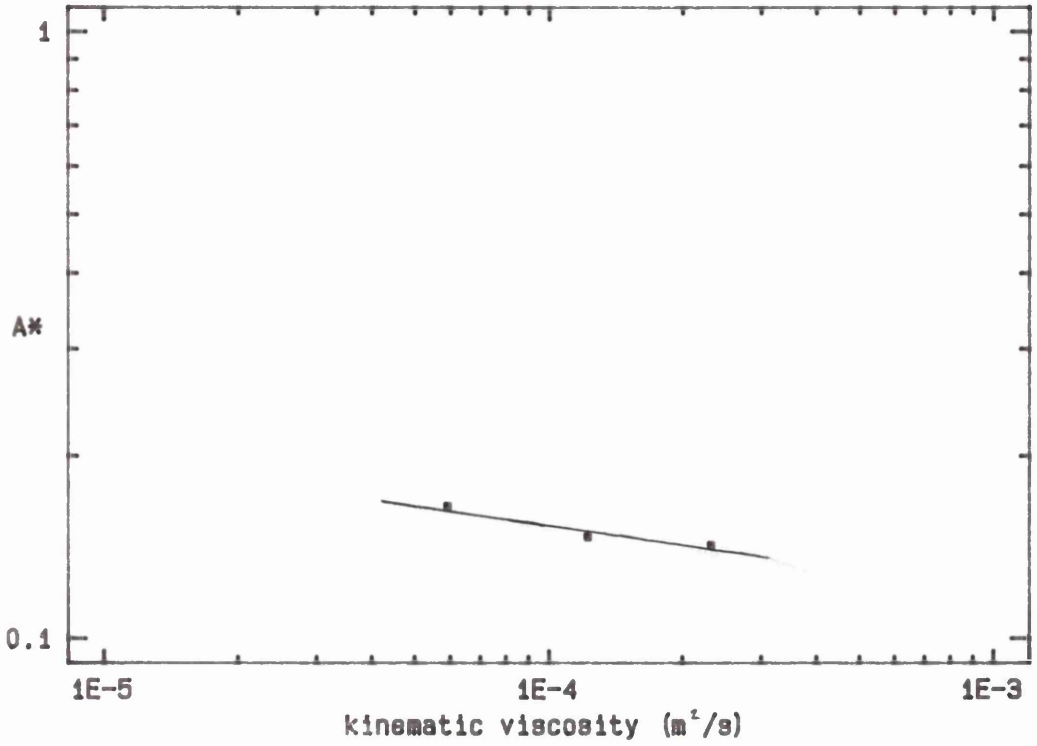

Figure 5.3.7
Plot of Velocity Profile for
83%wt Glycerol/Water

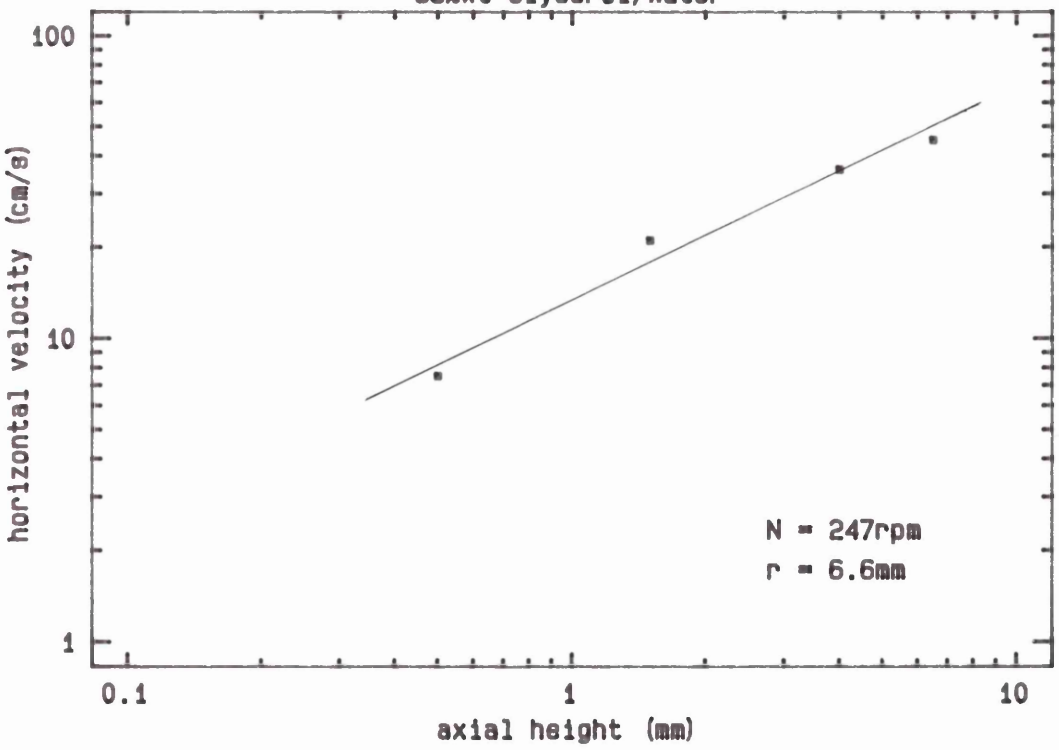

5.4 Comparison of Experimental Data with Quadratic Mean Flow Model

The Quadratic Mean Flow (QMF) model has been derived in Chapter Three. According to this model, N_{JS}, the just suspension speed, is related to the other design parameters by equation 3.1.20.

$$N_{JS} = \frac{-\frac{Bc_2}{d_p}\upsilon + \sqrt{\left[\frac{Bc_2}{d_p}\right]^2 \upsilon^2 + \frac{16}{3}\left[\frac{\rho_s - \rho_f}{\rho_f}\right]^2 gTA^2c_1}}{2\,A^2c_1\,D(D/T)} \qquad 5.4.1$$

This relatively simple model has not incorporated the influence of solids concentration. (See Appendix 5 for mathematical treatment to show effect of concentration).

a) evaluation of the composite constants for Newtonian liquids

In order to make use of 5.4.1 in a quantitative way, so as to predict values for N_{JS}, the two composite constants, A^2c_1 and Bc_2 need to be evaluated. However, these composite constant are themselves determined by the system geometry (including impeller clearance) and the viscous properties of the liquid. In 5.1.f, using liquids of intermediate viscosity (the glycerol/water mixtures), when the complex interactions between the impeller diameter and clearance are at their least significant, then A^2c_1 was found to be simply related to the kinematic viscosity by:

$$A^2c_1 \propto \left[\mu/\rho_f\right]^{-0.29} \qquad 5.4.2$$

Again for intermediate viscosity liquids, A^2c_1 was found to related to the impeller clearance by a simple proportionality:

$$A^2c_1 \propto \Delta Z^{-0.20} \qquad 5.4.3$$

Incorporating 5.4.1 and 5.4.2 together, then:

$$A^2c_1 \propto \Delta Z^{-0.20}\left[\mu/\rho_f\right]^{-0.29} \qquad 5.4.4$$

$$\text{or} \quad A^2c_1 = 5.0\left[\Delta Z/T\right]^{-0.20}\left[\mu/\rho_f\right]^{-0.29} \qquad 5.4.5$$

Assuming that within the composite constant, A^2c_1, c_1 is neither a function of ΔZ nor of υ; and furthermore, within the composite constant Bc_2, c_2 is not a function of ΔZ or υ, then for consistency, it should follow that:

$$Bc_2 \propto \Delta Z^{-0.10}\left[\mu/\rho\right]_f^{-0.115} \qquad 5.4.6$$

The evaluation of Bc_2 is much more difficult to achieve with a high degree of accuracy. Referring to equation 3.1.19 unless the Archemedes Number, Ar, is very small, then the term involving A^2c_1 will tend to dominate the term involving Bc_2. This means that the empirical evaluation of Bc_2 has to be achieved by the subtraction of one relatively large number from another, slightly larger number.

Analysis of the suspension speed data gives a value of 1.0 as being the most probable for the constant of proportionality in equation 5.4.6.

Substituting for A^2c_1 and Bc_2 into equation 5.4.1 (not fully substituted for lack of space)

$$N_{JS} = \frac{-\frac{1.0}{d_p}\left[\frac{\Delta Z}{T}\right]^{-0.1}\upsilon^{0.885} + \sqrt{\left[\frac{Bc_2}{d_p}\right]^2\upsilon^2 + \frac{16}{3}\left[\frac{\rho_s-\rho_f}{\rho_f}\right]^2 gTA^2c_1}}{10.0\left[\Delta Z/T\right]^{-0.20}\left[\mu/\rho_f\right]^{-0.29} D(D/T)} \qquad 5.4.7$$

Using equation 5.4.7 it is possible to calculate predicted values for N_{JS} in any size of flat-bottomed,

unbaffled, cylindrical tank where the agitation is caused by any "reasonable" size ($0.2 < D/T < 0.66$) of six-bladed 45 degree pitched turbine that pumps upwards causing a radial flow pattern.

Figure 5.4.1 shows a comparison between prediction and experimental values for N_{JS} using equation 5.4.7. The experimental values are taken from suspension speed measurements conducted in glycerol/water mixtures. The corresponding predictions show very good agreement with the points on the graph lying very close to the x=y diagonal. The average difference between the experimental and predicted values of N_{JS} is 5.1%.

Unfortunately, application of the model, using equation 5.4.7, to the much more viscous corn syrup/water mixtures does not yield satisfactory quantitative predictions. In general, equation 5.4.7 over-predicts N_{JS}, as compared with experimental data, sometimes by a factor of 3 or 4. A possible explanation for such overestimation may lie in the attempted extrapolation of the empirically determined correlations for A^2c_1 and Bc_2. The former of these two being the most significant. Since there is an over-prediction, this suggests that A^2c_1 is higher in the corn syrup/water mixtures than predicted using 5.4.4. Figure 5.4.2 shows a graph of predicted values of N_{JS} vs experimental values in corn syrup/water mixtures using the relationship:

$$N_{JS} = \frac{-\frac{1.0}{d_p}\left(\frac{\Delta Z}{T}\right)^{-0.1}\upsilon^{0.885} + \sqrt{\left(\frac{Bc_2}{d_p}\right)^2\upsilon^2 + \frac{16}{3}\left(\frac{\rho_s-\rho_f}{\rho_f}\right)^2 gTA^2c_1}}{100\left(\Delta Z/T\right)^{-0.20}\left(\mu/\rho_f\right)^{-0.23}D(D/T)} \qquad 5.4.8$$

where $$A^2c_1 = 50\left(\Delta Z/T\right)^{-0.20}\left(\mu/\rho_f\right)^{-0.23} \qquad 5.4.9$$

the constant of proportionality having been increased by a factor of ten compared to 5.4.4. Again, there is generally

good agreement between prediction and experiment except for the effect of varying impeller diameter. The average difference between prediction and experiment, using all the points in figure 5.4.2, is 16.8%.

The model predicts the effect of impeller diameter, D, on N_{JS} to follow the simple rule:

$$N_{JS} \propto {}^{1}/_{D^2} \qquad 5.4.10$$

However, the experimental data shows that varying the impeller diameter does not have such a dramatic effect on N_{JS}. For example, in the 30cm tank, containing a corn syrup/water mixture of viscosity 4.7 Pas, the ratio of N_{JS} values using a 6.5cm impeller and a 13cm impeller is only 4.28 to 2.95 /s (1.45), whilst the model was predicting a ratio of 4. The model does predict the correct ratios in the intermediate viscosity liquids. This discrepancy has already been noted and discussed in 5.1 and has been (partially) explained as being part of a complex interaction between the impeller diameter and its clearance in high viscosity systems.

Equation 5.4.9 has been modified from 5.4.8. by the simple expedient of substituting a value of 50 instead of 5.0. However, it may also be possible, and indeed quite likely, that the form of the relationship (5.4.4) would have to be completely altered in order to calculate values of A^2c_1 for all viscosities, impeller clearances and diameters so as to be in a position to accurately predict N_{JS}, i.e.

$$A^2c_1 \propto \Delta Z^{-\beta} \left[{}^{\mu}/_{\rho}\right]^{-\alpha} \qquad 5.4.11$$

where β and α are themselves functions of either D/T or υ or both. These functions have to be such that at intermediate viscosities, β tends to -0.20 and α tends to -0.23

The exponent, α, may follow a similar pattern to those exponents that govern the effect of particle diameter, d_p, and particle concentration, C_w. This means

that as the viscosity is increased, it has a diminishing effect on A^2c_1 so that α asymptotically tends to zero as the viscosity is increased.

i.e $\quad 0 < \alpha < 0.23$

The variation of viscosity may also have an influence on A^2c_1 through the function that relates the exponent β to the interaction between impeller clearance and diameter.

b) Evaluation of constants for non-Newtonian liquids

In a similar method to that used for the Newtonian liquids, the composite constants for the non-Newtonian fluids can also be evaluated.

In 5.1.h, a graph of A^2c_1 vs $k/\rho_f n$ is presented showing that:

$$A^2c_1 \propto \left(\frac{k}{\rho_f n}\right)^{-0.22} \qquad 5.4.12$$

The clearance was not altered for the non-Newtonian fluids investigated, but assuming a similarly simple relationship (as for the intermediate viscosity Newtonian liquids) then

$$A^2c_1 \propto \left(\frac{\Delta Z}{T}\right)^{-0.20}\left(\frac{k}{\rho_f n}\right)^{-0.22} \qquad 5.4.13$$

or $$A^2c_1 = 6.5\left(\frac{\Delta Z}{T}\right)^{-0.20}\left(\frac{k}{\rho_f n}\right)^{-0.22} \qquad 5.4.14$$

and for Bc_2:

$$Bc_2 = 1.0\left(\frac{\Delta Z}{T}\right)^{-0.20}\left(\frac{k}{\rho_f n}\right)^{-0.22} \qquad 5.4.15$$

substituting for A^2c_1 and Bc_2 from 5.4.14 and 5.4.15 and for υ by $k/\rho_f n$, then N_{JS} can be predicted using equation 5.4.1.

Figure 5.4.3 shows a comparison of predicted values of N_{JS} and experimentally measured values for suspension of particles in non-Newtonian fluids made with Carbonyl Methyl Cellulose (CMC) in water, with an average variation of 9.1%.

The only points which show significant deviation from the x=y diagonal are those that correspond to the suspension of acetate particles in 0.5%wt CMC, where the predicted values for N_{JS} are about 45% lower than the experimentally measured values. As mentioned in 5.1.f this might be caused by any elastic properties in the 0.5%wt CMC. These properties tend to be more significant at lower impeller speeds (those speeds required for the suspension of the relatively light acetate particles) but are diminished, in relative terms, at the higher speeds needed to suspend glass ballotini. Experiments were also conducted in 0.75 and 1.00%wt CMC solutions. However, these showed obvious signs of visco-elasticity (for more detailed observations of the suspension of particles in these fluids see Appendix 1).

Figure 5.4.1

Plot of Predicted vs Observed Njs Values for Glycerol/Water Mixtures

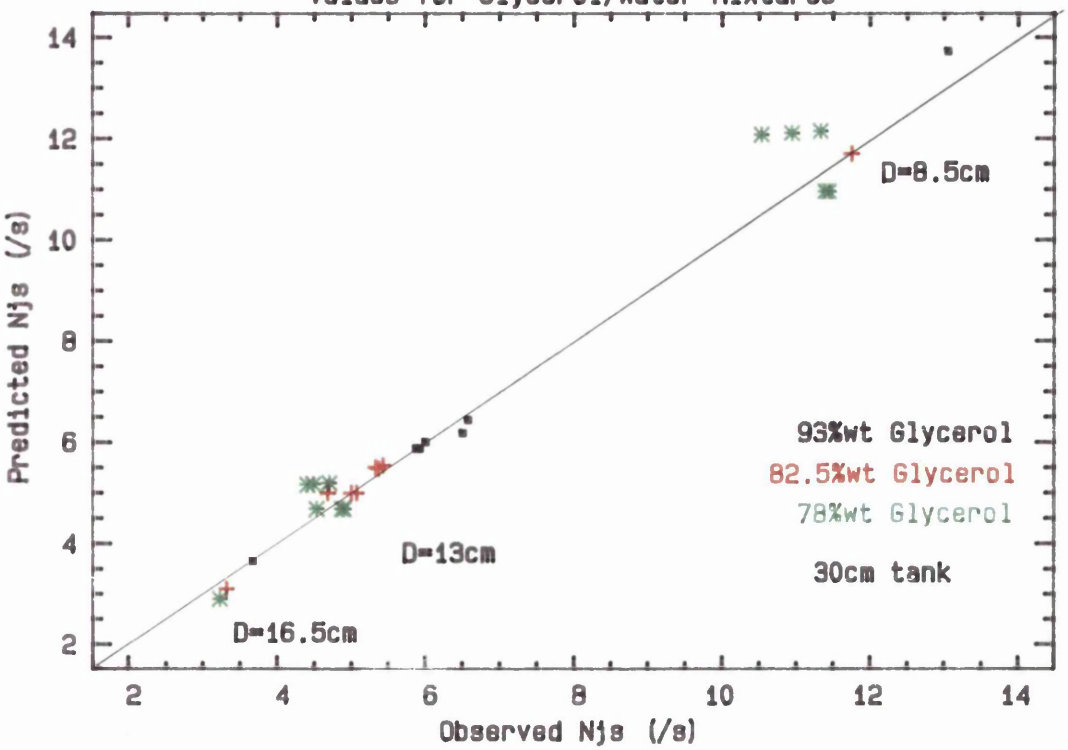

Figure 5.4.2

Plot of Predicted vs Observed Njs Values for Corn Syrup/Water Mixtures

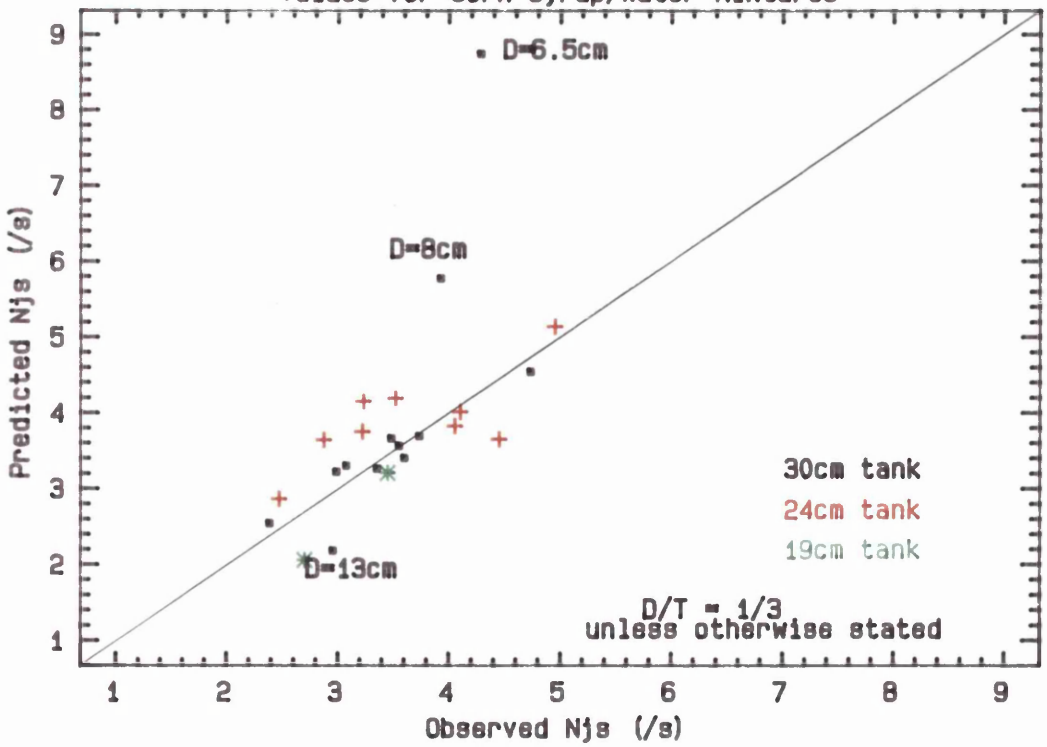

Figure 5.4.3

Plot of Predicted vs Observed Njs Values for CMC Solutions

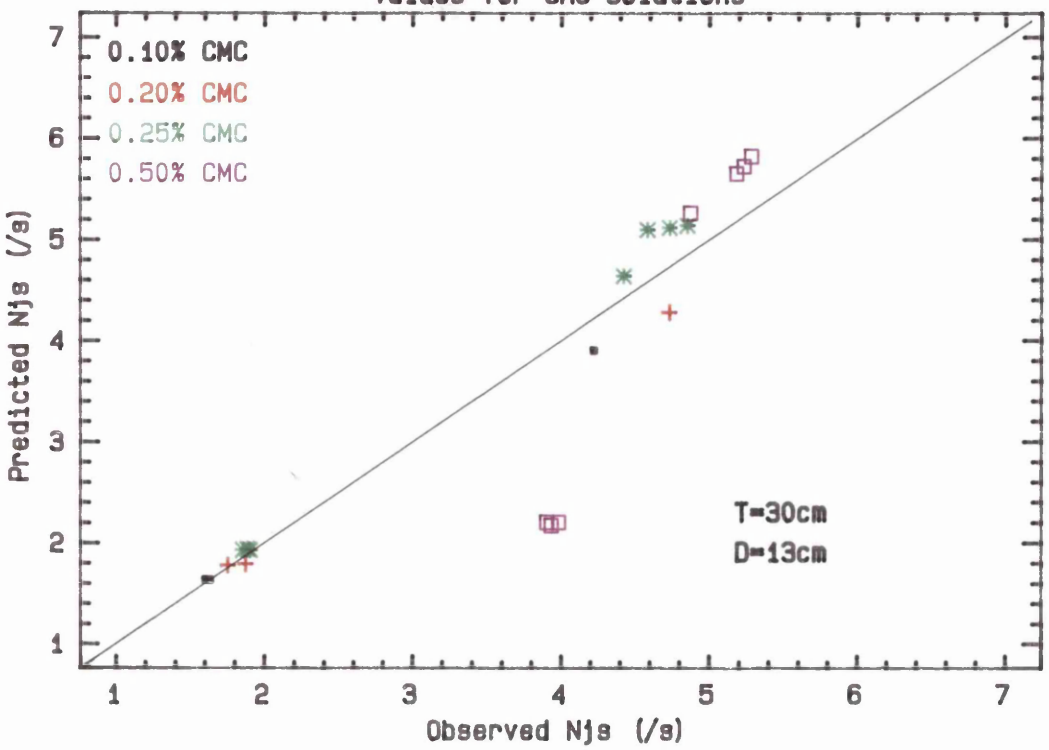

5.5 Comparison of Proposed Model with Previous Work

As stated before (see Chapter Two), there have many studies concerned with the suspension of solids in agitated vessels. Unfortunately, there has been very little work published (so far) of a systematic nature concerning the suspension of solids in liquids of viscosities orders of magnitude greater than water.

The agitation of water using any "mixed-flow" impeller (such as a pitched turbine) in conjunction with a set of baffles will normally lead to an axial flow pattern rather than the radial flow pattern reported for the viscous fluids used in this study. This axial flow pattern causes the last particles to lift into suspension at the periphery of the vessel's base, rather than at the centre. Since the geometry of the suspension mechanism is different for the two cases (the viscous and those liquids with a viscosity close to water), a quantitative comparison of the data and/or correlations from previous research with any predictions made using equation 5.4.8. is likely to prove fruitless. However, it has been postulated by this study that the mean flow mechanism is applicable even for cases where the impeller Reynolds Number might signify a high degree of turbulence in the bulk of the liquid. This means that the basic quadratic relationship for N_{JS}, equation 3.1.20, should still be a good approximation. In principle it should be possible to use some of the data taken from the researcher's data to calculate values for the composite constants Bc_2 and A^2c_1. These composite constants can than be substituted into 3.1.20 and the resulting equation used to calculate predictions of N_{JS} which can be compared with the rest of that researcher's data.

Comparison with Zweitering

The work of Zweitering (1958) remains the most complete set of empirical findings for the prediction of N_{JS}. As a consequence these findings are often used as a benchmark to which subsequent theoretical and empirical work can be compared. Zweitering's work is most

conveniently expressed by the following correlation:

$$N_{JS} = \frac{S\,\upsilon^{0.1}\,d_p^{0.2}\,C_w}{D^{0.85}}\left(\frac{\rho_f-\rho_s}{\rho_f}\right)^{0.45} g^{0.45} \qquad 5.5.1$$

and the quadratic mean flow model can be given by:

$$\frac{4}{3}\left(\frac{\rho_s-\rho_f}{\rho_f}\right)g = \frac{A^2c_1}{T}(ND)^2(D/T)^2 + \frac{Bc_2}{T}\frac{ND}{d_p}(D/T)\upsilon \qquad 5.5.2$$

Choosing a typical value for the geometric constant, S, of 6, N_{JS} can be found from 5.5.1 at the lowest viscosity used by Zweitering in combination with the highest particle diameter and density (i.e. at the highest Archemedes Number, Ar). In so doing the term involving Bc_2 will be dominated by the term involving A^2c_1 so that A^2c_1 can be approximated.

Using data taken with 850 μm sand particles suspended in acetone at 1.0%wt solids concentration, then:

$$N_{JS} = 7.67\ /s$$

where D/T = 0.13/0.30.

Using 5.5.2 when the first R.H.S. term >> second term

$$A^2c_1 = \frac{\frac{4}{3}\left(\frac{\rho_s-\rho_f}{\rho_f}\right)gT^3}{N_{JS}^2\,D^4} \qquad 5.5.3$$

substituting for the properties of the sand and acetone and taking the value of N_{JS} just calculated from 5.5.1 then:

$$A^2c_1 = 48.2$$

If A^2c_1 had been calculated by simply extrapolating from 5.4.5. then A^2c_1 would be about 100. This is is quite near considering the difference in geometrical factors.

To calculate Bc_2 most accurately from the Zweitering

data, N_{JS} should be calculated for the smallest, lightest particles in the most viscous liquid used by Zweitering. Using 125um sodium chloride particles in oil at 1.0%wt concentration, then 5.5.1 predicts N_{JS} as:

$$N_{JS} = 6.73 \text{ /s} \quad \text{(so that } Bc_2 = 106 \text{ using 5.5.2)}$$

The geometry has been kept the same as with acetone.

Before values for N_{JS} and A^2c_1 can be substituted into 5.4.1, A^2c_1 has to be corrected to take account of the difference in kinematic viscosities between acetone and oil. This means dividing by a factor K given by (see 5.4.2):

$$K = \left[\upsilon_{oil}/\upsilon_{acetone}\right]^{0.29} \qquad 5.5.4$$

so that the new value for A^2c_1 is 48.2/2.1. Substituting for A^2c_1 and Bc_2 into 5.4.1 (with Bc_2 = 106)

$$N_{JS} = \frac{-\frac{106}{d_p}\upsilon + \sqrt{\left[\frac{106}{d_p}\right]^2\upsilon^2 + \frac{16}{3}\left[\frac{\rho_s - \rho_f}{\rho_f}\right]^2 gT\frac{48.2}{2.1}}}{2 \times \frac{48.2}{2.1} D(D/T)} \qquad 5.5.5$$

where υ is about 1E-5 m^2/s. Using 5.5.5 it is then possible to compare the slope of any ln/ln plots of predicted N_{JS} vs any parameter, P, with the corresponding exponent for parameter P found empirically by Zweitering.

particle diameter

Figure 5.5.1. shows ln/ln plots of N_{JS} (as predicted by 5.5.5 with oil) vs d_p at the two different solid densities used by Zweitering. These are plots produced by the UNISTAT software package. These show that between 100 to 800μm, the predictions could be made to fit a straight line of slope approximately 0.20. With sodium chloride, the

slope is 0.1797, whilst for the denser sand, the slope is 0.1570. The errors in fitting a single straight line of slope 0.2 to what should be a shallow curve within the range 100 to 800μm are not large proving that there is good agreement between the findings of Zweitering and the quadratic mean flow model concerning the influence of particle diameter.

dimensionless density difference

Figure 5.5.2 shows ln/ln plots of N_{JS} vs the dimensionless density difference (again predicted for oil) at the extreme ranges of particle diameter used by Zweitering. These graphs are very accurately described by a single straight line. At the lower particle diameter (150μm), the slope is quite high 0.6424 whilst for the higher diameter (760μm), the slope has come down to 0.5295. If the particle diameter were increased further, then the slope would asymptotically reach a value of 0.5. This corresponds to the condition when the particle diameter no longer has any measurable influence on N_{JS}. This occurs at high Ar. Unfortunately, Zwietering's paper (1958) gives no indication of how many experiments were carried out at high or low Ar. The value of 0.45 is given without stating any variation in value.

The variation for the influence of gravity is given. According to Zwietering's 1958 paper, the exponent varied from 0.42 to 0.47. It might be supposed that the exponent governing the influence of the dimensionless density difference would also have varied from 0.42 to 0.47. This range of values can be compared with the range of values of 0.53 t0 0.64 as predicted from equation 5.4.16.

viscosity

Zwietering changed the kinematic viscosity from 0.39 x 10^{-6} (acetone) to 11.1 x 10^{-6} m^2/s (oil). Having previously calculated a value for A^2c_1 for acetone, the correction factor K, in equation 5.5.4, can be applied to

A^2c_1 to determine A^2c_1 at other, higher viscosities.

$$\text{i.e.} \quad A^2c_1 = \frac{48.2}{K} \quad \text{where} \quad K = \left[\upsilon / 0.39\times10^{-6}\right]^{0.29} \qquad 5.5.6$$

Bc_2 has been calculated from oil data, so a correction factor of K' should be applied to to calculate Bc_2 at other, lower viscosities

$$\text{i.e.} \quad Bc_2 = \frac{106}{K'} \quad \text{where} \quad K' = \left[\upsilon / 11.1\times10^{-6}\right]^{0.29/2} \qquad 5.5.7$$

Using K and K' it is then possible to calculate values for the composite constants A^2c_1 and Bc_2 which in turn can be substituted into 5.5.2 to evaluate N_{JS}.

$$N_{JS} = \frac{-\frac{106\upsilon}{d_p K'} + \sqrt{\left[\frac{106}{d_p}\right]^2 \frac{\upsilon^2}{K'^2} + \frac{16}{3}\left[\frac{\rho_s - \rho_f}{\rho_f}\right]^2 gT\frac{48.2}{K}}}{2\,\frac{48.2}{K}\,D(D/T)} \qquad 5.5.8$$

Figure 5.5.3. shows ln/ln plots of predicted N_{JS} vs. kinematic viscosity. One plot represents predictions made with the smallest and lightest particles used by Zwietering (150μm sodium chloride) whilst the other represents the largest and densest particles (760μm sand).

The most striking feature of the 150μm plot is that at a kinematic viscosity of about 4.5 x 10^{-6} m^2/s, N_{JS} peaks and then actually declines with increasing viscosity. The physical significance of this point lies in the relative values of the drag and lift forces acting on the particle. Increasing the viscosity of the liquid lowers the velocity of the liquid in the immediate vicinity of the suspending particles which lowers the lift force on the particle. However, the net effect on the drag is to increase the magnitude of the drag force acting upwards. When the Ar is sufficiently low, the drag force term

dominates the lift force term, with the consequence that increasing the viscosity will increase the total upward force on the particle, hence a lower N_{JS} is required to lift the particle. The Ar at this maximum is 2.9. Clearly one straight line cannot accurately describe all the points in the range 0.39 to 15 x 10^{-6} m^2/s. If the points to the right of the peak are ignored, then the slope of the best straight line is 0.06984. Zwietering did not report any such peak occurring for his data.

There is no such peak displayed for the 760μm plot. The minimum Ar in the range corresponding to a viscosity of 15 x 10^{-6} m^2/s is 40, well above the 2.9 value that corresponded to the N_{JS} peak of the 150μm plot. All the points in the range are accurately described by a single straight line of slope 0.09705. Increasing the viscosity beyond 15 x 10^{-6} m^2/s leads to the curve flattening out and reaching a maximum value of 10.32 /s. The Ar that corresponds to this peak is 18, which about 6 times higher than the value of Ar that corresponds to the peak of the 150μm plot. This means that the Archemedes Number cannot give a reliable means of determining the those conditions that will give rise to a peak.

Zwietering found that the exponent of μ varied between 0.05 and 0.16. Some of this variation was caused by the stirrer type used for agitation. The graphs of N_{JS} vs. υ are not linear and so the exponent will depend on the range of υ considered. If the range of υ is restricted to lower values of υ then the exponent will be increased. The predicted values for the exponent governing the influence lie between 0.06 and 0.10, which compares favourably with the range found by Zweitering.

impeller diameter and scale-up

Zwietering used a range of impeller types but did not use a six-bladed 45 degree pitched turbine. The closest type of impeller to that used by this study is the six-bladed flat turbine which will give the desired radial flow pattern, drawing in the particles to the centre of the

base prior to suspension. Figure 5.5.4. shows the variation of the geometrical constant, S, with T/D, presented in Zwietering's 1958 paper for a six-bladed flat turbine. For such a turbine, Zwietering found no measurable effect of clearance on N_{JS}. The graph can be used to calculate S at different T/D and hence find the influence of the impeller diameter on N_{JS}.

From the Unistat software,

$$N_{JS} \propto {}^{1}/_{D^{2.38}} \qquad 5.5.9$$

this compares with the inverse square relationship predicted from the model.

From the point of view of scale-up, the Zwietering relationship implies that for constant $\Delta Z/T$ and D/T,

$$N_{JS} \propto {}^{1}/_{D^{0.85}} \qquad 5.5.10$$

For the quadratic mean flow model, 5.4.1, the scale-up criterion is less obvious. At high Ar, 5.4.1

simplifies to $$N_{JS} \approx \frac{\sqrt{\frac{16}{3}\left[\frac{\rho_s - \rho_f}{\rho_f}\right] gTA^2 c_1}}{2\,A^2 c_1\, D(D/T)} \qquad 5.5.11$$

With low to intermediate viscosities such that there are no complex impeller diameter/clearance interactions, $A^2 c_1$ will be independent of D/T for constant $\Delta Z/T$, so that 5.5.11 implies

$$N_{JS} \propto \frac{\sqrt{T}}{D} \propto {}^{1}/_{D^{0.5}} \qquad 5.5.12$$

At lower Ar, when both R.H.S. terms of 5.5.2 are important, the scale-up rule will depend on the agitation conditions; the liquid and solid properties.

Taking equation 5.5.5 to exemplify this, varying d_p will vary the the scale-up rule. Dividing numerator and

denominator by D and keeping D/T constant at 1/3 then the variation of N_{JS} with D can be found at a given particle diameter. Figure 5.5.5. shows two ln/ln plots of N_{JS} vs. D for the extremes of the particle diameter range considered by Zweitering. The slopes vary from -0.44, for the smallest particles, to -0.49 for the largest particles. Both of these slopes imply a more conservative scale-up rule than that of Zwietering.

Figure 5.5.1
Predicted Effect of Particle Diameter

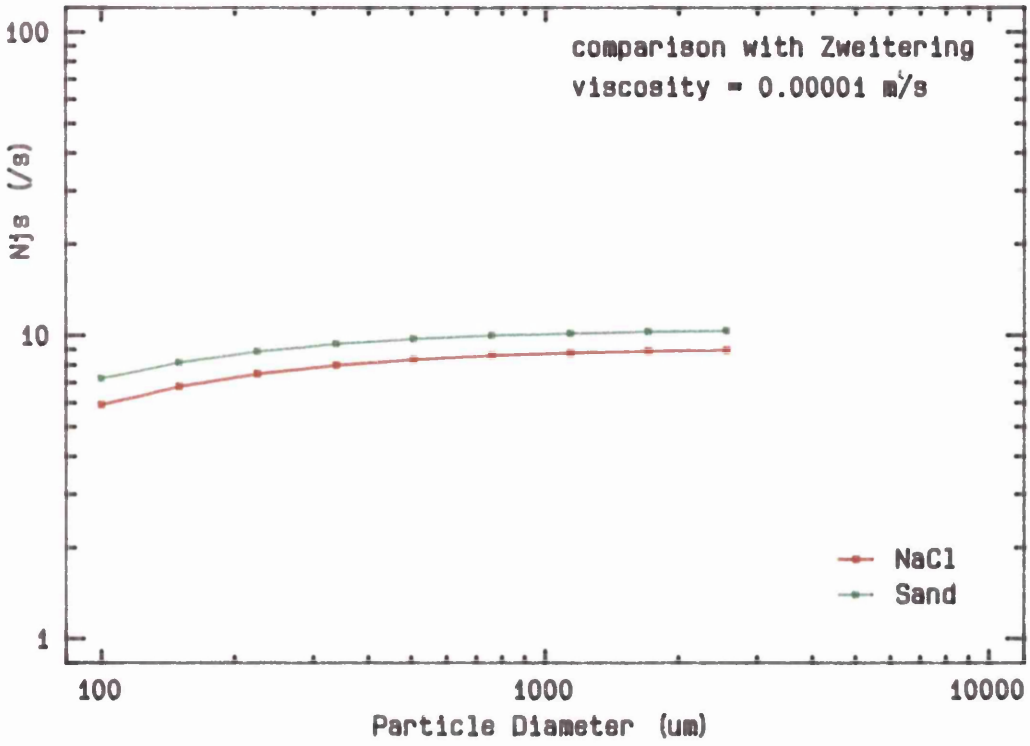

Figure 5.5.2
Predicted Effect of Dimensionless
Density Difference

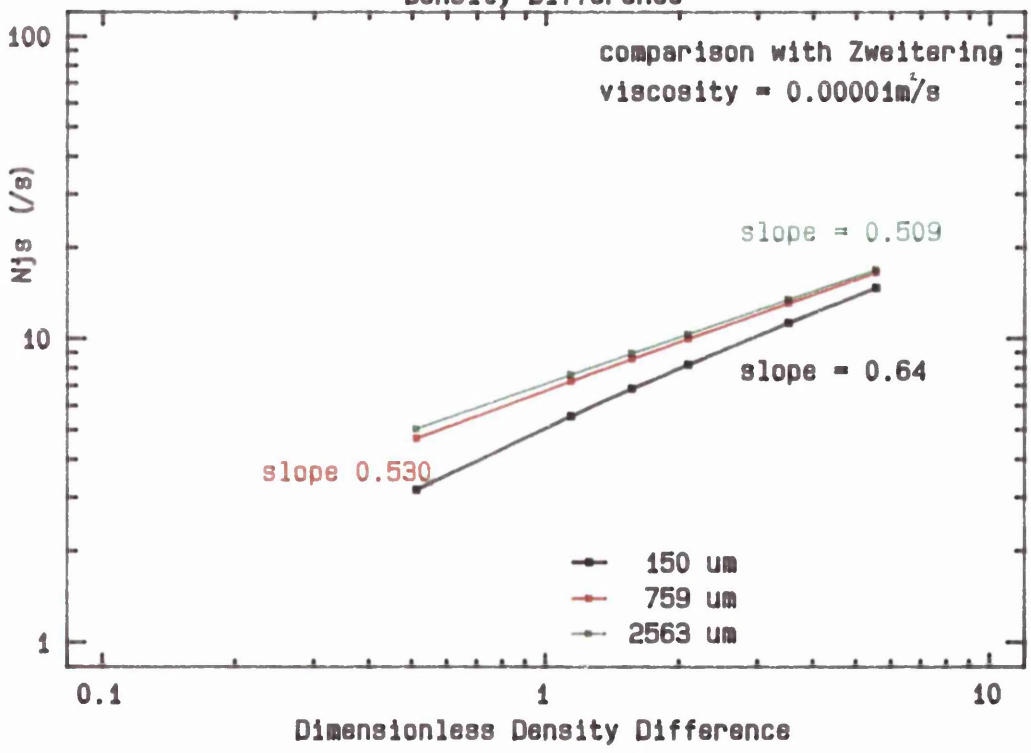

Figure 5.5.3
Predicted Effect of Viscosity

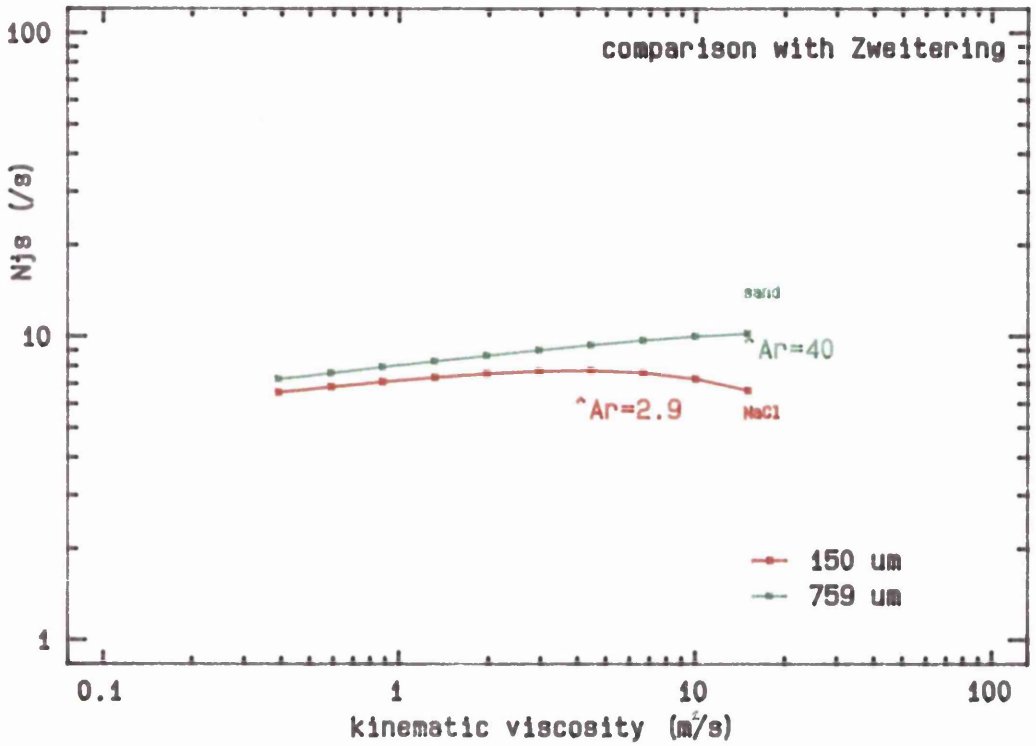

Figure 5.5.4
Variation of Zweitering Geometric
Constant for Six-Bladed Flat Turbine

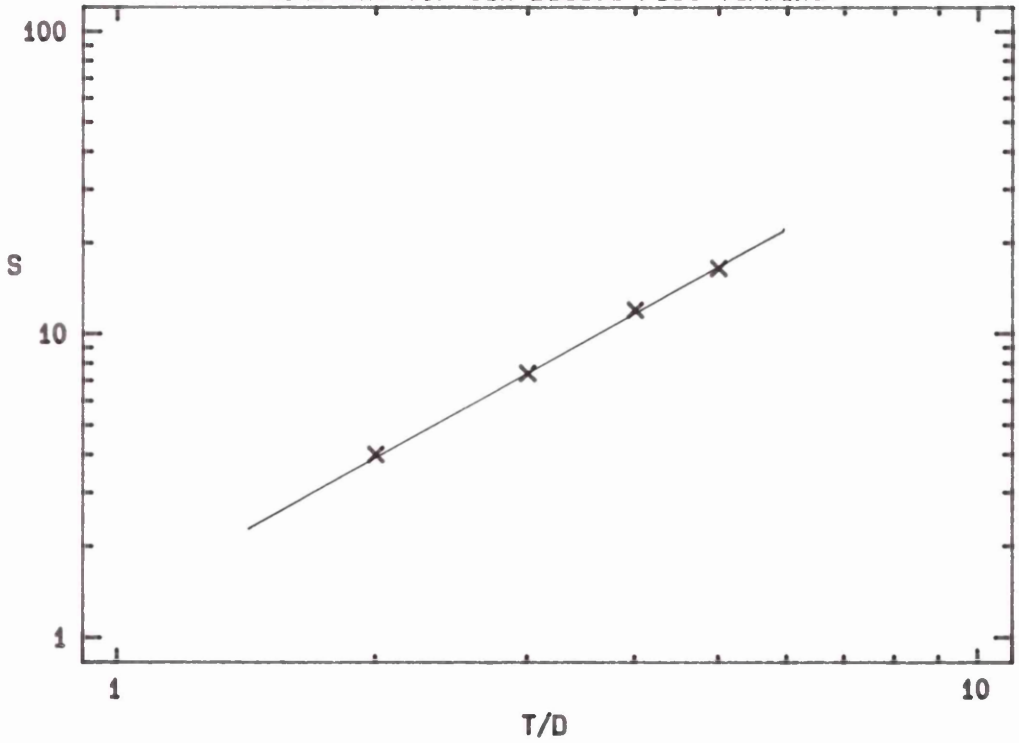

Figure 5.5.5
Predicted Scale-up Rule

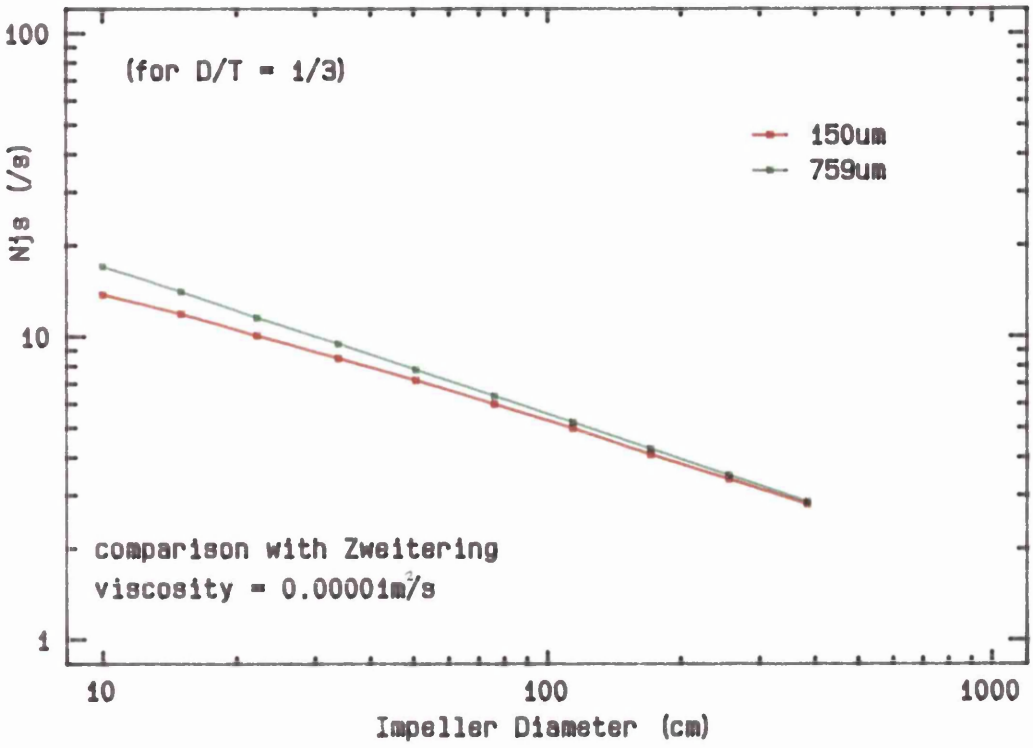

b) Other Researchers

Zwietering was not the only one to conduct empirical studies concerning the suspension of solids in mechanically agitated vessels (see Chapter Two). A selection of other researchers' equations and correlations are presented in table 5.5.1. Table 5.5.2 shows the range of exponents for each of the main design variables.

P	high	low	"consensus"	model*
d_p	0.25	0.0	≅ 0.20	0 -> 0.3
υ	0.10	0.0	≅ 0.10	0.06->0.10
D at constant T	-2.40	-0.73	≅ -2.20	-2.00
scale-up $N_{JS}D^{a}$ constant	-0.90	-0.50	≅ -0.70	-0.4->-0.5
$\frac{\rho_s - \rho_f}{\rho_f}$	0.60	0.45	≅ 0.50	0.5 -> 0.6
C_w	0.25	0.10	≅ 0.15	see App.5

*over Zweitering's experimental range

Table 5.5.2. Influence of Parameters, P, on the Just Suspension Condition

It should be remembered that all of the findings mentioned in table 5.5.1. resulted from experiments in low viscosity Newtonian liquids (such as water); these systems will tend to have high Ar.

Another team of researchers for whom the Ar was considered important is that of Ditl & Reiger, 1985. They conducted a wide range of experiments in water and found

that their experimental results could be summarized by the relationship:

$$Re \left[{}^{d_p}/_{T}\right]^{4/3} \left[{}^{T}/_{D}\right]^{1/3} \propto Ar^{a} \qquad 5.5.13$$

where for a typical set of results a=0.43
substituting for Re

$$N_{JS} \propto \frac{d_p^{-0.04} \upsilon^{0.14}}{D^{0.67}(D/T)} \left(\frac{\rho_s - \rho_f}{\rho_f}\right)^{0.43} g^{0.43} \qquad 5.5.14$$

The weak, negative dependence on the particle diameter, d_p,may be explained by the wide range of particle diameters (and hence Ar) tested by Ditl & Reiger. Figure 5.5.6. shows a typical plot of N_{JS} vs d_p for three different impellers. Below 1mm, there is a weak positive dependence on d_p. Above 1mm, N_{JS} appears to be independent of d_p. Averaged over the whole range of d_p (and Ar), the exponent governing the influence of d_p on N_{JS} will barely be above zero. The weak, negative dependence on N_{JS} (exponent = -0.04) might easily be caused by any experimental errors distorting the influence of Ar in equation 5.5.14. If the exponent of Ar had been 0.45 instead of 0.43, the dependence on d_p would have been 0.02 instead of -0.04. Plotting data on ln/ln scales tends to linearize any resulting graphs. Allowing for this, the graphs presented in figure 5.5.6.closely resemble the dependence on d_p found both by this set of experiments (see 5.1.a) and the dependence predicted by the quadratic mean flow model (using 5.5.5 to plot figure 5.5.1.).

Some of the relationships shown in table 5.5.1. seem to be more sophisticated than others. Whereas researchers such as Zwietering have presented their relationships as the product of constant exponent proportionalities, to give an overall expression for N_{JS}; others have acknowledged that the influence of some parameters is not constant. The relationship proposed by Staudinger is a good example of

this.

The constant A is itself a function of solids volume fraction. This constant, A, will in turn affect the degree to which d_p, T, υ , and $^{\Delta\rho}/_{\rho_f}$, will influence N_{JS}.

Figure 5.5.7. shows a graph of ln N_{JS} vs ln C_v as predicted by Staudinger. In view of the complexity of Staudinger's equation it is perhaps surprising that the points do seem lie so close to one straight line, so that for this set of conditions:

$$N_{JS} \propto C_v^{0.167} \qquad 5.5.15$$

As a consequence of varying C_v, the exponents for other variables also change. The most interesting is the change in exponent for d_p. At low volume fractions, the influence of d_p is predicted to be negative, so that increasing the particle diameter decreases the the just suspension speed. At higher volume fractions, the influence of d_p is positive. For a given C_v, the constant A will not vary, so that the influence of all other variables is also constant. This means that Staudinger could not predict the shape of N_{JS} vs d_p curves found and predicted by this study and Ditl & Reiger, 1985.

The relationship proposed by Zlokarnik and Judat uses an exponential function to describe the influence of impeller diameter and tank diameter (see figure 5.5.8.). Under these conditions there is a distinct minimum at D = 0.11m.

The experimental data gathered in this study, especially at the high viscosities associated with the corn syrup/water mixtures, also shows that it is not always valid that:

$$N_{JS} \propto {}^{1}/_{D^a} \qquad 5.5.16$$

(where a is some constant positive co-efficient for all D)

However, in contrast to figure 5.5.8., the experimental data gathered at high viscosities (see 5.1) shows a flattening-out of the curve of N_{JS} vs D, rather

than a distinct minimum. It is for this reason that any functions that relate the composite constants, A^2c_1 and Bc_2 to the impeller clearance to the impeller clearance have to be sophisticated enough to predict this flattening-out, through the complex interaction between ΔZ and D at high viscosities and yet, at low to intermediate viscosities yield the relatively straightforward relationship:

$$N_{JS} \propto \left(\frac{\Delta Z}{T}\right)^{0.1} {}^{1}/_{D^2} \qquad 5.5.17$$

for all "reasonable" ΔZ and D.

The relationship proposed by Lamadé does include a term that seems to depend on the interaction of impeller clearance and diameter.

$$N_{JS} \propto {}^{1}/_{D^{0.71}} \left({}^{\Delta Z}/_{D}\right)^{0.115(T/D)^{-1.5}} \qquad 5.5.18$$

However, this term does not include the influence of viscosity on the interaction of ΔZ and D. Indeed, viscosity is not included at all in Lamadé's expression. Figure 5.5.8. shows ln/ln plots of N_{JS} vs D at an impeller clearance of 9.0cm.

If D is kept constant, and ΔZ varied then the influence of ΔZ would be fixed by D/T for all ΔZ. Therefore equation 5.5.18 would not predict any minima or maxima in any plot of N_{JS} vs ΔZ. From equation 5.5.18, if

$$N_{JS} \propto \Delta Z^{a}$$

then $0 < a < 0.115$.

By using appropriate values for the constants, A^2c_1 and Bc_2, comparison of the predictions made by the model with the findings of Zwietering showed good agreement when the model was applied to the range of experimental

conditions considered by Zweitering except for the difference in scale-up rules. Comparison with other researchers showed both similarities and differences with the QMF model and experimental data gathered in this study.

Author	Equation
Gates et al 1976	$n_k = (\phi w'_{ss} d'^{-2.81})^{1/3.75}$ $\phi = 6.5 \times 10^{10}$ d' (in.) (agitation scale 3) w'_{ss} (ft/min)
Hobler & Zablocki 1966	$n_k = 10.325 \left(\frac{\rho_p - \rho}{\rho}\right)^{0.6} \left(\frac{\rho_p}{\rho}\right)^{0.17} g^{0.43} \nu^{0.1} d_p^{0.25} \left(\frac{h_R}{d}\right)^{0.19} \left(\frac{D}{d}\right) d^{-0.9} \left(\frac{c_v}{1 - c_v}\right)^{0.17}$
Knuele & Weinspach 1967	$n_k = 1.75 \left(\frac{g}{d} \frac{\rho_p - \rho}{\rho}\right)^{0.5} \left(\frac{1}{1 + \frac{\rho}{\rho_p} \frac{1 - c_v}{c_v}}\right)^{0.25} \left(\frac{D/d}{3.25}\right)^{5/3}$
Kotzek et al, 1969	$n_k = \left(\frac{c_{ps}}{c_p}\right)^{1/3} \left(\frac{\pi H}{4D}\right)^{0.319} \left(\frac{D}{d}\right)^{0.957} \left(\frac{g}{d} \frac{\rho_p - \rho}{\rho}\right)^{0.5} \left(\frac{1}{1 + \frac{\rho}{\rho_p} \frac{1 - c_v}{c_v}}\right)^{0.175} \left(\frac{d_p}{d}\right)^{0.21}$ $c_{ps} = 0.69$ $c_p = 0.4$
Lamadé 1966	$n_k = 5.57 \left(\frac{g}{d} \frac{\rho_p - \rho}{\rho}\right)^{0.5} \left(\frac{d_p}{d}\right)^{0.21} \left(\frac{1}{1 + \frac{\rho}{\rho_p} \frac{1 - c_v}{c_v}}\right)^{0.15} \left(\frac{h_R}{d}\right)^{0.115(D/d)^{-1.5}}$
Staudiger 1976	$n_k = 4.2^A \left(\frac{d_p^{0.5}(1 + 8c_v^{0.3})}{D^2 \left(\frac{d_p^2}{\nu}\right)^{0.5(1 - 1.85c_v^{1/3})}}\right)^{A/3} \left(g \frac{\rho_p - \rho}{\rho}\right)^{A/2} \left(\frac{D/d}{3}\right)^{5/3}$; $A = \frac{6}{7 - 1.85 c_v^{1/3}}$
Zlokarnik & Judat, 1969	$n_k = 7.08 \left(\frac{g}{d} \frac{\rho_p - \rho}{\rho}\right)^{0.5} \left(\frac{d_p}{d}\right)^{1/6} \left(\frac{1}{1 + \frac{\rho}{\rho_p} \frac{1 - c_v}{c_v}}\right)^{1/6} e^{(0.58 D/d) - 2.27}$
Zweitering, 1958	$n_k = 6.0 d^{-0.85} \nu^{0.1} d_p^{0.2} \left(g \frac{\rho_p - \rho}{\rho}\right)^{0.45} \left(100 \frac{\rho_p c_v}{\rho(1 - c_v)}\right)^{0.13}$
Einenkel & Mersmann, 1977	$n_k = 24.93 \frac{\nu^{0.0826}}{d^{0.7768}} \left(g w_{ss} c_v \frac{\rho_p - \rho}{\rho}\right)^{0.3058} \left(\frac{D/d}{3.175}\right)^{5/3}$

Table 5.5.1 Selected equations for predicting the just suspension speed (from Bohnet & Niesmak, 1980)

Figure 5.5.6
Effect of Particle Diameter
(Ditl & Rieger, 1985)

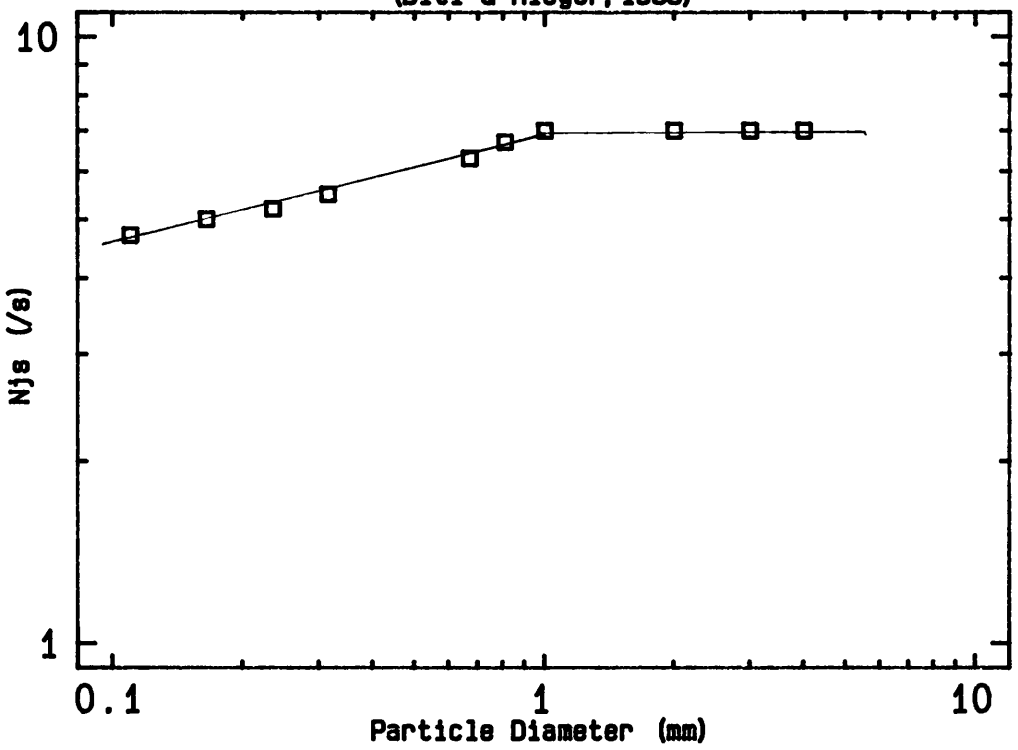

Figure 5.5.7
Effect of Cv using
Staudiger's Equation

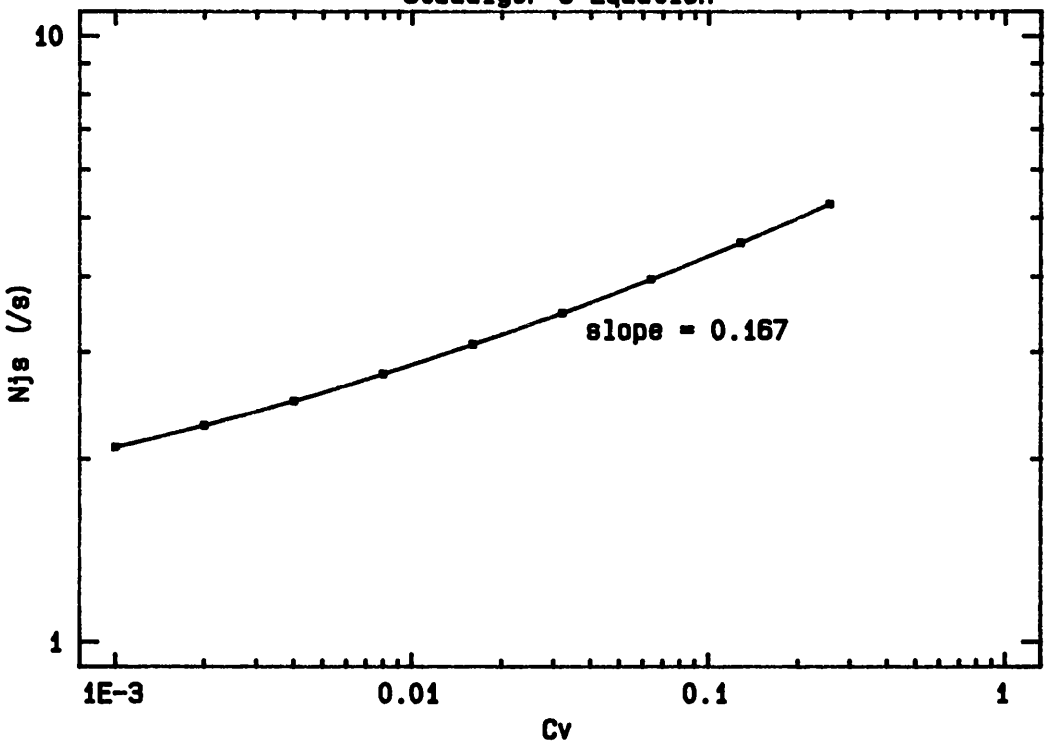

Figure 5.5.8
Effect of Impeller Diameter

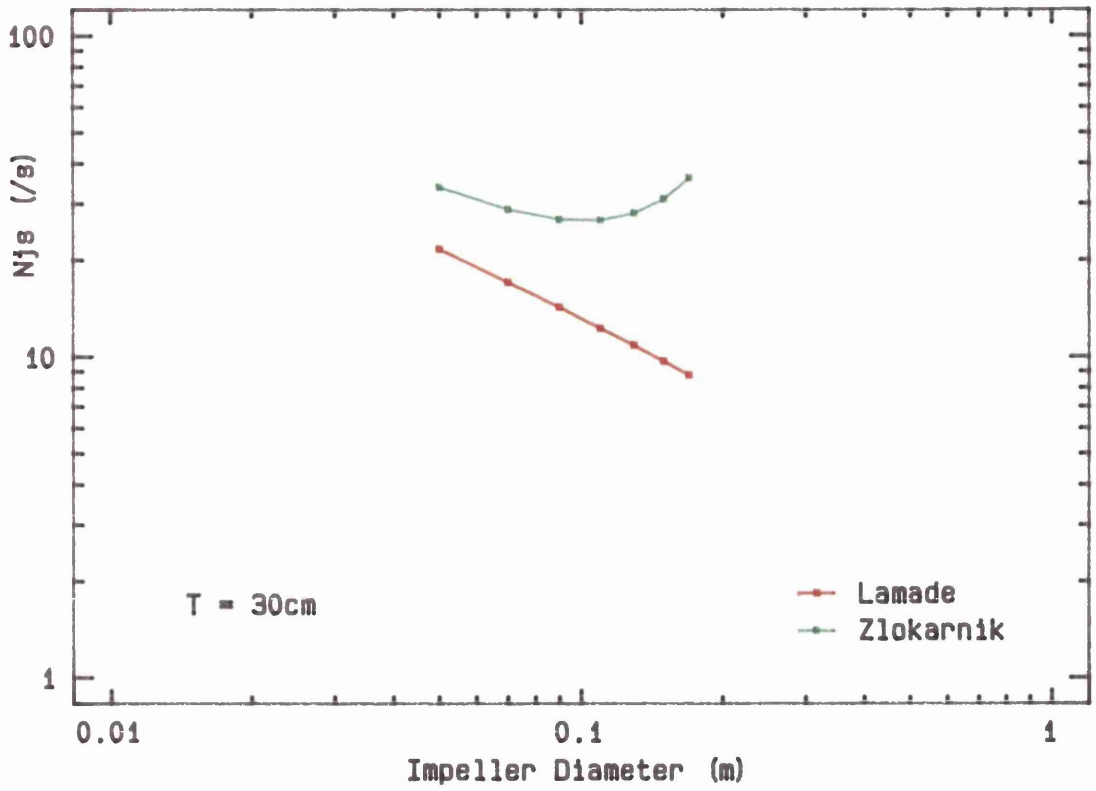

$T = 30cm;\ \upsilon = 10^{-5} m^2/s;\ d_p = 1000\mu m$

$$\frac{\rho_p - \rho_f}{\rho_f} = 1.0; \quad C_v = 0.01$$

CHAPTER SIX

Conclusions and Recommendations for Further Work

6.1 Conclusions

Just suspension speeds have been measured in viscous Newtonian and non-Newtonian liquids for low concentrations of solids. The kinematic viscosities of the Newtonian liquids used varied from 20×10^{-6} to 7.3×10^{-3} m^2/s. These were composed of mixtures of water with either glycerol or corn syrup. The non-Newtonian liquids were solutions of Carbonyl Methyl Cellulose (CMC) dissolved in distilled water. These solutions displayed pseudo-plastic behavior, well described by a power-law rheology. The flow index, n, varied from 0.95 to 0.79; whilst the consistency index varied from 0.012 to 0.17 (in consistent S.I. units). Agitation was provided by a range of six-bladed 45 degree pitched turbine impellers in flat-bottomed, transparent tanks. The impeller Reynolds Number was always less than 1000.

Experiments have confirmed that particles much denser than the surrounding liquid can be suspended in the absence of turbulence, at Reynolds Numbers less than 10.

Under such low Reynolds Numbers, those theoretical relationships that rely on fluid turbulence have proven unsatisfactory either as a means of explaining the suspension mechanism or for predicting the just suspension condition.

A new model has been proposed (the Quadratic Mean Flow equation 3.1.21) that attempts to explain the suspension mechanism and then use this mechanism to predict N_{JS} for unbaffled flat-bottomed tanks.

These equations have proved successful in predicting the influence of particle and liquid properties and impeller diameter for both non-Newtonian and Newtonian liquids (of intermediate viscosity). The scale-up rule implied by the model is such that if:

$$N_{JS} \propto {}^{1}/_{D^{a}}$$

then the value of a varies from about 0.44 to 0.50 depending on the liquid and particle properties.

However, at high viscosities, above 1 Pas, equation 5.4.7 no longer reliably predicts N_{JS}, and instead equation 5.4.8 can be used to predict N_{JS}. The difference between 5.4.7 and 5.4.8 being the ten-fold increase in the value of the composite constant A^2c_1. This has been explained by the interactions between liquid viscosity and the impeller's clearance and diameter that considerably complicate the functions that are used to calculate the constants A^2c_1 and Bc_2. As a result of these complex interactions at high viscosities, N_{JS} was found to be more sensitive to clearance but less sensitive to impeller diameter than expected from 5.4.8 or 5.4.7.

The use of baffles was found always to hinder the onset of the just suspension condition, especially for the CMC solutions.

Suspending solids of sufficient particle mass in liquids more viscous than 2.5 Pas led to a hysteresis. This means that having suspended the solids, the impeller speed could be reduced by upto 75% and still the particles would be maintained in suspension indefinitely.

If the basic approach taken by the modeling (in Chapter Three) is correct, then to improve the mechanical efficiency of the suspension process, the agitation system should be designed to maximize mean, bulk flow at the base of the tank, even if this means lowering the degree of turbulence. For example by using a fully profiled vessel without baffles.

The effect of viscosity in the suspension process is normally very slight except for systems that involve very low Archemedes Numbers. The most important effect of the viscosity of the liquid is to dampen the velocity of the liquid emerging from the impeller zone to the base of the tank.

The most important particle property to determine N_{JS} is the density, through its effect on the dimensionless density difference. This will be especially true for solids whose densities are only slightly greater than the

surrounding liquid.

The effect of solids concentration is normally slight. Concentration may be important for very dilute suspensions. The mean flow mechanism can be extended to explain why this is the case.

The Q.M.F. model explains why the effect of particle diameter on N_{JS} varies depending on the range of particle diameters investigated. Generally, the effect of particle diameter is low except for very low Archemedes Number systems ($<10^{o}$). As the particle diameter is increased, its influence declines. Increasing the particle diameter increases the weight of the particle (d_p^3)and leads to lower lift and drag co-efficient (d_p^{-1}). However, this is (at least partially) mitigated by the nature of the liquid's velocity profile at the base of the tank which leads to larger diameter particles experiencing greater relative velocities.

The observations, in this study as well as others, that the last particles are suspended, at a position on the base of the tank, where the mean relative velocity between the particle and the agitated liquid is at its peak provide a good confirmation of the mean flow approach. This is true even for low viscosity, high Reynolds Numbers systems where the position of the last particles also corresponds to the point of greatest mean relative velocity, which does not always correspond to the position of greatest intensity of turbulence.

Experimental data was also gathered to determine the distribution of suspended solids. These were performed using a non-intrusive, optical technique involving a laser and a photocell. This is a technique that has been used previously with proven success. Agitation was provided by six-bladed 45 degree pitch turbines in two geometrically similar fully profiled vessels using a variety of viscous Newtonian and non-Newtonian liquids (Reynolds Numbers in the range 500 to 2500).

The laser/photocell arrangement was used to determine axial and radial concentration profiles. The radial variation concentration in the bulk of the liquid was found

to be less significant than the axial, but still important enough not to be discounted. The axial profiles, for the two types of liquid, showed interesting differences both from each other and as compared with suspensions in liquids of low viscosity (such as water).

For the viscous Newtonian liquids examined (mixtures of glycerol and water), it was found that particles could be well distributed throughout the vessel without the need for agitation in the fully turbulent regime. However, in contrast to the less viscous Newtonian liquids, the axial profile showed that the local solids concentration could increase rather than decrease with height. Under such conditions, the application of any simple 1-dimensional models has proved unsatisfactory. However, for a given impeller speed, increasing the viscosity of the liquid did lead to a worse solids distribution.

For the non-Newtonian liquids (aqueous solutions of CMC), at impeller speeds close to, or below, N_{JS}, most of the suspended particles were to be found concentrated in a slowly rotating ring. This ring of particles was located between anywhere above the plane of the impeller, at the periphery of the vessel. The position of the ring depended on the liquid and solid properties. Increasing the impeller speed caused the ring to move to a higher plane. If the speed of the impeller were to be increased about 30% above N_{JS}, then the ring would break up and the distribution of solids would approach that of a Newtonian liquid with the same apparent viscosity. Increasing the degree of non-Newtonianness corresponded to more of the particles being found in the ring and a poorer solids distribution.

The use of baffles did not prove beneficial for improving the distribution of suspended solids.

6.2 Recommendations for Further Work

This study has been the first attempt to systematically study solids suspension in viscous Newtonian and non-Newtonian liquids. A mean flow model (QMF) has been proposed. This attempts to relate the just suspension condition, N_{JS}, to other design variables. Assumptions and

approximations have had to be made in the development of this model. Although experimental work was carried out to validate some of the assumptions, more accurate measurements need to be made concerning the liquid velocities around suspending particles and the pressure differences that give rise to the lift forces on the particle.

The velocities of liquids can be determined with increasing accuracy using the latest advances in Laser Doppler Anemometry (LDA). Such LDA techniques might be usefully employed to investigate the complex interactions that occur in high viscosity liquids between the impeller's diameter and clearance.

The hysteresis effect discovered in this study may have important industrial applications. If a reliable means can be found of predicting and encouraging the hysteresis effect, then this may lead to significant energy savings for suspension processes where a poor distribution of solids is acceptable.

The problem of solids distribution in viscous Newtonian and non-Newtonian liquids has also been addressed in this study. More systematic data is required, extending the range of liquid and particle properties as well as vessel sizes. This data would prove valuable for supporting any theoretical approaches to the problems of solids distribution and scale-up.

Nomenclature

A constant of proportionality defined by equation 3.1.17

Ar Archemedes Number

B constant of proportionality defined by equation 3.1.18

c_1 constant of proportionality defined by equation 3.1.10

c_2 constant of proportionality defined by equation 3.1.6

C_D drag co-efficient

C_L lift co-efficient

c_f friction factor

C_v solids concentration [%wt]

D impeller diameter [m]

d_p particle diameter [m]

Fr Froude Number

g acceleration due to gravity [m/s^2]

k consistency index [$kgm^{-1}s^{n-2}$]

M_c Mixing Co-efficient

N impeller speed [/s]

N_{JS} just suspension speed [/s]

Pe Péclet Number

Re Reynolds Number

S Zweitering's geometric constant defined by 2.3.1

T tank diameter [m]

u liquid velocity [m/s]

v' fluctuating velocity component [m/s]

V Volume [m^3]

Z_B Baldi et al's geometric constant defined by 2.3.6

ΔZ impeller clearance from vessel base [m]

Italic

l pathlength [m]

D_p particle diffusivity [m^2s]

D_f liquid diffusivity [m^2s]

l_e size of energy containing eddies [m]

$\dot{\gamma}$ shear rate [/s]

Γ liquid circulation [m^2/s]

μ absolute viscosity [Pas]

υ kinematic viscosity [m^2/s]

ρ density [kg/m^3]

τ shear stress [N/m^2]

θ_s angular displacement of stagnation point

σ^2 variance

ε dissapated power per unit volume [W/m^3]

ζ_p particle diffusion co-efficient [m^2/s]

Subscripts and Superscripts

h horizontal, or at height h

v vertical, or on volumetric basis

f fluid

s,p solid, particle

* modified

av average or effective

REFERENCES

Aeschbach S. & Bourne J.R., 1972, Chem.Eng.Sci., 27, 234

Baldi G., Conti R., and Alaria E., 1978 Chem.Eng.Sci., 33, 21

Barresi A. & Baldi G., 1987, Chem.Eng.Sci., 42, 534

Bohnet M. & Niesmak G., 1980, Ger.Chem.Eng., 3, 57

Bos A.S. & Heerens J.J., 1982, Chem.Eng.Comm., 16, 301

Bos A.S., Zuiderwerg F.J., and Weltewerde R., 1981,
CHISA conference, 4, 131

Bosart & Snoddy, 1928, Ind.Eng.Chem., 20, 1378

Bourne J.R. & Sharma M., 1974, Chem.Eng.Sci., 29, 243

Calderbank P. & Moo-Young M.B., 1961, Chem.Eng.Sci., 16, 39

Chapman C.M., 1981 phD thesis, University College, London.

Chapman C.M., Nienow A.W., Cooke M., & Middleton J.C., 1983,
Chem.Eng.Res.Des., 61, 71

Chudacek M.W., 1982, "4th European Conference of Mixing",
Netherlands, 275

Conti R. & Baldi G, 1978, International Symposium on Mixing,
Faculte Polytechnique de Mons

Darby R., 1976, Viscoelastic Fluids (Chemical Processing and
Engineering Volume 9), Marcel Dekker Inc, NY

Ditl P. & Reiger F., 1985, "5th European Conference of Mixing",
FDR, 53

Eichhorn S. & Small R., 1964, J.Fluid Mech., 20 , 513

Einenkel W.D., 1980, Ger.Chem.Eng., 3, 118
Einenkel W.D. & Mersmann A., 1977, Verfrabenstecknik, 11, 90

Einstein A.H. & El-Samni A., 1949, Revs.Mod.Phys., 21, 520

Gates L.E., Morton R.L., and Fondy P.L., 1976, Chem.Eng.J., 5, 144

Goren S.L. & O'Neill M.E., 1971, Chem.Eng.Sci., 26, 325

Gregory J. & Nelson D.W., 1986, Colloids and Surfaces, 18, 175

Gunkel A.A & Weber M.E., 1975, A.I.Ch.E.J., 21, 931

Harnby N., Edwards M.E., and Nienow A.W, 1975, Mixing in the Process Industries, Butterworths

Herringe R.A., 1979, "3rd European Conference of Mixing", BHRA, Cranfield, England,

Hinze J.O., 1975, Turbulence, McGraw-Hill, NY

Hirsekorn F.S. & Miller S.A., 1953, Chem.Eng.Prog., 49, 459

Hobler S. & Zablocki D., 1966, Chem.Tech. (Leipzig), 18(11), 650

Holmes D.B., Vonken R.M., Dekker T.A., Chem.Eng.Sci., 10, 201

Kneule F., 1956, Chem.Eng.Tech., 28, 221

Kneule F. & Weinspach S., 1967, Verfahrenstechnik (Mainz), 1(12) 531

Kolar V., 1967, Colln.Czech.Chem.Comm., 32, 526

Kotzek K., Langhans D., Kiepe P., and Weissgarber S., 1969, Mitt.Inst.Chem.Anal. 9(2), 53

Koutsakos E., 1989, phD thesis, University College, London

Leighton D. & Acrivos A., 1985, ZAMP, 36, (Jan)

Lemadé H., 1966, Verfahrenstechnik, (Mainz), 11(2), 72

Levins R.M. & Glastonbury J.G., 1972, Trans.Inst.Chem.Eng., 50, 32

Levich V.G., 1962, Physiochemical Hydrodynamics, Prentice-Hall, New Jersey

Machon V., Fort, Skrivanek, 1982, "4th European Conference of Mixing", Netherlands, 289

Massey B.S., 1979, Mechanics of Fluids, 4th Edition, Van Nostrand Reinhold

Mersmann A. & Laufhutte H.D., 1985, "5th European Conference of Mixing", FDR, 273

Metzner A.B. & Otto R.E., 1953, A.I.Ch.E.J, 3, 3

Molerus O. & Latzel W., 1987, Chem.Eng.Sci., 42, 1423

Musil L., 1976, Colln.Czech.Chem.Comm., 41, 839

Musil L. & Vlk J., 1978, Chem.Eng.Sci., 33, 1123

Musil L., Vlk J., and Jiroudvoka K., 1984, Chem.Eng.Sci., 39, 621

Nagata S., 1975, Mixing Principles and Applications, John Wiley, NY

Nayaranan S., Vinay K., Bhatia K., Guha D.K., and Roa M.N., Chem.Eng.Sci., 24, 223

Nienow A.W. & Barlett R., 1984, "1st European Conference of Mixing", BHRA, UK, B1-1

Nienow A.W. & Elson T., 1988, Chem.Eng.Res. & Des., 66, 234

Nienow A.W. & Miles D., 1978, Chem.Eng.J., 15, 13

Ohiaeri I.N., 1981, phD thesis, Univerisity of Bradford

Oldshue J.Y., 1983, Fluid Mixing Technology, McGraw-Hill

Pavlushenko I.S., Kostin, Matejev, 1957 J.App.Chem., USSR, 30, 1160

Periculeous K.A. & Patel M.K., 1987, Processing (Feb)

Reibel S. & Loffler J., 1989, Chem.Eng.Tech., 12, 433

Rouse H., 1938, "Proceedings of the 5th International Congress" publ. J.Wiley, NY., 550

Saffman P.G., 1965, J.Fluid Mech., 22, 385

Schlingting N., 1968, Boundary Layer Theory, 6th Edition, McGraw-Hill, NY

Schwartzburg H.G. & Treybal R.E., 1968, Ind.Eng.Chem.Fundls., 7, No.1, 1

Segre A. & Silverberg E., 1962, J.Fluid Mech., 14 , 115

Shamlou P.A. & Koutsakos E., 1986, Proc.of Euro.Conf.: "Colloque Agitation Mechanique" Toulouse, France

Shamlou P.A. & Koutsakos E., 1989, Chem.Eng.Sci.44, No.3, 529

Shamlou P.A. & Zolfagharian A., 1987, I.Chem.Eng. Symposium Series No 108, 195, University of Bradford

Sheeley M.L.,1932, Ind.Eng.Chem., 24, 1060

Staudiger G. & Moser F., 1976, Chem.Ing.Tech., 48, 1071

Subbaroa S. & Taneja V.K., 1979, "3rd European Conference of Mixing", BHRA, UK, B3-25

Sysova M., Fort I., Vanek T, 1984, Proc.Congress CHISA84, V3.49

Thomas D.G., 1961, A.I.Ch.E.J, 7, 423

Tojo K., Miyanami K., and Mitsui H., 1981, Chem.Eng.Sci., 36, 279

Uhl V.W. & Grey J.R., 19, 1986, Mixing Theory and Practice, Volume 3, 3rd Edition, Academic Press

Von Karman, 1935, Mech.Eng., 57, 407

Weisman J. & Efferding L.E., 1960, A.I.Ch.E.J., 6, No.3, 419

Wichterle K., 1988, Chem.Eng.Sci., 43 ,467

Yuan S.W., 1967, Foundations of Fluid Mechanics, Prentice-Hall, New Jersey

Yung B.P.K., Merry H., & Bott T.R., 1989, Chem.Eng.Sci., 44, 873

Zlokarnik M. & Judat H., 1969 Chem.Ing.Tech., 41(23)

Zwietering T.N., 1958, Chem.Eng.Sci., 8, 244

APPENDICES

A1 Experimental Observations

Whilst performing the suspension studies described in 5.1, there were many interesting observations concerning the behavior of particles both prior to suspension as well as the appearance of the suspension after the particles had been suspended. Some of these observed phenomena were general to all liquids and solids used, whilst some were limited to non-Newtonian liquids or to the very viscous corn syrup/water mixtures.

a) General

With all types of liquids used, agitation with a six-bladed 45 degree pitch turbine always gave a radial flow pattern. This meant that particles, randomly scattered on the (flat) base of the vessel, would be drawn into the centre of the base. This process of radial migration might very slow, especially for particles close to the periphery of the base. The particles slowly accelerate as they approach the centre. Seen from above, the particle motion described a spiral of of decreasing radius.

Near the centre, at impeller speeds below N_{JS} (about $0.5N_{JS}$), particles join other particles to form a circular monolayer. At higher impeller speeds, particles, at the outer reaches of the monolayer will be swept up by the liquid flow in such a way as to hop above other particles so as to form a mound of particles on top of the centre of the monolayer. Particles then climb up the mound to the summit, where the liquid has sufficiently high velocity to sweep up the particle into suspension. As the impeller speed is increased further, the rate at which this ascension process occurs also increases and eventually the mound and the monolayer are no longer discernible. Instead, particles are being suspended from the base of the tank with the aid of a few neighbouring particles. These neighbouring particles assist by allowing another particle to climb up one particle from the base to a faster moving region of liquid. If particles are suspended directly from

the base of the tank, without requiring the assistance of any neighbouring particles, then the just suspension speed has been achieved.

b) non-Newtonian Liquids

There is a similar suspension process as described in a) except for the 0.75%wt and 1.0%wt CMC solutions where the liquids exhibited some visco-elastic phenomena.

i) 0.75%wt CMC

1.Starting from rest, with a random arrangement of particles on the base of the vessel, if the impeller is rotated to some speed less than N_{JS}, the particles were either pushed outwards or inwards until all the particles, with the exception of those trapped in fillets at the corners, are rotating slowly in a distinct ring on the base of the tank.This ring rotates in the same direction as the impeller. Those particles that were initially at rest at radial positions further out than the radial position corresponding to this ring were drawn inwards by the action of the impeller. Those particles that were initially closer to the centre were pushed outwards (see figure A1.1). If the impeller speed is increased the radius of this ring diminishes.

The next stages in the suspension process depends on whether the impeller is being rotated clockwise (pumping downwards) or anticlockwise (pumping upwards).

2. If anticlockwise, then the particles come to the centre of the base and form a mound as before (except for the 2mm acetate particles, the lightest particles). But if the impeller is rotating clockwise, some of the particles lift from the ring, about 4 cm from the centre. In some cases, these particles only manage to rise a few centimeters before falling back. Figure A1.2 shows a representation of a conical "dead zone". If a particle should enter this zone, it becomes trapped there.

3. If the impeller speed is increased further, more particles that were in suspension manage to penetrate into this central dead zone. At lower speeds, they would have simply fallen out of suspension to the base of the tank and then slowly migrated inwards to the rotating ring before lifting off again. This rotating ring marks the circumference of the dead zone.

4. For a range of impeller speeds, if enough time is allowed (10 to 15 minutes),all the particles eventually end up in the central dead zone.The interesting exception to this phenomenon is the suspension of 2mm acetate spheres which always stay suspended. Whilst observing the suspension process, the shape of the dead zone became apparent because this region appeared to covered by a translucent "skin" that marked out the cone. Perhaps the 2mm particles lacked the momentum to penetrate this "skin".

5. When all the particles are within the central dead zone, a sufficient increase in impeller speed will eliminate the zone and the the particles come together to form a mound in the usual manner.

The behavior described in steps 2 to 5 can be summarized by the graphical representation shown in figure A1.3.

ii) 1.0%wt CMC

The behavior of particles undergoing the suspension process is similar to that described for 0.75%wt CMC except that steps 2 to 5 occur for all particles and for both anticlockwise as well as clockwise impeller rotation.

c) Corn syrup/water mixtures above 2.5 Pas

All corn syrup/water mixtures are Newtonian liquids. At high viscosities, the behavior of the particles in suspension differs from those suspensions involving less

viscous liquids. As described in 5.1.h, the suspension of particles of sufficient mass will lead to a hysteresis in a graph of fraction of solids suspended vs impeller speed.

The initial suspension process at speeds below N_{JS} is the same as a). However, once suspended, none of the particles will resettle. Instead, they rotate in a densely packed ring just beyond the tips of the impeller. Even at impeller speeds 1.5 or 2 times N_{JS}, this ring will not break up. This means that the solids distribution will remain poor.

For such cases, where a hysteresis occurs, N_{JS} is not a function of particle concentration. For "normal"(less viscous) systems, particles in suspension will tend to resettle and an equilibrium is set up between the rate at which particles resettle and the rate at which they are suspended. This equilibrium rate is a function of particle concentration. In Appendix 5, this result is used to show how particle concentration effects N_{JS}. For solid/particle systems that display the hysteresis there is no equilibrium rate because none of the particles ever resettle at impeller speeds close to or above N_{JS}.

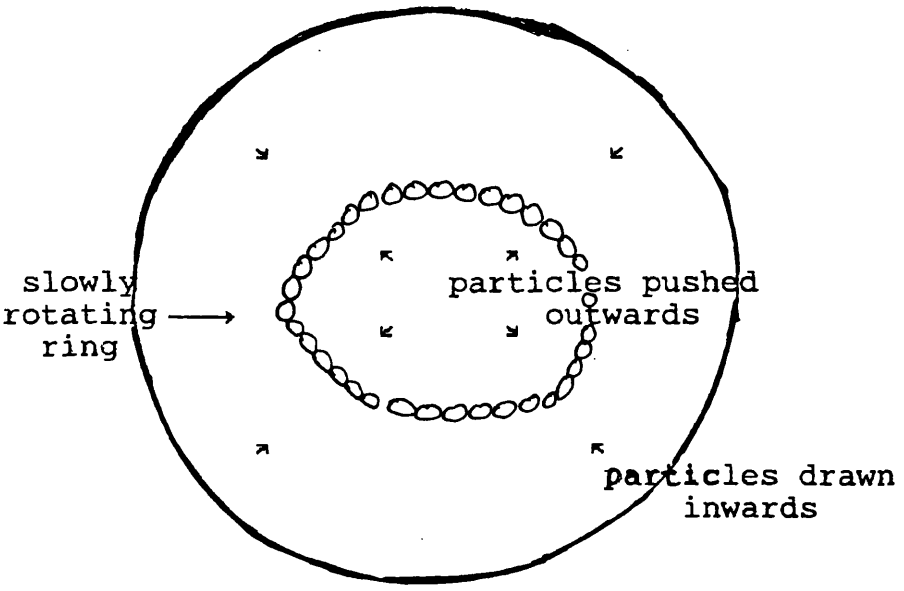

Figure A1.1 Plan view of ring formation on base of tank

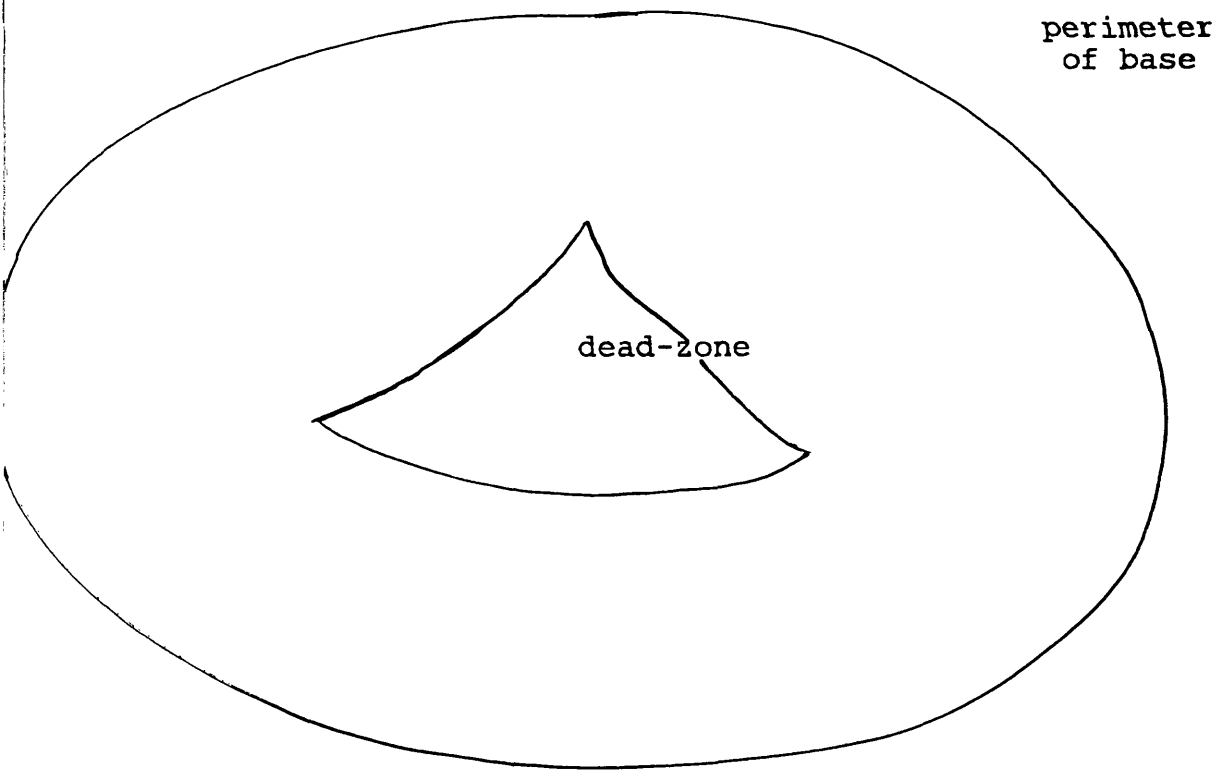

Figure A1.2 Illustration of the conical "dead-zone"

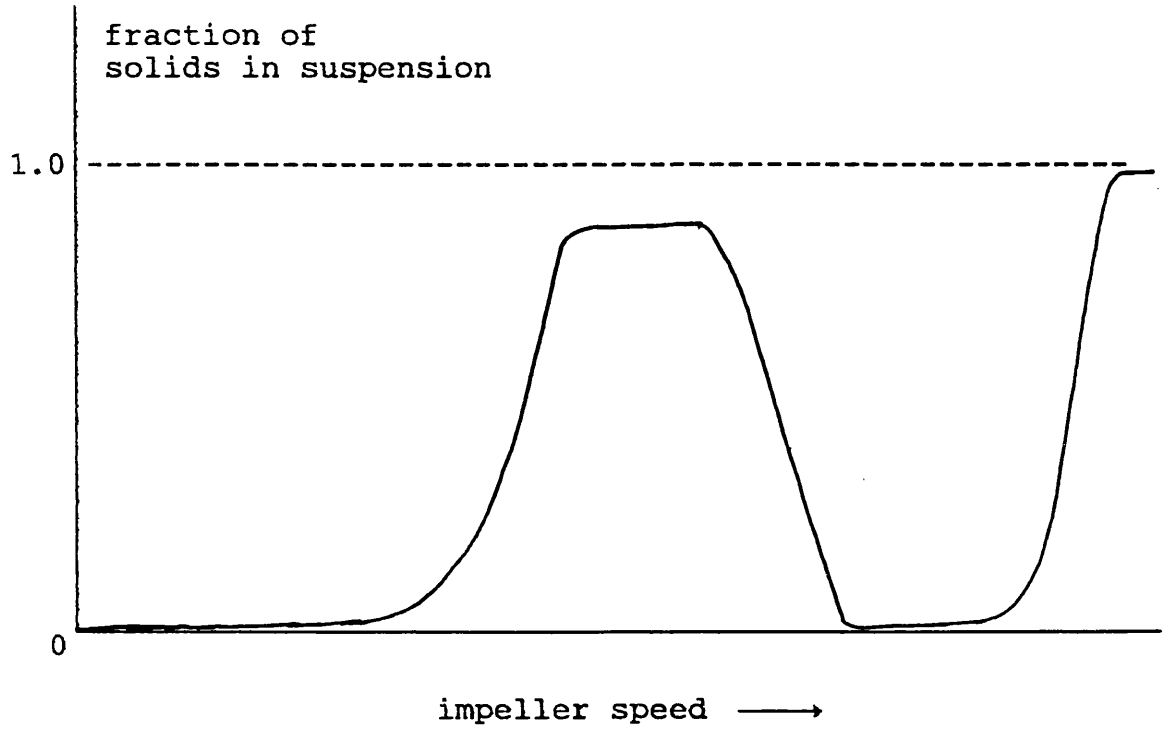

Figure A1.3 Sketch graph illustrating behavior of 0.75%wt and 1.0%wt CMC solutions

The non-Newtonian liquids used for this series of experiments were made up from dissolving known amounts of 7H4C Carbonyl Methyl Cellulose (CMC) powder in distilled water. The preparation of each liquid took place at the prevailing room temperature (20°C). The white CMC powder is added slowly to the water whilst the water is being mechanically agitated. Having prepared the non-Newtonian liquid, it should appear as a clear transparent liquid similar in appearance to water.

CMC is a long chain polymer which can be produced in a variety of chain lengths and molecular weights. The prefix, 7H4C, distinguishes this type of CMC from any other.

To determine the rheology of the non-Newtonian liquids, measurements must be made of shear stresses experienced by the liquid at different shear rates. The device chosen for these measurements was a Contraves Rheomat 30, using Measuring System B. System B has a fixed metal outer cylinder within which a metal cylindrical bob is rotated at variable angular speed by an electric motor (see figure A.2.1).

Associated with the motor are strain gauges that measure the torque experienced by the bob as it rotates at a given speed. The more viscous the sample and the faster the speed, the greater the torque encountered. To keep the sample at constant temperature (normally 20°C), the outer cylinder is immersed in a Grant water bath.

The Rheomat has 30 speed settings. Each setting corresponds to an average effective shear rate experienced by the sample. For each measuring system, there is a calibration table provided by the manufacturers, Contraves, to give the effective shear rate, $\dot{\gamma}$, for each speed setting. For Measuring System B, the possible variation of $\dot{\gamma}$ is from 0.0215 /s to 157.9 /s. However, it is not practicable to employ the full range of $\dot{\gamma}$. If the liquid is not very viscous, then operating at low shear rates will mean low torques to which the strain gauges will not be

sensitive enough to register accurately. For such liquids, the shear rates employed are confined to the higher end of the range. For the highly viscous liquids, it is advisable to to use the lower shear rates otherwise the resulting torque may go off-scale.

For each recorded torque (presented as a % by the Rheomat), there is a corresponding effective shear stress τ (the arithmetic average) experienced by the sample. For Measuring System B, this is simply a matter of multiplying the % torque display of the Rheomat by a constant factor, 0.4061 to give the effective shear stress in Pa. At least two samples are taken from each solution to ensure reproducibility.

Having recorded the shear stress at each shear rate, it is then possible to determine the rheology of the liquid by assuming that the relationship between the two is given by simple power-law equation.

$$\tau = k\dot{\gamma}^n \qquad \text{A2.1}$$

If A2.1 is valid then a graph of τ vs.$\dot{\gamma}$ on ln/ln scales should yield a straight line. The slope of the line will give n, the flow index, and k, the consistency index, is determined at $\dot{\gamma} = 1$.

For Newtonian liquids, n=1, so that k would correspond to the absolute viscosity, μ, of the liquid. For pseudoplastic liquids, such as CMC solutions, $n < 1$, whilst for dilatent liquids, $n > 1$. Figure A2.2 shows the flow curves for a range of CMC solutions.

The relationship described by equation A2.1 is not the only means by which τ can be related to $\dot{\gamma}$, merely the simplest. A good review of the progress made in the last decade in dealing with non-Newtonian liquids is that by Nienow and Elson, 1988. The following equations represent other relationships that can characterize the rheology of a non-Newtonian liquid.

a) Bingham Plastic

$$\begin{aligned} \tau &= \tau_o + \mu\dot{\gamma} \qquad \tau > \tau_o \\ \dot{\gamma} &= 0 \qquad\qquad\quad \tau < \tau_o \end{aligned} \tag{A2.2}$$

so that unless the shear rate is above some critical value, τ_o, the sample will exhibit the behavior of a solid.

b) Eyring

$$\tau = \mu_o B \operatorname{arcsinh}\left(\dot{\gamma}/_B\right) \tag{A2.3}$$

The model becomes Newtonian $\mu \to \mu_o$ as $\dot{\gamma} \to 0$ otherwise the model behaves as a pseudoplastic fluid.

c) Reiner-Philippoff

$$\tau = \left[\mu_\infty + \frac{\mu_o - \mu_\infty}{1 + (\tau/\tau_o)^2} \right] \dot{\gamma} \tag{A2.4}$$

This model exhibits high and low shear rate limiting viscosities:
as $\tau \to \infty$ the model becomes Newtonian $\mu = \mu_o$
as $\tau \to 0$ the model also becomes Newtonian $\mu = \mu_\infty$

d) Truncated Power Law

$$\begin{aligned} \tau &= k\dot{\gamma}^n \qquad \dot{\gamma} > \dot{\gamma}_1 \\ \tau &= \mu\dot{\gamma} \qquad \dot{\gamma} < \dot{\gamma}_1 \end{aligned} \tag{A2.5}$$

The advantage of this model over the simple power law equation, A2.1 is that it overcomes the problem of predicting either zero limiting viscosity for pseudoplastic and infinite limiting viscosity for dilatent liquids.

e) Ellis

$$\tau = \left[\frac{\mu_o}{1 + \left| \tau / \tau_{1/2} \right|^{\alpha-1}} \right] \dot{\gamma} \qquad \text{A2.6}$$

where $\tau_{1/2}$ is the value of τ at which $\mu = 1/2\mu_o$
as $\tau \rightarrow 0$, the model becomes Newtonian with $\mu = \mu_o$
whilst for $\mu \ll \mu_o$ it reduces to the power law with $1/\alpha \equiv n$

f) Meter

$$\mu = \mu_o \left[\frac{1 + \left| \tau/\tau_m \right|^{\alpha-1} \mu_\infty/\mu_o}{1 + \left| \tau/\tau_m \right|^{\alpha-1}} \right] \qquad \text{A2.7}$$

This model has four parameters. τ_m is the value of τ at which

$$\mu = \frac{\mu_o + \mu_\infty}{2}$$

As $\tau \rightarrow 0 \quad \mu = \mu_o$

$\tau \rightarrow \infty \quad \mu = \mu_\infty$

For intermediate τ the model behaves as a power law model with $1/\alpha \equiv n$

If $\mu \ll \mu_o$ the model reduces to the Ellis model, above.

g) Cross

$$\mu = \mu_\infty + \frac{\mu_o - \mu_\infty}{1 + (\dot{\gamma} t_1)P} \qquad \text{A2.8}$$

For $\mu_o \gg \mu \gg \mu_\infty$ this model reduces to the power law with

$$(1-P) = n$$

and

$$k = \mu_o (t_1)^{-P} \qquad \text{A2.9}$$

The parameter t_1 is a characteristic time constant and is

equal to the reciprocal of the value of $\dot{\gamma}$ at which:

$$\mu = \frac{\mu_o + \mu_\infty}{2}$$

h) Williams

$$\mu = \mu_\infty + \frac{\mu_o - \mu_\infty}{(1 + 2t_1^2\dot{\gamma})^P} \qquad \text{A2.10}$$

For $\mu_o \gg \mu \gg \mu_\infty$ and $\mu_o^{1/P} \gg \mu^{1/P}$ this model reduces to power law, with n = (1-2P) and

$$k = \mu_o(2t_1^2)^{-P}$$

The general characteristics of all the mentioned models are shown in the graph presented in figure A2.4.

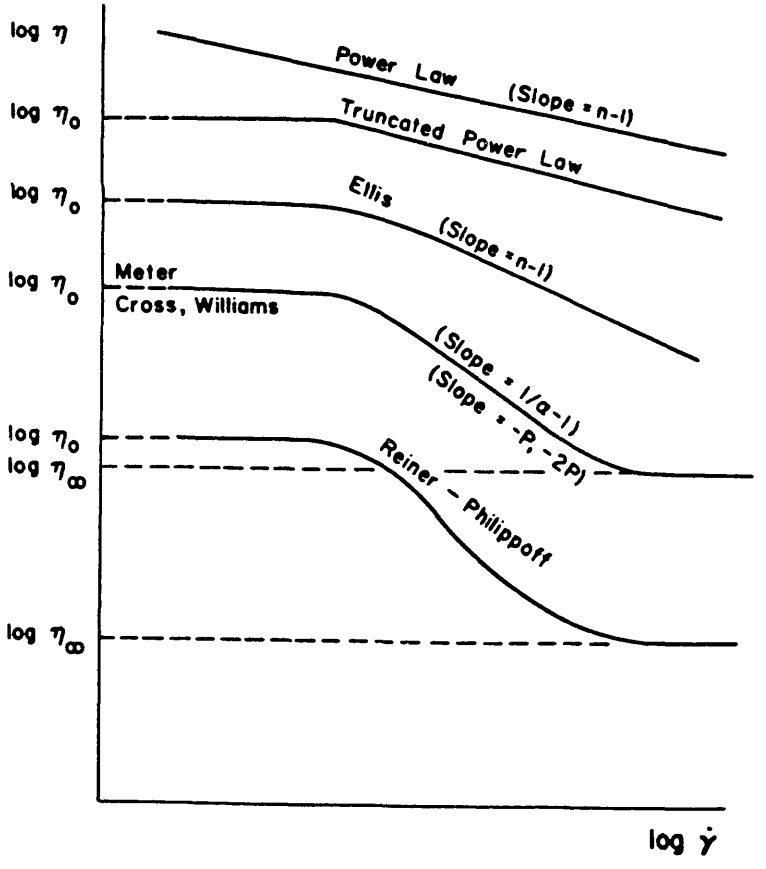

Figure A2.4 Sketch graph illustrating different types of non-Newtonian behavior (Darby, 1976)

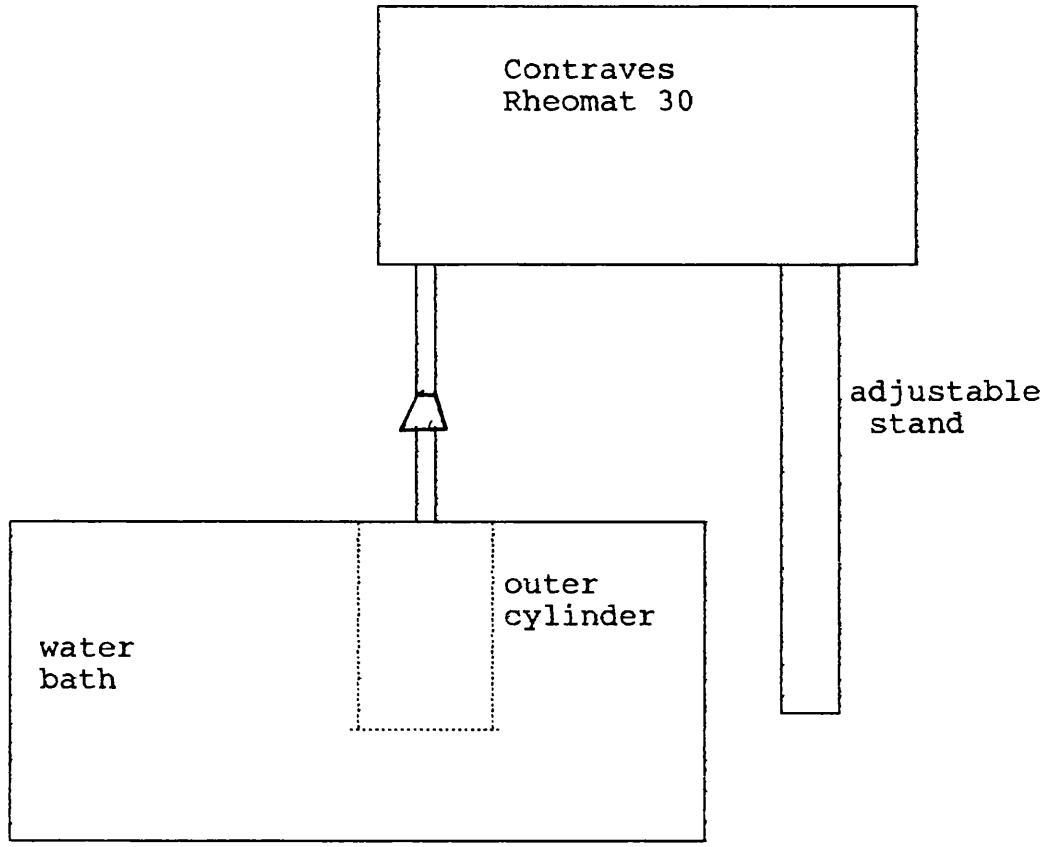

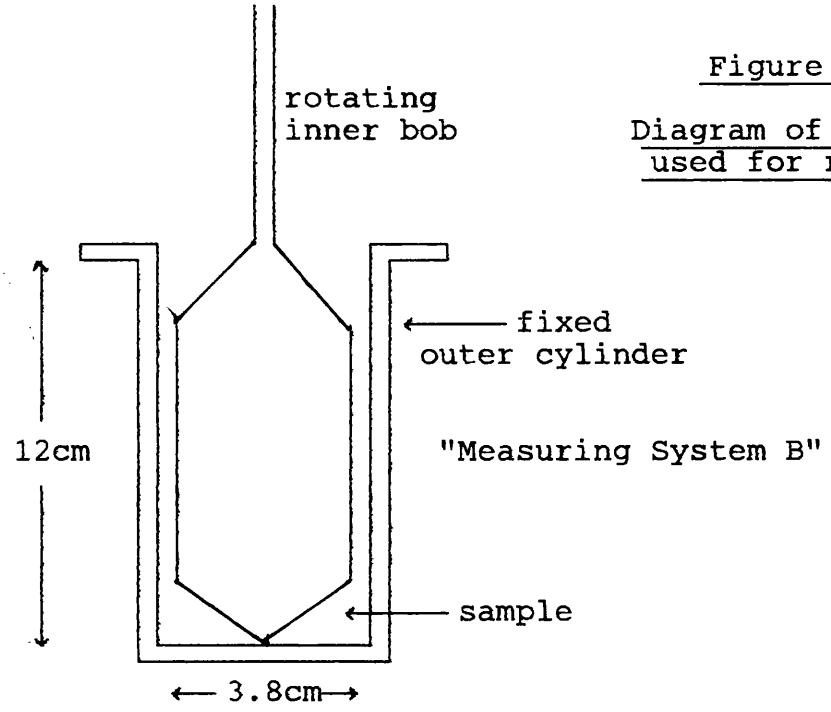

Figure A2.1

Diagram of equipment used for rheometry

Figure A2.2 Flowcurves for CMC solutions

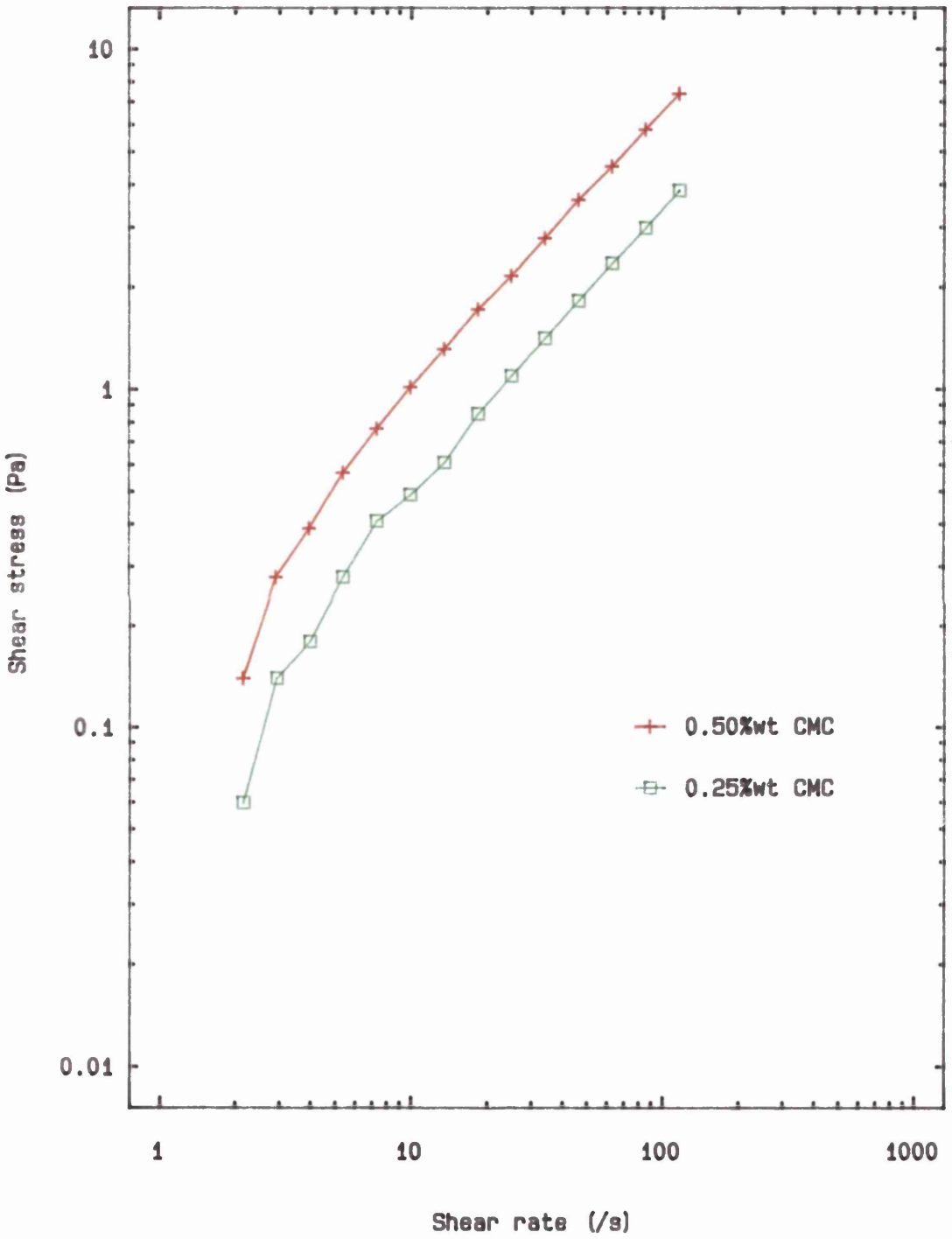

Figure A2.3

Plot of Refractive Index vs. Percentage Corn Syrup (at 26 deg.C)

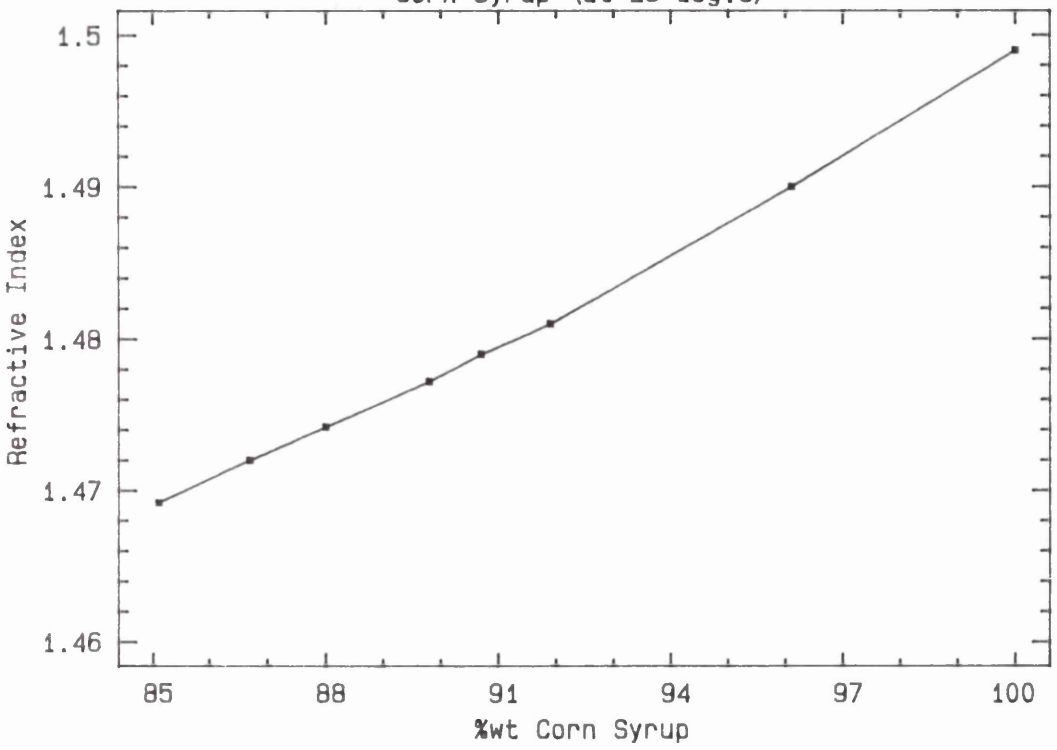

Figure A2.4

Plots of Power Number vs Reynolds Number

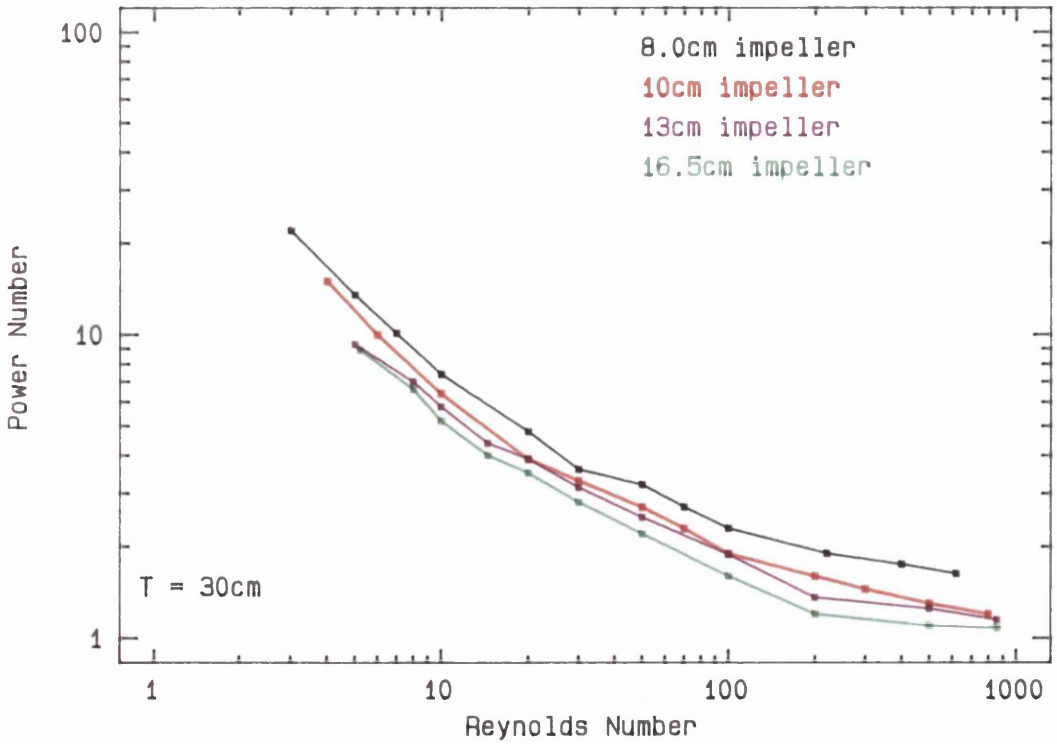

Appendix 3 Technical Specifications of Electric Motors and Ancilliary Equipment

Two D.C. electric motors have been used to rotate the various impellers used for this study; one with a greater power output than the other. Both of these motors have been manufactured by Anyspeed Ltd. Each motor is connected to a infinitely variable speed controller, with a range of 2000 rpm.

Parameter	Specification	
	Motor 1	Motor 2
Maximum power output	1.1kW	3.0kW
Maximum speed	2000rpm	2000rpm
Adjustible ramp	0.5 -> 15 sec	0.5 -> 15 sec
Mains supply	220/240 V	220/240 V
	50/60 Hz	50/60 Hz
Output - armature	160/180 V, DC	160/180 V, DC
- field	190/21 OV, DC	190/21 OV, DC
Operating Temperature	0 -> 40°C	0 -> 40°C

Table A3.1 Specifications of Electric Motors

Associated with each motor is a shaft mounted torque transducer (figure 4.3.4), manufactured by EEL (a division of Westland).The impeller speed was detected by a miniature light source and photo-transistor. These are incorperated within each torque transducer. On each of the transducer shafts are placed white reflective markings. As the motor is engaged, the transducer and impeller shafts (which are connected) rotate at a common frequency. The frequency of the photo-transistor signals caused by the periodic reflection of light emitted by the miniature light source corresponds to the frequency of impeller rotation.

The transducers are designed to detect the small angular distortions of the transducer shaft encountered during rotation. These distortions cause a change in the electrical resistance of the strain gauges attached to the shaft within each transducer. This change in resistance produces an electrical output which is directly proportional to the torque encountered by the shaft.

Parameter	Specification	
	Transducer 1	Transducer 2
Working range	0 -> 8 Nm	0 -> 20 Nm
Maximum speed	1500 rpm	2000 rpm
Operating temperature	0 -> 40^{o}C	0 -> 40^{o}C
Maximum error	± 0.2%	± 0.2%
Sensitivity	2.2mV ± 5%	2.2mV ± 5%
Overload	1.5x8 Nm	1.5x20 Nm
Rotation	both clockwise and anticlockwise	
Working life	100,000 miles peripheral distance	

Table A3.2 Specifications of Torque Transducers

The torque and impeller frequency signals were directed into a display unit, the TM 30/3, also manufactured by EEL. This was initially calibrated by the manufacturers but requires periodic recalibration in accordance with manufacturers' instruction manual. Outlets at the rear of the TM 30/3 allowed the output to connected to other display units such as a voltmeter to give a digital display of the torque or shaft frequency.

APPENDIX 4: Safety Procedures for Operation of Laser System

The laser/photocell arrangement shown in figure 4.3.3 was designed to comply the University's safety regulations ("Safety in the Use of Lasers", Policy Statement for University College, London, Health and Safety at Work Act, 1974) for lasers emitting less than 0.5mW.

Whenever the laser was switched on, the gun, the mixing vessel, and the photocell were always enclosed by a thick curtain as shown in figure 4.3.3.

Before any changes were made to the positioning of the laser beam (see 4.3), the following safety procedures were observed:

1) Starting Procedure (see figure 4.3.3)
a) The intermediate on/off switch {2} on the laser gun was placed in the upper position, thus completely obscuring the laser beam outlet.
b) The laser power supply was turned on using the security key switch {16} attached onto the power supply. The laser was allowed approximately 45 minutes to achieve a stable state.

2) Procedure for Alignment of Laser
a) With the laser beam completely blocked, the laser was placed at the required position using the adjusting screws on the vertical {1} and horizontal {8} rails. The position of the photocell {6} at the other side of the mixing vessel was aligned in a similar way.Often fine adjustment was required to ensure that the laser beam was directly incident onto the convex lens of the photocell.
b) The curtains surrounding the laser/vessel/cell system were drawn and secured onto the main frame so that no stray reflections could escape the enclosure.
c) The cover on the level adjusting screws {1} was removed; this automatically introduces an optical filter {3} which reduces the laser power to about 2/3.

d) The intermediate laser shutter {2} was pushed down allowing the laser beam to escape from the laser gun through the optical filter and to pass through the glass vessel to be collected by the photocell.
e) The procedure described in Appendix 8 was followed and the voltage corresponding to the intensity of the laser beam incident onto the photocell was displayed by the screen monitor connected to the microcomputer.
f) Using the fine adjusting screws {1} or {8}, the laser beam could be more accurately directed to the photocell such that the beam was exactly perpendicular to the vertically positioned photocell and laser gun. This condition was reached when the data acquisition system showed the maximum voltage value, V_o.
g) The cover on the fine adjustment screws {1} was replaced. In so doing, the optical filter was automatically removed, allowing the full power of the laser beam to pass through. The system is then ready to commence the data acquisition procedure, described in Appendix 8.

APPENDIX 5

Effect of Solids Concentration

Empirically, many workers have found that the effect of concentration on the just suspension speed is small (see table 3.1.4). Others (Pavleshenko et al, 1957) have reported that particle concentration has its most significant influence at low concentrations and then has a progressively smaller effect as the concentration rises to about 15%wt. The shape of any graph of N_{JS} against concentration, C_w, would be similar to that for d_p (figure 3.6).

Even some of those who tried to derive theoretical models to predict N_{JS} have had to rely on experimental data to take account of concentration. As yet, there seems to be a lack of agreement between the various workers on the means by which the particle concentration influences N_{JS}.

The "quadratic mean flow" model presented earlier in Chapter Three can be used a starting point from which to explain, theoretically, why concentration has such a small influence on N_{JS}, and why even that small influence diminishes with increased concentration. The following analysis outlines how this might be done. The quadratic mean flow model is based on a balance of vertical forces exerted upon a solitary particle resting on flat plane. The net upward force on the particle causes the the particle to lift and thereby gain potential energy as it rises from the plane (by one particle diameter, say) into suspension. The potential energy, P.E., gained in such a process will be

$$P.E. = -\int_{d_p/2}^{3d_p/2} F(z)\, dz \qquad A5.1$$

where the limits of integration represent the initial and final axial positions of the centre of mass of the particle.

From 3.1.2 (with some modification)

$$F(z) = F_D(z) + F_L(z) - F_G \qquad \text{A5.2}$$

F_D and F_L will not be constant as the particle moves upwards away from the plane, and are therefore expressed as $F_D(z)$ and $F_L(z)$. However, the other variables can be expressed as simple functions of z so that $F_D(z)$ and $F_L(z)$ can be found and the integral A5.1 can be performed.

$$u_h(z) = \frac{Az}{T} ND(D/T) \qquad \text{A5.3}$$

$$u_v(z) = \frac{Bz}{T} ND(D/T) \qquad \text{A5.4}$$

$$C_L = \frac{c_1' T}{z} \qquad \text{A5.5}$$

$$C_D = \frac{c_2' \mu}{\rho_f u_v d_p} \qquad \text{A5.6}$$

c_1 and c_2 may change slightly to c_1' and c_2' respectively once the particle has stopped touching the base of the tank, but for the purposes of this analysis, they will be assumed to be unchanged from before.

Once the P.E. for one particle has been found, this can be related to the other particles in the tank by considering the rate of suspension of particles at N_{JS}, $\dot{S}$ By multiplying the P.E. for one particle by $\dot{S}$, the rate at which energy is required at N_{JS} can be determined.

$$\text{i.e.} \quad \dot{E}_{P.E.} = -\dot{S} \int_{d_p/2}^{3d_p/2} F(z)\, dz \qquad \text{A5.7}$$

where $\dot{S}$ is a function of the particle concentration.

The power requirement to suspend particles must come from the kinetic energy contained within that flow of liquid which is in the immediate vicinity of the suspending particles.

The kinetic energy of a "lump" of liquid of mass, m,

with speed, u, is given by

$$K.E. = \frac{1}{2} m u^2 \qquad A5.8$$

The kinetic power of "lumps" of liquid will be

$$\dot{E}_{K.E.} = \frac{1}{2} \dot{m} u^2 \qquad A5.9$$

where $\dot{m}$ is the mass flowrate of those lumps, which in turn is proportional to u. This means that the rate at which liquid K.E. passes through a given region is proportional to u^3. As these lumps of liquid pass close to the suspending particles, they will experience some retardation by some proportion, W, so that their speed is diminished to (1-W)u. Therefore, the rate at which the liquid loses K.E. because of the suspension of particles will be proportional to:

$$u^3 - (1 - W)^3 u^3 = W^3 u^3 \qquad A5.10$$

If the liquid velocity, u, is in turn proportional to the impeller speed (equations 3.1.13 and 3.1.14) then the rate at which K.E. is lost is proportional to N^3.

Equating the rate at which the liquid loses K.E. to the rate at which the particles gain P.E., then

$$-\dot{S} \int_{d_p/2}^{3d_p/2} F(z)\, dz \quad \propto \quad N^3 \qquad A5.11$$

substituting for F(z)

$$\dot{S} \int_{d_p/2}^{3d_p/2} F_G - \{F_D(z) + F_b(z)\}\, dz \quad \propto N^3 \qquad A5.12$$

after performing the integration, the resulting equation will have the form

$$\frac{N^3}{a_1 - a_2N^2 - a_3N} \propto \dot{S} \qquad \text{A5.13}$$

where a_1, a_2, and a_3 are all positive co-efficient.

Using a video camera and recorder, film of suspending particles, at N_{JS}, could be analyzed frame by frame. By knowing the frame speed of the camera and counting the number of particles being suspended in each frame, one can estimate the rate of solids suspension, $\dot{S}$. By adding different concentrations of solids it was found that as a good approximation

$$\dot{S} \propto C_w^{0.5} \qquad \text{A5.14}$$

substituting for $\dot{S}$ in equation A5.13

$$\frac{N^3}{a_1 - a_2N^2 - a_3N} \propto C_w^{0.5} \qquad \text{A5.15}$$

With a equation of this type, a small change in N_{JS} will result in a much larger change in C_w, i.e:

$$\frac{dC_w}{dN_{JS}} \text{ is large so } \frac{dN_{JS}}{dC_w} \text{ must be small}$$

The exact value of dN_{JS}/dC_w will depend on the relative values of the co-efficient a_1, a_2, and a_3. If a_2 and a_3 are large enough so that:

$$a_2N^2 + a_3N \rightarrow a_1 \qquad \text{A5.16}$$

then $$\frac{dN_{JS}}{dC_w} \rightarrow 0 \qquad \text{A5.17}$$

meaning that there is no influence of C_w on N_{JS}.

Even if

$$a_2N^2 + a_3N \ll a_1 \qquad \text{A5.18}$$

so that A5.15 can be approximated by:

$$\frac{N_{JS}^3}{a_1} \propto C_w^{0.5} \qquad \text{A5.19}$$

then the most that N_{JS} can depend on C_w is such that:

$$N_{JS} \propto C_w^{0.17} \qquad \text{A5.20}$$

so if, in general,

$$N_{JS} \propto C_w^{a} \quad \text{then} \quad 0 < a < 0.17 \qquad \text{A5.21}$$

Therefore, a relationship of the type shown by equation A5.15 would explain not only why C_w has such a small influence on N_{JS} but also why, as N_{JS} increases (because C_w has been increasing) and A5.16 is approached, even that small influence has been reduced to zero.

The analysis presented to explain the effect of particle concentration on the just suspension condition requires further theoretical and empirical work before all the constants of proportionality can be determined. Once this is done, then a general equation of the form shown by A5.15 can be used to give quantitative predictions for N_{JS} for a given agitation system.

The mathematical modeling presented in this Appendix and in chapter 3 has been based on the hydrodynamics and particle/fluid interactions predicted from considering only the mean (or time-averaged) velocities of an agitated liquid close to the region of solids suspension. In this manner a simplified "quadratic mean flow" model has been developed to predict N_{JS} . This model arises from a force balance on a solitary particle resting on the base of an agitated vessel. This simplified model does not take into account the particle concentration. However, the analysis of forces on one particle can be used to formulate an energy balance between the rate at which potential energy is required by the particles lifting into suspension, and

the rate at which the surrounding liquid can supply this energy by transferring some of its kinetic energy. This energy balance leads to a more general relationship for N_{JS} which includes the (small) influence of particle concentration.

For the purposes of this study, the quadratic mean flow model has been examined to see how the predictions for N_{JS} compare with experimental data.

APPENDIX 6: Experimental Results

CMC SUSPENSION SPEED DATA

All experiments conducted with a 13cm six-bladed 45° pitched turbine at a clearance, ΔZ, of 9.0cm in a 30cm flat-bottomed, unbaffled tank.

A) 0.25%wt CMC

Acetate

	pumping down		pumping up		
d_p/mm	N_{JS}/RPM	μ_{av}/cP	N_{JS}/RPM	μ_{av}/cP	
2	147	38	111	39	ρ_s=1270kg/m
4	156	38	114	39	C_b= 0.03%wt
5	157	38	113	39	

d_p/mm	N_{JS}/RPM	ρ_s/kg/m^3	μ_{av}/cP	
390	275	2900	36	Glass pumping up
530	284	2900	36	
1100	291	2900	36	C_b= 0.5%wt
1840	265	2540	36	

Variation with particle concentration:

390μm

C_b (%wt)	N_{JS} (RPM)
0.1	271
0.2	273
0.5	275
1.0	280

530μm

C_b (%wt)	N_{JS} (RPM)
0.1	284
0.2	285
0.5	284
1.0	289

1100μm

C_b (%wt)	N_{JS} (RPM)
0.1	287
0.2	288
0.5	291
1.0	287

1840μm

C_b (%wt)	N_{JS} (RPM)
0.1	266
0.2	265
0.5	265
1.0	266

μ_{av} calculated from Metzner & Otto (k_s = 13)

B) 0.5%wt CMC Acetate ρ_s =1270kg/m^3

	pumping down		pumping up	
d_p/mm	N_{JS}/RPM	μ_{av}/cP	N_{JS}/RPM	μ_{av}/cP
2	348	68	236	74
4	349	68	239	74
5	349	68	234	74

C_b = 0.03%wt

d_p/μm	N_{JS}/RPM	ρ_s/kg/m^3	μ_{av}/cP
390	311	2900	70
530	314	2900	70
1100	317	2900	70
1840	292	2540	72

Glass
pumping up

C_b=0.5%wt

Variation with particle concentration:

390μm

C_b (%WT)	N_{JS} (RPM)
0.1	305
0.2	307
0.5	311
1.0	314

530μm

C_b (%WT)	N_{JS} (RPM)
0.1	307
0.2	311
0.5	314
1.0	313

1100μm

C_b (%WT)	N_{JS} (RPM)
0.1	315
0.2	318
0.5	317
1.0	319

1840μm

C_b (%WT)	N_{JS} (RPM)
0.1	279
0.2	287
0.5	292
1.0	292

C) 0.1%wt CMC
Acetate ρ_s=1270kg/m^3

	pumping down		pumping up		
d_p/mm	N_{JS}/RPM	μ_{av}/cP	N_{JS}/RPM	μ_{av}/cP	
2	94	10	97	10	
4	93	10	98	10	
5	96	10	96	10	

Glass ρ_s=2540kg/m^3, d_p=1840μm

C_b (%WT)	N_{JS} (RPM)	μ_{av} (cP)
0.1	245	9.8
0.2	248	9.8
0.5	253	9.8
1.0	257	9.8

Only the 1840μm particles could be investigated because the other glass ballotini were too dense to be suspended without the nadir of the vortex reaching the plane of the impeller.

D) 0.20%wt CMC Acetate ρ_s=1270kg/m^3

	pumping down		pumping up		
d_p/mm	N_{JS}/RPM	μ_{av}/cP	N_{JS}/RPM	μ_{av}/cP	
2	161	18	105	19	
4	165	18	111	19	
5	166	18	112	19	

Glass ρ_s = 2540kg/m^3, d_p = 1840μm

C_b (%WT)	N_{JS} (RPM)	μ_{av} (cP)
0.1	274	17
0.2	279	17
0.5	284	17
1.0	288	17

Other, denser, glass ballotini were not able to be suspended because the nadir of the vortex reached the impeller.

Solids Suspension Experiments with Glycerol/Water Mixtures

C_b (%WT)	ΔZ (M)	93%WT Glycerol N_{JS}/s^{-1}			78%WT Glycerol N_{JS}/s^{-1}			82.5%WT Glycerol N_{JS}/s^{-1}			d_p (mm)
		0.13	0.085	0.165	0.13	0.085	0.165	0.13	0.085	0.165	
0.1	0.09	6.00			4.40	10.53		5.37			0.390
0.1	0.07	5.87			4.28			5.12			0.390
0.1	0.05	5.80			4.02			4.83			0.390
0.1	0.11	6.08			4.53			vortex			0.390
0.1	0.11	6.58			4.65			vortex			0.530
0.1	0.07	6.42			4.37			5.00			0.530
0.1	0.05	6.20			4.25			4.68			0.530
0.1	0.09	6.50			4.48	10.94		5.33			0.530
0.1	0.09	6.57			4.70	11.33		5.43			1.100
0.1	0.07	6.40			4.45			5.30			1.100
0.1	0.05	6.20			4.33			5.17			1.100
0.1	0.11	6.70			4.82			vortex			1.100
0.1	0.11	6.00			4.70			5.00			1.840
0.1	0.07	5.70			4.28			4.50			1.840
0.1	0.05	5.50			4.05			4.10			1.840
0.1	0.09	5.90			4.53	11.39		4.68			1.840
0.2	0.09	5.87	13.05	3.67	4.87	11.44	3.23	5.00	11.75	3.32	1.840
0.2	0.07	5.67	12.88	3.60	4.78	11.19	3.13	4.87	11.25	3.16	1.840
0.2	0.05	5.50	12.50	3.50	4.68	10.76	3.03	4.37	11.14	3.13	1.840
0.2	0.11	6.00	13.15	3.80	4.95	11.88	3.43	5.10	11.95	3.47	1.840
0.5	0.09	5.92			4.90	11.48		5.07			1.840

For particles 0.390 to 1.100mm, $\rho_s = 2900 kg/m^3$

For particles of diameter 1.840mm, $\rho_s = 2540 kg/m^3$

kinematic viscosity of 93%WT glycerol = 0.572/1242 m^2/s

of 78%WT glycerol = 0.049/1202 m^2/s

of 82.5%WT glycerol = 0.099/1216 m^2/s

Variation with particle concentration

ΔZ=0.09m, T=0.30m using 78%wt glycerol/water

i) d_p=1.840mm

C_b (%wt)	N_{JS}/s^{-1} D=0.13m	D=0.085m
0.1	4.53	11.39
0.2	4.87	11.44
0.5	4.90	11.48
1.0	4.95	11.53

ii) d_p=1.100mm

C_b (%wt)	N_{JS}/s^{-1} D=0.13m	D=0.085m
0.1	4.70	11.33
0.2	4.90	11.42
0.5	4.93	11.47
1.0	4.95	11.51

iii) d_p= 0.530mm

C_b (%wt)	N_{JS}/s^{-1} D=0.13m	D=0.085m
0.1	4.48	10.94
0.2	4.68	11.00
0.5	4.73	11.05
1.0	4.83	11.11

Hysteresis Experiments in 15.3cm Tank

D=6.5cm, ΔZ=3.6cm, using corn syrup/water mixture
μ= 4.7Pas, ρ_f = 1377kg/m^3

A) Glass ballotini ρ_s = 2900kg/m^3

i) d_p = 6mm, mass of each particle = 3.28x10^{-4}kg

C_b (%WT)	N_{JS} (RPM)	N_D (RPM)
0.02	288	60
0.08	290	75
0.21	289	120
0.45	291	170
0.71	291	291

N_D is the impeller speed at which the first particle drops out of suspension. If there is no column for N_D, then no hysteresis.

ii) d_p = 4mm, mass = 9.68x10^{-5}kg

C_b (%WT)	N_{JS} (RPM)	N_D (RPM)
0.04	276	65
0.17	278	96
0.57	281	125
0.65	279	279

iii) d_p = 2mm, mass = 1.21x10^{-5}kg

C_b (%WT)	N_{JS} (RPM)
0.05	263
0.22	270
0.66	280
1.29	288

iv) d_p = 1.100mm, mass = 2.01x10^{-6} kg

C_b (%WT)	N_{JS} (RPM)
0.04	254
0.16	264
0.53	267
1.17	268

v) d_p = 0.780mm, mass = 7.17x10^{-7}kg

C_b (%WT)	N_{JS} (RPM)
0.04	242
0.13	260
0.39	270
0.66	271

B) Glass ballotini, ρ = 2540 kg/m^3

i) d_p = 10mm, mass = 1.33x10^{-3}kg

C_b (%WT)	N_{JS} (RPM)	N_D (RPM)
0.03	235	60
0.15	233	65
0.49	239	95
1.13	232	155
1.27	234	234

ii) d_p = 3.265mm, mass = 4.63x10^{-3}kg

C_b (%WT)	N_{JS} (RPM)	N_D (RPM)
0.04	234	75
0.09	233	115
0.21	235	175
0.43	232	232

C) Zirconium oxide, $_s\rho$ = 3820kg/m^3

d_p = 1.85mm, mass = 1.27x10^{-5}kg

C_b (%WT)	N_{JS} (RPM)
0.03	330
0.18	342
0.60	345
1.38	344

D) PTFE, $_s\rho$ = 2140kg/m^3

d_p = 3.175mm, mass = 3.59x10^{-5}kg

C_b (%WT)	N_{JS} (RPM)
0.03	204
0.17	211
0.51	214
0.87	213

Suspension Experiments with Corn Syrup in 19cm tank

viscosity of syrup = 11.30 Pas, density = 1384 kg/m^3

all experiments conducted with 6.5cm six-bladed 45^{o}pitched turbine impeller at a clearance of 3.6cm.

Suspension studies at 0.1%wt concentration

d_p/mm	ρ_s/kg/m^3	N_{JS}/RPM	HYSTERESIS
6.0	2900	231	YES
10.0	2540	219	YES
4.0	2900	225	YES
3.265	2540	192	YES
3.175	2140	162	YES
1.85	3820	284	YES
2.0	2900	213	YES
1.1	2900	241	NO
0.78	2900	294	NO

Variation with particle concentration

i) 6mm glass ballotini

C_b/%wt	N_{JS}/RPM	N_D/RPM
0.04	230	45
0.10	231	70
0.28	231	110
0.37	232	125
0.44	231	170
0.56	231	190
0.67	232	232

Effect of impeller diameter at 0.1%wt for 6mm ballotini

D/cm	N_{JS}/RPM	N_D/RPM
6.5	231	70
8.0	207	65
10.0	185	60

ii) 1.1mm glass ballotini

C_b/%WT	N_{JS}/RPM	N_D/RPM
0.03	193	75
0.13	241	241
0.36	290	290
0.91	295	295

Effect of impeller diameter at 0.9%WT for 1.1mm ballotini

D/cm	N_{JS}/RPM
6.5	295
8.0	270
10.0	252

iii) 0.78mm glass ballotini

C_b/%WT	N_{JS}/RPM
0.04	256
0.14	294
0.37	316
0.95	319

Suspension Experiments with Corn Syrup in 24cm tank

viscosity of syrup = 4.7 Pas, density = 1374kg/m^3, ΔZ=3.6cm

A) 10mm glass ballotini, ρ_s = 2540kg/m^3
D=6.5cm

C_b/%WT	N_{JS}/RPM	N_D/RPM
0.07	225	120
0.21	226	140
0.41	225	190
0.54	227	205
0.66	227	227

Effect of impeller diameter for C_b= 0.66%WT

D/cm	N_{JS}/RPM
6.5	227
8.0	193
10.0	175
13.0	173

B) 6mm glass ballotini, ρ_s = 2900kg/m^3
D=8.0cm

C_b/%WT	N_{JS}/RPM	N_D/RPM
0.06	209	70
0.21	211	160
0.33	208	175
0.44	209	209

C) 4mm glass ballotini, ρ_s = 2900kg/m^3
D=8.0cm

C_b/%WT	N_{JS}/RPM	N_D/RPM
0.07	194	60
0.21	195	80
0.34	194	145
0.61	200	175
0.75	203	203

D) 3.265mm glass ballotini, ρ_s = 2540kg/m^3

D=8.0cm

C_b/%WT	N_{JS}/RPM	N_D/RPM
0.08	170	70
0.23	172	80
0.38	173	110
0.53	171	125
0.67	172	172

E) 2mm glass ballotini

ρ_s = 2900kg/m^3

D=8.0cm

C_b/%WT	N_{JS}/RPM
0.08	241
0.23	246
0.45	260
0.78	263

F) 1.1mm glass ballotini

ρ_s = 2900kg/m^3

D=8.0cm

C_b/%WT	N_{JS}/RPM
0.07	230
0.21	243
0.48	264
0.85	268

G) 0.78mm glass ballotini, ρ_s = 2900kg/m^3

D=8.0cm

C_b/%WT	N_{JS}/RPM
0.07	245
0.25	267
0.48	274
0.85	276

H) 1.85mm Zirconium

ρ_s = 3820kg/m^3

D=8.0cm

C_b/%WT	N_{JS}/RPM
0.07	284
0.22	297
0.56	299
0.93	301

I) 3.175mm PTFE

ρ_s = 2140kg/m^3

D=8.0cm

C_b/%WT	N_{JS}/RPM
0.06	140
0.21	148
0.45	159
0.85	161

Suspension Experiments with Corn Syrup in 30cm Tank

viscosity of syrup = 4.7Pas, density = 1374kg/m^3, ΔZ=3.6cm, D=10cm

A) 6mm glass ballotini

ρ_s = 2900kg/m^3

C_b/%WT	N_{JS}/RPM
0.03*	215*
0.13	224
0.36	235
0.71	240

*with baffles 222rpm

Effect of impeller diameter at 0.03%wt

D/cm	N_{JS}/RPM
6.5	257
8.0	235
10.0	215
13.0	177

B) 4mm glass ballotini, ρ_s = 2900kg/m^3

C_b/%WT	N_{JS}/RPM
0.03	204
0.13	209
0.28	217
0.47	225
0.72	227

C) 10mm glass ballotini, ρ_s = 2540kg/m^3

C_b/%WT	N_{JS}/RPM	N_D/RPM
0.04	181	165
0.11	184	184
0.25	189	189
0.47	191	191

D) 3.265mm glass ballotini
ρ_s = 2540 kg/m^3

C_b/%WT	N_{JS}/RPM
0.05	172
0.14	179
0.27	183
0.49	182

E) 3.175mm PTFE
ρ_s = 2140kg/m^3

C_b/%WT	N_{JS}/RPM
0.03	143
0.10	148
0.26	151
0.41	153

F) 2mm glass ballotini
ρ_s = 2900kg/m^3

C_b/%WT	N_{JS}/RPM
0.03	200
0.12	213
0.26	223
0.52	233

G) 1.1mm glass ballotini
ρ_s = 2900kg/m^3

C_b/%WT	N_{JS}/RPM
0.03	190
0.15	216
0.35	232
0.62	238

H) 0.78mm glass ballotini
ρ_s = 2900kg/m^3

C_b/%WT	N_{JS}/RPM
0.03	179
0.13	201
0.31	220
0.58	229
0.75	231

I) 1.85mm Zirconium
ρ_s = 3820kg/m^3

C_b/%WT	N_{JS}/RPM
0.03	244
0.12	284
0.28	294
0.51	296

Single Particle Suspension Speed Experiments

All experiments conducted with mixtures of corn syrup and water in a 30cm unbaffled tank.

1) Viscosity of liquid = 10.0Pas, density = 1383kg/m^3

a) effect of particle ΔZ=3.6cm, D=10.0cm
using six-bladed 45^{o}pitched turbine
pumping upwards

d_p/mm	ρ_s/kg/m^3	$\frac{\rho_s - \rho_f}{\rho_f}$	N_{JS}/RPM
10.0	2580	0.866	185
6.0	2900	1.097	206
4.0	2900	1.097	196
3.265	2580	0.866	178
3.175	2140	0.547	138
1.85	3820	1.762	246
2.0	2900	1.097	187
1.1	2900	1.097	179
0.78	2900	1.097	175

b) effect of impeller diameter and clearance
using a single 6.0mm glass particle

D=10.0cm

ΔZ/cm	N_{JS}/RPM
2.9	226
3.6	206
4.1	195
4.7	195
5.2	196
5.7	217
7.1	227
7.7	236

D=13.0cm

ΔZ/cm	N_{JS}/RPM
2.9*	188*
3.6	178
4.9	171
5.5	151
5.8	151
6.7	163
7.4	172
7.9	192

*pumping down 213rpm

D=8.0cm

ΔZ/cm	N_{JS}/RPM
2.3	234
2.8	212
3.1	196
3.4	213
4.2	233
4.7	245
6.0	264
6.6	280

D=16.0cm

ΔZ/cm	N_{JS}/RPM
4.1	169
6.4	159
7.6	175

2) viscosity of syrup = 2.0Pas, density = 1358kg/m^3

effect of impeller diameter and clearance
using six-bladed 45^{o}pitched turbines pumping upwards
and a single 6.0mm glass particle

D=10.0cm

ΔZ/cm	N_{JS}/RPM
3.0	305
3.6	340
4.1	412
5.4	685

D=13.0cm

ΔZ/cm	N_{JS}/RPM
3.7	482
5.4	468
6.4	445
6.6	422

D=8.0cm

ΔZ/cm	N_{JS}/RPM
2.9	286
3.5	323
4.1	388
4.6	570
5.1	>840*

*violent vibration

D=16.0cm

ΔZ/cm	N_{JS}/RPM
2.3	323
2.8	340
3.5	390
4.4	393
4.8	366
5.8	330
6.1	315
6.6	292
7.7	260

3) viscosity of syrup = 1.0Pas, density = 1343kg/m^3

effect of particle ΔZ=3.6cm, D=10.0cm
using six-bladed 45° pitched turbine
pumping upwards

d_p/mm	ρ_s/kg/m^3	$\frac{\rho_s - \rho_f}{\rho_f}$	N_{JS}/RPM
10.0	2580	0.921	371
6.0	2900	1.159	400
4.0	2900	1.159	394
3.265	2580	0.921	359
3.175	2140	0.593	302
1.85	3820	1.844	441
1.84	2580	0.921	356
2.0	2900	1.159	385
1.1	2900	1.159	372
0.78	2900	1.159	365

4) viscosity of syrup = 0.5Pas, density = 1323kg/m^3

effect of impeller diameter and clearance
using six-bladed 45^{o}pitched turbines pumping upwards
and a single 6.0mm glass particle

D=10.0cm

ΔZ/cm	N_{JS}/RPM
1.9	554
2.4	435
2.9	353
3.2	358
3.6	319
3.7	324
4.1	527
4.4	510
4.9	514
5.6	476
6.0	462
6.1	442
6.8	380

D=8.0cm

ΔZ/cm	N_{JS}/RPM
1.8	561
2.2	477
2.7	399
3.2	383
3.6	482
4.1	390
4.4	850
4.5	>900*
4.7	>900*
4.9	822
5.5	732
7.0	>600**

*violent vibration
**vortex reaching impeller

(continued on next page)

(continued from previous page)

D=13.0cm

ΔZ/cm	N_{JS}/RPM
2.4	391
3.2	355
3.8	353
4.2	336
4.7	313
5.3	295
6.2	261
7.0	243
7.4	251
7.8	242
8.3	239
9.0	234
9.6	228

D=16.0cm

ΔZ/cm	N_{JS}/RPM
2.3	>345**
3.2	340
3.5	292
4.0	259
4.5	239
4.8	226
5.2	210
5.7	195
6.2	188
6.6	179
7.0	169
7.3	167
7.9	165
8.2	155
9.3	156
9.7	154

5) viscosity of syrup = 0.19Pas, density = 1295kg/m^3

effect of particle ΔZ=3.6cm, D=10.0cm
using six-bladed 45°pitched turbine
pumping upwards

d_p/mm	ρ_s/kg/m^3	$\frac{\rho_s - \rho_f}{\rho_f}$	N_{JS}/RPM
10.0	2580	0.992	247
6.0	2900	1.239	254
4.0	2900	1.239	251
3.265	2580	0.992	235
3.175	2140	0.653	201
1.85	3820	1.950	320
1.84	2580	0.992	223
2.0	2900	1.239	241
1.1	2900	1.239	229
0.78	2900	1.239	220

Effect of viscosity
using throughout a 6mm glass sphere, density 2900kg/m^3, in mixturesof corn syrup and water. T=30cm, D=10cm. Impeller is a six-bladed 45^0 pitched turbine.

A) ΔZ=3.6cm

μ_f/Pas	ρ_f/kg/m^3	N_{JS}/RPM
10.0	1383	206
8.2	1378	203
7.3	1374	201
6.0	1369	200
5.0	1367	203
4.3	1366	216
3.2	1364	236
2.9	1361	247
2.5	1360	277
2.2	1359	319
2.0	1358	340
1.8	1353	371
1.6	1351	402
1.4	1350	410
1.3	1348	409
1.1	1346	402
1.0	1343	400
0.88	1340	391
0.79	1337	378
0.70	1334	367
0.65	1331	359

CONTINUED ON NEXT PAGE

(CONTINUED FROM PREVIOUS PAGE)

μ_f/Pas	ρ_f/kg/m^3	N_{JS}/RPM
0.57	1326	341
0.53	1324	333
0.50	1323	319
0.44	1321	311
0.38	1318	303
0.30	1314	286
0.27	1311	280
0.25	1308	277
0.22	1300	259
0.19	1295	254
0.16	1288	247

B) ΔZ=4.4cm

μ_f /Pas	ρ_f /kg/m^3	N_{JS} /RPM
10.0	1383	195
7.1	1375	194
5.8	1372	193
5.0	1370	192
4.4	1368	192
3.7	1366	203
3.2	1363	230
2.5	1362	282
2.0	1360	459
1.7	1354	484
1.6	1353	498
1.4	1352	445
1.1	1345	440
0.87	1340	428
0.76	1336	434

Rheology Experiments

Preparation of Carbonyl Methyl Cellulose (CMC) solutions in distilled water at room temperature. The rheology was investigated using a Contraves Rheomat 30. Measuring system B was employed (co-axial cylinders).
The cylinders were placed in a water bath kept at 20°C.

A) 0.5%wt CMC

speed setting	nominal torque % run1	run2	actual torque/Nm^{-2}
0	0.6	0.8	0.0
16	1.0	1.1	0.14
17	1.3	1.5	0.28
18	1.6	1.7	0.39
19	2.0	2.2	0.57
20	2.5	2.7	0.77
21	3.1	3.3	1.02
22	3.8	4.1	1.32
23	4.8	5.1	1.73
24	5.8	6.3	2.17
25	7.3	7.9	2.80
26	9.4	9.9	3.63
27	11.7	12.1	4.55
28	14.9	15.2	5.83
29	19.0	19.0	7.43

The "actual torque" is the average of runs 1 and 2 and represents the "Arithmetic Average Shear Stress" experienced by the sample trapped between the two cylinders.

B) 0.75%wt CMC

speed setting	nominal torque % run1	run2	actual torque/Nm^{-2}
0	0.8	0.8	0.0
16	2.2	2.4	0.61
17	3.6	3.8	1.18
18	4.4	4.7	1.52
19	5.5	5.8	1.97
20	6.8	7.2	2.52
21	8.5	9.0	3.23
22	10.7	11.1	4.10
23	13.1	13.6	5.10
24	16.3	17.0	6.44
25	20.2	20.8	8.00
26	24.9	25.2	9.85
27	30.3	30.4	12.00
28	36.1	37.1	14.70
29	44.8	45.0	17.91

C) 1.0%wt CMC

speed setting	nominal torque % run1	run2	actual torque/Nm^{-2}
0	0.5	0.9	0.0
16	2.6	3.0	0.85
17	4.0	4.8	1.50
18	5.2	5.9	1.97
19	6.5	7.3	2.52
20	8.1	9.0	3.19
21	10.1	11.2	4.04
22	12.8	14.1	5.18
23	15.7	17.2	6.40
24	19.6	21.3	8.02
25	24.1	26.1	9.91
26	29.8	32.0	12.26
27	36.5	38.9	15.03
28	44.3	46.8	18.21
29	53.2	56.0	24.80

D) 0.25%wt CMC

speed setting	nominal torque % run1	run2	actual torque/Nm^{-2}
0	0.3	0.0	0.0
16	0.4	0.2	0.06
17	0.6	0.4	0.14
18	0.7	0.5	0.18
19	1.0	0.7	0.28
20	1.3	1.0	0.41
21	1.5	1.2	0.49
22	1.8	1.5	0.61
23	2.4	2.1	0.85
24	3.0	2.7	1.10
25	3.8	3.5	1.42
26	4.8	4.5	1.83
27	6.1	5.8	2.36
28	7.7	7.4	3.00
29	9.8	9.5	3.86

Axial Concentration Profiles

All experiments conducted in fully profiled vessels, which were unbaffled except if stated otherwise. Impellers used were six-bladed 45° pitched turbines, unless stated otherwise. Solids concentration always 1.0%wt. Glass ballotini, density 2900kg/m^3, always used.

A) Experiments in 15cm tank

D=8.5cm, ΔZ=8.3cm (above base of cone), d_p=0.53mm, H_L=25.5cm

all at midradial position

1) 0.5%wt CMC

N (RPM)	h=3cm C_w/%wt	h=7cm C_w/%wt	h=11cm C_w/%wt	h=14cm C_w/%wt	h=19cm C_w/%wt	h=23cm C_w/%wt	Divergence σ
200	0.022	0.004					0.9977
300	0.090	0.067					0.9818
400	0.892	0.895	0.835	1.879	0.568	0.071	0.4961
440*	0.828	0.874	0.802	1.822	0.541	0.038	0.5051
460	0.807	0.639	0.741	1.592	0.513		0.5319
480	0.759	0.620	0.716	1.739	0.520		0.5680
500	0.743	0.593	0.691	1.210	0.582	0.041	0.4627
520	0.751	0.590	0.700	1.073	0.651	0.398	0.3692
540	0.768	0.632	0.711	0.744	0.815	0.303	0.3726
560	0.767	0.718	0.737	0.749	0.923	0.711	0.2698
580	0.759	0.659	0.650	0.655	1.199	0.711	0.2716
600	0.722	0.634	0.629	0.637	0.834	0.768	0.3353
620	0.628	0.609	0.598	0.616	0.612	0.867	0.3859

2) 0.25%wt CMC

N (RPM)	h=3cm C_w/%WT	h=7cm C_w/%WT	h=11cm C_w/%WT	h=14cm C_w/%WT	h=19cm C_w/%WT	h=23cm C_w/%WT	Divergence σ
200							1.000
250	0.048	0.050	0.061	0.045			0.970
300	0.551	0.361	0.620	0.501	0.584	0.646	0.491
320*	0.658	0.580	1.372	0.769	0.704	0.610	0.376
340	0.610	0.510	0.747	0.769	0.716	0.640	0.365
360	0.611	0.520	0.768	0.784	0.775	0.648	0.344
380	0.617	0.523	0.616	0.801	0.771	0.663	0.363
400	0.624	0.530	0.595	0.725	0.815	0.697	0.364
420	0.637	0.540	0.602	0.585	0.845	0.750	0.372
440	0.656	0.566	0.631	0.600	0.731	0.784	0.377
460	0.698	0.596	0.667	0.628	0.739	0.837	0.349
480	0.725	0.615	0.697	0.641	0.664	0.780	0.349
500	0.746	0.627	0.708	0.652	0.681	0.716	0.359

3) 0.20%wt CMC

N (RPM)	h=3cm C_w/%WT	h=7cm C_w/%WT	h=11cm C_w/%WT	h=14cm C_w/%WT	h=19cm C_w/%WT	h=23cm C_w/%WT	Divergence σ
200							1.000
240	0.143	0.061	0.041	0.056	0.049	0.058	0.944
260	0.275	0.161	0.271	0.315	0.360	0.336	0.728
280	0.522	0.792	1.380	1.051	0.860	0.817	0.253
300*	0.860	0.721	1.683	1.028	0.889	0.820	0.280
320	0.833	0.716	1.150	1.085	0.927	0.856	0.195
340	0.786	0.703	0.748	1.076	0.948	0.877	0.208
360	0.792	0.686	0.688	1.057	0.998	0.917	0.200
380	0.797	0.678	0.698	1.039	1.083	0.961	0.207
400	0.800	0.682	0.710	1.061	1.091	1.032	0.208
420	0.810	0.673	0.725	0.760	1.146	1.097	0.260
440	0.832	0.691	0.752	0.808	1.121	1.196	0.252
460	0.867	0.727	0.794	0.841	0.812	1.224	0.248

4) 70%wt glycerol/water
μ=0.022Pas, ρ_f=1180kg/m^3

N (RPM)	h=3cm C_w/%WT	h=7cm C_w/%WT	h=11cm C_w/%WT	h=14cm C_w/%WT	h=19cm C_w/%WT	h=23cm C_w/%WT	Divergence σ
100							1.000
140	0.043	0.009					0.995
160	0.070	0.017	0.009		0.016	0.016	0.985
180	0.243	0.200	0.124	0.119	0.187	0.106	0.852
200	0.608	0.531	0.458	0.598	0.583	0.394	0.503
220*	1.050	0.962	0.742	0.777	0.811	0.571	0.251
240	1.067	1.013	0.806	0.852	0.877	0.649	0.199
260	1.101	1.043	0.844	0.899	0.927	0.732	0.170
280	1.108	1.050	0.866	0.938	0.950	0.785	0.148
300	1.095	1.039	0.874	0.951	0.967	0.809	0.135
320	1.094	1.038	0.887	0.978	0.998	0.854	0.114
340	1.098	1.034	0.893	0.994	1.024	0.872	0.112
360	1.081	1.023	0.894	0.999	1.033	0.897	0.106

5) 77%wt glycerol/water
μ=0.044Pas, ρ_f=1200kg/m^3

N (RPM)	h=3cm C_w/%WT	h=7cm C_w/%WT	h=11cm C_w/%WT	h=14cm C_w/%WT	h=19cm C_w/%WT	h=23cm C_w/%WT	Divergence σ
100							1.000
140							1.000
160	0.096	0.053	0.036	0.042	0.071	0.038	0.950
180	0.627	0.392	0.338	0.359	0.372	0.452	0.622
200	1.081	0.851	0.631	0.844	0.728	0.682	0.279
220	1.203	0.920	0.690	0.949	0.880	0.862	0.189
240*	1.268	0.950	0.728	0.983	0.956	0.888	0.157
260	1.284	0.976	0.756	0.999	0.973	0.901	0.140
280	1.287	0.974	0.771	1.012	0.993	0.922	0.133
300	1.315	0.980	0.773	1.020	1.013	0.905	0.139
320	1.317	0.989	0.776	1.045	1.036	0.937	0.142
340	1.313	0.994	0.788	1.054	1.036	0.939	0.140
360	1.317	0.988	0.793	1.053	1.060	0.969	0.141

6) 82%wt glycerol/water
μ=0.077Pas, ρ_f =1215kg/m^3

N (RPM)	h=3cm C_w/%WT	h=7cm C_w/%WT	h=11cm C_w/%WT	h=14cm C_w/%WT	h=19cm C_w/%WT	h=23cm C_w/%WT	Divergence σ
140	0.044	0.028	0.058	0.016	0.015		0.977
160	0.198	0.088	0.090	0.162	0.141	0.012	0.896
180	0.550	0.339	0.306	0.397	0.340	0.028	0.706
200	0.936	0.592	0.543	0.566	0.614	0.041	0.507
220	1.080	0.726	0.751	0.771	0.763	0.028	0.385
240	1.117	0.743	0.821	0.840	0.877	0.878	0.251
260*	1.133	0.751	0.821	0.840	0.877	0.878	0.212
280	1.146	0.754	0.831	0.854	0.904	0.912	0.197
300	1.146	0.757	0.841	0.864	0.916	0.924	0.193
320	1.170	0.752	0.850	0.870	0.926	0.932	0.186
340	1.178	0.751	0.853	0.873	0.935	0.939	0.183
360	1.183	0.746	0.853	0.879	0.941	0.949	0.180
380	1.174	0.750	0.856	0.882	0.954	0.961	0.173

7) 0.20%wt CMC with 1.1mm glass ballotini

N (RPM)	h=3cm C_w/%WT	h=7cm C_w/%WT	h=11cm C_w/%WT	h=14cm C_w/%WT	h=19cm C_w/%WT	h=23cm C_w/%WT	Divergence σ
200							1.000
250		0.042					0.993
300	0.228	0.304	0.606	0.341	0.369	0.369	0.641
320	0.612	0.497	0.724	0.685	0.661	0.520	0.416
340*	0.601	0.497	0.731	0.728	0.649	0.561	0.404
360	0.590	0.493	0.754	0.745	0.671	0.602	0.398
380	0.649	0.482	0.778	0.771	0.679	0.653	0.368
400	0.650	0.480	0.655	0.805	0.719	0.676	0.370
420	0.660	0.483	0.651	0.776	0.719	0.712	0.368
440	0.686	0.485	0.664	0.716	0.735	0.746	0.368
460	0.685	0.508	0.678	0.676	0.786	0.802	0.350
480	0.704	0.506	0.688	0.644	0.765	0.846	0.351
500	0.719	0.510	0.693	0.656	0.720	0.871	0.352

8) 0.25%wt CMC with 1.1mm glass ballotini

N (RPM)	h=3cm C_w/%WT	h=7cm C_w/%WT	h=11cm C_w/%WT	h=14cm C_w/%WT	h=19cm C_w/%WT	h=23cm C_w/%WT	Divergence σ
250							1.000
300	0.327	0.112	0.367	0.200	0.144	0.136	0.813
320	0.583	0.386	0.591	0.487	0.418	0.380	0.565
340*	0.662	0.439	1.219	0.708	0.520	0.499	0.441
360	0.677	0.463	1.018	0.755	0.581	0.547	0.376
380	0.668	0.456	0.761	0.780	0.671	0.564	0.387
400	0.653	0.449	0.738	0.848	0.710	0.606	0.367
420	0.635	0.441	0.721	0.823	0.736	0.649	0.365
440	0.607	0.440	0.645	0.807	0.785	0.666	0.370
460	0.622	0.435	0.629	0.815	0.808	0.683	0.363
480	0.630	0.447	0.641	0.878	0.837	0.723	0.334
500	0.640	0.452	0.659	0.680	0.835	0.779	0.359
520	0.650	0.453	0.680	0.660	0.790	0.815	0.362

9) 82%wt glycerol/water with 1.1mm glass ballotini

μ=0.077Pas, ρ_f =1215kg/m^3

N (RPM)	h=3cm C_w/%WT	h=7cm C_w/%WT	h=11cm C_w/%WT	h=14cm C_w/%WT	h=19cm C_w/%WT	h=23cm C_w/%WT	Divergence σ
200	0.124	0.050	0.051	0.028	0.033	0.002	0.962
240	0.571	0.409	0.274	0.244	0.358	0.128	0.707
260	0.776	0.541	0.447	0.405	0.525	0.291	0.554
280	0.872	0.570	0.535	0.521	0.645	0.463	0.456
300*	0.878	0.575	0.570	0.608	0.643	0.577	0.417
320	0.923	0.581	0.619	0.687	0.695	0.704	0.361
340	0.958	0.586	0.652	0.709	0.739	0.712	0.338
360	1.007	0.588	0.674	0.731	0.752	0.711	0.326
380	1.027	0.571	0.678	0.743	0.824	0.736	0.309
400	1.064	0.573	0.688	0.754	0.869	0.741	0.297
420	1.072	0.555	0.681	0.770	0.882	0.745	0.296
440	1.082	0.548	0.687	0.769	0.885	0.745	0.297
500	1.151	0.521	0.662	0.786	0.973	0.748	0.289

10) 77%wt glycerol/water with 1.1mm glass ballotini

μ=0.044Pas, ρ_f =1200kg/m^3

N (RPM)	h=3cm C_w/%WT	h=7cm C_w/%WT	h=11cm C_w/%WT	h=14cm C_w/%WT	h=19cm C_w/%WT	h=23cm C_w/%WT	Divergence σ
200	0.146	0.147	0.100	0.067	0.016	0.037	0.927
240	0.551	0.419	0.273	0.246	0.196	0.233	0.724
260	0.766	0.556	0.419	0.404	0.327	0.309	0.594
280*	0.934	0.634	0.467	0.472	0.424	0.399	0.515
300	0.975	0.661	0.514	0.541	0.457	0.433	0.476
320	1.038	0.701	0.545	0.584	0.507	0.496	0.437
340	1.075	0.707	0.545	0.587	0.537	0.576	0.420
360	1.154	0.718	0.549	0.632	0.570	0.593	0.406
380	1.133	0.716	0.549	0.630	0.562	0.650	0.398
400	1.169	0.712	0.533	0.666	0.579	0.668	0.391
420	1.191	0.717	0.617	0.678	0.594	0.730	0.364
440	1.199	0.709	0.608	0.695	0.605	0.769	0.356
500	1.279	0.701	0.499	0.689	0.613	0.878	0.364

B) Experiments in 29cm tank

ΔZ=15.5cm (above base of cone), D=16.5cm, d_p=0.53mm

11) 77%^{wt} glycerol/water (at midradial position)

N (RPM)	h=8cm C_w/%wt	h=12cm C_w/%wt	h=19cm C_w/%wt	h=24cm C_w/%wt	h=28cm C_w/%wt	h=32cm C_w/%wt	h=36cm C_w/%wt	Divergei σ
120	0.724	0.647	0.592	0.619	0.627	0.589	0.534	0.412
140	0.777	0.699	0.643	0.681	0.700	0.651	0.610	0.354
160	0.791	0.725	0.683	0.717	0.727	0.705	0.653	0.320
180*	0.795	0.736	0.705	0.735	0.747	0.721	0.690	0.303
200	0.795	0.742	0.721	0.752	0.761	0.743	0.719	0.288
220	0.804	0.751	0.718	0.762	0.773	0.759	0.740	0.279
260	0.800	0.757	0.748	0.772	0.783	0.786	0.771	0.263

12) 77%^{wt} glycerol/water (at midradial +3.5cm position)

N (RPM)	h=8cm C_w/%wt	h=12cm C_w/%wt	h=19cm C_w/%wt	h=24cm C_w/%wt	h=28cm C_w/%wt	h=32cm C_w/%wt	h=36cm C_w/%wt	Divergenc σ
120	0.880	0.794	0.771	0.759	0.728	0.667	0.660	0.284
140	0.889	0.855	0.850	0.833	0.835	0.847	0.752	0.198
160	0.931	0.903	0.892	0.882	0.870	0.873	0.784	0.160
180*	0.941	0.914	0.913	0.909	0.907	0.922	0.844	0.131
200	0.945	0.929	0.932	0.928	0.928	0.955	0.879	0.111
220	0.945	0.934	0.944	0.944	0.946	0.973	0.904	0.098
260	0.943	0.946	0.957	0.963	0.965	1.006	0.953	0.080

13) 77%wt glycerol/water (at midradial -3.5cm position)

N (RPM)	h=8cm C_w/%wt	h=12cm C_w/%wt	h=19cm C_w/%wt	h=24cm C_w/%wt	h=28cm C_w/%wt	h=32cm C_w/%wt	h=36cm C_w/%wt	Divergenc σ
120	0.612	0.659	0.523	0.458	0.437	0.458	0.384	0.512
140	0.737	0.694	0.582	0.506	0.524	0.513	0.439	0.454
160	0.745	0.718	0.606	0.548	0.544	0.531	0.600	0.416
180*	0.754	0.729	0.623	0.564	0.563	0.550	vortex	
200	0.756	0.745	0.632	0.575	0.575	0.569	vortex	
220	0.757	0.742	0.635	0.573	0.585	0.583	vortex	
260	0.753	0.735	0.625	0.575	0.594	vortex	vortex	

14) 77%wt glycerol/water (at midradial position) with baffles

N (RPM)	h=8cm C_w/%wt	h=12cm C_w/%wt	h=19cm C_w/%wt	h=24cm C_w/%wt	h=28cm C_w/%wt	h=32cm C_w/%wt	h=36cm C_w/%wt	Divergenc σ
150	0.015							0.999
200	0.360	0.186	0.286	0.226	0.226	0.289	0.254	0.759
240	0.623	0.529	0.518	0.638	0.520	0.487	0.479	0.486
260	0.834	0.620	0.638	0.673	0.596	0.607	0.582	0.390
280*	0.755	0.667	0.673	0.662	0.642	0.647	0.654	0.362

15) 77%wt glycerol/water (at midradial+3.5cm position) with baffles

N (RPM)	h=8cm C_w/%WT	h=12cm C_w/%WT	h=19cm C_w/%WT	h=24cm C_w/%WT	h=28cm C_w/%WT	h=32cm C_w/%WT	h=36cm C_w/%WT	Divergence σ
150	0.015							0.999
200	0.410	0.327	0.256	0.238	0.225	0.310	0.287	0.729
240	0.764	0.650	0.668	0.624	0.613	0.644	0.555	0.387
260	0.884	0.764	0.759	0.768	0.714	0.730	0.661	0.284
280*	1.055	0.801	0.826	0.818	0.767	0.775	0.714	0.235

16) 77%wt glycerol/water (at midradial-3.5cm position) with baffles

N (RPM)	h=8cm C_w/%WT	h=12cm C_w/%WT	h=19cm C_w/%WT	h=24cm C_w/%WT	h=28cm C_w/%WT	h=32cm C_w/%WT	h=36cm C_w/%WT	Divergence σ
150	0.015							0.999
200	0.446	0.403	0.361	0.287	0.312	0.331	0.298	0.668
240	0.746	0.601	0.585	0.547	0.507	0.531	0.512	0.534
260	0.772	0.655	0.674	0.614	0.618	0.601	0.576	0.387
289*	0.743	0.677	0.739	0.654	0.640	0.629	0.619	0.356

17) 0.25%wt CMC (at midradial position)

N (RPM)	h=8cm C_w/%WT	h=12cm C_w/%WT	h=19cm C_w/%WT	h=24cm C_w/%WT	h=28cm C_w/%WT	h=32cm C_w/%WT	h=36cm C_w/%WT	Divergenc σ
140	0.602	0.267	0.480	0.595	0.449	0.456	0.523	0.558
180	0.618	0.582	0.595	0.782	0.673	0.631	0.672	0.391
200	0.621	0.593	0.598	0.715	0.695	0.659	0.596	0.389
220*	0.633	0.606	0.609	0.616	0.770	0.683	0.624	0.381
240	0.659	0.628	0.637	0.637	0.676	0.728	0.858	0.348
260	0.674	0.640	0.650	0.650	0.657	0.708	vortex	

18) 0.25%wt CMC (at midradial-3.5cm position)

N (RPM)	h=8cm C_w/%WT	h=12cm C_w/%WT	h=19cm C_w/%WT	h=24cm C_w/%WT	h=28cm C_w/%WT	h=32cm C_w/%WT	h=36cm C_w/%WT	Divergenc σ
140	0.098	0.229	0.111	0.267	0.244	0.484	0.353	
180	0.581	0.558	0.606	0.632	0.567	0.499	0.505	
200	0.582	0.558	0.547	0.667	0.592	0.521	vortex	
220*	0.590	0.563	0.551	0.653	0.619	0.532	vortex	
240	0.622	0.583	0.572	0.565	0.556	vortex	vortex	
260	0.638	0.598	0.579	0.562	0.526	vortex	vortex	

19) 0.25%wt CMC (at midradial+3.5cm position)

N (RPM)	h=8cm C_w/%WT	h=12cm C_w/%WT	h=19cm C_w/%WT	h=24cm C_w/%WT	h=28cm C_w/%WT	h=32cm C_w/%WT	h=36cm C_w/%WT	Divergence σ
140	0.657	0.342	0.333	0.770	0.732	0.708	0.676	0.456
180	0.682	0.651	0.847	0.849	0.802	0.764	0.704	0.267
200	0.697	0.661	0.709	0.801	0.857	0.789	0.725	0.285
220*	0.717	0.678	0.726	0.717	0.911	0.815	0.751	0.276
240	0.749	0.700	0.753	0.740	0.804	0.893	0.802	0.259
260	0.779	0.722	0.764	0.761	0.800	0.886	0.826	0.247

20) 77%wt glycerol/water (at midradial position) with 1.1mm glass

N (RPM)	h=8cm C_w/%WT	h=12cm C_w/%WT	h=19cm C_w/%WT	h=24cm C_w/%WT	h=28cm C_w/%WT	h=32cm C_w/%WT	h=36cm C_w/%WT	Divergence σ
120	0.183	0.154	0.067	0.035	0.048	0.049	0.013	0.928
140	0.648	0.524	0.215	0.233	0.206	0.190	0.105	0.723
160	0.866	0.656	0.349	0.332	0.285	0.291	0.181	0.613
180	0.924	0.745	0.405	0.402	0.350	0.355	0.270	0.545
200*	0.953	0.754	0.444	0.443	0.405	0.411	0.348	0.505
220	0.931	0.755	0.466	0.468	0.421	0.463	0.431	0.480
260	0.909	0.718	0.498	0.482	0.452	0.605	0.475	0.453

21) 77%wt glycerol/water (at midradial +3.5cm position) with 1.1mm glas

N (RPM)	h=8cm C_w/%WT	h=12cm C_w/%WT	h=19cm C_w/%WT	h=24cm C_w/%WT	h=28cm C_w/%WT	h=32cm C_w/%WT	h=36cm C_w/%WT	Divergence σ
120	0.226	0.104	0.095	0.099	0.056	0.007	0.008	0.926
140	0.695	0.442	0.309	0.314	0.268	0.188	0.109	0.670
160	0.866	0.623	0.491	0.471	0.408	0.365	0.180	0.548
180	0.993	0.726	0.579	0.560	0.535	0.469	0.312	0.447
200	1.028	0.765	0.644	0.621	0.604	0.578	0.404	0.385
220	1.068	0.791	0.684	0.661	0.632	0.642	0.518	0.345
260	1.057	0.801	0.735	0.717	0.704	0.745	0.600	0.292

22) 77%wt glycerol/water (at midradial position) using 1.1mm glass (anticlockwise) agitation provided by a 3-bladed 15cm marine propeller

N (RPM)	h=8cm C_w/%WT	h=12cm C_w/%WT	h=19cm C_w/%WT	h=24cm C_w/%WT	h=28cm C_w/%WT	h=32cm C_w/%WT	h=36cm C_w/%WT	Divergence σ
180	0.326	0.278	0.170	0.136	0.096	0.090	0.008	0.850
220	0.590	0.489	0.313	0.258	0.222	0.186	0.062	0.714
240	0.657	0.519	0.365	0.310	0.256	0.249	0.095	0.690
260*	0.719	0.552	0.412	0.345	0.306	0.290	0.112	0.632
280	0.770	0.581	0.455	0.384	0.354	0.334	0.151	0.593
320	0.806	0.661	0.514	0.446	0.417	0.403	0.229	0.530

23) 77%wt glycerol/water (at midradial+3.5cm position) using 1.1mm gl
(anticlockwise) agitation provided by a 3-bladed 15cm marine propelle

N (RPM)	h=8cm C_w/%WT	h=12cm C_w/%WT	h=19cm C_w/%WT	h=24cm C_w/%WT	h=28cm C_w/%WT	h=32cm C_w/%WT	h=36cm C_w/%WT	Divergence σ
180	0.408	0.273	0.232	0.173	0.160	0.131		0.817
220	0.691	0.494	0.406	0.346	0.304	0.287	0.054	0.655
240	0.745	0.558	0.451	0.392	0.364	0.342	0.078	0.607
260*	0.818	0.639	0.503	0.446	0.421	0.392	0.145	0.548
280	0.857	0.664	0.551	0.495	0.506	0.476	0.163	0.500
320	0.929	0.747	0.601	0.563	0.562	0.552	0.242	0.435

24) 0.25%wt CMC (at midradial position) using 1.1mm glass

N (RPM)	h=8cm C_w/%WT	h=12cm C_w/%WT	h=19cm C_w/%WT	h=24cm C_w/%WT	h=28cm C_w/%WT	h=32cm C_w/%WT	h=36cm C_w/%WT	Divergenc σ
140	0.056	0.046	0.097	0.080	0.076	0.074	0.077	0.929
180	0.483	0.427	0.605	0.615	0.541	0.514	0.498	0.492
200	0.507	0.481	0.541	0.560	0.593	0.544	0.531	0.486
220*	0.525	0.501	0.557	0.544	0.622	0.573	0.546	0.471
240	0.549	0.528	0.569	0.536	0.651	0.615	0.572	0.451
260	0.570	0.545	0.588	0.553	0.583	0.633	0.587	0.445

25) 0.25%wt CMC (at midradial+3.5cm position) using 1.1mm glass

N (RPM)	h=8cm C_w/%WT	h=12cm C_w/%WT	h=19cm C_w/%WT	h=24cm C_w/%WT	h=28cm C_w/%WT	h=32cm C_w/%WT	h=36cm C_w/%WT	Divergen σ
140	0.099	0.086	0.182	0.141	0.101	0.153	0.117	0.876
180	0.570	0.461	0.655	0.577	0.638	0.637	0.564	0.439
200	0.584	0.475	0.601	0.598	0.680	0.666	0.619	0.428
220*	0.599	0.492	0.614	0.667	0.710	0.702	0.639	0.400
240	0.608	0.502	0.628	0.596	0.738	0.737	0.681	0.392
260	0.633	0.525	0.639	0.621	0.675	0.792	0.716	0.378

26) 0.25%wt CMC (at midradial position) using 1.1mm glass
ΔZ=9.0cm above base of cone

N (RPM)	h=12cm C_w/%WT	h=19cm C_w/%WT	h=24cm C_w/%WT	h=28cm C_w/%WT	h=32cm C_w/%WT	h=36cm C_w/%WT	Divergence σ
140	0.166	0.166	0.161	0.121	0.154	0.131	0.856
160	0.503	0.493	0.463	0.428	0.400	0.352	0.576
180*	0.563	0.645	0.567	0.532	0.551	0.437	0.467
200	0.612	0.753	0.642	0.591	0.601	0.515	0.398
220	0.622	0.677	0.656	0.612	0.648	0.548	0.397
260	0.648	0.595	0.633	0.645	0.707	vortex	

27) 0.25%wt CMC (at midradial) using 1.1mm glass (antclockwise) agitation provided by 15cm 3-bladed marine propeller

N (RPM)	h=8cm C_w/%wt	h=12cm C_w/%wt	h=19cm C_w/%wt	h=24cm C_w/%wt	h=28cm C_w/%wt	h=32cm C_w/%wt	h=36cm C_w/%wt	Divergenc σ
180	0.103	0.078	0.084	0.092	0.065	0.044	0.076	0.927
220	0.548	0.472	0.465	0.464	0.393	0.356	0.240	0.596
240*	0.565	0.483	0.514	0.501	0.444	0.405	0.322	0.556
260	0.583	0.496	0.560	0.549	0.477	0.441	0.353	0.525
280	0.593	0.510	0.578	0.576	0.512	0.480	0.418	0.497
320	0.622	0.535	0.542	0.637	0.546	0.516	0.480	0.473

APPENDIX 7 Optical technique for measurement of local solids concentrations

In Chapter Four, the experimental procedures by which the local solids concentrations are determined have been described. This Appendix sets out to explain the theory that lies behind the laser/photocell technique for measurement local solids concentrations.

If a coherent beam of light, such as that from a laser, is passed through a liquid containing solid particles, it will be partially scattered by those particles that stray within the beam. Only some fraction of the energy contained within the original beam of light will pass through the suspension to be detected by the photocell (see figure A7.1). That light that does manage to pass through the suspension causes a mean, time averaged, voltage to be generated by the photocell, $\bar{V}$.

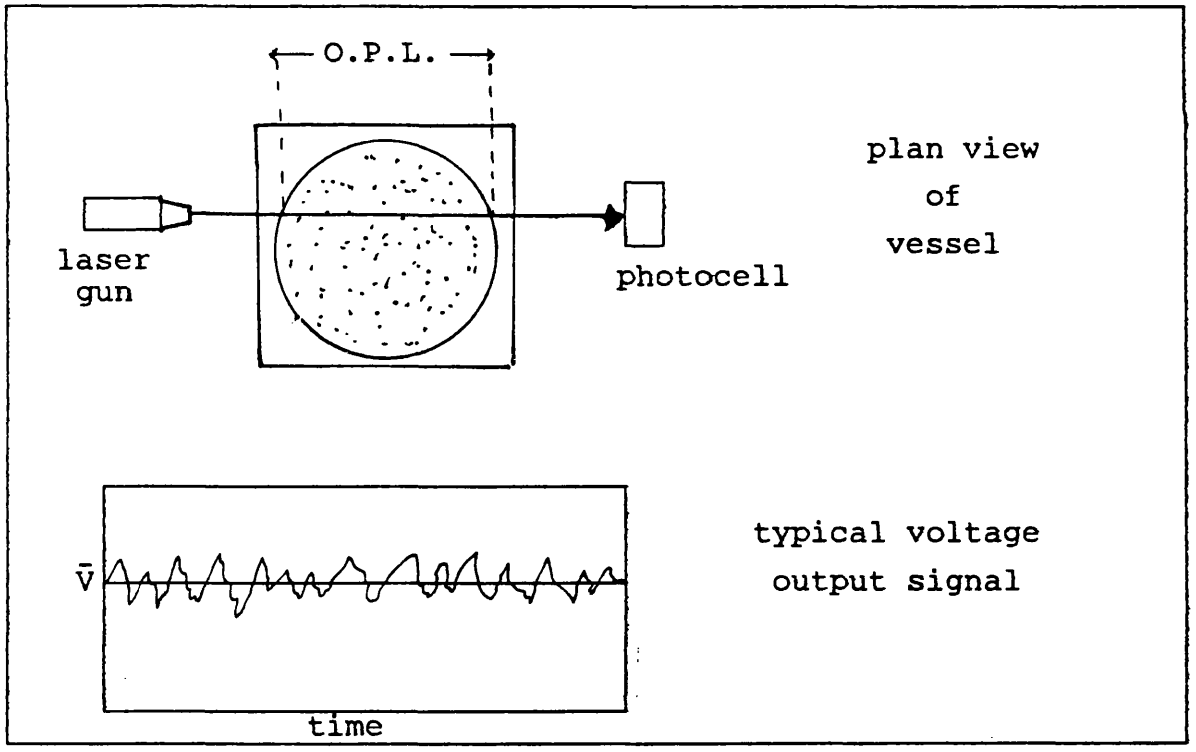

Figure A7.1 Schematic diagram of laser beam passing through a suspension

This value of $\bar{V}$ is proportional to the amount of light energy that is transmitted through the suspension. When there are no particles in suspension, the voltage generated by the photocell will be higher, V_o. The difference, $V_o - \bar{V}$, is a direct function of the number of particles present (local solids concentration, C_w), within the volume described by the laser beam; the optical path volume (cf Chapter 5.2). This function is also determined by the particle diameter, d_p, and the optical pathlength, L_o.

What has just been described is very similar to the well established Beer-Lambert Law (Bos & Heerens, 1982) for the transmission of light through a dilute suspension. Beer and Lambert expressed the ratio of the intensity of the light, $\bar{I}$, after passing through a pathlength, L, of the suspension, to the original intensity, I_o, by the following:

$$\ln(I_o / \bar{I}) = \phi\, C_w L \qquad \text{A7.1}$$

where ϕ is the light scatter co-efficient.
However, since the voltage, V, generated by the photocell is proportional to the intensity, I, A7.1 can rewritten:

$$\ln(V_o / \bar{V}) = \phi\, C_w L \qquad \text{A7.2}$$

If this relationship is applied to the study of solids suspensions, it might be expected that value of $\ln(V_o / \bar{V})$would be a function only of $(\phi\, C_w L/d_p)$. However, over wide range of experiments (Koutsakos, 1989), the results indicated that:

$$\ln(V_o / \bar{V}) = \phi\, C_w L/d_p + k \qquad \text{A7.3}$$

where k is a constant. A7.3, therefore, deviates from the expectations of the Beer-Lambert Law. This might be caused by the very dilute solutions and small optical pathlengths considered for A7.1. Similar deviations were observed by others (Bos & Zuiderwerg, 1981; Bos & Heerens, 1982). More

recently when Gregory & Nelson, 1986, also used a similar optical technique to measure the solids concentration, deviations were found.

Figure A7.2 shows the calibration curve determined by Koutsakos, 1989,of $V_o - \bar{V}$ against the ratio $C_w L/d_p$. The calibration curve can be represented by two straight lines intersecting at a point where $C_w L/d_p = 607$. This intersection point agrees well with Gregory & Nelson, 1986. Although the laser/photocell technique has some limitations, the technique was found to give reproducible results both for this study as well as for a previous study (Koutsakos, 1989).

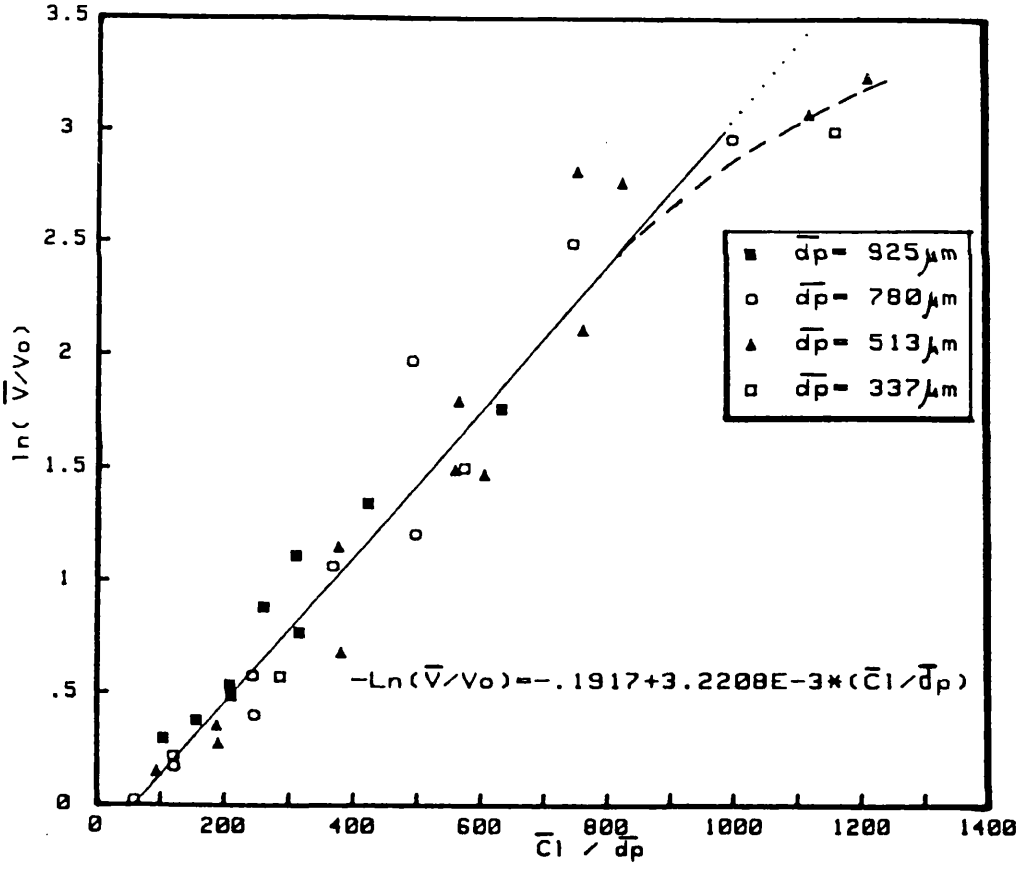

Figure A7.2 Calibration curve determined by Koutsakos, 1989

APPENDIX 8: Computer Programs and Procedures for data acquisition and data processing

The program for data acquisition is listed on page and is loaded by pressing simultaneously the "shift" and "break" keys. The menu shown in figure A8.1 then appears on the screen. The program assigns the computer certain function keys for subroutines. These subroutines are:

F0 "Collect data"; this initiates the collection and storage of real time voltage signals transmitted from the photocell via an A/D converter.

F1 "Real time display"; this displays the the instantaneous voltage signal from the photocell onto the screen monitor in both a graphical and digital form (see figure 4.3.5).

F2 "Catalog disc"; this displays the names of the data files stored on the diskette (which has been inserted into the other disc drive).

F3 "Set block count"; this specifies the number of "blocks" of data to be collected and stored. The longer the block count then, in principle, the more accurate any eventual calculation will become. However, the computer will take a correspondingly long time to perform the calculation.

F4 "Set range"; this selects one of seven voltage ranges (15-25, 25-50, 50-100, 100-150, 150-200, 200-250, 250-350mV)

F5 "Display data"; this key is pressed for VDU display and/or printing of the stored data.

F6 "Exit"; to quit from the main acquisition program.

Procedure for data acquisition:

a) Insert the data acquisition disc into drive 1 and and insert a formatted disc into drive 2.

b) Load the program by depressing the "break" and "shift" keys at the same time.

c) Press F1; from the VDU displayed signal determine the maximum value of the voltage signal, V_o. Return to the menu.

d) Press F4 to select the appropriate voltage range, usually 250-350 mW.
e) Set the voltage range on the A/D amplifier to accommodate the maximum voltage determined in c) and voltage range in d)
f) Press F3 to set the required block count. This was usually set at 25 at a frequency of 10 kHz.
g) Press F0 to initiate the collection of voltage signals from the photocell. Before any data is collected, a sub-menu is displayed on the screen enabling the operator to name the data file and the details of the experimental conditions. When this information is inserted, the data acquisition commences, using the diskette in drive 2 as storage space. At the end of the data collection and storage, the main menu reappears.

Data processing

In order to retrieve any data collected, the function key, F5, must be pressed when the menu appears. This is followed by the name of datafile required. When the data file is loaded onto the ROM of the microcomputer, the screen will show "PLOTS/STATS". If PLOTS is chosen, then the voltage signal will appear on the monitor and/or printed. An example of the printed voltage signal is shown in figure A7.1 If STATS is typed, then the computerwill calculate and display the time averaged voltage signal, $\bar{V}$,collected over the block count selected.If required, the computer can also calculate the standard deviation of the voltage signals from the time average voltage.
This value of $\bar{V}$ is then subtracted from the maximum value, V_o. Then using the calibration curve shown in Appendix 7, the mean local solids concentration can be calculated.

```
 10 MODE 7
 20 REM **MAIN PROGRAM**
 30 :
 40 REM **DEFINE FUNCTION KEYS**
 50 :
 60 *FX200,1
 70 *KEY0 £
 80 *KEY1 $
 90 *KEY2 %
100 *KEY3 &
110 *KEY4 '
120 *KEY5 (
130 *KEY6 )
140 :
150 REM **ZERO PAGE LOCATIONS**
160 :
170 BUFFEND=&72:REM   End of buffer address high byte
180 RANGEBIT=&73:REM   250mV/350Mv Flag
190 OFSET%=&20:REM  Buffer high byte offset
200 :
210 REM **INSTALL CHECK**
220 :
230 IF ?&74<>&55 THEN 290
240 IF ?&75<>&AA THEN 290
250 GOTO 380
260 :
270 REM **PUT IN DEFAULTS**
280 :
290 BLKCOUNT%=&5C
300 ?BUFFEND=BLKCOUNT%+OFSET%
310 RANGE%=1
320 ?RANGEBIT=RANGE%
330 ?&74=&55:?&75=&AA
340 :
350 :
360 REM **STARTUP VALUES**
370 :
380 COLECT=FALSE
390 EDATA%=&FF:REM  End of data flag
400 BLKCOUNT%=?BUFFEND-OFSET%
410 @%=&00000002:REM Print Format
420 RANGE%=?RANGEBIT
430 IF RANGE%>2 THEN RANGE%=-1*(256-RANGE%)
440 :
450 REM **LOAD M/CODE FILES**
460 :
470 *LOAD O.LOAD
480 *LOAD O.DISC
490 :
500 REM **MAIN MENU CONTROL**
510 :
520 PROCmenu
530 REPEAT
540 KEY=INKEY(0)
550 IF KEY=35 THEN PROCdetails
560 IF KEY=36 THEN CHAIN "REALPLT"
570 IF KEY=37 THEN PROCcat
580 IF KEY=38 THEN PROCblockcount
590 IF KEY=39 THEN PROCrangeselect
600 IF KEY=40 THEN CHAIN "DISPLAY"
610 IF COLECT=TRUE THEN CHAIN "COLECT"
620 UNTIL KEY=41
630 CLS
640 @%=10:REM       Reset print format
```

```
650 *FX200,0
660 END
670 :
680 REM **DISPLAY MENU**
690 :
700 DEF PROCmenu
710  CLS
720 PRINT:PRINT
730 VDU141:PRINT"      Waveform Analyser V3.0"
740 VDU141,131:PRINT"     Waveform Analyser V3.0"
750 PRINT
760 VDU131:PRINT"        (C) MRV Systems 86"
770 PRINT:PRINT:PRINT
780 PRINT" F0=Collect Data        F4=Set Range"
790 VDU131:PRINT"F1=Real Time Display  F5=Display Data"
800 PRINT" F2=Catalog Disc        F6=Exit"
810 VDU131:PRINT"F3=Set Block Count"
820 PRINT
830 PRINT "System Parameters"
840 PRINT
850 PRINT"Block Count ="
860 PRINT"A/D range   ="
870 PRINT
880 PRINT "Press required function key >";
890 PRINT TAB(14,16) ~BLKCOUNT%
900 UPDATE=TRUE:PROCrangeselect
910 PRINT TAB(29,19);
920 ENDPROC
930 :
940 REM **CATALOG DRIVE 1**
950 :
960 DEF PROCcat
970 CLS
980 *CAT 1
990 PRINT:PRINT "Press any key"
1000 REPEAT
1010 KEY=INKEY(0)
1020 UNTIL KEY <> -1
1030 PROCmenu
1040 ENDPROC
1050 :
1060 REM **DISC & EXP DETAILS ROUTINE**
1070 :
1080 DEF PROCdetails
1090 CLS
1100 PRINT TAB(0,5)
1110 PRINT"Enter disc filename for data after"
1120 PRINT"collection or enter to quit"
1130 PRINT:PRINT
1140 INPUT "Filename  ";FDATA$
1150 PRINT:PRINT:PRINT "     ** Details of experiment **"
1160 PRINT
1170 IF LEN(FDATA$)=0 THEN 1340
1180 COLECT=TRUE
1190 INDEX%=&AC0
```

```
1200 PROCparamfill
1210 INPUT "          Vessel Geometry  ";FDATA$
1220 PROCparamfill
1230 INPUT "        Type of particles  ";FDATA$
1240 PROCparamfill
1250 INPUT "Particles mean diam (mm)  ";FDATA$
1260 PROCparamfill
1270 INPUT "    % Solid concentration  ";FDATA$
1280 PROCparamfill
1290 INPUT "       Vessel height (Cm)  ";FDATA$
1300 PROCparamfill
1310 INPUT "     Impeller speed (RPM)  ";FDATA$
1320 PROCparamfill
1330 ?INDEX%=EDATA%
1340 IF COLECT=FALSE THEN PROCmenu
1350 ENDPROC
1360 :
1370 REM **BUFFER PARAMETER FILL**
1380 :
1390 DEF PROCparamfill
1400 FDATA$=LEFT$(FDATA$,7)
1410 IF LEN(FDATA$)=0 THEN FDATA$="£££££"
1420 FOR N=1 TO LEN(FDATA$)
1430 ?INDEX%=ASC(MID$(FDATA$,N,1))
1440 INDEX%=INDEX%+1
1450 NEXT N
1460 ?INDEX%=&0D
1470 INDEX%=INDEX%+1
1480 ENDPROC
1490 :
1500 REM **SET BLOCK COUNT ROUTINE**
1510 :
1520 DEF PROCblockcount
1530 BLKCOUNT%=BLKCOUNT%+1
1540 IF BLKCOUNT%=&5D THEN BLKCOUNT%=0
1550 ?BUFFEND=BLKCOUNT%+OFSET%
1560 PRINT TAB(14,16) ~BLKCOUNT%
1570 PRINT TAB(29,19);
1580 ENDPROC
1590 :
1600 REM **SET A/D RANGE ROUTINE**
1610 :
1620 DEF PROCrangeselect
1630 IF UPDATE=TRUE THEN 1650
1640 RANGE%=RANGE%+1
1650 IF RANGE%=3 THEN RANGE%=-5
1660 IF RANGE%=-5 THEN PRINT TAB(14,17)"15mV ";
1670 IF RANGE%=-4 THEN PRINT TAB(14,17)"25mV ";
1680 IF RANGE%=-3 THEN PRINT TAB(14,17)"50mV ";
1690 IF RANGE%=-2 THEN PRINT TAB(14,17)"100mV";
1700 IF RANGE%=-1 THEN PRINT TAB(14,17)"150mV";
1710 IF RANGE%=0 THEN PRINT TAB(14,17)"200mV";
1720 IF RANGE%=1 THEN PRINT TAB(14,17)"250mV";
1730 IF RANGE%=2 THEN PRINT TAB(14,17)"350mV";
1740 ?RANGEBIT=RANGE%
1750 PRINT TAB(29,19);
1760 UPDATE=FALSE
1770 ENDPROC
```

"MYMIX" PROGRAM

```
 10  DIM LO(50)
 20  DIM C(50)
 30  DIM OPV(50)
 40  DIM Z(50)
 50  DIM SV(50)
 60  DIM DV(50)
 70  DIM WA(50)
 80 PRINT "INPUT TANK RADIUS(M)"
 90 INPUT R
 91 R=0.145
100 PRINT "VOLUME(M3)AND HEIGHT(M) OF LIQUID"
110 INPUT VL
111 VL=0.024
120 INPUT ZL
121 ZL=0.385
130 PRINT "LASER BEAM WIDTH(M)"
140 INPUT BW
141 BW=0.009
150 PRINT "SOLID BULK CONCENTRATION(%WT)"
160 INPUT CB
161 CB=1.0
170 PRINT "YOU NOW NEED THE OPTICAL PATHLENGTHS AT EACH HEIGHT"
180 PRINT "HOW MANY HEIGHTS SAMPLED?"
190 INPUT NV
191 NV = 7
200 PRINT "STARTING FROM THE BASE UP"
210 FOR I=1 TO NV
220 PRINT "INPUT SAMPLE HEIGHT"
230 INPUT Z(I)
231 Z(1) = 0.08
232 Z(2) = 0.125
233 Z(3) = 0.195
234 Z(4) = 0.24
235 Z(5) = 0.28
236 Z(6) = 0.32
237 Z(7) = 0.36
240 PRINT "INPUT OPTICAL PATHLENGTH"
250 INPUT LO(I)
251 LO(1) = 0.224
252 LO(2) = 0.241
253 LO(3) = 0.251
254 LO(4) = 0.251
255 LO(5) = 0.251
256 LO(6) = 0.251
257 LO(7) = 0.251
259 PRINT "LOCAL CONCENTRATION"
260 INPUT C(I)
270 NEXT I
280 RL = 0.5*LO(NV)
```

```
290 Z(NV +1)=ZL
300 C(NV+1)=0
310 FOR J=1 TO NV
320 OPV(J)=3.142*BW^2*LO(J)/4
330 NEXT J
340 OPV(NV+1)=OPV(NV)
350 PRINT "FINE SO FAR"
360 FOR I=1 TO NV
370 IF Z(I)<R AND Z(I+1)<R THEN GOTO 400
380 IF Z(I)<R AND Z(I+1)>R THEN GOTO 420
390 IF Z(I)>R AND Z(I+1)>R THEN GOTO 440
400 SV(I)=2*BW*RL^2*(ATN((R-Z(I))/RL)-ATN((R-Z(I+1))/RL))
410 GOTO 450
420 SV(I)=2*BW*RL^2*(ATN((R-Z(I))/RL))+2*BW*RL*(Z(I+1)-R)
430 GOTO 450
440 SV(I)=2*BW*RL*(Z(I+1)-Z(I))
450 NEXT I
460 PRINT "SUBTENDED VOLUMES CALCULATED"
470 FOR I=1 TO NV
480 DV(I)=ABS(C(I)-CB)
490 NEXT I
500 DV(NV+1)=CB
510 FOR I=1 TO NV
520 WA(I)=((DV(I)*OPV(I))+(DV(I+1)*OPV(I+1)))/(OPV(I)+OPV(I+1))
530 NEXT I
540 SUM=0
550 FOR I=1 TO NV
560 SUM=SUM+(WA(I)*SV(I))
570 NEXT I
580 SLIVOL=0
590 FOR I=1 TO NV
600 SLIVOL=SLIVOL+SV(I)
610 NEXT I
620 DVSLI =SUM/SLIVOL
630 PRINT "THE VOLUME OF THE SLICE"
640 PRINT SLIVOL
650 PRINT "THE DIVERGENCE IN THE SLICE"
660 PRINT DVSLI
670 STOP
680 END
```